AD NUMBER

AD857490

NEW LIMITATION CHANGE

TO

Approved for public release, distribution unlimited

FROM

Distribution authorized to U.S. Gov't. agencies and their contractors; Critical Technology; JUN 1969. Other requests shall be referred to Naval Weapons Center, China Lake, CA.

AUTHORITY

USNWC ltr dtd 30 Aug 1974

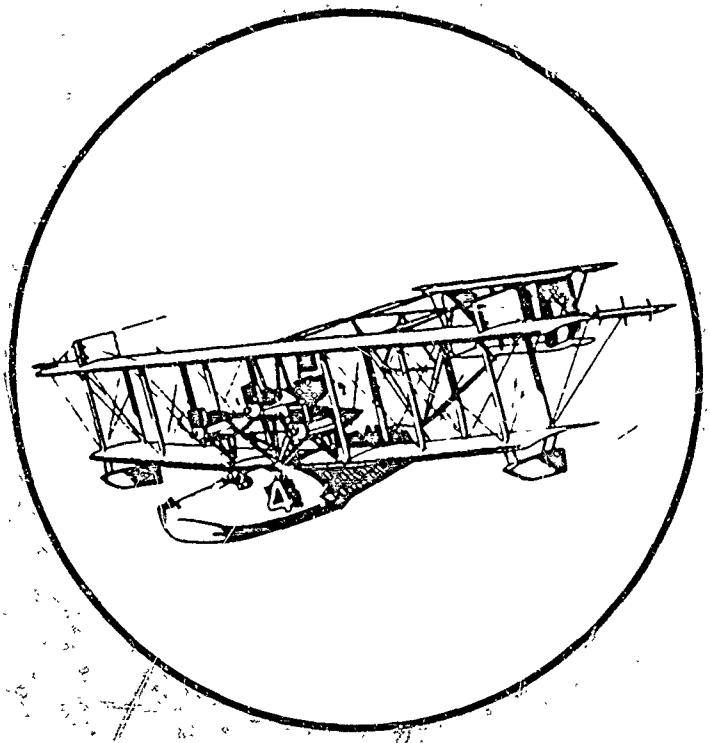

PROCEEDINGS OF THE 8TH NAVY SYMPOSIUM ON AEROBALLISTICS

VOLUME 4

6, 7, 8 MAY 1969

NAVAL WEAPONS CENTER • Corona Laboratories • Corona, California

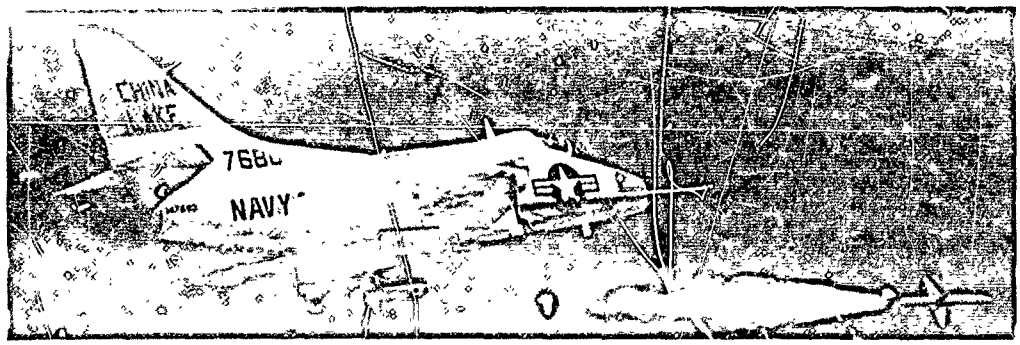

SPONSORED BY THE NAVAL AEROBALLISTICS ADVISORY COMMITTEE
FOR THE
NAVAL AIR SYSTEMS COMMAND•NAVAL ORDNANCE SYSTEMS COMMAND

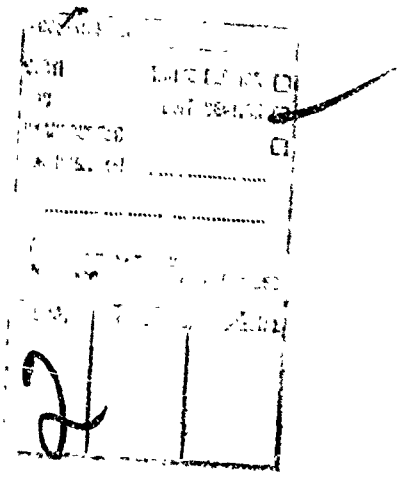

50TH ANNIVERSARY COMMEMORATED

Appropriately, the closing date of the Symposium marked the 50th anniversary of a significant milestone in aviation. On 8 May 1919, three naval aircraft left Long Island to attempt the first crossing of the Atlantic. Of the three Curtiss flying boats that started that historic 3,925-nautical-mile flight, the NC-4 (shown on cover), commanded by LCDR A. C. Read, was successful, making the first Atlantic crossing via Newfoundland, the Azores, and Portugal, finally arriving at Plymouth, England.

The Secretary of the Navy designated May 1969 a commemorative period, and it was especially appropriate that the Symposium salute the aeronautical pioneers who made history in May 1919.

PROCEEDINGS OF THE
8TH NAVY SYMPOSIUM
ON AEROBALLISTICS

VOLUME 4

6, 7, 8 MAY 1969

NAVAL WEAPONS CENTER • Corona Laboratories • Corona, California

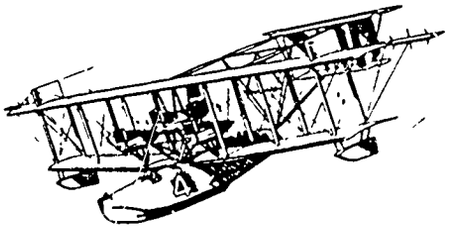

SPONSORED BY THE NAVAL AEROBALLISTICS ADVISORY COMMITTEE
FOR THE
NAVAL AIR SYSTEMS COMMAND•NAVAL ORDNANCE SYSTEMS COMMAND

NAVAL WEAPONS CENTER • CHINA LAKE, CALIFORNIA

JUNE 1969

FOREWORD

These *Proceedings,* published in five volumes, comprise the 49 papers presented at the Eighth Navy Symposium on Aeroballistics held at the Naval Weapons Center Corona Laboratories, Corona, Calif., 6, 7, and 8 May 1969.

This symposium was the eighth in a series begun in 1950 under the sponsorship of the then Bureau of Ordnance Committee on Aeroballistics, and currently conducted by the Naval Aeroballistics Advisory Committee as sponsoring committee for the Naval Air Systems Command and the Naval Ordnance Systems Command. The continuing purpose of the symposiums has been to disseminate the results of aeroballistics research and to bring the research findings of industry, the universities, and government laboratories to bear upon the Navy's aeroballistics research and development programs.

Over 200 research scientists representing more than 72 organizations attended this eighth symposium. Sessions 1 and 2 covered the subjects of heat transfer and aerophysics, nozzles and jet effects; Sessions 3 and 4 were concerned with aerodynamics and missile stability; and Session 5 dealt with structures and aeroelasticity, and external carriage and store separation.

The papers in these *Proceedings* have been reproduced in facsimile. They appear in the order of presentation except that all classified papers have been taken out of sequence and grouped together as Volume 5, a confidential volume. Volumes 1 through 4 are unclassified. This is Volume 4.

Requests for or comments on individual papers should be addressed to the respective authors.

RAY W. VAN AKEN
General Chairman
Symposium Committee

Published by the Publishing Division of the Technical Information Department, NWC; first printing, June 1969, 250 copies.

CONTENTS
Volume 1

Volume 2

Vol. 4

Volume 3

Volume 4

Volume 5
(Classified Papers)

AUTHORS

Paper No. 38

STRUCTURAL QUALIFICATION OF THE LOW SPEED FAE WEAPON DISPENSER (U)

(Paper UNCLASSIFIED)

by

Jack D. Brannan
Honeywell Inc.
Ordnance Division
St. Louis Park, Minn. 55416
and
Wallace W. Parmenter
Naval Weapons Center
China Lake, Calif. 93555

ABSTRACT. (U) Structural qualification of external airborne ordnance has, historically, been an arbitrary process. An effort was made to qualify the LSFAE weapon dispenser to criteria that more closely represented the use environment. Three distinct tests were performed:

1. Aircraft vibration
2. Transportation vibration
3. Static loads

Historically, the most severe of these test environments is aircraft vibration, while transportation vibration is the least severe.

(U) Aircraft vibration testing is usually done to that spectrum of MIL-STD-810B which is believed to simulate the use environment of the item tested. In qualifying the LSFAE dispenser, a composite spectrum was established for each axis by flying a fully instrumented LSFAE weapon on a UH-1E helicopter and an OV-10A fixed wing aircraft (the two primary carrier aircraft). These spectra, which were several times more severe than MIL-STD-810B, were then used as input in the qualification test.

(U) The static loads test was divided into three parts:

1. Flight loads
2. Handling loads
3. Pressurization as required

The flight loads test was designed to meet the requirements of MIL-A-8591C. The handling loads were defined as 35 g's in all axis when the weapon was mounted in its shipping container. The pressurization load, 90 psig, was the vapor pressure of the fuel at 165°F.

(U) The transportation vibration test was designed according to MIL-STD-810B, modified.

(U) The most significant improvement in the structural qualification program was in the aircraft vibration test. Had the spectrum of MIL-STD-810B been used, an undertest would have resulted, and the dispenser might well have failed structurally when in its use environment.

INTRODUCTION

(U) The process for establishing the structural design and qualification testing criteria for airborne ordnance has usually consisted of selecting standard tests from military specifications, and designating them as development requirements. This process sometimes resulted in nonrepresentative testing to a degree proportional to the contracting agencies experience. The most questionable of the specs selected was in the aircraft vibration regime. In the LSFAE program, a systematic attempt was made to define the probable use environment insofar as aircraft vibration was concerned. This was done by flight testing a weapon on the required aircraft, and recording the accelerometer histories at various points on it. From these measured data, a composite specification was established to which the dispenser was designed and tested. The LSFAE weapon is shown in Fig. 1.

(U) This paper will attempt to delineate the procedures followed in establishing the aircraft vibration environment, define the methods used to reduce the flight test data, describe the test methods and instrumentation, and briefly outline procedures recommended for future weapons development. The data presented are by no means complete; however, they represent the composite of all the data recorded during the development program.

(U) The paper is divided into four sections as follows:

1. Aircraft vibration
2. Transportation vibration
3. Static loads
4. Discussion and recommendations.

AIRCRAFT VIBRATION

ENVIRONMENTAL CAPTIVE-FLIGHT RESPONSE MEASUREMENTS

(U) Captive-flight vibration measurements were made on the LSFAE weapon during tests on the UH-1E helicopter and the OV-10A aircraft. Measurement of the weapon response was performed early in the development program for inclusion into aircraft vibration test specifications. This was extremely valuable for a more realistic evaluation during the preliminary design phase and subsequent operational integrity and safety tests. The flight tests were conducted at the U. S. Naval Weapons Center, China Lake, California, using prototype hardware. The purpose of these tests was to provide support and improvement of the vibration test curves presented in MIL-STD-810B.

(U) The LSFAE weapon installation on the UH-1E helicopter is shown in Fig. 2. Details of the UH-1E installation are depicted more clearly in Fig. 3. Also shown is the compartment area where the airborne magnetic tape recorder and the instrumentation electronics were carried.

(U) Fig. 4 shows the weapon installation on the OV-10A aircraft. A detailed view of the LSFAE mounted on an Aero 65A bomb rack of Station 1 is shown in Fig. 5. The OV-10A aircraft installation carried the tape recorder and associated electronics in the fuselage cargo compartment.

INSTRUMENTATION SYSTEM

(U) The instrumentation system for acquiring the vibration data consisted of transducers (piezoelectric and strain-gauge types), signal conditioning equipment and shielded cables. The instrumentation used during the flight tests are listed in Table 1. Fig. 6 shows the installation of Endevco Model 2213C accelerometers in the forward end at the base of the dispenser fuze. System calibrations were performed by mounting the transducers on an electrodynamic vibration exciter and recording their outputs for known vibration levels and frequencies. The transducer signals and the observer's voice were recorded on 1-inch wide magnetic tape. Annotation of the tape facilitated event correlation during subsequent playbacks. Transducer locations on the weapon and bomb rack are shown in Fig. 7.

CAPTIVE-FLIGHT TESTS

(U) Various maneuvers and flight profiles were included in the captive-flight tests. For the OV-10A aircraft, this consisted of airfield take-offs, turns, dives and airfield landings. The instrumented weapon was carried at Stations 1, 3 and 5, with several combinations of adjacent weapons, such as a 4-round Zuni launcher, a 2.75-inch 7- and 19-round launcher, and a centerline fuel tank. Also, transducer signals were recorded during the firing of a Mk 16 Mod II Zuni and during minimum and maximum engine-power settings.

(U) Test flights with the UH-1E helicopter consisted of lift-offs, straight and level flights at constant speeds of from 20 knots to the maximum of 120 knots, deceleration and acceleration runs, steep and shallow turns, dives, and landings. Vibration responses were recorded during firing of the M-60C machine guns.

METHODS OF DATA ANALYSIS

(U) Oscillograph records were obtained during playbacks of the magnetic tapes. The observer's comments concerning the flight conditions were marked on the oscillograms. The records were then viewed and the areas of vibration having maximum amplitudes were

selected to be analyzed. The method of data analyses is outlined in Fig. 8. For the almost periodic data from the UH-1E helicopter tests, amplitude versus frequency plots were obtained using a Spectral Dynamics Company tracking filter, Model 101. The filter bandwidths used for this analysis were 5 Hz and 20 Hz, with switch over occurring at 150 Hz.

(U) The more random data from the OV-10A aircraft flight tests were digitized and analyzed using a spectral analysis program with a CDC 3300 computer. The plotted output consisted of power spectral density (PSD) graphs. The analysis was performed with an effective bandwidth of 15.6 Hz and 104 degrees of freedom.

ANALYSIS RESULTS

(U) Examination of the oscillograph records clearly showed the most severe vibration conditions. These occurred during machine gun firing and straight and level flight at 120 knots for the UH-1E helicopter. For the OV-10A aircraft, the worst condition occurred at maximum power setting during a dive at low altitude. The resulting curves from the respective analyses were then enveloped to provide specification levels for laboratory vibration tests. For purposes of conciseness, the individual plots for each transducer are not presented in this paper; only the maximum composite spectra levels are shown.

(U) Fig. 9 shows the maximum composite plot for the response measured in the vertical axis of the weapon when mounted on the UH-1E helicopter. Similarly, the maximum composite plots for the transverse and longitudinal axes are shown in Fig. 10 and Fig. 11, respectively. If one were to view the individual PSD plots of the accelerometers, one would observe discrete periodic signals traceable to:

1. The machine gun firing rate (at about 9 Hz)
2. Rotating parts of the engine (primary frequency is at 115 Hz)
3. Rotor blade downwash (at about 5.5 and 11 Hz).

(U) As mentioned earlier, the environmental vibration data obtained from the OV-10A aircraft could be better described in terms of statistical methods of random analysis. Typical PSD levels obtained are shown in Fig. 12. These spectra shapes are typical of the other plots produced, which, again for conciseness, are not presented in this paper. An envelope was simply drawn around the maximum captive-flight PSD spectra. The resulting envelope curve was then used as the laboratory vibration test curve (see Fig. 12).

LABORATORY VIBRATION TESTS

(U) The laboratory vibration tests to be performed on the LSFAE weapon for environmental qualification use the test curves derived by the methods outlined above, along with the normal test

procedures presented in MIL-STD-810B. The laboratory vibration tests attempt to simulate two major portions of the life cycle of the LSFAE weapon: transportation and aircraft captive-flight vibration. The transportation vibration environment is the least severe insofar as the structural integrity of the dispenser is concerned.

TRANSPORTATION VIBRATION TEST

(U) The laboratory vibration test specification for the transportation environment is taken directly from MIL-STD-810B. The sinusoidal test curve employed is shown in Fig. 13 and is applied individually to each of the three axes with the weapon loaded in the shipping container. The test temperature is at 70° ± 10°F. The test levels from MIL-STD-810B are reduced to the maximum allowable, which is 50%.

(U) Typical laboratory test set-ups at the Naval Weapons Center are shown in Fig. 14 and 15. The electrodynamic vibration exciter (Ling, Model A 300B) is rated at 8000 force-pounds. Schematically, the test installation is shown in Fig. 16. For the transverse and longitudinal axes tests, the vibration fixture is attached to a slip table. Additional accelerometers monitored locations throughout the container and weapon. Thermocouples attached to the container shock mounts are monitored during the tests. The accelerometer output signals are amplified (Endevco, Model 2711) and recorded, using a Sanborn magnetic tape recorder (Model 150). During the cycling part of the tests, several real-time plots are made. Frequencies for resonance dwells are chosen from the plots where an amplification of 1.5 or more is evident. The shipping container and weapon are subjected to a total vibration time for cycling and resonance dwells of 105 minutes in each axis as outlined in Table 2.

(U) An additional resonance search of the shipping container with the LSFAE weapon was conducted from 2 to 5 Hz. This was performed to determine if any resonances existed that would not normally be observed during the MIL-STD-810B transportation tests. No resonances were found in this frequency region.

AIRCRAFT CAPTIVE-FLIGHT VIBRATION

(U) In a similar manner as above, and with the procedures outlined in MIL-STD-810B, the sine vibration tests are performed on the individual fully assembled LSFAE weapon. The test levels used are those previously mentioned and shown in Figs. 9, 10 and 11 for the respective axes. Three different specimens are selected for vibration at 5° ± 5°F, 125° ± 5°F and 70° ± 10°F, respectively. These temperatures represent the estimated extremes in the areas of the world where the LSFAE weapon is to be used. After each axis of sine vibration test, the weapon is vibrated for 30 minutes of random testing to the level shown in Fig. 12. During the tests, the control accelerometer is

located near the forward lug on the strongback. The weapon is rigidly mounted to the support fixture during the vibration tests at the Naval Weapons Center laboratory, as shown in Figs. 17, 18 and 19.

STATIC LOADS

(U) The static loads acting on the LSFAE weapon dispenser can be divided into the following loading categories:

1. Flight loads
   - Airborne inertial and aerodynamic loads
   - Catapult loads
   - Arrested landing loads
2. Handling loads, including cradling
3. Pressurization as required.

Each category is unique, in that the magnitude of the load involved, and the internal structural load paths required to react the load, are distinctly different. Because of this, each load category will be treated as an entity, and the discussion of each will include the following:

1. Design philosophy
2. Design loads
3. Test philosophy
4. Loads application scheme
5. Applied loads
6. Instrumentation
7. Summary.

FLIGHT LOADS

Design Philosophy

(U) MIL-A-8591C was the specification to which the LSFAE dispenser was designed. A development requirement stated that the strongback and cargo section skin, and their attachments, be structurally compatible with high speed carriage (M = 1.2 at sea level) to permit the basic structure to be used for future high speed flight testing. Because of this, all airborne inertial and aerodynamic design loads were directed solely to high speed carriage, and the low speed loads were discarded as insignificant. The design bomb rack-aircraft configuration was the inboard shoulder station of a TER rack on the outboard wing Pylon of an F4 aircraft. All available data indicated that this combination would provide the most severe structural loading. The lug and swaybrace reactions for the catapult and arrested landing conditions were calculated, but were found to be far less severe than the flight loads. Furthermore, when the longitudinal loads were compared to those of the handling and pressurization conditions (to be discussed later), they were found to be insignificant and were discarded.

The tail fins were designed to be compatible with 450 knot carriage even though the maximum low speed velocity is only 300 knots. This was to allow the weapon to be flown to the target at speeds in excess of the maximum release speed; furthermore, the tail fins as used on the low speed dispenser would be different than those on future high speed applications so the high speed requirement would not apply.

Design Loads

(U) The design loads as described here are the loads that theoretically act at the store C. G. as calculated by MIL-A-8591C. It is these loads that have to be transferred internally to the strongback where they are reacted out by the bomb rack. Fig. 20 describes the symbolism and sign convention. The limit design loads were as follows:

1. P_x – 3396. pounds
2. P_y – 4335. pounds
3. P_z – 337. pounds
4. M_y – 9320. inch-pounds
5. M_z – 47076. inch-pounds.

(U) The tail fins were designed to a limit load of 250 pounds. The load was assumed to act at the 30 percent chord and at the 60 percent span.

Test Philosophy

(U) The intent of the test program was to simulate as nearly as possible the actual loading environment of the design conditions. Because of the design of the BLU-73/B bombs (Fig. 21), all inertia loads of the weapon were introduced into the dispenser by direct bearing of the bomb bulkheads on the inside of the cargo section skin. Furthermore, the critical design condition resulted in the dispenser being critical in ring bending, with the maximum stress occurring at either edge of the strongback. To simulate this condition, it was necessary to load the bombs from the outside of the dispenser, pulling their bulkheads into the skin. At the same time, the axial load had to be simulated; therefore, it was necessary to either pull or push on the end of the dispenser. The actual details of the loading scheme are described in the next section. The applied loads, P_y, P_z, M_y, and M_z were matched by the following iterative procedure:

1. The net loads P_y and P_z were equally distributed between all load points.

2. They were then increased or decreased linearly, in proportion to their location from the weapon C. G. until the sum of the

products of each load and its distance from the C. G. equalled the desired moment;

$$\sum_{1}^{n} P_{yi} \overline{X}_i = M_z \qquad (1)$$

$$\sum_{1}^{n} P_{zi} \overline{X}_i = M_y \qquad (2)$$

3. The process was iterated until both the net load, $\sum_{1}^{n} P_{yi}$ and $\sum_{1}^{n} P_{zi}$, equalled the desired load, P_y or P_z; and the net moments, $\sum_{1}^{n} M_{yi}$ and $\sum_{1}^{n} M_{zi}$ equalled the desired moment, M_y or M_z.

(U) The intent of the fin test was to simulate the aerodynamic fin load both in magnitude and location.

Loads Application Scheme

(U) Fig. 22 describes the flight loading scheme. There were four loading points to simulate P_y, P_z, M_y, and M_z, and one loading point to simulate P_x. Each load represented the resultant of the loads P_{yi} and P_{zi} at that point, and, because of the necessity to match M_y and M_z, each resultant was in a unique direction and had a unique magnitude.

(U) The loads were introduced into the weapon by tension rods which penetrated the skin through small holes, and tied through swivels, to a steel rod that ran the length of the dispenser on the bomb centerline. The holes in the skin were small and were located in areas of relatively low stress. Each tension rod was secured to a hydraulic piston actuator through an electronic load cell. The load cells were calibrated on a Tinius-Olsen testing machine within the load range they were to measure. The end load was in the aft direction and was introduced into the dispenser through the rear bulkhead. It was generated by a hydraulic piston actuator acting through an electronic load cell.

(U) Fig. 23 shows a cross section of the dispenser at one of the bomb bulkheads located under the strongback with no loads acting on the bomb. Fig. 24 shows the same cross section, but with the bombs loaded as they were in the static test. The deflected shape is indicative of the actual deflection.

(U) The fin load was applied by means of a hydraulic piston actuator acting through an electronic load cell. It was introduced into the fin by means of a tension rod and a bearing pad at the location of the theoretical center of pressure. Fig. 25 describes the loading scheme.

Applied Loads

(U) Table 3 shows the magnitude of the applied limit flight loads. It should be re-emphasized that the loads were monitored electrically by the load cells rather than by pressure gages located in the hydraulic lines. Experience has shown that significant (10% to 15%) errors can result from monitoring the pressures. The primary reason is system friction.

(U) Table 4 shows the magnitude of the applied load error when compared to the design limit load.

(U) The applied limit fin load was 250 pounds.

Instrumentation

(U) Fig. 26 shows the location of the strain gages used to verify the internal stresses. Three-axis rosettes were used at each corner of the strongback (the ends of the welds) to determine the principle stresses and their directions.

(U) Instrumentation of the fin consisted of two axial strain gages mounted circumferentially on the dispenser skin adjacent to the forward fin pivot block, and on a circumference passing through the center of the block. Fig. 27 describes the instrumentation.

Summary

(U) The flight load test was conducted to 200% of limit load. No failure resulted at 200% and no permanent set at 115%.

(U) The fin was tested to 200% of limit. No failure resulted at 200% and no permanent set at 115%.

HANDLING AND CRADLING LOADS

Design Philosophy

(U) The design philosophy regarding handling loads was that the dispenser should be able to withstand the design loads as if they were statically applied. The actual loading times are discussed in the next section. Furthermore, because the handling loads, by definition, occur while the weapon is in its shipping container, only axial loads were considered significant. This was due primarily to the diametrical constraints imparted by the container to the dispenser. The

cradling loads were established from MIL-A-8591C. The areas on the dispenser that react the loads were also defined by this specification.

Design Loads

(U) The weapon shipping container (CNU-120/E) design criteria permitted the weapon to experience handling loads up to 35 g's in any direction. Review of the shipping container qualification tests disclosed measured responses of 25 g's and time durations to 0.056 seconds, with peak rise times of 0.021 seconds. Because of the long time durations, the assumption was made that the load was static. This assumption is not as conservative as it might at first seem because of the bomb load path into the dispenser. At the forward end, the load path is direct shear into the dispenser skin through the bulkhead-skin attachment weld. At the aft end, the load is introduced into the rear bulkhead through rubber compression members located approximately 3 inches in from the periphery, and directly over the structural ribs. The load then goes to the bulkhead flange, through the bulkhead mounting bolts in tension, and into the rear ring which is welded to the skin. Fig. 28 shows the rear bulkhead assembly and the load path from the bombs into the dispenser mounting screws.

(U) The cradling limit load, as described by MIL-A-8591C, was 3 g's acting through 6 inches of line contact, distributed over at least two support points.

Test Philosophy

(U) The test philosophy, in the case of the handling loads, was to simulate the design load introduced into the bulkheads by the bombs. The loads were applied on a Tinius-Olsen testing machine at a low rate of application. After reviewing the load paths, it was felt that a handling test on the front bulkhead would be unnecessary since shear was the only significant stress mechanism involved. The test was therefore limited to the rear bulkhead assembly.

(U) The cradling test was designed to satisfy the cradling requirements of MIL-A-8591C.

Loads Application Scheme

(U) Fig. 29 describes the loading scheme for the handling loads test. The load was introduced into the rear bulkhead through the spacer cruciform and a simulated bomb. The rear bulkhead was secured to the aft ring by the proper screws, and the ring was welded to a short section of skin. The loads were reacted out of the skin segment by a cylindrical section secured to the skin with radially oriented screws. The entire test assembly was then loaded on a Tinius-Olsen Testing Machine. The bulkhead deflection was monitored by a dial indicator located between the bulkhead and the machine base.

(U) Fig. 30 describes the cradling loads application scheme. The cradle had four load points for a total of 6 inches of line contact. The loads were introduced into the dispenser by weights that were placed in a saddle located on the top of the weapon. This method satisfied the requirements of MIL-A-8591C.

Applied Loads

(U) The limit applied handling load was 14, 000 pounds. The limit applied cradling load was 1, 500 pounds.

Instrumentation

(U) As mentioned earlier, the bulkhead deflection was measured in the handling test with a dial indicator. No other instrumentation was utilized in either test.

Summary

(U) The handling test was stopped at 140% of limit load, due to the capacity of the testing machine; however, no permanent set was experienced at this load, so it was felt that further testing would be unnecessary. The dispenser was measured after the cradling load test to insure compliance with the design requirements. No permanent set was experienced as a result of the applied loads.

PRESSURIZATION LOADS

Design Philosophy

(U) The LSFAE dispenser was designed to withstand the internal pressure that would result if a bomb ruptured at the maximum safety test temperature of 165°F delineated in WR-50. This requirement was established to preclude any potential safety hazard to personnel handling the weapon.

Design Loads

(U) The design limit pressure was 90 psig.

Test Philosophy

(U) The test setup was designed to satisfy three objectives:

1. Test the dispenser to the defined ultimate load.
2. Provide the capability for introducing large pressure surges.
3. Provide the maximum safety to the test personnel.

Loads Application Scheme

(U) The pressurization medium was nitrogen over water. The dispenser was completely filled with water before nitrogen pressure was applied. The pressure source was a fully pressurized nitrogen tank. The nitrogen was introduced through a pressure regulator and an electronically operated solenoid valve. The static pressure was accomplished first with the ultimate load being achieved in approximately five minutes. The pressure regulator was then fixed at the ultimate pressure, the solenoid valve shut off, and the pressure in the dispenser reduced to 20 psig. The solenoid valve was then opened, and the pressure surged through limit pressure in approximately half a second, and stabilized at the ultimate pressure after about 5 seconds.

Applied Loads

(U) The limit test pressure was 90 psig. Ultimate pressure was 135 psig. The total pressure surge was 115 psi. The pressure surge to limit pressure was 70 psi.

Instrumentation

(U) The only instrumentation was a pressure gage mounted between the solenoid valve and the rear bulkhead of the dispenser.

Summary

(U) The dispenser was visually examined after the pressurization test. No structural damage was observed.

DISCUSSION AND RECOMMENDATIONS

(U) The vibration procedures described in this paper are typical of the steps a given organization should at least follow during the development and qualification of new ordnance or a piece of associated airborne equipment. The test facility (or some cognizant group) should at least see that the specified vibration levels adequately cover the actual environmental spectra. If this is not observed, severe overtesting or undertesting of the item can result. Figs. 9, 10, 11 and 12 graphically illustrate this point.

(U) Careful consideration of seemingly minor details often will determine whether or not a satisfactory test has been performed. Care must be exercised so that the control accelerometer is properly located and mounted, and is not at a node point. Needless to say, adequate laboratory test equipment should be used and calibrated systematically. Good test fixture design is important in order to eliminate harmful fixture resonance.

(U) Environmental vibration response data must be correctly obtained with consideration given to the subsequent types of analyses and format of data presentation. The simple placement of an accelerometer has to be judicially selected (the accelerometer measures the vibration response at that point of location). This may seem to be an extremely elementary statement, but often the actual placement is really determined by a technician applying the transducer. Thus, an accelerometer or cable may be exposed in an area susceptible to boundary layer turbulence. The result will be erroneous measurements due to microphonics. The entire data acquisition system must have an overall frequency response and signal-to-noise ratio commensurate with the requirements of the structural dynamicist. Suitable transducers, signal conditioners and recording instruments must be selected.

(U) The overall aspect of a laboratory vibration test should be continuously reviewed, when formulating a series of laboratory vibration tests into a specification. The purpose of a vibration test specification should be to provide a correct detailed description for performing a series of vibration tests upon the item of concern. This vibration specification can be used during the R and D phase or during procurement of the item for inclusion into a contract. Before a specification writer can begin, he must first decide if the tests will:

1. Simulate the actual environment,
2. Simulate the damaging effect of the environment, or
3. Provide a severe enough overtest using engineering judgment.

(U) The final choice depends upon the intent of the particular vibration specification for the ordnance. Closely associated with this choice is the definition as to what constitutes a failure.

(U) Future efforts should be directed towards more realistically simulating in the laboratory the environment of airborne ordnance by:

1. Determining frequency response functions (or impedance functions)
2. Determining the apparent weight of the item
3. Determining the cumulative fatigue damage of ordnance during their life history from stockpile to target.

(U) The static test procedures described herein are typical of the sequence that should be followed for most items of airborne ordnance. Probably the most significant task in preparing a static test is the definition of the important load paths, and the resultant probable modes of failure during service. An example of the potential problems that could be experienced if load paths were not determined would be premature shear failure due to a nonrepresentative shear distribution, if the item was critical in beam bending; that is, if the bending moment was matched, but the shear was too high because of

the load distribution, a premature failure could occur without ever testing the critical condition. The reverse could also be true; a bending failure could occur before the critical shear condition was reached.

(U) A significant improvement in the design static flight loads could be realized by determining the actual lug and swaybrace loads from instrumented captive flight tests. These measured data could then be used in place of those calculated by the methods of MIL-A-8591, and would be more representative of the actual conditions encountered.

(U) The test procedures related in this paper demonstrate methods of improving the really questionable areas of any qualification structural test program for airborne ordnance. It is felt by the authors that the requirements for structural design and test need to be improved to more closely simulate the use environment of the item being developed.

TABLE 1. LSFAE Vibration Data Acquisition Systems

CARRIER	TRANSDUCERS	SIGNAL CONDITIONERS	MAGNETIC TAPE RECORDER
UH-1E HELICOPTER	ENDEVCO MODEL 2221 AND CEC MODEL 4-202	ENDEVCO MODEL 4606 AND GULTON MODEL FT-3612	AMPEX MODEL CP-100 60 IPS, 108 KH_Z CENTER FREQUENCY, ± 40% DEVIATION.
OV-10A AIRCRAFT	ENDEVCO MODEL 2213C	UPHOLTZ-DICKIE MODEL 8PMCV	SANGAMO MODEL 3500 15 IPS, KH_Z CENTER FREQUENCY, ± 40% DEVIATION, ± 5 KH_Z RESPONSE.

TABLE 2. LSFAE Laboratory Transportation Vibration Tests

DIRECTION OF VIBRATION	TIME OF CYCLING	RESONANCES	DWELL TIME
VERTICAL	THREE 15-MIN.	12 AND 18Hz	30 MIN. EACH
TRANSVERSE	THREE 15-MIN.	16 AND 29Hz	30 MIN. EACH
LONGITUDINAL	THREE 15-MIN.	14 AND 16Hz	30 MIN. EACH

NOTE: THE INPUT EXCITATION IS SHOWN IN FIGURE (13). THE LSFAE WEAPON IS CLAMPED WITHIN THE SHIPPING CONTAINER.

TABLE 3. Applied Limit Flight Loads

LOAD	FORCE (LBS.)	θ IN
P_{i1}	1432	90°
P_{i2}	1403	86°
P_{i3}	913	78°
P_{i4}	452	55°
P_X	3396	-

TABLE 4. Applied Load Errors

	% ERROR
P_X	0.4
P_R*	1.2
M_R*	4.7

$$*P_R = \sqrt{P_Y^2 + P_Z^2}$$

$$M_R = \sqrt{M_Y^2 + M_Z^2}$$

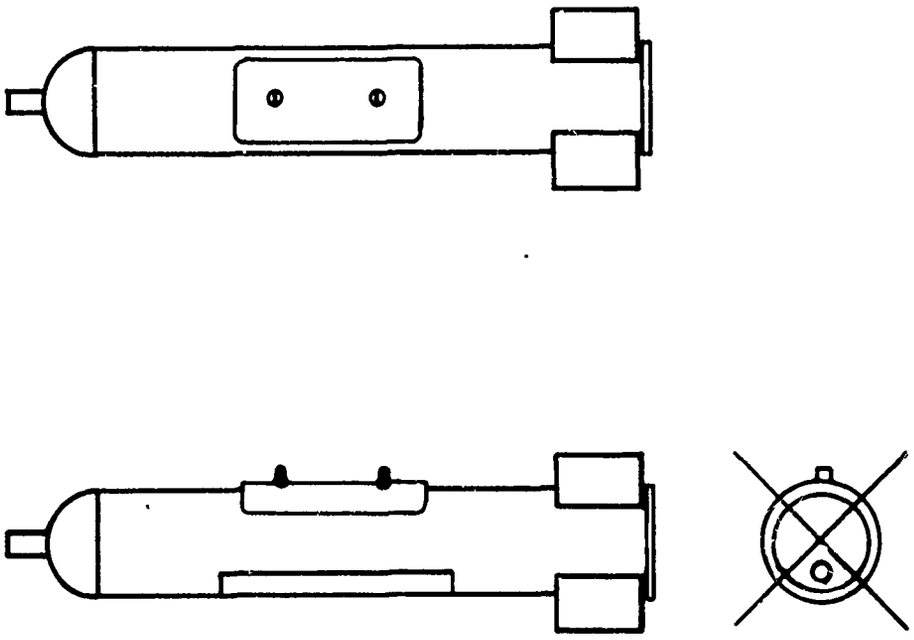

WEIGHT 510 POUNDS
LENGTH 89 INCHES
DIAMETER 14 INCHES
DESCRIPTION:
FREE FALL CLUSTER WEAPON WITH FOLDING FINS WHICH ARE LOCKED OPEN PRIOR TO FLIGHT"

FIG. 1. Low Speed Fuel-Air Explosive Weapon (CBU-55/B)

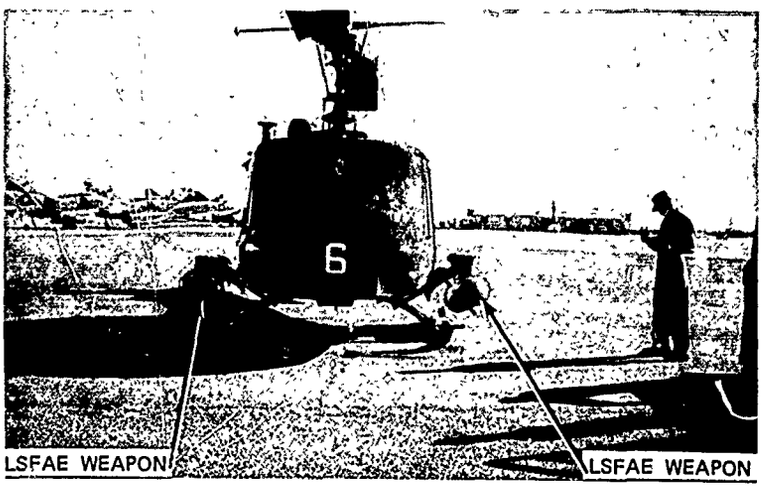

FIG. 2. LSFAE Weapons Mounted on the UH-1E Helicopter.

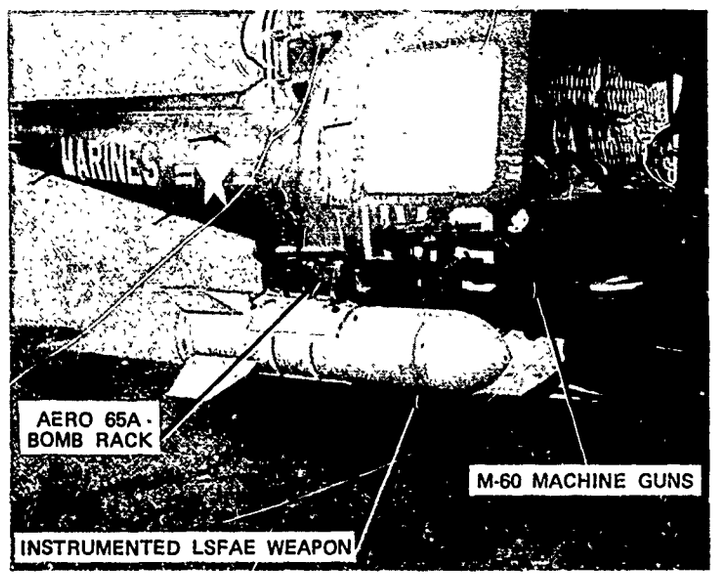

FIG. 3. Instrumented LSFAE Weapon Mounted on the Starboard Side of the UH-1E Helicopter.

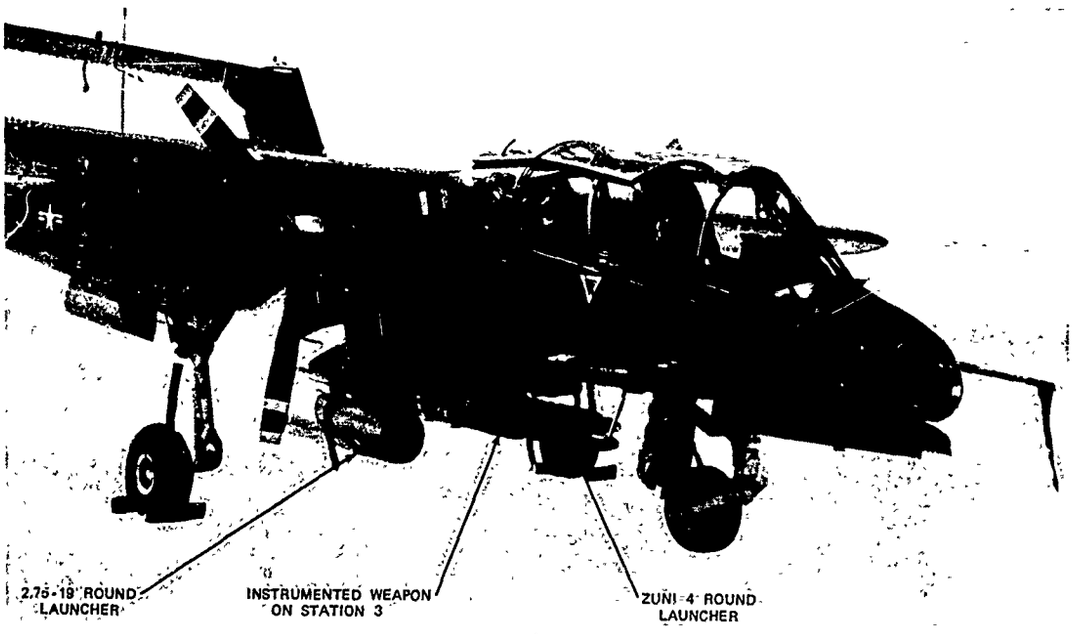

FIG. 4. General View of the Instrumented LSFAE Weapon Mounted at the Centerline Position (Station 3) of the OV-10A Aircraft.

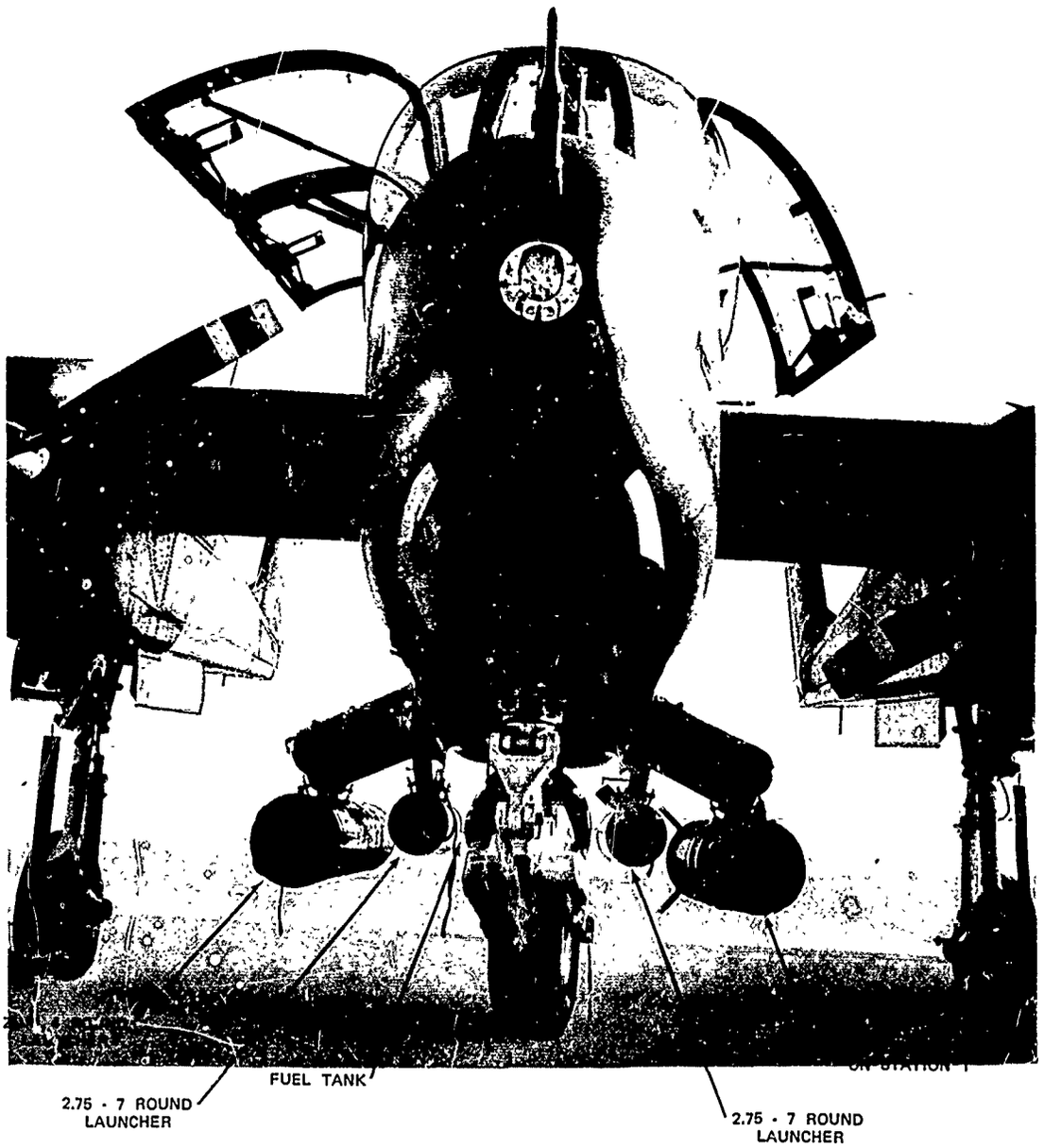

FIG. 5. Close-Up View of the OV-10 Setup. The Instrumented LSFAE Weapon is Mounted at Station 1.

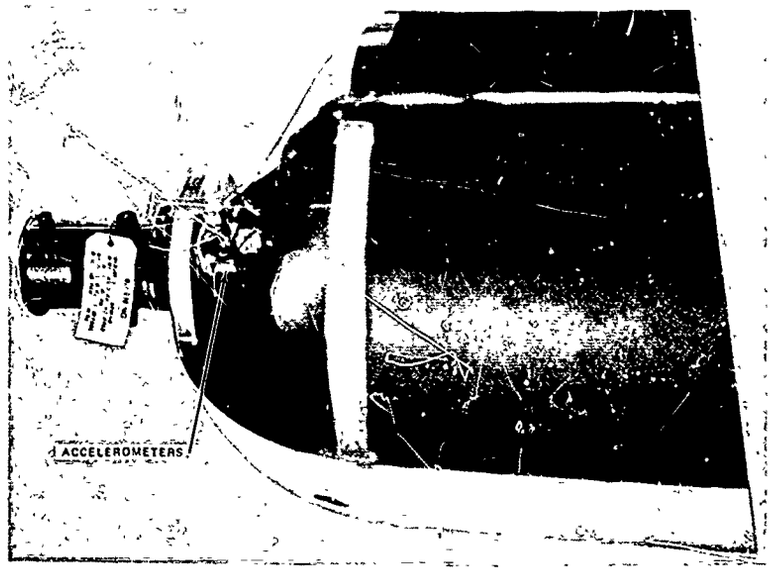

FIG. 6. Detailed View of the Accelerometer Installation at the Base of the Dispenser Fuse.

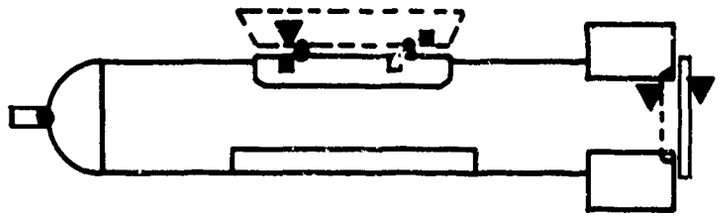

▼ UH-1E TESTS ONLY

■ OV-10A TESTS ONLY

● COMMON TO BOTH TESTS

FIG. 7. General View of the LSFAE Weapon Depicting the Accelerometer Locations.

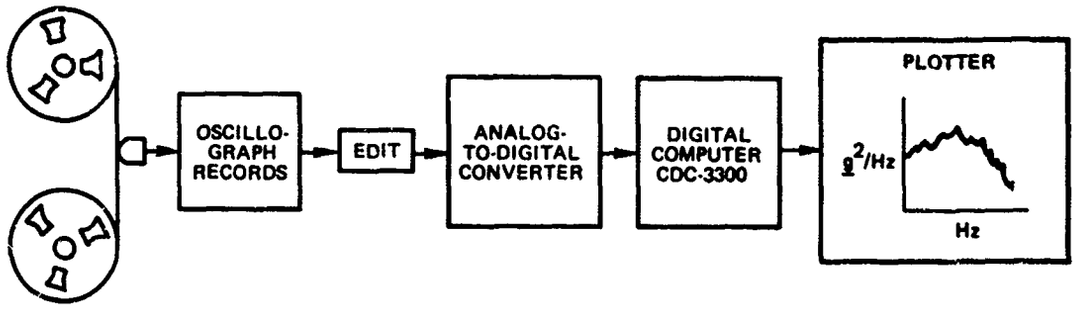

A. PROCEDURE FOR THE OV-10A VIBRATION DATA

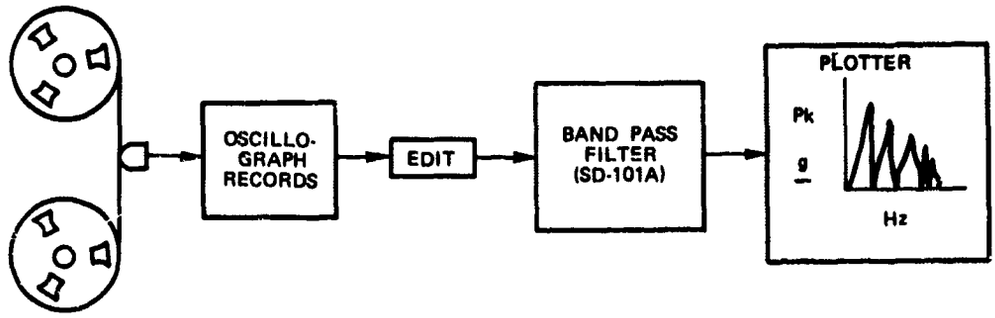

B. PROCEDURE FOR THE UHI-E VIBRATION DATA

FIG. 8. Analysis Procedures for the Environmental Vibration Data

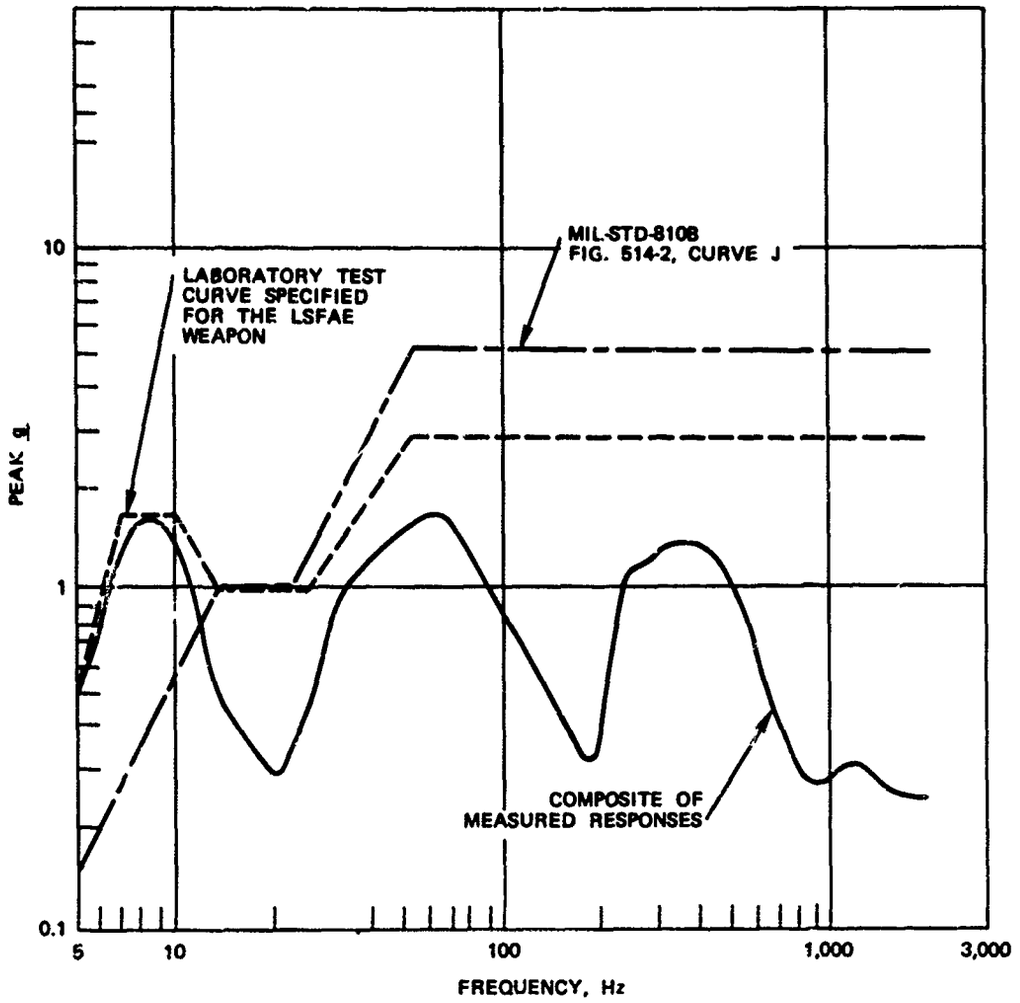

FIG. 9. Comparison of the Maximum Vertical Measured Responses on the UH-1E Helicopter with the Specified and MIL-STD-810B Curves

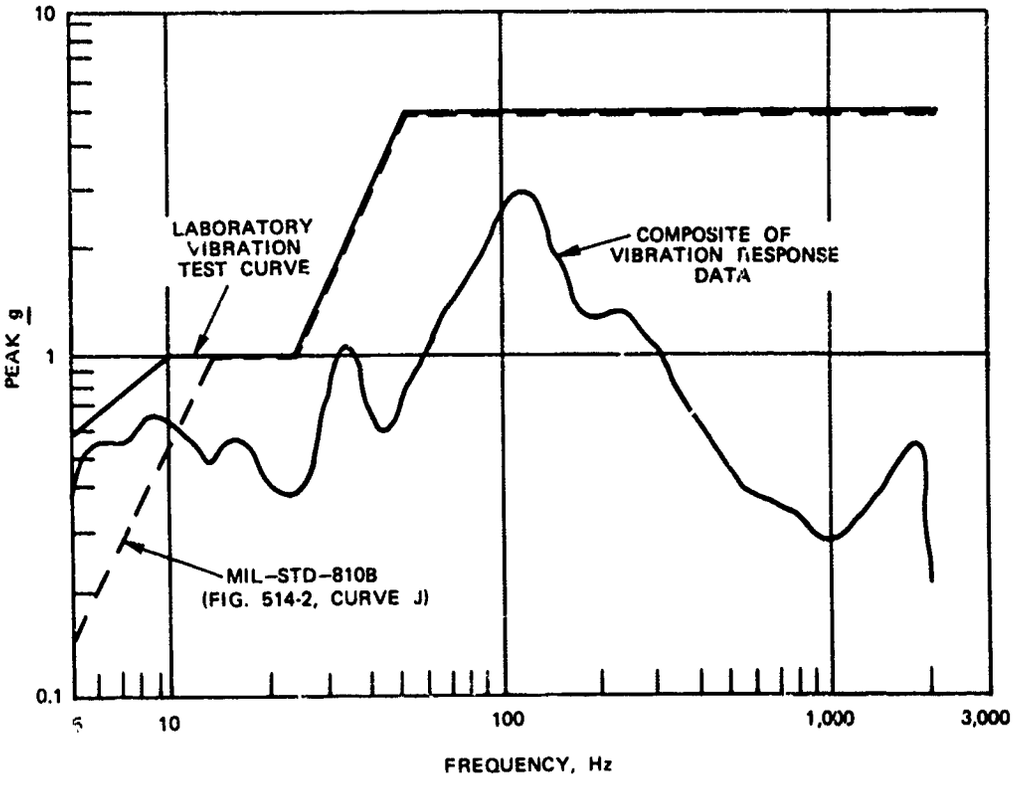

FIG. 10. Comparison of the Maximum Transverse Measured Responses on the UH-1E Helicopter with the Specified and MIL-STD-810B Curves

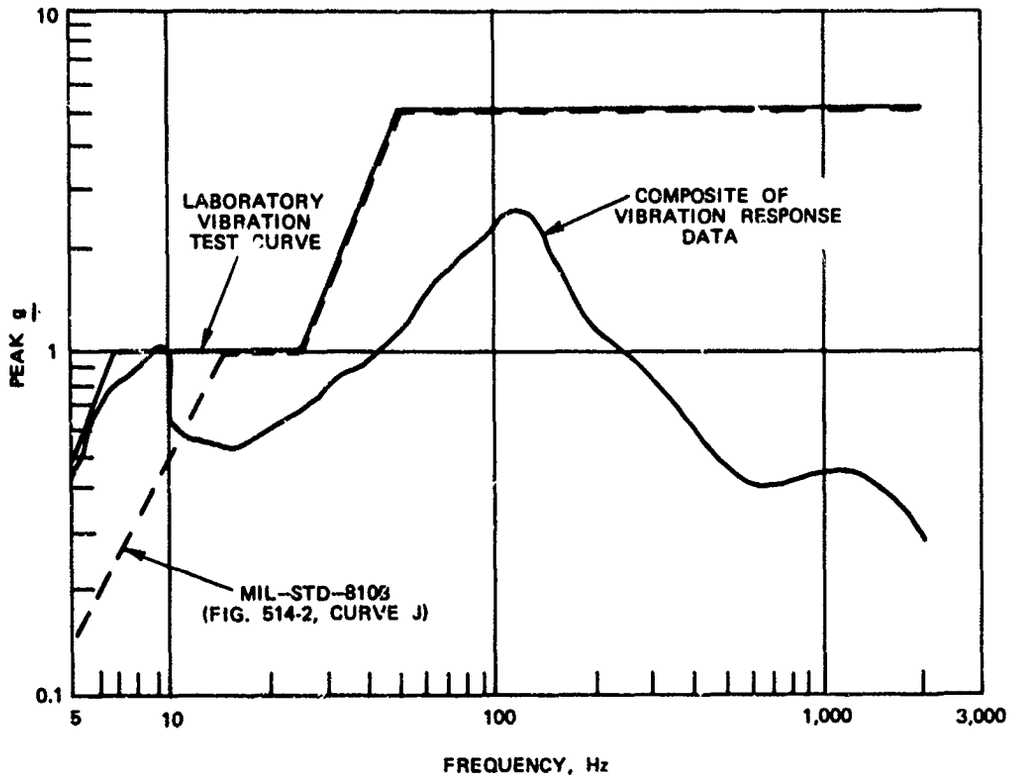

FIG. 11. Comparison of the Maximum Longitudinal Measured Responses on the UH-1E Helicopter with the Specified and MIL-STD-810B Curves

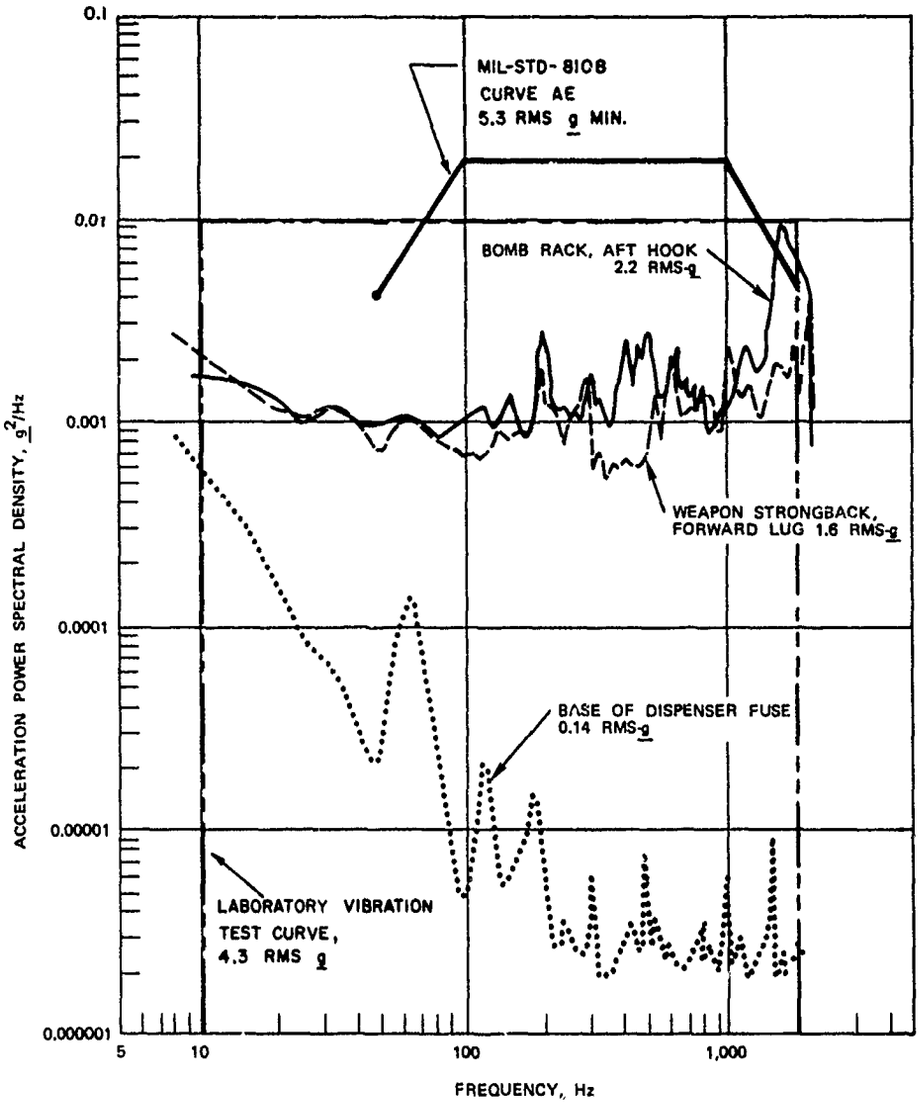

FIG. 12. Maximum Vertical Responses Measured on the OV-10A Aircraft During Maximum Aircraft Power and Dynamic Pressure

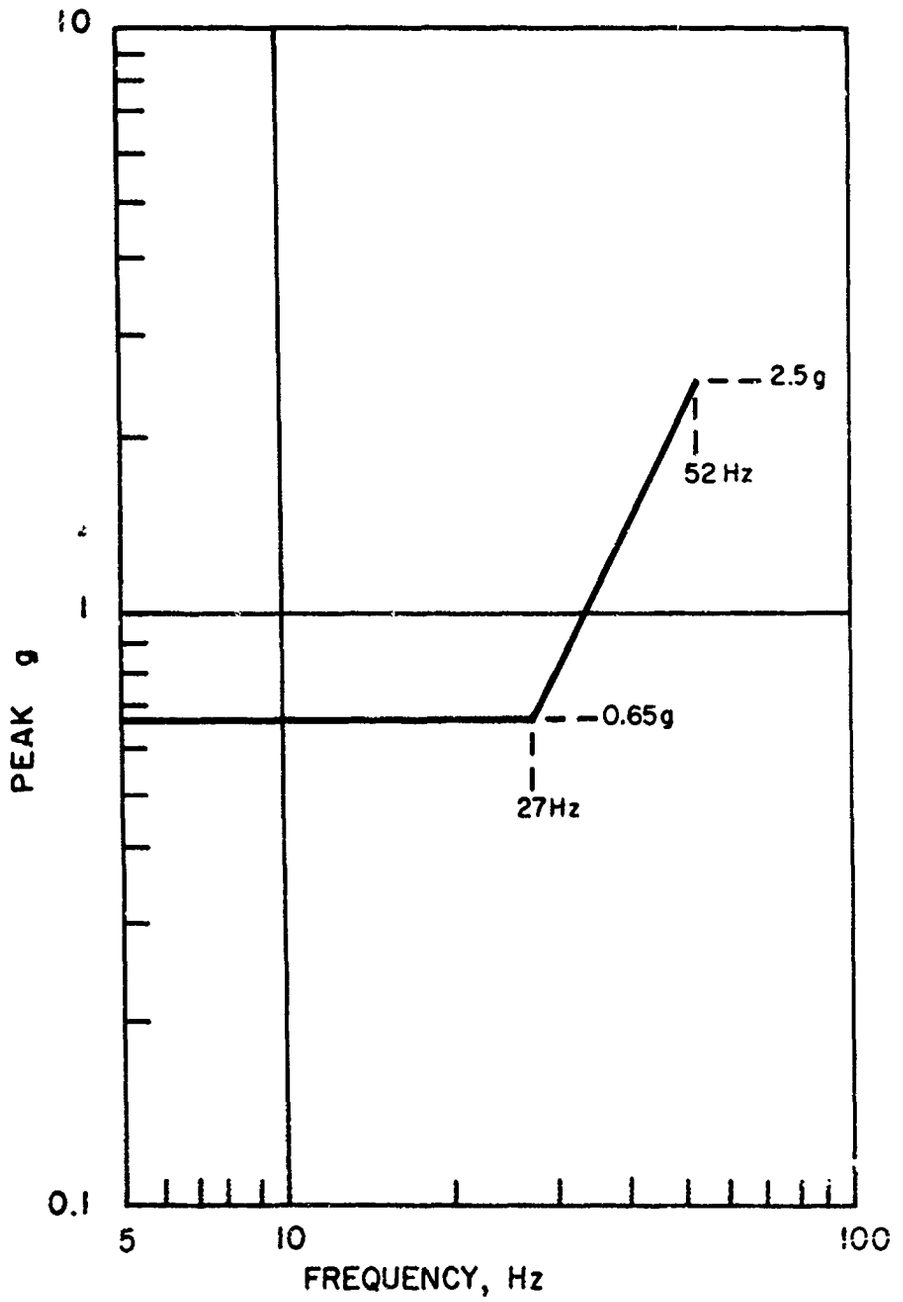

FIG. 13. Laboratory Vibration Test Specification for Transportation Environment (Ref. Mil-Std-810B).

FIG. 14. Laboratory Test Setup for Vertical Excitation of the Assembled LSFAE Weapon Within the Shipping Container.

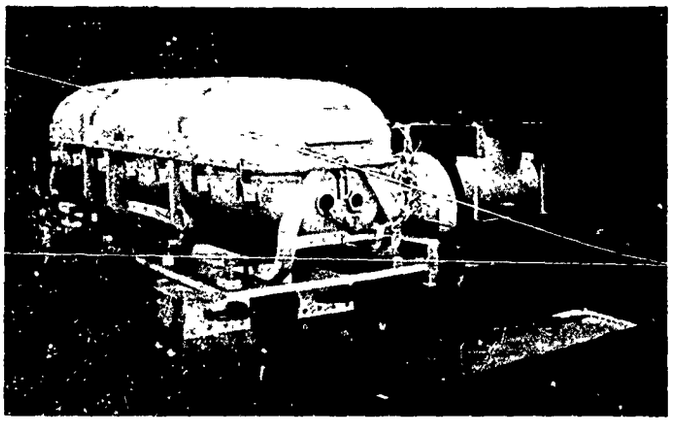

FIG. 15. Laboratory Test Setup for Transverse Excitation of the Assembled LSFAE Weapon Within the Shipping Container.

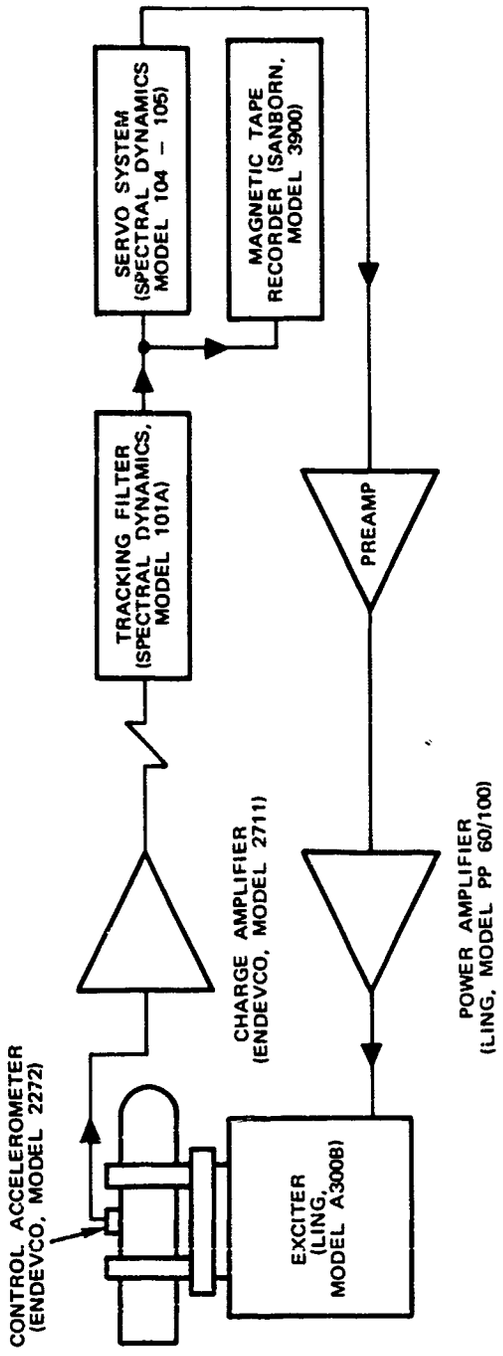

FIG. 16. Schematic Diagram for the Laboratory Vibration Tests

FIG. 17. Laboratory Test Setup for Vertical Excitation of the Assembled LSFAE Weapon

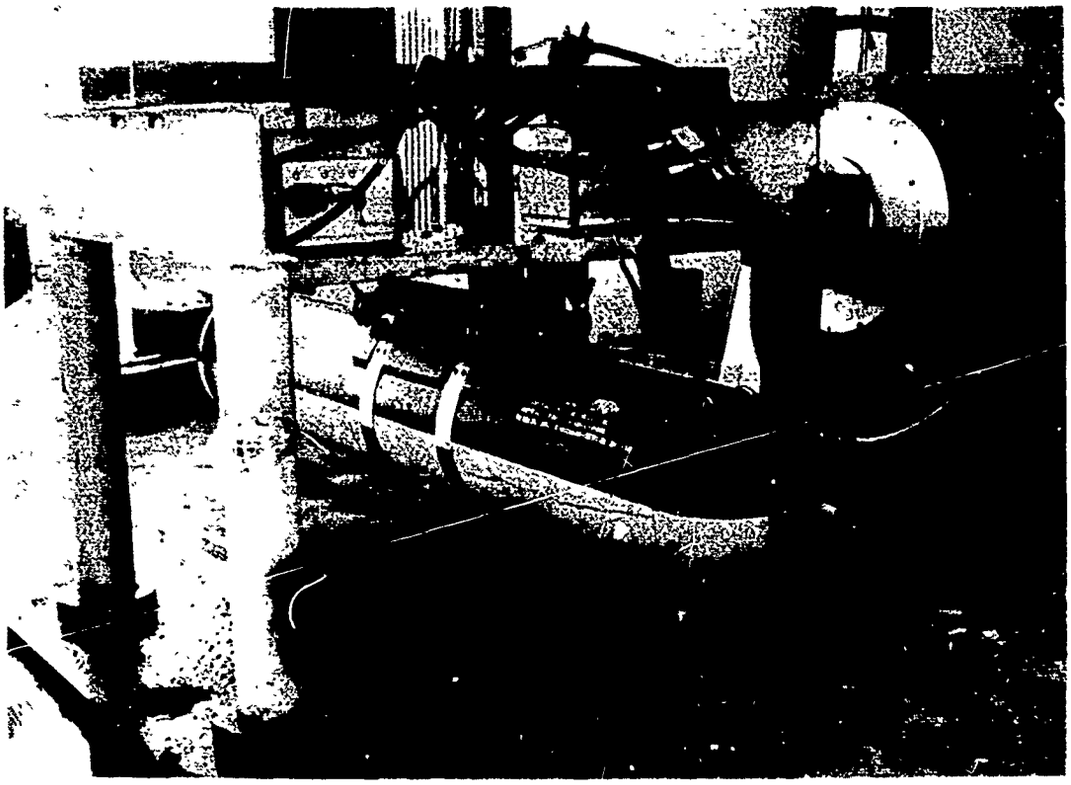

FIG. 18. Laboratory Test Setup for Transverse Excitation of the Assembled LSFAE Weapon.

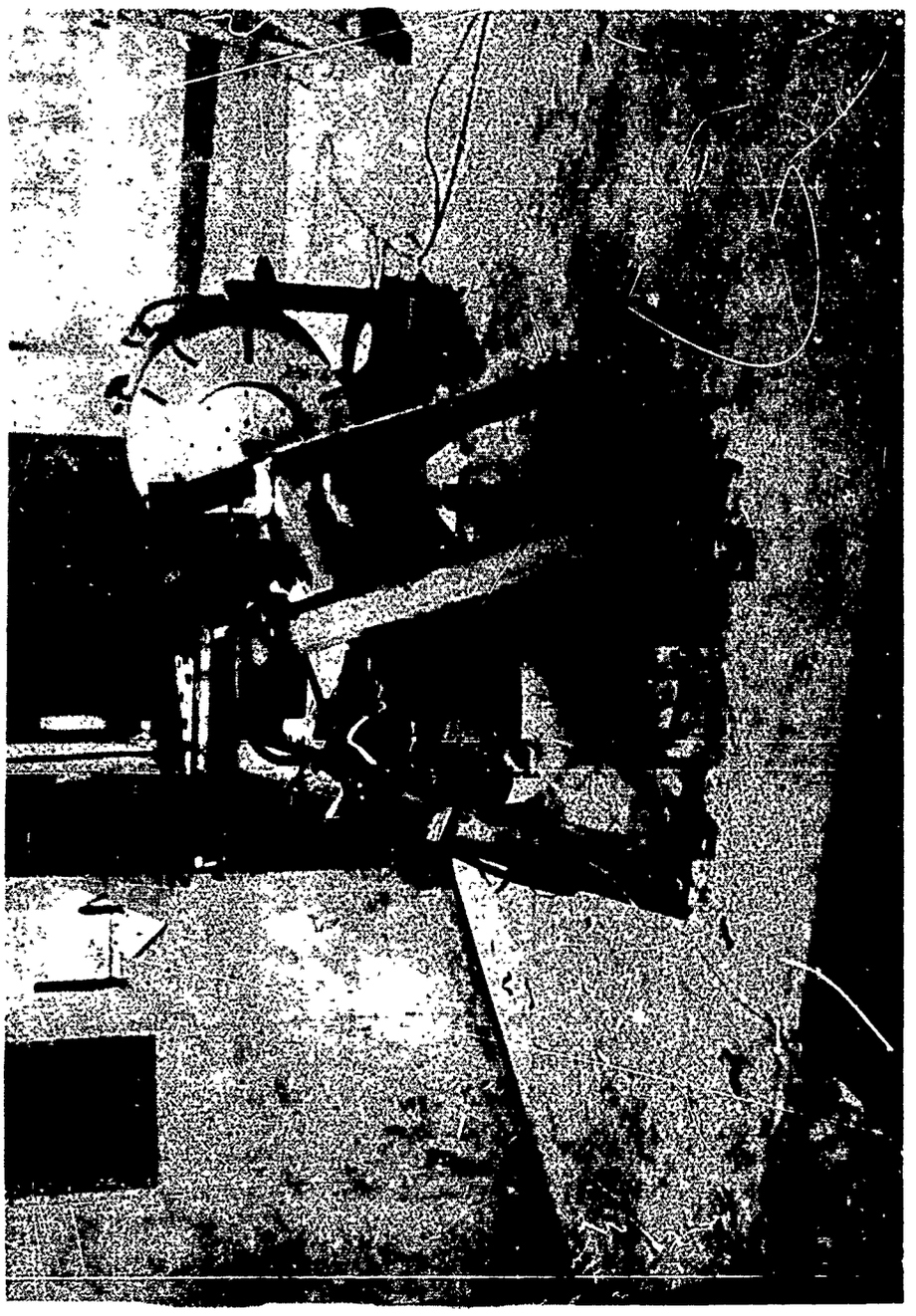

FIG. 19. Laboratory Test Setup for Longitudinal Excitation of the Assembled LSFAE Weapon

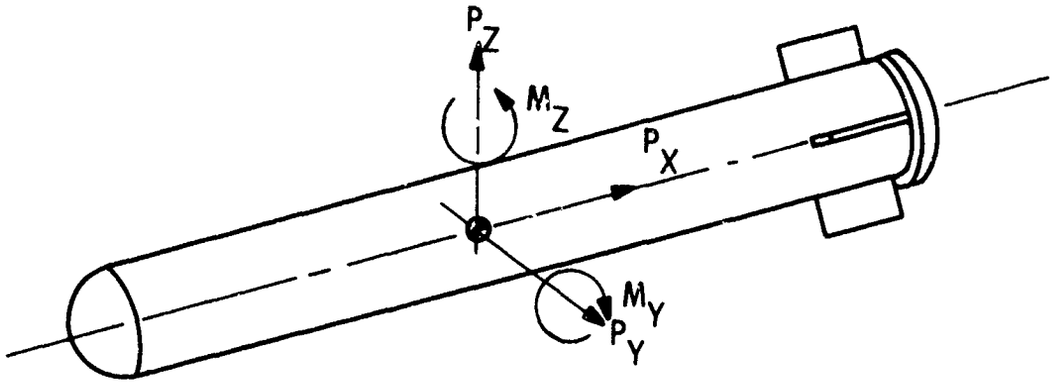

FIG. 20. Static Loads Sign Convention

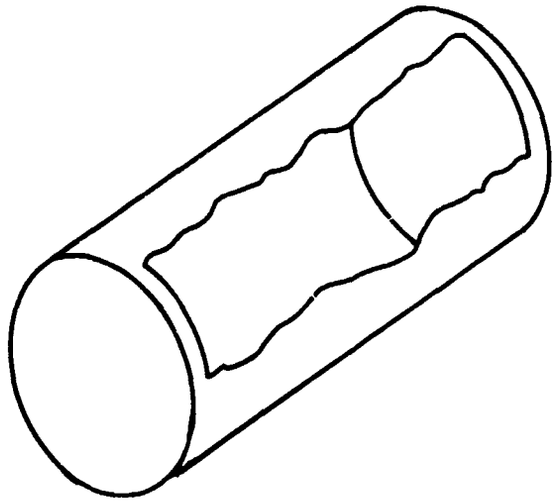

DIAMETER	13.5 INCHES
LENGTH	22.0 INCHES
BULKHEADS	STEEL 0.375 INCHES THICK

FIG. 21. BLU-73/B Bomb Schematic

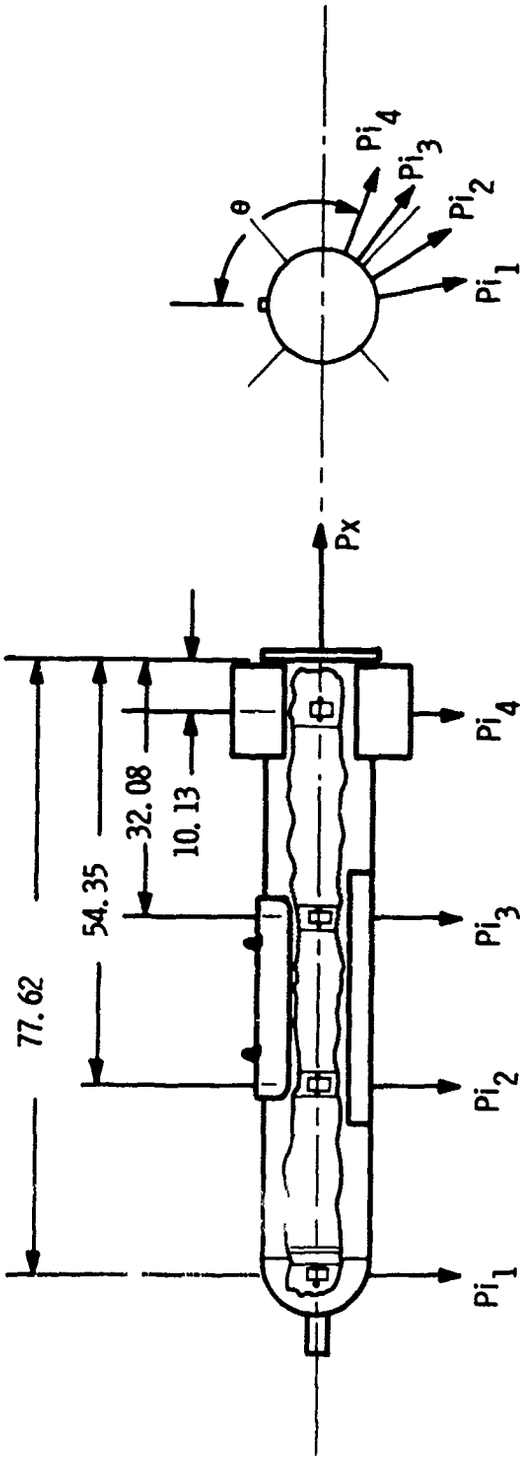

FIG. 22. Flight Loading Schematic

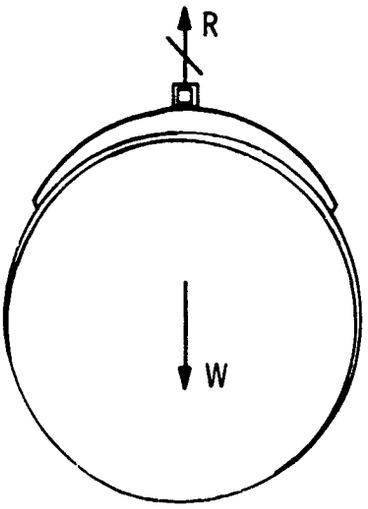

FIG. 23. Cross Section of Weapon Unloaded

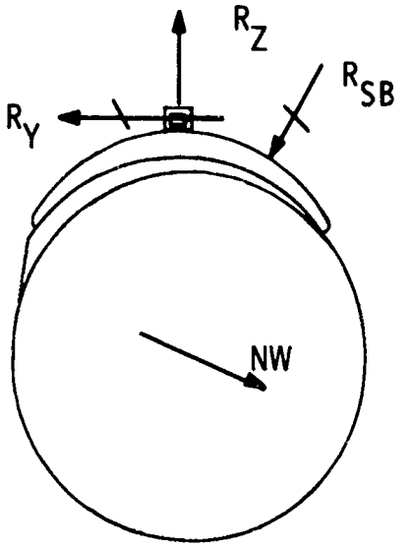

FIG. 24. Cross Section of Weapon Loaded

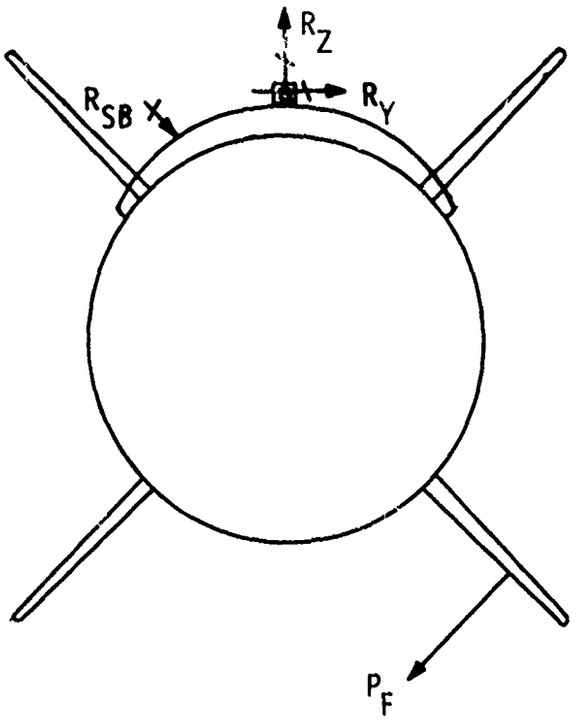

FIG. 25. Fin Loading Schematic

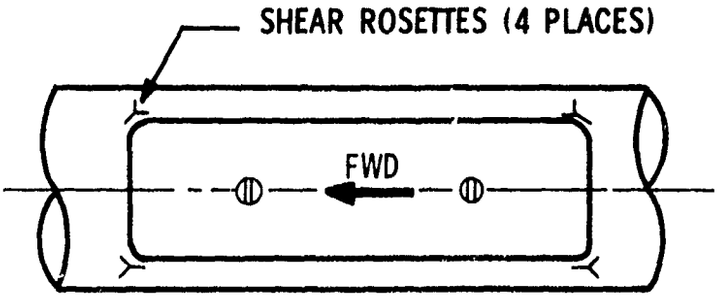

FIG. 26. Strain Gage Locations - Flight Loads

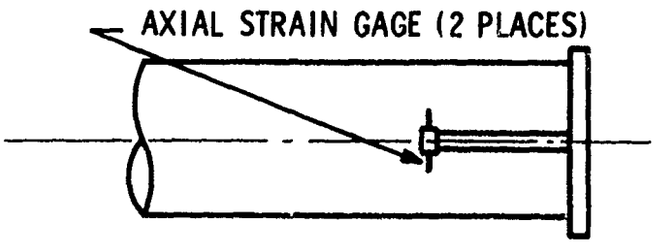

FIG. 27. Strain Gage Locations - Fin Loads

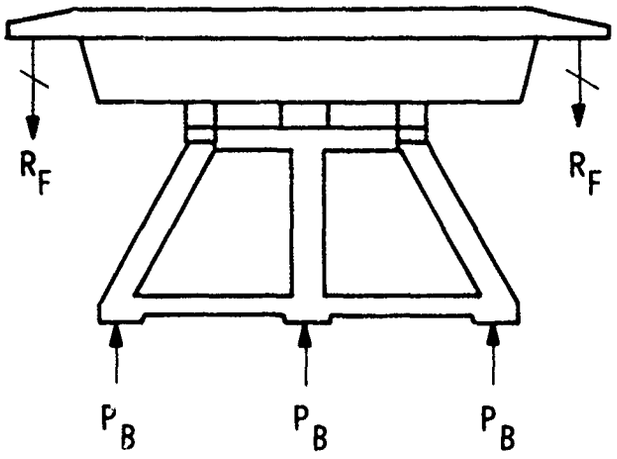

FIG. 28. Rear Bulkhead Assembly

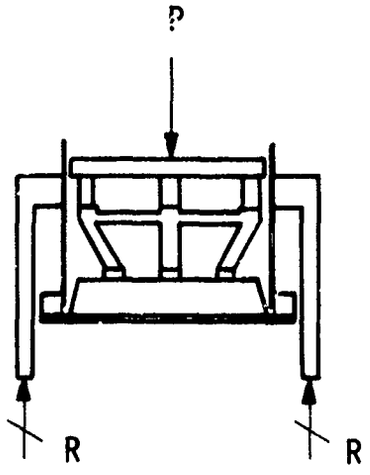

FIG. 29. Rear Bulkhead Loading Schematic

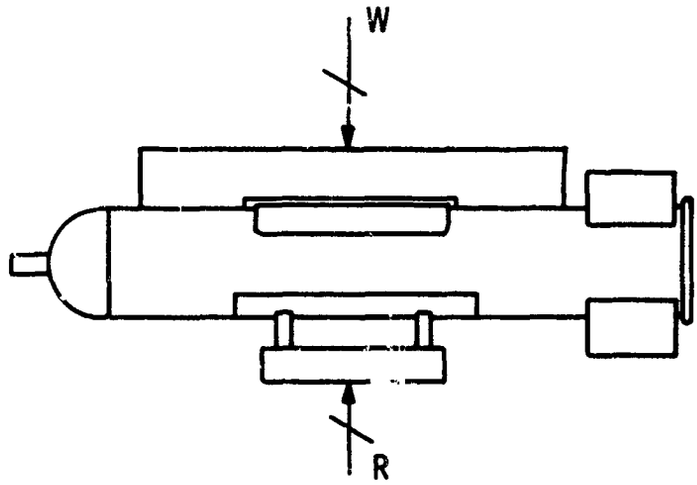

FIG. 30. Cradling Load Schematic

BLANK PAGE

Paper No. 40

STIFFNESS MATRIX FOR MISSILE STRUCTURES USING THIN SHELL THEORY (U)

(Paper UNCLASSIFIED)

by

Pao C. Huang
U.S. Naval Ordnance Laboratory
White Oak, Silver Spring, Md. 20910

ABSTRACT. For the static and dynamic analysis of a missile structure, a stiffness matrix will be employed in the solution. The accuracy of the solution will in general depend upon the quality of the stiffness matrix.

At present an idealized model is commonly used in the analysis which consists of small flat-plate elements that are connected at finite joints and approximately follow the contour of the structure.

The principal disadvantage of the system, aside from the approximation of a curved element by a flat plate, lies in the incompatibility of the adjacent elements between any two finite joints.

This paper will present a precise method for the development of a stiffness matrix using thin shell theory. The analytical approach will be outlined for a general arbitrary shell configuration in terms of Gaussian coordinates. The structure will be treated as a continuum rather than a discrete model.

INTRODUCTION

This paper describes a method for obtaining the stiffness equations for a thin shell analysis. In this procedure the principle of potential energy is employed, wherein the shell structure is treated as a continuous medium. The development retains the usual thin shell assumptions such as the Kirchhoff hypothesis and other simplifications which have been successfully employed by other investigators. The general equations for the stiffness matrix presented in Eqs. (44), (45) and (46) can be applied to most isotropic thin shell problems which need not be defined in an orthogonal curvilinear coordinate system.

The principle of potential energy can be expressed as

$$\delta \Pi = \delta U - \delta W \tag{1}$$

where

Π = Total potential energy of the system
U = Total strain energy of the system
W = Total work done to the system

Let q_i be the generalized coordinates, then the strain energy formulation is quadratic in q_i

$$U = \frac{1}{2} \sum_{i=1}^{n} \sum_{j=1}^{n} K_{ij} q_i q_j \tag{2}$$

and its variation is

$$\delta U = \sum_{i=1}^{n} \frac{\partial U}{\partial q_i} \delta q_i \tag{3}$$

Since K_{ij} is symmetric in i and j, the variational energy calculated from Eq. (2) is

$$\delta U = \sum_{i=1}^{n} \sum_{j=1}^{n} K_{ij} q_j \delta q_i \tag{4}$$

comparing Eqs. (3) and (4) we have

$$\frac{\partial U}{\partial q_i} = \sum_{j=1}^{n} K_{ij} q_j \tag{5}$$

Eq. (5) can be used in the development of the stiffness matrix, K_{ij}, simply by differentiating q_j

$$K_{ij} = \frac{\partial^2 U}{\partial q_i \partial q_j} \tag{6}$$

The expression for work done can be written as

$$\left.\begin{aligned} W &= \sum_{i=1}^{n} C_i q_i \\ \text{Hence} \qquad \delta W &= \sum_{i=1}^{n} C_i \delta q_i \end{aligned}\right\} \tag{7}$$

For the case when the actual displacement components are treated as generalized coordinates, q_i, then the C_i become the concentrated loads acting at discrete points on the shell surface.

Applying the principle of potential energy a set of simultaneous stiffness equations can be obtained of the form,

$$\sum_{j=1}^{n} K_{ij}\, q_j = C_i \tag{8}$$

In matrix notation Eq. (8) can be written as

$$[K]\{q\} = \{C\} \tag{9}$$

where K is the stiffness matrix, which is symmetric.

Once the K-matrix is developed, Eq. (9) can be used for the solution of q_i and eventually the structural response of the shell can be investigated. For dynamic analyses, the Lagrange equations which also utilize the K-matrix may be employed.

GEOMETRY; STRAIN-DISPLACEMENT RELATIONS

Referring to Fig. 1, let the Gaussian surface coordinates u^1 and u^2 be imprinted on the middle surface (ms) of a shell imbedded in a three-dimensional X^i space.

At any material point P, a right-hand triad is used in the development which consists of $\vec{e}_3$ normal to the middle surface and base vectors $\vec{a}_\alpha$ tangent to the coordinate curves. A repeated Greek index denotes summation from 1 to 2, and a repeated Latin index from 1 to 3.

A material point $\underline{P}$ in the interior of the shell is located by the vector $\vec{\underline{r}}$; consequently

$$\vec{\underline{r}} = \vec{r} + \eta\, \vec{e}_3 \tag{10}$$

The base vectors $\vec{g}_\alpha$ parallel to u^α are obtained by differentiating $\vec{r}$ with respect to u^α, thus

$$\vec{g}_\alpha = \vec{r}_{,\alpha} = (\delta^\beta_\alpha - \eta b^\beta_\alpha)\,\vec{a}_\beta \tag{11}$$

where δ^β_α is the Kronecker delta and $b_{\alpha\beta}$ is the second fundamental magnitude for the middle surface.

At the middle surface where $\eta = 0$ and $\underline{\vec{r}} = \vec{r}$ we have

$$\vec{g}_\alpha = \vec{a}_\alpha$$

and

$$\vec{g}_3 = \vec{r}_{,3} = \vec{e}_3$$

The metric tensor $g_{\alpha\beta}$ can now be obtained by the following equation.

$$g_{\alpha\beta} = \vec{g}_\alpha \cdot \vec{g}_\beta = a_{\alpha\beta} - 2\eta b_{\alpha\beta} + \eta^2 b_{\alpha\lambda} b^\lambda_\beta \tag{12}$$

where $a_{\alpha\beta}$ is the metric tensor at the middle surface.

When $\underline{P}$ displaces to $\underline{P}'$, as indicated by the displacement vector $\underline{\vec{V}}$, a new triad is formed by the three vectors $\vec{e}_3'$ and $\vec{g}_\alpha'$. At this stage, the Kirchhoff hypothesis of $\vec{e}_3'$ being normal to the deformed surface, and the normal displacement component w, being uniform through the thickness along a normal to the middle surface, is effected. Accordingly, one has

$$\underline{\vec{V}} = \vec{V} + (\vec{e}_3' - \vec{e}_3)\eta \cong \vec{V} + \eta\vec{\Theta} \tag{13}$$

and

$$\left.\begin{aligned} \underline{\vec{V}} &= \underline{V}_\alpha \vec{a}^\alpha + \underline{w}\, \vec{e}_3 \\ \vec{V} &= V_\alpha \vec{a}^\alpha + w \vec{e}_3 \\ \vec{\theta} &= \theta_\alpha \vec{a}^\alpha \end{aligned}\right\} \tag{14}$$

From Eqs. (13) and (14) one obtains

$$\left.\begin{aligned} \underline{V}_\alpha &= V_\alpha + \eta \theta_\alpha \\ \underline{w} &= w \end{aligned}\right\} \tag{15}$$

The unit normal vector $\vec{e}_3'$ to the deformed middle surface is derived in the following manner.

Since

$$\vec{r}' = \vec{r} + \vec{V} \tag{16}$$

$$\vec{a}_\alpha' = \vec{a}_\alpha + \vec{V}_{,\alpha} \tag{17}$$

The scalar product of $\vec{a}_\alpha'$ and $\vec{a}_\beta'$ yields

$$a'_{\alpha\beta} = a_{\alpha\beta} + 2\gamma_{\alpha\beta} \tag{18}$$

where the strain tensor $\gamma_{\alpha\beta}$ is, after dropping the nonlinear terms,

$$2\gamma_{\alpha\beta} \doteq V_{\alpha|\beta} + V_{\beta|\alpha} - 2b_{\alpha\beta} w \tag{19}$$

The symbol $V_{\alpha|\beta}$ denotes the covariant derivative of V_α with respect to u^β.

Using the following relations for the permutation tensor $\epsilon_{\alpha\beta}$

$$\epsilon_{\alpha\beta}\,\epsilon^{\alpha\beta} = 2 \;; \qquad \epsilon_{\alpha\beta}\,\epsilon^{\lambda\beta} = \delta^{\lambda}_{\alpha}$$

$$\epsilon'_{\alpha\beta} \cong \epsilon_{\alpha\beta}$$

and

$$\epsilon'_{\alpha\beta}\ \vec{e}'_3 = \vec{a}'_\alpha \times \vec{a}'_\beta \tag{20}$$

the linearized expression for $\vec{e}'_3$ is found to be

$$\vec{e}'_3 \cong (1 + V^\alpha|_\alpha - b^\alpha_\alpha w)\,\vec{e}_3 - (w_{,\alpha} + b_{\alpha\beta} V^\beta)\,\vec{a}^\alpha \tag{21}$$

Substituting Eq. (21) into Eq. (13), the rotation vector θ_α may be found as

$$\theta_\alpha = -(w_{,\alpha} + b_{\alpha\beta} V^\beta) \tag{22}$$

The covariant derivatives of V_α and θ_α may be expressed as,

$$V_\alpha|_\beta = V_{\alpha,\beta} - \Gamma^\lambda_{\alpha\beta} V_\lambda \tag{23}$$

$$\theta_\alpha|_\beta = -(w_{,\alpha}|_\beta + b_{\alpha\lambda}|_\beta V^\lambda + b_{\alpha\lambda} V^\lambda|_\beta) \tag{24}$$

where

$$b_{\alpha\lambda}|_\beta = b_{\alpha\lambda,\beta} - \Gamma^\mu_{\alpha\beta} b_{\mu\lambda} - \Gamma^\mu_{\lambda\beta} b_{\alpha\mu} \tag{25}$$

and the Christoffel symbol $\Gamma^{\lambda}_{\alpha\beta}$ is

$$\Gamma^{\lambda}_{\alpha\beta} = \frac{1}{2} a^{\lambda\mu}\left(a_{\mu\beta,\alpha} + a_{\alpha\mu,\beta} - a_{\alpha\beta,\mu}\right) \tag{26}$$

STRAIN ENERGY FOR THIN SHELLS

For an isotropic thin shell analysis, the following simplifications are made:

$$g_{\alpha\beta} \cong a_{\alpha\beta} \tag{27}$$

$$\gamma_{\alpha\beta} \cong \gamma_{\alpha\beta} + \frac{\eta}{2}\left(\Theta_{\alpha|\beta} + \Theta_{\beta|\alpha}\right) \tag{28}$$

$$\underline{T}^{\alpha\beta} = \underline{C}^{\alpha\beta\lambda\rho}\,\underline{\gamma}_{\lambda\rho} \cong C^{\alpha\beta\lambda\rho}\,\underline{\gamma}_{\lambda\rho} \tag{29}$$

where $\gamma_{\alpha\beta}$, $\Theta_{\alpha|\beta}$ have been defined in Eqs. (19) and (24). Eqs. (29) are the constitutive equations where $T^{\alpha\beta}$ is the stress tensor. The Hookean constants for isotropic materials are expressed as

$$C^{\alpha\beta\lambda\rho} = \frac{E}{1-\nu^2}\left[(1-\nu)\,a^{\alpha\lambda}a^{\beta\rho} + \nu a^{\alpha\beta}a^{\lambda\rho}\right] = \frac{E}{1-\nu^2}\,E^{\alpha\beta\lambda\rho} \tag{30}$$

It should be noted that the constitutive equations are written for general curvilinear coordinates which are not necessarily orthogonal. The modulus of elasticity E and Poisson's ratio ν are two constants employed for isotropic but nonhomogeneous materials. The strain energy can now be expressed as,

$$U = \iiint U_o \sqrt{a}\, d\eta\, du^1 du^2 \tag{31}$$

where

$$a = \det (a_{\alpha\beta})$$

U_o is the strain energy density which can be expressed in terms of displacement components as follows

$$\begin{aligned} U_o &= \frac{1}{2} \underline{T}^{\alpha\beta} \underline{\gamma}_{\alpha\beta} = \frac{1}{2} C^{\alpha\beta\lambda\rho} \underline{\gamma}_{\lambda\rho} \underline{\gamma}_{\alpha\beta} \\ &= \frac{1}{8} C^{\alpha\beta\lambda\rho} \left[V_{\lambda|\rho} + V_{\rho|\lambda} - 2 b_{\lambda\rho} w + \eta (\Theta_{\lambda|\rho} + \Theta_{\rho|\lambda}) \right] \\ &\quad \times \left[V_{\alpha|\beta} + V_{\beta|\alpha} - 2 b_{\alpha\beta} w + \eta (\Theta_{\alpha|\beta} + \Theta_{\beta|\alpha}) \right] \end{aligned} \tag{32}$$

Integrating Eq. (31) and defining,

$$\left.\begin{aligned} D &= \int_{-\frac{t}{2}}^{\frac{t}{2}} \frac{E}{1-\nu^2}\, d\eta = \frac{E t}{1-\nu^2} \\ K &= \int_{-\frac{t}{2}}^{\frac{t}{2}} \frac{E \eta^2}{1-\nu^2}\, d\eta = \frac{E t^3}{12(1-\nu^2)} \end{aligned}\right\} \tag{33}$$

one has

$$U = \frac{1}{8}\left[\iint D E^{\alpha\beta\lambda\rho}(V_{\lambda|\rho} + V_{\rho|\lambda} - 2b_{\lambda\rho}w)(V_{\alpha|\beta} + V_{\beta|\alpha} - 2b_{\alpha\beta}w)\sqrt{a}\, du^1 du^2 + \iint K E^{\alpha\beta\lambda\rho}(\Theta_{\lambda|\rho} + \Theta_{\rho|\lambda})(\Theta_{\alpha|\beta} + \Theta_{\beta|\alpha})\sqrt{a}\, du^1 du^2\right] \tag{34}$$

The first integral on the right-hand side is the membrane energy of the shell while the second integral is the bending energy.

At this stage, the stiffness matrix can be readily obtained by integration once the admissible displacement functions for a thin shell structure are assumed. However, for optimum use of high-speed digital computers, a solution by numerical integration may prove to be the most flexible and convenient procedure.

Referring to Fig. 2, let us replace the continuous curvilinear coordinates with a discrete system which has gridpoints uniformly spaced in Δu_1, and Δu_2 on the u^1 = constant and u^2 = constant coordinate lines. It should be noted that along any u^α line the length of a shell element between any two neighboring gridpoints may not be a constant under this system.

At gridpoint (0,0), a covariant derivative can be written in a finite difference form as follows,

$$V_{1|1} = \frac{1}{2\Delta_1}\left[(V_1)_{(\Delta_1,0)} - (V_1)_{(-\Delta_1,0)}\right] - \Gamma_{11}^1 (V_1)_{(0,0)} - \Gamma_{11}^2 (V_2)_{(0,0)} \tag{35}$$

If U_0 can be taken as constant at this gridpoint for an elemental area,

$$A = \sqrt{a}\ \Delta_1 \Delta_2 \tag{36}$$

then the strain energy over this area is

$$U_{(0,0)} = (U_0 A)_{(0,0)} \tag{37}$$

and the total strain energy for the shell is

$$U = \sum_{i=1}^{N} (U)_i = \sum_{i=1}^{N} (U_0 A)_i \tag{38}$$

where N is the total number of gridpoints in the network.

Writing out Eq. (38) one has

$$U = \sum_{i=1}^{N} \left\{ \frac{AE}{8}^{\alpha\beta\lambda\rho} \left[D(V_{\lambda|\rho} + V_{\rho|\lambda} - 2b_{\lambda\rho}w)(V_{\alpha|\beta} + V_{\beta|\alpha} - 2b_{\alpha\beta}w) + K(\Theta_{\lambda|\rho} + \Theta_{\rho|\lambda})(\Theta_{\alpha|\beta} + \Theta_{\beta|\alpha}) \right] \right\}_i \tag{39}$$

and the variational energy is

$$\begin{aligned} \delta U &= \sum_{i=1}^{N} \left\{ \frac{AE}{4}^{\alpha\beta\lambda\rho} \left[D(V_{\lambda|\rho} + V_{\rho|\lambda} - 2b_{\lambda\rho}w)(\delta V_{\alpha|\beta} + \delta V_{\beta|\alpha} - 2b_{\alpha\beta}\delta w) \right. \right. \\ &\qquad \left. \left. + K(\Theta_{\lambda|\rho} + \Theta_{\rho|\lambda})(\delta\Theta_{\alpha|\beta} + \delta\Theta_{\beta|\alpha}) \right] \right\}_i \\ &= \sum_{i=1}^{N} \left\{ (G^{\alpha\beta} - H^{\rho\beta} b_{\rho}^{\alpha}) \delta V_{\alpha,\beta} + \left[(\Gamma_{\rho\mu}^{\alpha} b_{\beta}^{\rho} - b_{\beta|\mu}^{\alpha}) H^{\beta\mu} \right. \right. \\ &\qquad \left. - G^{\beta\mu} \Gamma_{\beta\mu}^{\alpha} \right] \delta V_{\alpha} - H^{\alpha\beta} \delta w_{,\alpha\beta} + H^{\alpha\beta} \Gamma_{\alpha\beta}^{\rho} \delta w_{,\rho} \\ &\qquad \left. - G^{\alpha\beta} b_{\alpha\beta} \delta w \right\}_i \end{aligned} \tag{40}$$

where

$$G^{\alpha\beta} = \left(\frac{AD}{2}\right)\left(\frac{E^{\alpha\beta\lambda\rho}+E^{\beta\alpha\lambda\rho}}{2}\right)\left(V_{\lambda}|_{\rho} + V_{\rho}|_{\lambda} - 2b_{\lambda\rho}w\right) \quad (41)$$

$$H^{\alpha\beta} = \left(\frac{AK}{2}\right)\left(\frac{E^{\alpha\beta\lambda\rho}+E^{\beta\alpha\lambda\rho}}{2}\right)\left(\Theta_{\lambda}|_{\rho} + \Theta_{\rho}|_{\lambda}\right) \quad (42)$$

The bracketed expression in Eq. (40) represents the variational energy associated with the ith gridpoint. It should be noted that due to the presence of derivatives behind the variational operator δ, there is an energy contribution from the ith point to itself and to the eight surrounding points. Expanding Eq. (40) completely and rearranging the expression in groups of variations with V_1, V_2 and w being the ith, jth and kth generalized coordinates at a gridpoint, one has

$$\delta U = \sum_{p=1}^{N}\left\{\left[\sum_{m=1}^{3N} K_{im}q_m\right]\delta V_1 + \left[\sum_{m=1}^{3N} K_{jm}q_m\right]\delta V_2 + \left[\sum_{m=1}^{3N} K_{km}q_m\right]\delta w\right\}_p \quad (43)$$

Eq. (43) indicates that at any gridpoint p there are three equations available for the three unknown linear displacement components.

In a practical solution the stiffness matrix, K_{ij}, is banded along the diagonal. The nonzero elements of K_{ij} when considering gridpoint (0,0) are expressed in the following form:

$$\sum_{m=1}^{3N} K_{im}q_m = \left[-\Gamma'_{\alpha\beta}G^{\alpha\beta} + \left(\Gamma'_{\rho\beta}b^{\rho}_{\alpha} - b'_{\alpha}|_{\beta}\right)H^{\alpha\beta}\right]_{(0,0)}$$
$$+\left[\frac{1}{2\Delta_2}\left(G'^{2} - b'_{\alpha}H^{\alpha 2}\right)\right]_{(0,-\Delta_2)} + \left[\frac{-1}{2\Delta_2}\left(G'^{2} - b'_{\alpha}H^{\alpha 2}\right)\right]_{(0,+\Delta_2)}$$
$$+\left[\frac{1}{2\Delta_1}\left(G'' - b'_{\alpha}H^{\alpha 1}\right)\right]_{(-\Delta_1,0)} + \left[\frac{-1}{2\Delta_1}\left(G'' - b'_{\alpha}H^{\alpha 1}\right)\right]_{(+\Delta_1,0)} \quad (44)$$

$$\sum_{m=1}^{3N} K_{jm} q_m = \left[-\Gamma^2_{\alpha\beta} G^{\alpha\beta} + \left(\Gamma^2_{\rho\beta} b^{\rho}_{\alpha} - b^{2}_{\alpha|\beta} \right) H^{\alpha\beta} \right]_{(0,0)}$$
$$+ \left[\frac{G^{22} - b^{2}_{\alpha} H^{\alpha 2}}{2\Delta_2} \right]_{(0,-\Delta_2)} + \left[-\frac{G^{22} - b^{2}_{\alpha} H^{\alpha 2}}{2\Delta_2} \right]_{(0,+\Delta_2)}$$
$$+ \left[\frac{G^{21} - b^{2}_{\alpha} H^{\alpha 1}}{2\Delta_1} \right]_{(-\Delta_1,0)} + \left[-\frac{G^{21} - b^{2}_{\alpha} H^{\alpha 1}}{2\Delta_1} \right]_{(+\Delta_1,0)} \qquad (45)$$

$$\sum_{m=1}^{3N} K_{km} q_m = \left[-G^{\alpha\beta} b_{\alpha\beta} + 2\left(\frac{H^{11}}{\Delta_1^2} + \frac{H^{22}}{\Delta_2^2} \right) \right]_{(0,0)}$$
$$+ \left[-\frac{H^{22}}{\Delta_2^2} + \frac{\Gamma^2_{\alpha\beta} H^{\alpha\beta}}{2\Delta_2} \right]_{(0,-\Delta_2)} + \left[-\frac{H^{22}}{\Delta_2^2} - \frac{\Gamma^2_{\alpha\beta} H^{\alpha\beta}}{2\Delta_2} \right]_{(0,+\Delta_2)}$$
$$+ \left[-\frac{H^{11}}{\Delta_1^2} + \frac{\Gamma^1_{\alpha\beta} H^{\alpha\beta}}{2\Delta_1} \right]_{(-\Delta_1,0)} + \left[-\frac{H^{11}}{\Delta_1^2} - \frac{\Gamma^1_{\alpha\beta} H^{\alpha\beta}}{2\Delta_1} \right]_{(+\Delta_1,0)}$$
$$+ \left[-\frac{H^{12} + H^{21}}{4\Delta_1\Delta_2} \right]_{(-\Delta_1,-\Delta_2)} + \left[\frac{H^{12} + H^{21}}{4\Delta_1\Delta_2} \right]_{(-\Delta_1,+\Delta_2)}$$
$$+ \left[\frac{H^{12} + H^{21}}{4\Delta_1\Delta_2} \right]_{(+\Delta_1,-\Delta_2)} + \left[-\frac{H^{12} + H^{21}}{4\Delta_1\Delta_2} \right]_{(+\Delta_1,+\Delta_2)}$$

(46)

Eqs. (44), (45) and (46) are used to develop the stiffness matrix. They are completely general in formulation and are applicable to most isotropic thin shell structures of double curvature defined by any curvilinear coordinate system, not necessarily orthogonal. The geometry of the shell is described by the Christoffel symbols, $\Gamma^{\gamma}_{\alpha\beta}$, and the second fundamental magnitudes, $b_{\alpha\beta}$, while the generalized forces and moments are expressed by $G^{\alpha\beta}$ and $H^{\alpha\beta}$ as indicated in Eqs. (41) and (42).

APPLICATIONS TO CYLINDRICAL AND SPHERICAL SHELLS

Cylindrical and spherical shells are the two most frequently employed configurations in missile structures. The stiffness matrix calculation for these configurations will be demonstrated in the following examples.

CYLINDRICAL SHELL

The generalized coordinates (see Fig. 3) are taken as θ and z, hence

$$\{u_\alpha\} = \{\theta, z\}$$

$$a_{\alpha\beta} = \begin{bmatrix} r^2 & 0 \\ 0 & 1 \end{bmatrix} \; ; \quad a^{\alpha\beta} = \begin{bmatrix} \frac{1}{r^2} & 0 \\ 0 & 1 \end{bmatrix}$$

$$a = \det(a_{\alpha\beta}) = r^2$$

$$\Gamma^{\gamma}_{\alpha\beta} = 0$$

$$b_{\alpha\beta} = \begin{bmatrix} -r & 0 \\ 0 & 0 \end{bmatrix} \; ; \quad b^{\alpha}_{\beta} = \begin{bmatrix} -\frac{1}{r} & 0 \\ 0 & 0 \end{bmatrix}$$

$$b^{\alpha}_{\beta}|_{\rho} = 0$$

The material constants are

$$E^{1111} = \frac{1}{r^4} \quad ; \quad E^{1122} = \frac{\nu}{r^2}$$

$$E^{1212} = \frac{1-\nu}{r^2} \quad ; \quad E^{2121} = \frac{1-\nu}{r^2}$$

$$E^{2211} = \frac{\nu}{r^2} \quad ; \quad E^{2222} = 1$$

all other $E^{\alpha\beta\lambda\rho} = 0$

$$\because \quad V_1 = r u \quad ; \quad \delta V_1 = r \delta u$$

$$V_2 = v \quad ; \quad \delta V_2 = \delta v$$

The generalized forces and moments are

$$G^{12} = G^{21} = \frac{(1-\nu) AD}{2 r^2} [r u_{,z} + v_{,\theta}]$$

$$G^{11} = \frac{AD}{r^2} [\frac{1}{r} (u_{,\theta} + w) - \nu v_{,z}]$$

$$G^{22} = AD [v_{,z} + \frac{\nu}{r} (u_{,\theta} + w)]$$

$$H^{12} = H^{21} = - \frac{(1-\nu) AK}{2 r^2} [2 w_{,\theta z} - u_{,z}]$$

$$H^{11} = - \frac{AK}{r^2} [\frac{1}{r^2} (w_{,\theta\theta} - u_{,\theta}) + \nu w_{,zz}]$$

$$H^{22} = - AK [w_{,zz} + \frac{\nu}{r^2} (w_{,\theta\theta} - u_{,\theta})]$$

Vol. 4

The stiffness equations using u, v, w as the generalized coordinates then reduce to:

$$\sum_{m=1}^{3N} K_{im} q_m = \left[\frac{rG^{12}+H^{12}}{2\Delta_2}\right]_{(0,-\Delta_2)} + \left[-\frac{rG^{12}+H^{12}}{2\Delta_2}\right]_{(0,+\Delta_2)}$$
$$+\left[\frac{rG^{11}+H^{11}}{2\Delta_1}\right]_{(-\Delta_1,0)} + \left[-\frac{rG^{11}+H^{11}}{2\Delta_1}\right]_{(+\Delta_1,0)}$$

$$\sum_{m=1}^{3N} K_{jm} q_m = \left[\frac{G^{22}}{2\Delta_2}\right]_{(0,-\Delta_2)} + \left[\frac{-G^{22}}{2\Delta_2}\right]_{(0,\Delta_2)} + \left[\frac{G^{21}}{2\Delta_1}\right]_{(-\Delta_1,0)} + \left[\frac{-G^{21}}{2\Delta_1}\right]_{(+\Delta_1,0)}$$

$$\sum_{m=1}^{3N} K_{km} q_m = \left[rG^{11} + 2\left(\frac{H^{11}}{\Delta_1^2} + \frac{H^{22}}{\Delta_2^2}\right)\right]_{(0,0)}$$
$$+\left[-\frac{H^{22}}{\Delta_2^2}\right]_{(0,-\Delta_2)} + \left[-\frac{H^{22}}{\Delta_2^2}\right]_{(0,\Delta_2)} + \left[\frac{-H^{11}}{\Delta_1^2}\right]_{(-\Delta_1,0)} + \left[\frac{-H^{11}}{\Delta_1^2}\right]_{(\Delta_1,0)}$$
$$+\left[-\frac{H^{12}}{2\Delta_1\Delta_2}\right]_{(-\Delta_1,-\Delta_2)} + \left[\frac{H^{12}}{2\Delta_1\Delta_2}\right]_{(-\Delta_1,\Delta_2)} + \left[\frac{H^{12}}{2\Delta_1\Delta_2}\right]_{(\Delta_1,-\Delta_2)}$$
$$+\left[-\frac{H^{12}}{2\Delta_1\Delta_2}\right]_{(+\Delta_1,+\Delta_2)}$$

SPHERICAL SHELL

The generalized coordinates are taken as ϕ and θ in this example (see Fig. 4). Then,

$$\{u_\alpha\} = \{\phi, \theta\}$$

$$a_{\alpha\beta} = \begin{bmatrix} R^2 & 0 \\ 0 & R^2 \sin^2\phi \end{bmatrix}; \quad a^{\alpha\beta} = \begin{bmatrix} \frac{1}{R^2} & 0 \\ 0 & \frac{1}{R^2 \sin^2\phi} \end{bmatrix}$$

$$a = \det(a_{\alpha\beta}) = R^4 \sin^2\phi$$

from

$$\Gamma^{\alpha}_{\beta\gamma} = \frac{1}{2} a^{\alpha\lambda}(a_{\lambda\beta,\gamma} + a_{\lambda\gamma,\beta} - a_{\beta\gamma,\lambda})$$

we have

$$\Gamma^{1}_{22} = -\sin\phi\cos\phi$$

$$\Gamma^{2}_{12} = \Gamma^{2}_{21} = \cot\phi$$

all other $\Gamma^{\alpha}_{\beta\gamma}$ vanish

$$\because \quad b_{\alpha\beta} = \begin{bmatrix} -R & 0 \\ 0 & -R\sin^2\phi \end{bmatrix}; \quad b^{\alpha}_{\beta} = \begin{bmatrix} -\frac{1}{R} & 0 \\ 0 & -\frac{1}{R} \end{bmatrix}$$

all $\quad b_{\alpha\beta}|_{\rho} = 0$

$$E^{1111} = \frac{1}{R^4} \quad ; \qquad E^{1122} = \frac{\nu}{R^4 \sin^2\phi}$$

$$E^{1212} = \frac{1-\nu}{R^4 \sin^2\phi} \quad ; \qquad E^{2121} = \frac{1-\nu}{R^4 \sin^2\phi}$$

$$E^{2211} = \frac{\nu}{R^4 \sin^2\phi} \quad ; \qquad E^{2222} = \frac{1}{R^4 \sin^4\phi}$$

$$\because \quad V_1 = R\,u \quad ; \qquad V_2 = R \sin\phi\, v$$

$$\therefore \quad \delta V_1 = R\,\delta u \quad ; \qquad \delta V_2 = R \sin\phi\, \delta v$$

The generalized forces are

$$G^{11} = \frac{AD}{R^3}\left[u_{,\phi} + w + \frac{\nu}{\sin\phi}\left(v_{,\theta} + \cos\phi\, u + \sin\phi\, w\right)\right]$$

$$G^{12} = G^{21} = \frac{(1-\nu)AD}{2R^3 \sin^2\phi}\left[u_{,\theta} + \sin\phi\, v_{,\phi} - \cos\phi\, v\right]$$

$$G^{22} = \frac{AD}{R^3 \sin^2\phi}\left[\nu\left(u_{,\phi} + w\right) + \frac{1}{\sin\phi}\left(v_{,\theta} + \cos\phi\, u + \sin\phi\, w\right)\right]$$

The generalized moments are

$$H^{11} = -\frac{AK}{R^4}\left\{w_{,\phi\phi} - u_{,\phi} + \frac{\nu}{\sin^2\phi}\left[w_{,\theta\theta} + \sin\phi\cos\phi\left(w_{,\phi} - u\right) - \sin\phi\, v_{,\theta}\right]\right\}$$

$$H^{12} = H^{21} = -\frac{(1-\nu)AK}{R^4 \sin^2\phi}\left[w_{,\theta\phi} - \cot\phi\, w_{,\theta} - \frac{1}{2}\left(u_{,\theta} + \sin\phi\, v_{,\phi} - \cos\phi\, v\right)\right]$$

$$H^{22} = -\frac{AK}{R^4 \sin^2\phi}\left\{\nu\left(w_{,\phi\phi} - u_{,\phi}\right) + \frac{1}{\sin^2\phi}\left[w_{,\theta\theta} + \sin\phi\cos\phi\left(w_{,\phi} - u\right) - \sin\phi\, v_{,\theta}\right]\right\}$$

The stiffness equations at (0,0) with the physical components of the displacement vector as the generalized coordinates are then,

$$\sum_{m=1}^{3N} K_{im} q_m = \left[-\Gamma_{22}^{1}(RG^{22}+H^{22})\right]_{(0,0)} + \left[\frac{RG^{12}+H^{12}}{2\Delta_2}\right]_{(0,-\Delta_2)} + \left[-\frac{RG^{12}+H^{12}}{2\Delta_2}\right]_{(0,+\Delta_2)}$$
$$+ \left[\frac{RG^{11}+H^{11}}{2\Delta_1}\right]_{(-\Delta_1,0)} + \left[-\frac{RG^{11}+H^{11}}{2\Delta_1}\right]_{(+\Delta_1,0)}$$

$$\sum_{m=1}^{3N} K_{jm} q_m = \left[-\Gamma_{12}^{2}\sin\phi(RG^{12}+H^{12})\right]_{(0,0)} + \left[\frac{\sin\phi(RG^{22}+H^{22})}{2\Delta_2}\right]_{(0,-\Delta_2)}$$
$$+ \left[-\frac{\sin\phi(RG^{22}+H^{22})}{2\Delta_2}\right]_{(0,+\Delta_2)} + \left[\frac{\sin\phi(RG^{21}+H^{21})}{2\Delta_1}\right]_{(-\Delta_1,0)}$$
$$+ \left[-\frac{\sin\phi(RG^{21}+H^{21})}{2\Delta_1}\right]_{(+\Delta_1,0)}$$

$$\sum_{m=1}^{3N} K_{km} q_m = \left[R(G^{11}+G^{22}\sin^2\phi)+2\left(\frac{H^{11}}{\Delta_1^2}+\frac{H^{22}}{\Delta_2^2}\right)\right]_{(0,0)} + \left[-\frac{H^{22}}{\Delta_2^2}+\frac{\Gamma_{12}^{2}H^{12}}{\Delta_2}\right]_{(0,-\Delta_2)}$$
$$+ \left[-\frac{H^{22}}{\Delta_2^2}-\frac{\Gamma_{12}^{2}H^{12}}{\Delta_2}\right]_{(0,+\Delta_2)} + \left[-\frac{H^{11}}{\Delta_1^2}+\frac{\Gamma_{22}^{1}H^{22}}{2\Delta_1}\right]_{(-\Delta_1,0)}$$
$$+ \left[-\frac{H^{11}}{\Delta_1^2}-\frac{\Gamma_{22}^{1}H^{22}}{2\Delta_1}\right]_{(+\Delta_1,0)} + \left[-\frac{H^{12}}{2\Delta_1\Delta_2}\right]_{(-\Delta_1,-\Delta_2)} + \left[\frac{H^{12}}{2\Delta_1\Delta_2}\right]_{(-\Delta_1,+\Delta_2)}$$
$$+ \left[\frac{H^{12}}{2\Delta_1\Delta_2}\right]_{(+\Delta_1,-\Delta_2)} + \left[-\frac{H^{12}}{2\Delta_1\Delta_2}\right]_{(+\Delta_1,+\Delta_2)}$$

CONCLUSIONS

In the development of the stiffness equations the principle of potential energy has been employed and the relevant formulations are expressed in a general curvilinear coordinate system. Consequently this approach has the following advantages:

1. The advantage of having to satisfy only the essential displacement boundary conditions is preserved.

2. The constitutive equations and the stiffness equations are presented in general Caussian surface coordinates which need not be orthogonal.

3. The shell structure may have variable thickness and may be of a nonhomogeneous but isotropic material.

4. The equations are general for any arbitrary shell configuration.

5. The stiffness equations can be easily programmed for automatic computation.

6. The stiffness matrix will be symmetrical and banded along the diagonal, hence the simultaneous equations may be rapidly solved.

BIBLIOGRAPHY

Martin Marietta Corp. Theory of Thin Shells, by P. C. Huang. Martin, Balto., September 1963. (RM-163).

Martin Marietta Corp. Elasto-Plastic Analysis for Thin Shells of Revolution, by P. C. Huang. Martin, Balto., November 1965. (RR-63).

Martin Marietta Corp. Analysis of Frame Stiffened Arbitrary Hull Segments Typical of Submarine Construction, by P. C. Huang and R. J. Edwards. Martin, Balto., May 1967. (RR-80).

John Wiley Co. Tensor Analysis Theory and Application, by I. S. Sokolnikoff. 1958.

Oxford Press. Theoretical Elasticity by A. E. Green and W. Zerna. 1960.

McGraw-Hill. Theory of Plates and Shells, by S. Timoshenko and S. Woinowsky-Krieger. 1959.

Noordhoff Ltd. The Theory of Thin Shells, by V. V. Novozhilov. 1959.

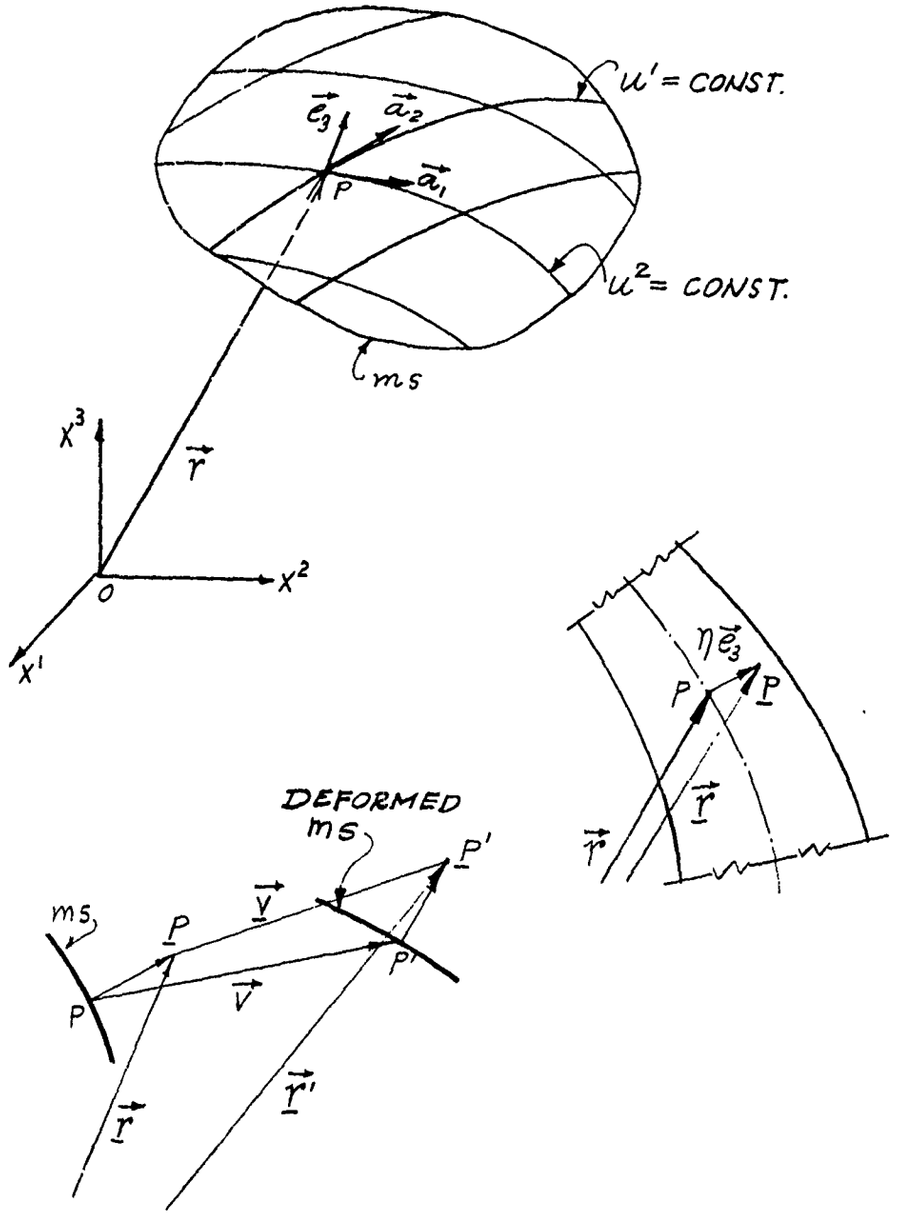

(U) FIG. 1 Thin Shell Coordinate System.

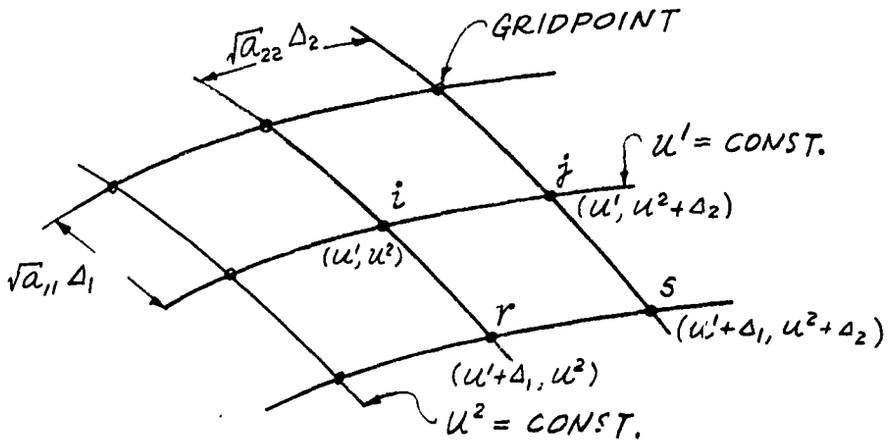

(U) FIG. 2 Discrete Gaussian Surface Gridwork.

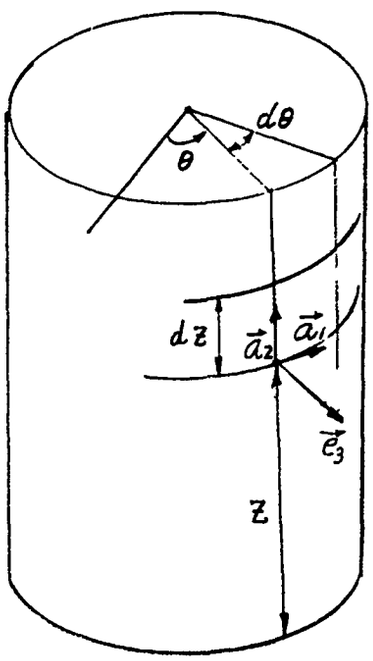

$$\{u^1, u^2\} = \{\theta, z\}$$

(U) FIG. 3 Coordinate System for Cylindrical Shell.

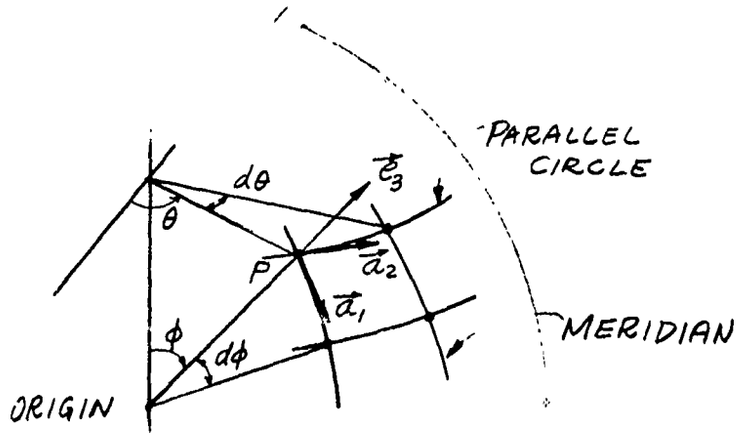

$$\{u^1, u^2\} = \{\phi, \theta\}$$

(U) FIG. 4 Coordinate System for Spherical Shell.

Paper No. 41

AN EXPERIMENTAL INVESTIGATION OF AIRCRAFT/MISSILE INTERFERENCE EFFECTS (U)

(Paper UNCLASSIFIED)

by

C. Franklyn Markarian
Naval Weapons Center
China Lake, Calif. 93555

ABSTRACT. A study is being conducted to investigate the influence of the carrying aircraft on the flow field about captive flight ordnance. Results of the program have application to problems in store separation, aerodynamic heating and structural loads. A store instrumented to measure surface pressure distributions was flown over a broad range of flight conditions aboard high performance aircraft. Captive flight pressure distributions were obtained at speeds up to Mach 2 and altitudes to 40,000 feet. Wind tunnel tests of a pressure instrumented scale model of the captive flight round were conducted in order to provide interference-free reference pressure distributions for comparison with the captive flight data. Significant interference effects such as impinging shock waves are evident in the captive flight data. The test program is discussed, and captive flight pressure distributions are presented along with comparisons with wind tunnel data.

INTRODUCTION

Most work in aircraft/missile interference effects is concentrated on the measurement and prediction of gross loads on captive flight stores, and there has been less emphasis, particularly of an experimental nature, on the study of the captive flight flow field. In addition to applications in the study of aerodynamic loads and the store separation problem in general, a knowledge of the flow field is essential in aerodynamic heating and structural studies of airborne ordnance.

Although flow field and aerodynamic heating parameters about a simple body under free stream conditions can be predicted with reasonable accuracy, when the same body is placed on an aircraft in the vicinity of the launcher assembly and adjoining stores the problem becomes extremely complex. Resulting interference effects, which may take such forms as redirection of flow or shock wave impingement, can cause major variations in surface pressure distributions and aerodynamic heating rates. Altered pressure distributions could have adverse effects on aerodynamic loads on captive flight stores as evidenced by the difficulties currently being experienced in achieveing satisfactory separation of certain stores from aircraft. Increased heating rates caused by shock wave impingement may create serious problems, particularly if impingement occurs at a sensitive location such as the warhead or motor of a missile.

Most of the work done to date on the flow field aspects of interference effects has been limited to analytical studies of simplified shapes and wind tunnel investigations. Relatively little full scale data is available. In view of the lack of full scale information and the extensive flight test facilities available at the Naval Weapons Center, the approach was taken of captive flight testing of a suitably instrumented store. In order to aid in the identification of flow disturbances, wind tunnel tests were conducted using a scale model of the captive flight round. The purpose of the wind tunnel tests was to provide interference-free reference data for comparison with the captive flight results.

Data obtained in this program can be used for comparison with the results of analytical and wind tunnel investigations, and in addition, will provide insight into the nature and magnitude of full scale captive flight flow disturbances.

PROCEDURE

A detailed investigation of interfering flow fields requires knowledge of a wide variety of local flow parameters such as pressure, heat transfer coefficient, flow direction and skin friction. For an experimental program, the measurement of pressure offers the advantage of being the least complicated and expensive source of the accurate and detailed distributions of data necessary for detection of localized flow disturbances. In addition, pressure measurements can be related to several of the other local flow parameters and, as noted below, are directly applicable to the major areas of interest in this program.

1. Store separation - Pressure distributions give an indication of flow direction and may be integrated to obtain aerodynamic loads. A knowledge of captive flight pressure distributions can complement measurements of gross loads on captive flight stores such as obtained with airborne balances.
2. Aerodynamic heating - Surface pressure distributions may be used to determine local flow properties for use in calculating aerodynamic heat transfer coefficients. A detailed pressure distribution can detect the location and strength of impinging shock waves and be used to estimate the peak heating rates in shock impingement regions.
3. Structural analysis - Integrating the pressure distribution will give the distribution of aerodynamic loads over a store in complex captive flight flow fields.

For the reasons described above, the captive flight round used in the test program was instrumented to measure surface pressure distributions.

DESIGN OF TEST VEHICLE

In order that as much existing hardware and circuitry as possible could be utilized in the program, the launcher and circuitry requirements and the basic airframe of the test vehicle were designed around the Shrike missile. Although in final configuration the only similarity between the test vehicle and Shrike was an 8 inch diameter and the same hangers and detents, the Shrike launcher and aircraft circuitry, including control panel, were utilized. Advantages of the Shrike installation were the availability of a large number of wires for carrying data from the round to a recorder in the aircraft and a relatively large diameter, which facilitated installation of pressure tubing and packaging of the instrumentation system. The primary disadvantage was the limitation of the system to aircraft, specifically stations on aircraft, configured for Shrike. In this respect, a completely self contained round, requiring only electrical power at a pylon would be desirable.

The basic configuration of the round, shown in Fig. 1, consists of an 8 inch diameter cylinder with a spherically tipped, tangent-ogive nose. Wings and fins are not used as they would normally occupy positions aft of the last pressure ports.

Development of instrumentation techniques for high accuracy airborne measurements was as important a part of the program as the investigation of interference effects. Complete descriptions of the design and operation of the instrumentation system developed for the program are given in Ref. 1 & 2. Detection of localized flow disturbances such as impinging shock waves requires an extremely dense distribution of pressure taps over the surface of the round. This is accomplished by using Scanivalve multiple pressure scanning devices and a skin which can be rotated in flight (Fig. 1). Each Scanivalve, using a 0 to 25 psia pressure transducer, samples 48 pressure readings in two seconds. Two of the Scanivalves sample the 77 taps aligned in the pitch and yaw planes on the ogive and nose cap. Several of the taps on the nose cap are sampled more than once per scan in order to obtain frequent data for determining variations in angle of attack and stagnation pressure. The two remaining Scanivalves each scan one of the two rows of taps spaced 180 degrees apart on the cylindrical portion of the round. By indexing the cylinder through 180 degrees and back in 30 degree increments, and sampling all of the nose and cylinder pressure taps at each roll position, a complete circumferential pressure distribution is obtained. The pressure sampling sequence is initiated by the pilot and terminates automatically when the cycle has been completed. The complete cycle, during which the circumferential pressure distribution is measured twice, takes approximately one minute. Pressures are measured at 653 geometrically distinct locations over the forward half of the round during the cycle. The system may also be operated with the cylindrical section locked in any desired roll position. In this mode the pilot initiates the sequence, and the pressure taps are scanned with three second pauses between scans until the pilot terminates operation.

Although the rotating skin and use of Scanivalves result in a mechanically complex system, the cost of an equivalent alternative system using 653 pressure transducers would be prohibitive. The lack of pressure taps over the aft portion of the round eliminates the possibility of integrating the pressure data to obtain gross aerodynamic loads. However, since the main emphasis of the program was on the detection of localized flow disturbances, the decision was made to concentrate the maximum practical number of pressure taps over the forward half of the round.

DATA ACQUISITION AND REDUCTION

Recording of Data

All data from the round is recorded on an FM magnetic tape recorder carried in the aircraft. The following signals are monitored:

1. Amplified pressure outputs from Scanivalves

2. Pilot remarks on flight conditions (Mach no., altitude, etc.)
3. Timing signal and reference frequency for tape speed compensation
4. Miscellaneous signals indicating supply voltage levels, roll position of rotating cylinder and pressure tap identification.

In addition to the data recorded on tape, one channel is transmitted to a ground station during the flight. This allows the performance of the round to be monitored during a test, and also serves as a source for the ground tracking equipment used to obtain the aircraft flight profile.

Flight Conditions

Meaningful interpretations of the pressure data require that aircraft flight conditions, in particular Mach number, true air speed, altitude and angle of attack, be accurately known throughout each test run. This task was somewhat simplified by the fact that all data was collected during constant altitude and, except for some acceleration runs, constant speed flight.

The most convenient method of obtaining flight conditions is to record the pilot's readings of the aircraft instruments. This method has the following disadvantages:

1. A discreet number of readings are obtained rather than a continuous record. Small variations in conditions may be missed.
2. There can be a lag between the pilot's reading and recording of instrument settings. An extra burden is placed on the pilot, especially in low level or high speed runs.
3. Instrument errors, particularly the altimeter, can be significant.

A photopanel arrangement was attempted in order to alleviate the first two factors mentioned above. A camera operating at one frame per second was focused on the instrument panel, however, satisfactory results were never obtained, primarily because of poor lighting.

The most accurate, but most expensive, method of determining flight conditions is by ground tracking. The last several flights of the program were made with the aircraft tracked by MIDAS (missile intercept data acquisition system). MIDAS gives the aircraft position, heading and ground speed relative to a tangent plane coordinate system. Since most of the flights covered relatively long distances, corrections for curvature of the earth must be made in order to obtain geometric altitudes. Preliminary indications show the MIDAS data to improve considerably as the aircraft approaches the receiving antennas.

While the aircraft flight profile can be determined as described above, none of these methods provide information on angle of attack. The aircraft angle of attack indicator is calibrated in arbitrary units

which have no unique conversion to degrees. This data must be estimated from the aircraft flight manual which provides charts of angle of attack as a function of aircraft weight, altitude and Mach number.

Information on atmospheric conditions such as temperature, pressure and wind velocity as functions of altitude on the day of a flight is obtained from the daily weather balloon (Rawinsonde). This data is needed to convert aircraft ground speed provided by MIDAS to true airspeed and Mach number and is a source of ambient pressure for use in calculating pressure coefficients.

Data Reduction

Reduction of the captive flight data is performed almost entirely by computer. The analog flight tape is first digitized so that another tape is produced with all data expressed as voltages. The digitized data, along with flight parameters and pressure-voltage relations for each Scanivalve, is then input to a computer program which calculates pressure coefficients and outputs plots of circumferential and longitudinal pressure coefficient distributions.

ENVIRONMENTAL CHECKOUT

Before flight testing began, the captive flight round was subjected to proof load and altitude chamber tests. Proof load tests were conducted to verify the structural integrity of the round. The round was subject to maximum expected bending moments while deflections and the ability of the cylindrical section to rotate under load were monitored. Performance of the instrumentation system was checked out in altitude chamber tests in which the round was exposed to low temperature and pressure extremes.

CAPTIVE FLIGHT TESTS

A total of 25 flights were made in the test program. Two checkout flights were made aboard an A-4C aircraft (Ref. 3) while all remaining tests were flown on an F-4B (Fig. 2). As mentioned previously, because of launcher and circuitry requirements, all F-4B flights were made with the round carried on the left outboard station. A three-view drawing depicting the round on the F-4B is shown in Fig. 3. Although the first flight of the round was made in November 1964, modifications and refinements were continually made to improve the accuracy and reliability of the system, and the majority of the successful data flights were made from May to October 1968.

Data was collected over conditions ranging from 400 knots "on the deck" to Mach 2.0 at altitudes over 40,000 feet. While most flights consisted of constant speed and altitude runs, data was also collected during constant altitude acceleration with the rotatable cylindrical section locked so that the two rows of ports were aligned in either

the pitch or yaw planes. Flight conditions under which pressure distributions were obtained are summarized in Table 1.

TABLE 1. Summary of Flight Test Conditions

Altitude (Feet MSL)	Speed (KIAS or Mach No.)
Low Level	400 KIAS (Knots, Indicated Air Speed)
Low Level	500 KIAS
5,000	400 KIAS
5,000	500 KIAS
10,000	400 KIAS
10,000	500 KIAS
20,000	Acceleration from Mach 0.9 to 1.35*
20,000	Acceleration from Mach 0.9 to 1.32**
20,000	Mach 0.7
20,000	Mach 0.8
20,000	Mach 0.9
20,000	Mach 1.0
20,000	Mach 1.1
20,000	Mach 1.2
40,000	Acceleration from Mach 0.9 to 1.9*
40,000	Acceleration from Mach 0.9 to 1.91**
40,000	Mach 0.7
40,000	Mach 0.8
40,000	Mach 0.9
40,000	Mach 1.0
40,000	Mach 1.1
40,000	Mach 1.2
40,000	Mach 1.4
40,000	Mach 1.54
40,000	Mach 2.0

*Rotatable cylinder locked with rows of ports aligned in pitch plane
**Rotatable cylinder locked with rows of ports aligned in yaw plane

WIND TUNNEL TESTS

Wind tunnel tests of a pressure instrumented, quarter-scale model of the captive flight round were conducted in order to provide interference-free, reference pressure distributions for comparison with the captive flight data. The model, shown in Fig. 4, contains one row of pressure taps along a streamline and is rolled in order to obtain the complete circumferential pressure distribution. Tests were conducted over a broad range of Mach numbers and angles of attack in order to cover the captive flight conditions. Supersonic tests at Mach numbers of 1.54 and 2.05 were conducted at the Naval Ordnance Laboratory, White Oak (NOL) in May 1966. Tests at Mach numbers from 0.7 to 1.1 were performed in the transonic wind tunnel at the Naval Ship Research and Development Center (NSRDC) in February 1969. A summary of wind tunnel test conditions is given in Table 2.

TABLE 2. Wind Tunnel Test Conditions

Mach No.	Angle of Attack (Degrees)	Roll Angle* (Degrees)	Wind Tunnel
0.7	0,±2,±4,±6,±8,±10	0,15,30,60,90	NSRDC
0.8	0,±2,±4,±6,±8,±10	0,15,30,60,90	NSRDC
0.9	0,±2,±4,±6,±8,±10	0,15,30,60,90	NSRDC
1.0	0,±2,±4,±6,±8,±10	0,15,30,60,90	NSRDC
1.1	0,±2,±4,±6,±8,±10	0,15,30,60.90	NSRDC
1.54	-11.5 to +11.5	0,30,60,90	NOL
2.05	-11.5 to +11.5	0,15,30,60,90	NOL

* Roll angle is 0 degrees when the row of pressure taps is on top of the model.

RESULTS

While most of the data obtained in the program is still being reduced and evaluated, preliminary results indicate significant interference effects in all pressure distributions. Some typical examples of the results obtained are described below. All data presented is from flights aboard the F-4B aircraft.

LONGITUDINAL PRESSURE DISTRIBUTIONS

Comparisons between captive flight and wind tunnel longitudinal pressure distributions at Mach numbers of 1.0 and 1.54 are shown in Fig. 5. The captive flight data was obtained at an altitude of 20,000 feet in the Mach 1.0 run and 40,000 feet in the Mach 1.54 run. Angle of attack of the round relative to the free stream was estimated to be between plus or minus one degree for both cases. The distribution along the top of the round is shown, as this roll position displayed the largest disturbances during the flight tests. Pressure data in this and following figures is presented as pressure coefficient, C_p, calculated from the expression

$$C_p = \frac{P - P_\infty}{0.7\ P_\infty\ M^2}$$

where P is the measured surface pressure, P_∞ is the free stream pressure and M is the free stream Mach number.

Mach 1.0

The Mach 1.0 pressure distribution shows very good agreement between the captive flight data and the NSRDC wind tunnel data up to the forward portion of the cylindrical section. From this point the captive flight data diverges from the wind tunnel data, rising to a peak in front of the launcher. The captive flight pressure distribution then decreases in a complex manner indicating the acceleration of the flow as it passes between the launcher and the top of the round. The disturbance along the top of the cylinder is attributed primarily to the launcher, however, the pylon and leading edge of the wing are also in a position to influence the flow over this portion of the round.

Mach 1.54

The pressure distribution along the top of the round at Mach 1.54 is distinguished by (a) a disturbance on the ogive, possibly caused by the inboard pylon (see Fig. 3), (b) relatively undisturbed flow over the forward portion of the cylinder, (c) a sharp increase in pressure immediately in front of the launcher and (d) extremely complex flow beneath the launcher.

The pressure spike is caused by impingement of a launcher generated shock wave and represents an increase of 2.1 times the free stream pressure. As part of this program a study was made of heat transfer in shock wave-boundary layer interaction regions (Ref. 4). The following empirical expression relating the peak heat transfer coefficient to the peak pressure in the interaction region of a shock wave and a turbulent boundary layer was developed in Ref. 4.

$$\frac{h_{pk}}{h_{fp}} = \left(\frac{P_{pk}}{P_{fp}}\right)^{0.85}$$

The subscripts pk and fp represent the peak value and the undisturbed or flat plate value respectively. Based on this expression, the shock in peak heat transfer coefficient of 90%. At higher Mach numbers pressures as high as 2.5 times free stream have been measured, representing peak heat transfer coefficients of 2.2 times the undisturbed value.

CIRCUMFERENTIAL PRESSURE DISTRIBUTIONS

Circumferential pressure distributions at three longitudinal stations on the cylinder at Mach 1.0 and 1.54 are shown in Fig. 6. This data is from the same flight tests as that in Fig. 5. These distributions show the relatively uniform flow at the forward part of the cylinder, high pressures concentrated on the top of the round just in front of the launcher and low pressures underneath the launcher at the farthest aft station shown.

VARIATION OF PRESSURE DISTRIBUTION WITH MACH NUMBER

Longitudinal pressure distributions on the top and bottom of the round at Mach numbers of 0.9, 1.1 and 1.5 are shown in Fig. 7. This data was obtained during an acceleration run at an altitude of 40,000 feet with the cylindrical section of the round locked so that the two rows of pressure taps were aligned in the pitch plane. The pressure distribution along the top of the round is characterized by a gradual increase in pressure along the cylinder at Mach 0.9 which shortens in length and increases in magnitude with increasing Mach number, becoming a distinct shock induced pressure spike at Mach 1.5. While the flow beneath the launcher is quite complex, the pressure distribution shows basically the same shape for the three Mach numbers. A disturbance on the ogive, similar to that in Fig. 5(b), is evident on the Mach 1.5 distribution, but not at the lower Mach numbers.

As would be expected, interference effects along the bottom of the round are much less severe than those on the top. Mild pressure increases related to the higher increases on the top appear on the ogive at Mach 1.5 and on the cylinder at Mach 1.1 and 1.5. These pressure rises are located farther aft than the corresponding increases on the top of the round indicating the swept nature of the disturbances. The rearward sweep of the disturbances would tend to increase the downward pitching moment which might be expected from the high pressures on the top of the forward half of the round. However, since the data provides no knowledge of the pressure distribution over the aft portion of the round, no definite conclusions as to moments can be made.

Pressure distributions on the nose cap have given indications of changes in free stream flow direction relative to the round with changing

Mach number (other than angle of attack effects), but further investigation of this occurrence is required.

ACCURACY

Overall accuracy of the captive flight pressure data is difficult to determine because of the lack of a reliable reference pressure source in flight. One port of each of the two Scanivalves in the nose is connected to a common source, and the same is done with the Scanivalves in the cylindrical section. This allows each pressure transducer to be checked against one other. Maximum variation between the common readings is almost always within 0.15 psi, or less than 1% of full range.

Another approximate check of the accuracy of the system is obtained using the measured stagnation pressure. Mach numbers calculated from the ratio of free stream pressure to measured stagnation pressure generally agree within 5% of indicated Mach number and in many cases the agreement is within 1% or less. Deficiencies in this type of a comparison are as follows:

1. The local Mach number at the nose cap is not necessarily the same as that of the aircraft because of interference effects.
2. If the round is at angle of attack the true stagnation pressure might not be measured.

In addition, the accuracy with which the indicated Mach number and the free stream pressure are known is probably no better than the accuracy of the pressure data. In spite of these factors, it is felt that the relatively good agreement obtained in the comparisons which are made indicate a reasonably high degree of accuracy for an airborne instrumentation system.

FUTURE PLANS

Along with further reduction, evaluation and analysis of the data from the pressure measurement phase of the program, plans are being made to install thermal measurement instrumentation in the captive flight round. Flight tests will be conducted to measure local heat transfer coefficients in regions indicated by the pressure data to exhibit significant interference effects.

The possibility of measuring local flow direction over the surface of the round using a system more sophisticated than the usual tuft studies is being investigated. Vane driven potentiometers have been evaluated, but a less vulnerable sensor, preferably one which would mount flush with the skin is desirable.

SUMMARY AND CONCLUSIONS

Pressure distributions on a round of typical missile configuration have been measured during captive flight aboard an F-4B aircraft over a broad range of subsonic and supersonic flight conditions. Significant flow interference effects, particularly impinging shock waves, have been evident in the data. These disturbances can create major variations in expected aerodynamic loads and aerodynamic heating rates. Interference-free, reference pressure distributions for comparison with the captive flight data were obtained from wind tunnel tests of a pressure instrumented, quarter-scale model of the captive flight round.

Although the scope of the program is currently limited in that the data represents a single configuration on one station of one type of aircraft, much needed full scale data has been obtained which provides an insight into the nature and magnitude of captive flight flow disturbances. Results of the test program may also be used for comparison with analytical techniques and results of wind tunnel investigations.

An additional benefit of the program has been the development of techniques for obtaining accurate, high density, airborne measurements. If desired, the pressure measurement system developed for the program could be installed in an existing ordnance shape to provide data for a specific problem or in experimental configurations for the purpose of obtaining design information.

REFERENCES

1. Naval Ordnance Test Station. Design Description of Aircraft-Missile Interference-Effects Vehicle, by Dwight L. Weathersbee. China Lake, Calif., NOTS, April 1966. 30 pp. (NOTS TP 4067).

2. Naval Missile Center. Aircraft-Missile Interference Effects, by C.F. Markarian and C.M. Martin. Pt. Mugu, Calif., NMC, 7-9 June 1966. 19 pp. (Proceedings of the Seventh U.S. Navy Symposium on Aeroballistics.)

3. Naval Ordnance Test Station. Results of Aircraft-Missile Interference Effects Round Flights Aboard an A-4C Aircraft, by C.F. Markarian. China Lake, Calif., NOTS, 23 April 1965. 33 pp. (NOTS TN 4061-123).

4. Naval Weapons Center. Heat Transfer in Shock Wave-Boundary Layer Interaction Regions, by C.F. Markarian. China Lake, Calif., NWC, November 1968. 78 pp. (NWC TP 4485).

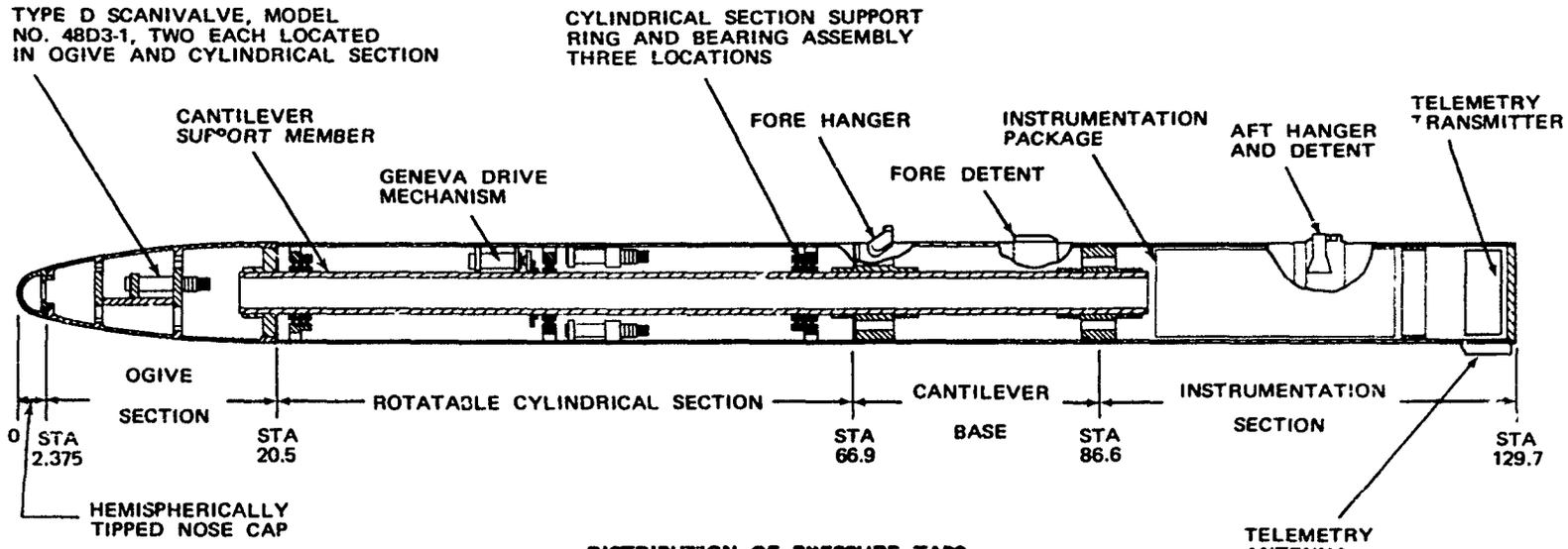

DISTRIBUTION OF PRESSURE TAPS

NOSE CAP & OGIVE:	TOTAL OF 653 GEOMETRICALLY DISTINCT TAP LOCATIONS
ONE CENTERLINE TAP	
FOUR ROWS OF 19 TAPS EACH ALIGNED IN PITCH AND YAW PLANES	
CYLINDER:	
TWO ROWS OF 48 TAPS EACH SPACED 180 DEG APART	
(CYLINDER ROTATES THROUGH 180 DEG AND BACK IN 30 DEG INCREMENTS)	

FIG. 1. SECTIONAL VIEW OF AIRCRAFT-MISSILE INTERFERENCE EFFECTS VEHICLE

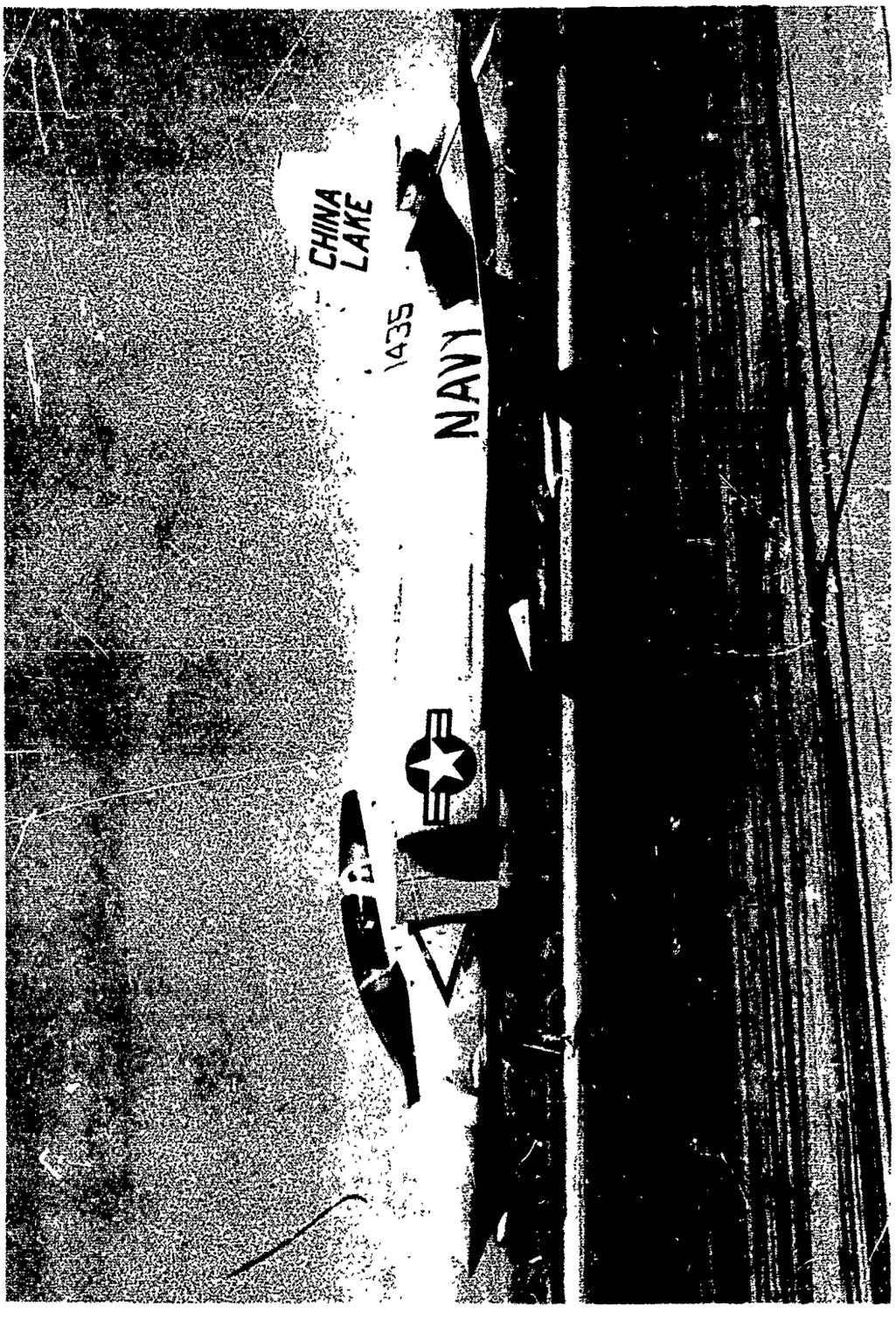

FIG. 2. AIRCRAFT-MISSILE INTERFERENCE EFFECTS VEHICLE ON F-4B AIRCRAFT

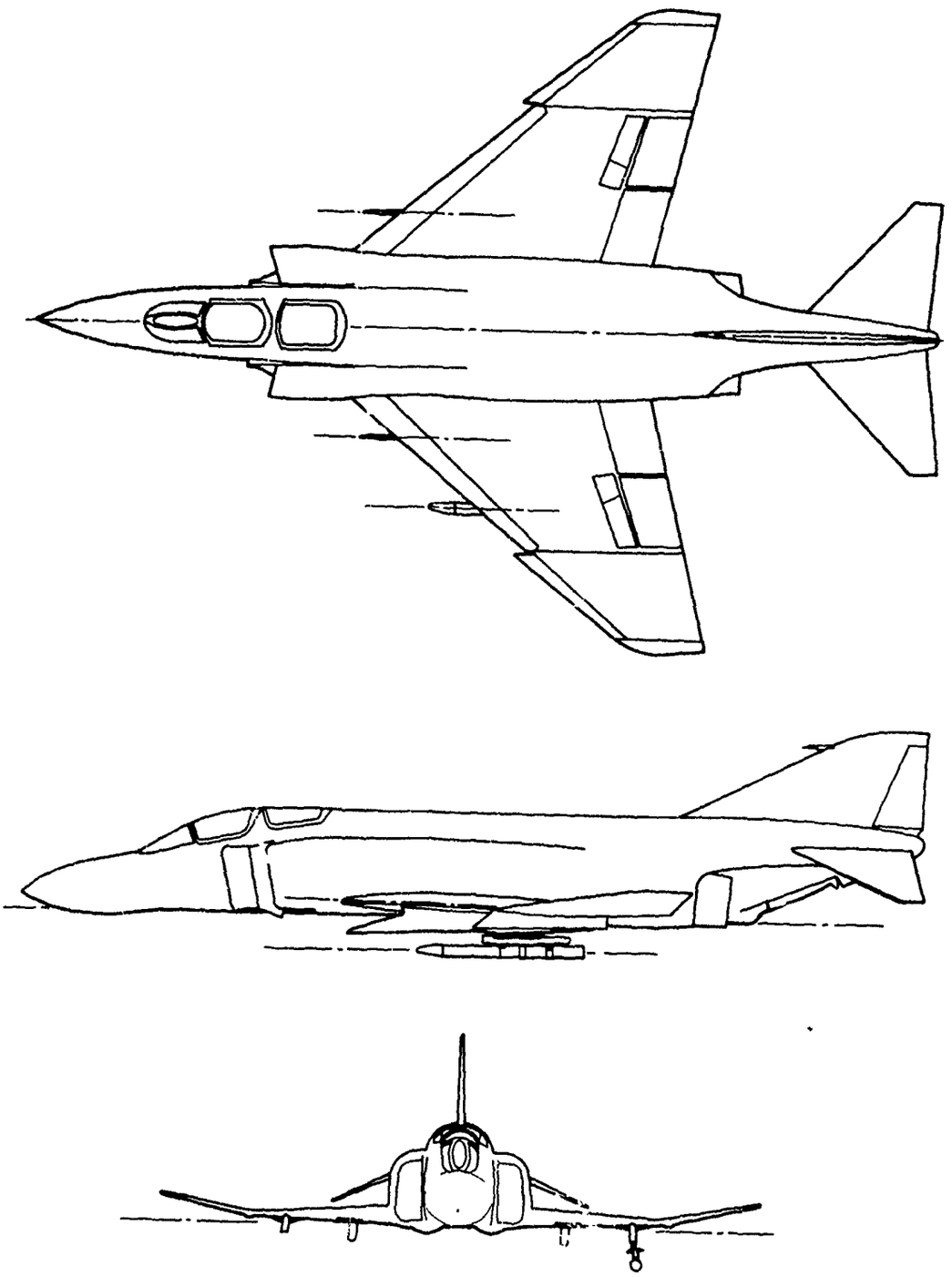

FIG. 3. AIRCRAFT-MISSILE INTERFERENCE EFFECTS
VEHICLE ON LEFT OUTBOARD STATION OF F-4B

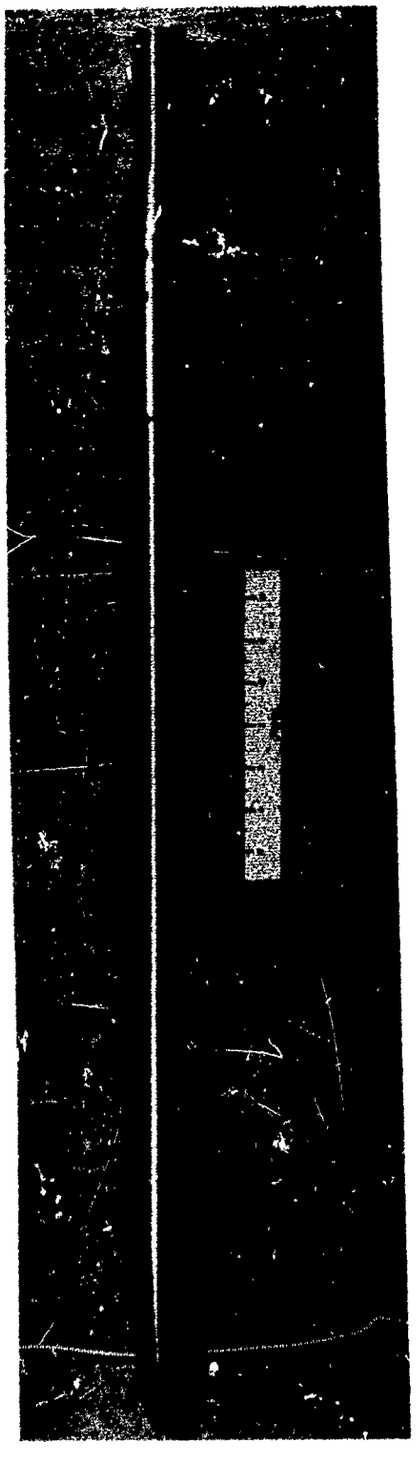

FIG. 4. QUARTER-SCALE, WIND TUNNEL MODEL OF AIRCRAFT-MISSILE INTERFERENCE EFFECTS VEHICLE

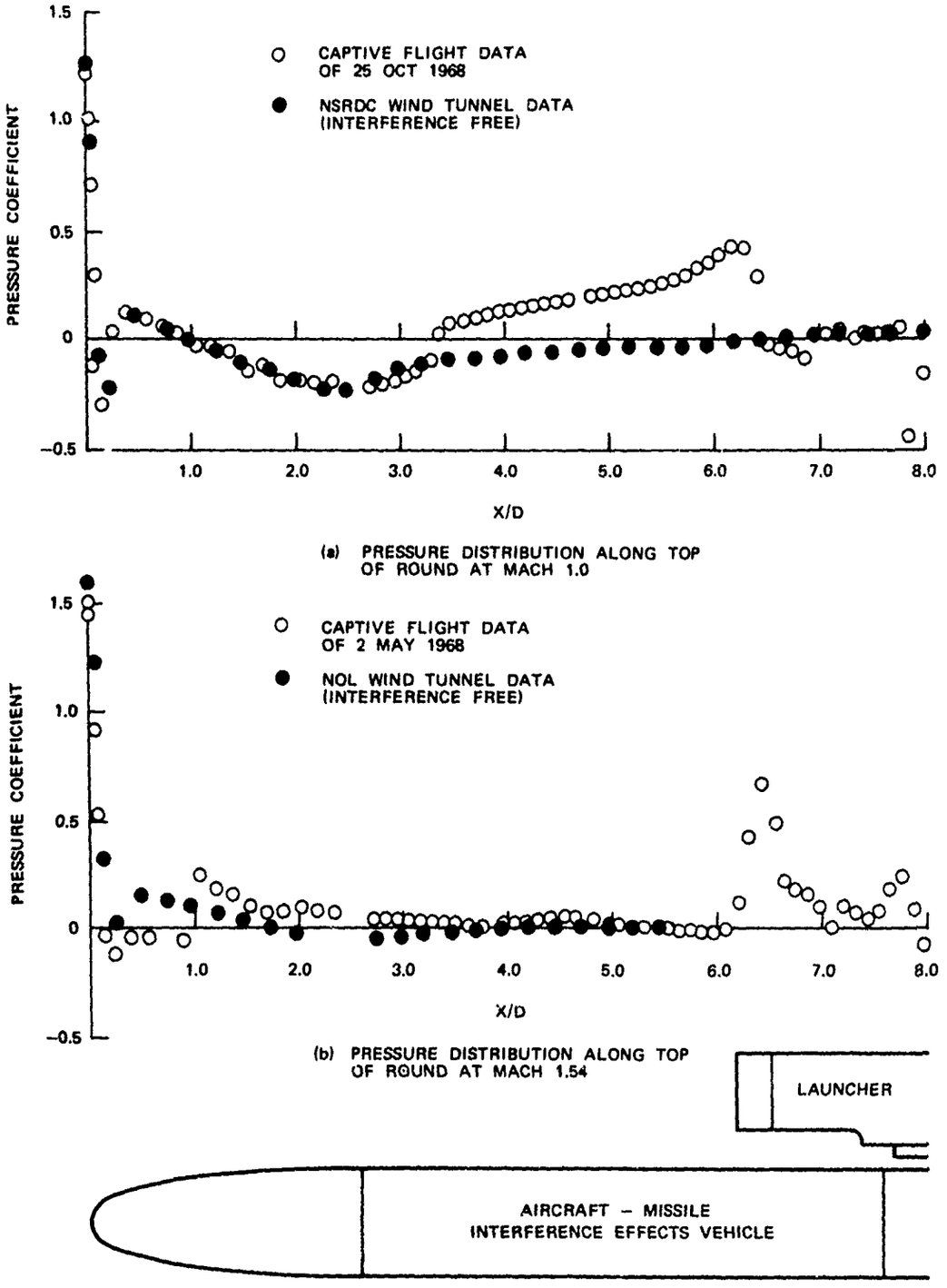

FIG. 5. COMPARISON OF CAPTIVE FLIGHT AND WIND TUNNEL PRESSURE DISTRIBUTIONS

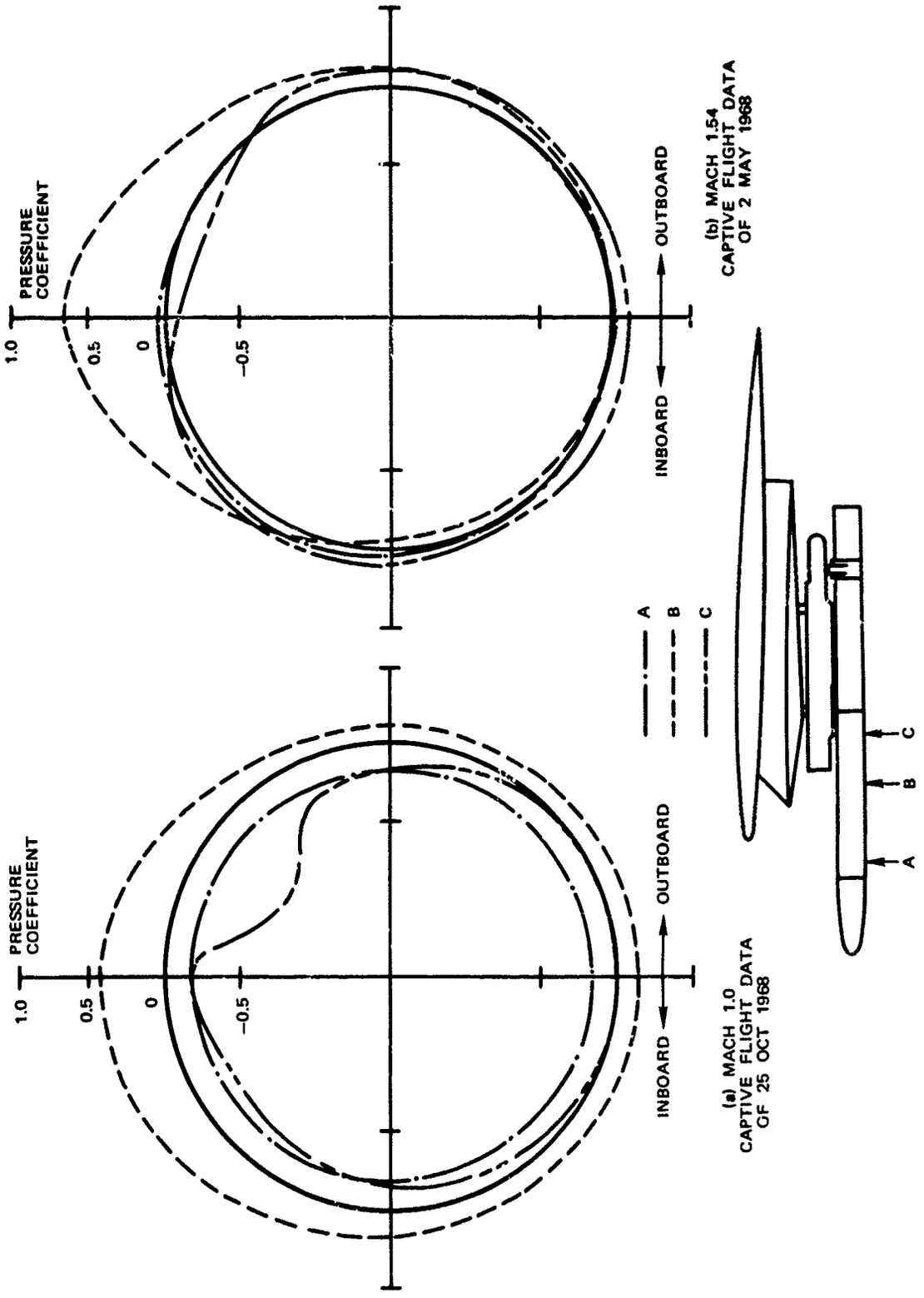

FIG. 6. CIRCUMFERENTIAL PRESSURE DISTRIBUTIONS AT MACH 1.0 and 1.54

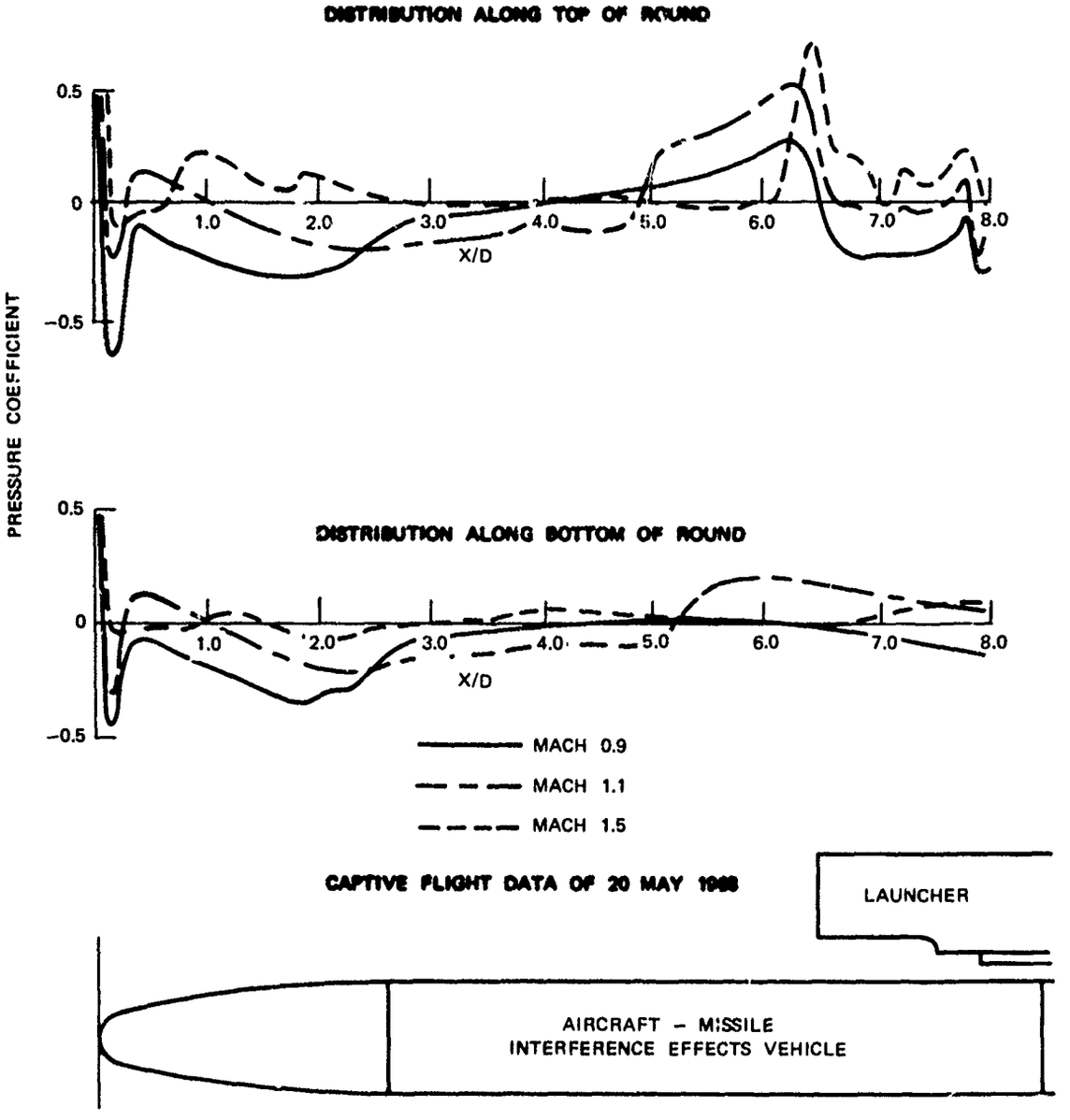

FIG. 7. VARIATION OF LONGITUDINAL PRESSURE DISTRIBUTION WITH MACH NUMBER

Paper No. 42

STORE SEPARATION FROM THE MCDONNELL DOUGLAS F-4 AIRCRAFT (U)

(Paper UNCLASSIFIED)

by

David L. Schoch
McDonnell Douglas Corporation
St. Louis, Mo. 63166

ABSTRACT. (U) This paper discusses the prediction of external store separation and jettison characteristics using theoretical techniques. It discusses the empirical approaches that have evolved at McDonnell during the certification of over thirty stores for the Navy/Air Force which has involved over 900 flights to accumulate the necessary information.

(U) The correlation of the flight data with the physical characteristics of the store is shown for a specific case and the usefulness of this technique in reducing the scope of a flight program and its inherent safety hazards is discussed.

(U) The correlation of wind tunnel data with flight data is presented and the applicability of the above technique to wind tunnel testing to further reduce the cost of certification is proposed.

INTRODUCTION

(U) Until recently the problems associated with external store separation and *jettison from aircraft have been given only a cursory examination during the design of aircraft and/or the stores themselves. This is understandable for two reasons: 1) the designer is primarily concerned with the aircraft performance which will sell his design, and 2) the main design mission of recent fighter-bombers, including the F-4, has been air-to-air and the air-to-ground mission has been a fall out. The F-4 is ideal for the study of the external store and jettison problem because of the large variety of stores which it can carry.

(U) In studying the separation problem we are concerned only with the store's motion from the instant of release until it is determined that the possibility of the store contacting the aircraft no longer exists. This portion of the store's trajectory is referred to as its separation characteristic or separation trajectory. During this initial phase of the store's total trajectory to the ground, its motion can be greatly influenced by the aircraft's flow field. The amount of influence that the flow field may have is determined to a great extent by the store's physical characteristics and its static aerodynamic characteristics. Therefore, for the purpose of separation analysis, external stores can be divided into four general categories:

1) Aerodynamically stable, high density
2) Aerodynamically stable, low density
3) Aerodynamically unstable, high density
4) Aerodynamically unstable, low density

(U) This paper is directed toward the study of the stores in categories (3) and (4) since the unstable nature of these stores is more likely to cause a collision with the aircraft than those in categories (1) and (2). A collision could seriously damage or even cause the loss of an aircraft.

*In this paper jettison will refer to the release of a store plus MER/TER combination.

THE F-4 AIRCRAFT AND ARMAMENT STATIONS

(U) Figure 1 illustrates the basic F-4 aircraft with the armament stations noted and pylons and ejector racks shown. There are nine armament stations; B.L. 0.0, left and right hand B.L. 81.50 stations, left and right hand B.L. 132.50 stations, and the four fuselage Sparrow III missile stations. Multiple ejector racks (MER) can be carried at the centerline (B.L. 0.0) and outboard (B.L. 132.50) stations. Triple ejector racks (TER) can be carried at all stations on the F-4B/J/K aircraft but only at the inboard stations (B.L. 81.50) on the F-4C/D/E aircraft. Separation of stores from the MER and TER is initiated by a single foot ejector inputing an average force of approximately 2000 lbs.

(U) Sketches of the MER and TER appear in Figures 2 and 3 which show the numbering system for the rack stations.

(U) Figures 4 through 9 are sketches of external stores mentioned in the text. These stores were selected for this paper because they are in categories (3) and (4) and flight test and wind tunnel test separation data are available for them.

FLIGHT TEST DATA

(U) Throughout this paper frequent mention will be made of separation trajectories obtained from flight tests. These trajectories are the result of reducing to time history form the translational and angular displacements of the store obtained from high speed, (200 frames per second) onboard, bore sighted, movie cameras. The data are reduced from camera pairs that allow triangulation. A computer program has been written to handle the calculations required.

(U) High confidence is placed in the accuracy of this data.

(U) Figures 10 through 14 illustrate the repeatability of the flight test data reduced in this matter and substantiate the high level of confidence.

SAFE SEPARATION CRITERIA

(U) The criteria for safe separation used by MCAIR during store separation flight test programs is dependent upon both the store and the aircraft armament station and rack station under consideration. The point or plane on the aircraft most likely to be contacted by the store at the given location is selected. Through this point or plane it is assumed passes an infinite horizontal plane. The store's center of gravity (c.g.) is displaced vertically from its stowed position and the store rotated nose up and nose down until contact with the infinite

plane occurs. This process is repeated at other vertical displacements (Z) and a plot of pitch angle (θ) versus ( ) is then made which represents a loci of contact points of the store with the selected plane. An illustration of a collision boundary is shown in Figure 15.

(U) Since it is inconvenient to correlate the histories of store pitch and vertical displacement with these physical collision boundaries, the variable time is eliminated by plotting the store pitch angle versus the vertical displacement of its center of gravity. Thus the store trajectories can be compared directly to a collision boundary. Any infringement of this boundary by the actual trajectory plots indicates contact with the aircraft or violation of the criteria established for safe separation from the aircraft.

(U) In the initial phase of the F-4 separation programs only three degrees of freedom were considered (longitudinal and vertical translational displacements and pitch angular displacement). Experience with the F-4 has shown that in most cases this is a valid simplification and that, if a problem is encountered in the yaw plane, an adjustment in the selection of the limiting horizontal plane, upon which the safe separation criteria is based, will in effect eliminate any situation where yaw would cause collision with the aircraft. An illustration would be to lower the collision plane to the bottom of the 370 gallon wing tank carried at B.L. 132.50 when concerned with the yawing outboard of stores separated from the B.L. 81.50 station.

(U) Another plot found extremely useful is a plot of pitch angle (θ) versus equivalent airspeed (V_{KEAS}) at store release for constant vertical displacements of the store center of gravity. It is realized that this plot assumes no Mach number effects and the flight data substantiate this assumption, i.e., the dominant effects are dynamic pressure and aircraft angle of attack. On these plots the previously discussed collision boundaries can be superimposed and the maximum and minimum safe separation/jettison speeds easily determined by a tangent line to the boundaries as illustrated in Figure 16. This plot, which is easily obtained by cross-plotting θ versus Z plots for varying release speeds, also is applicable only for a given aircraft and rack station.

(U) Recognizing this trend in separation characteristics with speed is a useful tool in MCAIR's empirical approach to separation/jettison analysis. Another obvious fall out from this type presentation is that it immediately identifies whether or not the store has critical separation characteristics. The more critical a store the steeper the slopes of the constant Z lines.

ANALYTICAL APPROACH TO PROBLEM

(U) Separation of an external store from an aircraft is a highly complex phenomena requiring detailed knowledge of the aircraft's flow

field influence on the store, the store's aerodynamic and physical characteristics, the release mechanism used, the dynamic characteristics of the store, and the physical installation of the store on the aircraft.

(U) In the process of certifying a number of Navy weapons and most of the Air Force "Seek Eagle" weapons, several theoretical approaches to predict store separation and jettison have been considered and ultimately dropped for various reasons. It is not the intention of the author to deny the usefulness of a theoretical solution to the problem but rather to indicate the limitations of the approaches considered in the day to day process of determining safe separation and jettison flight conditions in support of a flight test program where time available to do an analysis is often a limiting factor.

(U) There are two major problem areas in the analysis of store separation. The first is predicting the store's static stability characteristics. The second is determining the effect of the aircraft flow field on the store.

(U) The first problem area can usually be solved readily and with accuracy if the store is relatively simple, i.e., a body of revolution without bluff faces or bases. However, several of the more critical stores in category (4) have flat bottoms that are also open when empty. In these cases wind tunnel stability curves are a requirement since the analytical techniques available are inadequate.

(U) The second problem area is much more complex. Most techniques in the literature use potential flow theory (i.e., do not include viscous effects) with lifting line vortex theory. Special assumptions, such as an infinite cylinder or other body of revolution, are required in order to develop the flow field for the fuselage.

(U) The following analytical approaches or techniques are being or were considered by MCAIR in an attempt to obtain a suitable approach.

(U)] Flow angularities about the F-4 wing were calculated using Reference (1) and input to a six-degree-of-freedom computer program as a function of x, y, and z position. A comparison of a trajectory calculated using these data with a flight test trajectory is shown in Figure 17 for a BLU-1/B Napalm bomb carried directly on the pylon at the inboard station. The agreement is good when it is considered that the angle of attack at the c.g. of the store will not necessarily be the effective angle of attack on the total body, i.e., some adjustment must be made for the fact that the nose of the store may be in the wing upwash, etc. Methods of averaging the local angles of attack or dividing the body into sections and considering the α's on the various sections are being investigated.

(U) A similar comparison was made for the BLU-1/B separated from a TER at the inboard station (Figure 18). In this case the correlation is not as good as the previous one and indicates that the effect of the

rack on the flow field is significant. The results are not considered satisfactory and there is no technique within Reference (1) to account for the effect of the pylon-rack-multiple body on the flow field.

(U) 2. The approach used in Reference (11) has been tried and modified. This technique involves using the stowed store loads obtained from wind tunnel tests and assuming that the aircraft's influence will disappear entirely at some vertical displacement from the aircraft. A simple ramp and/or step function was used without satisfactory correlation with the flight test data.

(U) The loads were then assumed to vary in the same matter as the downwash angle was found to vary from Reference (1). A comparison of a simulated trajectory and flight test data is shown in Figure 19. The results are very good. However, measured stowed loads for all the possible store combinations are often not available prior to separation flight testing.

(U) 3. A computer program, Reference (8), has been written using potential theory to calculate the pressure distribution about an aircraft and any attached body or multiple bodies in the aircraft's flow field. Once the pressure distributions are determined, they must be integrated into forces and moments for input into the equations of motion. Then a step integration can be conducted over a small time increment and the whole process repeated until sufficient aircraft clearance is obtained. This technique is under consideration at the present but no results have been obtained to date.

(U) The requirements placed on a completely analytical approach obviously are high and are probably best illustrated by examples.

(U) A. The technique must take into account the actual fuselage shape and any small protuberances. An illustration of the effect of small changes in configuration moldline on store separation is illustrated in Figures 20 through 23. Figure 20 shows the difference in nose shape between the F-4E and F-4C aircraft. Figure 21 shows reduced flight test data for BLU-1/B is released at the same flight condition from an F-4E and F-4C. In the case of the F-4C a clean separation was obtained whereas from the F-4E the store contacted the aircraft as indicated. Comparison of similar data on other stores indicates the same trends.

(U) As another example, Figure 22 illustrates the moldline change between the F-4B and F-4K aircraft. The difference in separation characteristics obtained at the same flight condition is shown in Figure 23.

(U) B. The approach must also account for the effect of all bodies in the vicinity of the store being separated. This would include the pylon, MER or TER, and other stores being carried at the other rack stations. An illustration of the differences caused by the presence of other bodies is illustrated by the in-flight separation of five unfinned

CBU-39's from the left and right inboard armament station of an F-4C. As can be seen in Figure 24, the outboard stations rotated sharply nose up while the inboard stores rotated nose down. This difference is most likely caused by a combination of effects. The two dominant effects are (1) the differences in B.L. location, i.e., the outboard stores extend further forward of the wing leading edge, and (2) the presence of the pylon and rack and their effect on the spanwise flow and the local flow field. The differences in separation trajectories between the two outboard and between the two inboard stores can be attributed directly to the presence of another store, i.e., the L/H outboard store was released with the inboard store attached, while the R/H outboard store was the last store to be released.

(U) In summary, there are theoretical techniques available to provide useful information concerning a store's separation characteristics. However, addition techniques must be developed to provide complete theoretical solution.

MCDONNELL'S APPROACH TO ANALYSIS

(U) During the last five years McDonnell has flown over 900 flights for the purpose of separating or jettisoning external stores from an F-4 aircraft. Each of these flights required estimates of the separation characteristics of the store prior to flight. The following outlines the procedures used by McDonnell during this period. These approaches to the problem of determining weapon release placards have evolved over the years with refinements being made as more experience and flight test data were obtained.

(U) At the initiation of F-4 testing of a particular store, applicable flow field information is not always available and an alternate approach to calculating a flow field is undertaken. A rough estimate of the separation trajectory can, of course, be made assuming no aircraft influence and in the case of a heavy, highly stable store the error may not be large. However, this can lead to serious errors when analyzing low density, high volume, unstable stores. To account for this possibility a "flow field" is superimposed and a so-called "sensitivity" study is conducted on the store. The "flow field" imposed is nothing more than a gross flow angularity. The "sensitivity" study is a parametric study, with aircraft speed and flow angularities the variables to establish the initial flight test point. The determining criteria is to test initially at that speed where large variations in the input flow field will not cause the store to collide with the aircraft.

(U) The "best" or "safest" speed at which to initiate the flight program is usually determined by assuming no flow field effects and varying air speed only. A plot of pitch angle versus air speed for constant vertical displacements is made and the speed at which the

least rotation occurred (as noted in Figure 16) was selected. Permutations in flow angularity ($\pm 5°$) are superimposed on the freestream at this speed to determine the store's sensitivity to these changes. For a low density unstable store this study is repeated at several speeds on either side of the indicated best speed and the speed at which the variations in flow field produce the least changes in the store's separation characteristics is selected to initiate flight testing.

(U) Once the initial flight test is conducted and time histories of the trajectory obtained from the onboard cameras, the flight test data is compared to the various estimates to determine which gross flow angularity provides the best "simulation." This flow field approximation is then used to predict trajectories at small increments above and below the tested point (usually 25 to 50 knot increments). If at these speeds the trajectories are acceptable (no collision indicated) additional separations are conducted at these conditions. Once flight test data at these conditions are obtained a plot of θ versus V_{KEAS} is made. Extrapolation of the flight data is then made based on the three flight points obtained and the separation envelope expanded in increments of approximately 25 knots until the collision boundary on the extrapolation indicates unsafe separation.

(U) A refinement to this approach is to eliminate the parametric study on flow angularities for a new store. To permit this, the previously tested store most similar to the new one is chosen and the gross flow angularity providing the best best flight "match" is used to obtain predicted trajectories for the new item. Again the results are summarized in a θ versus V_E plot and the store's collision boundary superimposed. Reasonable increments in speed, considering flight safety, from the high and low ends of the predicted safe envelope are selected and the store flight tested at these conditions. The same technique described above is applied as the collision boundaries are approached.

(U) An attempt to further refine the analysis and better determine the flow field and its effects of separation has been conducted. This method consists of utilizing flight test time histories and graphical techniques to find accelerations, thus forces and moments as a function of time. These forces and moments are then converted to coefficient form and plotted against store pitch angle which in turn can be related to the store's freestream anlge of attack. The freestream static stability characteristics are then superimposed and the increment in coefficients from this curve are then assumed to be the effects of the aircraft's flow field which can be determined as a function of Z. This flow field information is then used to predict the trajectory of similarly shaped stores or to extrapolate the release characteristics of the same store to a higner speed.

(U) In general, the approaches have been very successful. Figures 25 and 26 are comparisons between flight data and predictions. Out of an approximate total of 2000 different separation and jettisons, less

than one percent resulted in any type of contact with the aircraft and all but one of these were of a minor nature.

(U) The sensitivity of some of the stores tested on the F-4 to speed (i.e., flow field) is extremely high and therefore dangerous to flight test. For example, the Suu 13 dispenser, a flat open bottom unstable store of low density, has extremely critical separation and jettison characteristics. In fact, the entire separation envelope is a single speed at the outboard armament station (B.L. 132.5). Although each store individually may be safe over a small speed range, 400 KCAS is the only speed compatible with all stations. Without previous flight data on other stores and the application of the analysis techniques developed by McDonnell, it is doubtful that this single safe separation speed could have been predicted.

(U) Similar problems were encountered with other stores and accurately predicted. The Suu 41/A, another dispenser very similar from separation considerations to the Suu-13/A, does not have a single speed for safe separation that is compatible with all three rack stations. This situation was predicted using the gross flow angularity and verified by flight test. The results were the bottom rack position was cleared at the single speed of 310 KCAS below 20,000 feet, the inboard shoulders over the speed range 310 - 350 KCAS below 20,000 feet and the outboard shoulder at the single speed, 350 KCAS below 20,000 feet.

JETTISON

(U) The discussion so far has centered on separation. Some particular attention should be given to the jettison of a store or stores plus MER/TER combination. This is by far the more difficult of the two releases to predict since the freestream aerodynamic characteristics of the rack and store combinations are extremely difficult to arrive at analytically. Also the flow field influence is larger due simply to the larger size, particularly the longer length when jettisoning a MER.

(U) Air Force and Navy criteria for jettison limits require that the limits that appear in the Pilot's Handbook must be applicable to any partial loading of the store on the rack that can occur. This amounts to a total of 64 combinations for a MER unless carried at the centerline where symmetry will halve that number. Of course, the object is to test only those loadings considered the most critical, thereby clearing the rest. This obviously assumes that the critical loadings can be determined using an analytical approach. Many of the loadings can be eliminated by a simple comparison of the weights and moments of inertia with the force and moment coefficients developed. McDonnell has developed what are considered to be critical loadings from the results of many jettisons made in flight. These configurations are usually one or two stores forward or aft on the MER. For

the TER at 81.50 it is a single store on either the outboard or inboard shoulder.

(U) As in the case of separation, the same partial loading is not the most critical for both the nose up and nose down cases. The object again is to find the speed range where the two critical configurations will overlap.

(U) Jettison of MER/store combinations from the B.L. 132.50 and centerline stations is accomplished by "free fall." This is merely opening the hooks retaining the MER and allowing it to drop away. This method is used because of the large center of gravity shifts that occur for partial loadings on the MER. A forced ejection would induce large pitching moments making an overlapping speed for all partial loadings very difficult, if not impossible, to achieve.

(U) The TER's at B.L. 81.50 on Air Force aircraft (F-4C/D/E) are force ejected from the pylon while on Navy aircraft (F-4B/J) the 81.50 TER's are jettisoned along with the pylon which is constrained at the rear to pivot through an angle of 11° before releasing from the wing.

(U) The criteria for safe jettison is the same as that for safe separation (i.e., the collision boundaries are established in the same matter). The analysis and methods used to predict separation were used also to predict jettison. The same trends with speed hold also.

(U) Since the static stability characteristics of a rack/store combination are extremely hard to estimate; the data obtained from "flight matches" using the gross flow angularity or incremental coefficient approach must be approached with caution. Such data may contain hidden adjustments to the static stability required to obtain proper correlation. However, if a consistent procedure is used to obtain these stability characteristics, the adjustment required should be similar and the extrapolation from store to store valid.

(U) In general, the results using these techniques to analyze jettison were considered very acceptable.

CORRELATION OF TRAJECTORIES AND PHYSICAL CHARACTERISTICS

(U) As the inventory of external stores carried on the F-4 aircraft grew and the effort required to support a flight test weapon separation/jettison program increased, it became obvious that a correlation between the store's physical characteristics (i.e., known quantities) and its separation characteristics would provide a very valuable asset, would eliminate the need for flight matches to obtain flow fields, and could reduce the scope of flight programs.

(U) All the factors affecting a separation trajectory were listed in detail. They were the store's static stability characteristics; its weight, moment of inertia and c.g. position; the aircraft armament

station and TER or MER station; and the flight condition (speed, altitude, load factor, dive angle and angle of attack). Since a plot of θ versus Z is the ultimate goal of a trajectory analysis, the correlation must involve these two parameters. Obviously the aircraft station and rack station did not relate to the store's physical characteristics and so it was determined that they should remain fixed. The same was true for the flight condition at release. The remaining parameters were weight, moments of inertia, and the store's stability. Examination of these parameters suggested the possibility of relating the store's accelerations to its vertical and angular displacement. The forces and moments, if one choses to forget the aircraft's influence temporarily, are primarily related to the store's aerodynamic characteristics, i.e., C_{M_α} and C_{N_α}. The "acceleration" terms then become C_{M_α}/Iy and C_{N_α}/W. It was desired to only have one term to define the store since both θ and Z are required to define the trajectory and four variables become awkward. Therefore, the parameter

$$\frac{C_{M_\alpha}}{Iy} \quad \frac{C_{N_\alpha}}{W}$$

was selected. Another parameter affecting the store's trajectory is the ejector foot-center of gravity relationship. In order that this would not initially confuse the picture, it was decided to correlate centerline "free fall" MER jettison results. It was found that a correlation did exist and that if a factor were introduced to account for a $C_{M_O} \neq 0$, better correlation was obtained. Another modification to refine it further was necessary in the case of stable configurations to account for the fact that they tend to oscillate about a trim angle of attack. This was accomplished by adjusting the pitch angle to account for the configuration trim angle of attack. The final results appear in Figure 27 which shows the correlation established for the jettison of a store located on the aft shoulder of the MER at the aircraft centerline station at a speed of 400 KEAS. Flight data is available at the point indicated. Similar correlations at 350 and 450 KEAS are presented in Figures 28 and 29.

(U) Similar charts for separation of a store from station 2 of the R/H 81.50 armament station were constructed. Since forced ejection is used, thereby inducing additional store pitching moments, the variations in c.g. position relative to the ejector foot must be considered. To arrive at these charts the flight data was first matched as indicated earlier to obtain a flow field effect. Then trajectories for variations in c.g. position were calculated. The results appear in Figures 30 and 32 for the specific case indicated.

(U) A note of caution; in as much as this correlation is highly dependent on the stability characteristics estimated, the same method should be used for each configuration. If different methods give different results for the same store, they obviously can not be interchanged in the correlation. However, as long as a consistent approach

is used, the correlation is valid.

(U) With a series of these curves covering a speed range, the previously discussed plot of θ versus V_{KEAS} can be constructed for a given rack station. The collision boundary for a new store can readily be developed and superimposed to determine the limiting conditions. The benefits of having this type of correlation to predict the characteristics of a new item are 1) it is quick, 2) it reduces the flight test safety hazard, 3) it reduces the flight test program required to certify the store, and 4) it eliminates the need to know the flow field for each separation. The emphasis in this preliminary study was on unstable stores since, usually, they represent the majority of separation problems. The data included is specifically for the F-4. However, the trends and correlation methods established are applicable to other aircraft.

(U) It would be advantageous to establish these charts for a new aircraft using methods other than flight data, e.g., wind tunnel techniques.

WIND TUNNEL TECHNIQUES

(U) At present there are three types of wind tunnel testing available to aid in predicting store separation characteristics. They are: 1) captive trajectory, 2) grid survey, and 3) dynamic drop techniques. Each has limitations and areas where one can be favored over the other. For example, the captive trajectory technique can simulate missile launches where the dynamic drop test cannot. However, the captive trajectory is not as suitable for unstable store separation and jettison where high pitch rates are involved, i.e., sting model interference and physical travel limitations on the driving mechanism are often encountered. It is not the purpose of this paper to examine the pros and cons or limitations of the techniques but to present the results of some tests conducted by McDonnell and discuss the usefulness of these results in conjunction with the correlation methods established. Comparison of captive trajectory testing results for several conditions and stores is shown in Figures 33 through 36. The agreement of the data shown in Figures 33 and 34 is good but in the case of highly unstable stores the amount of data obtained before sting interference occurs leaves something to be desired. However, the initial trends are in agreement with the flight data. The data shown in Figures 35 and 36 does not agree as well as would be desired in the pitch plane for the highly unstable stores. This is probably due to the fact that these data were obtained by linearly interpolating data at .5° and 3.4° aircraft angles of attack to the flight test angle of attack, while the actual variation may not be linear.

(U) An alternate approach using the same system is the grid survey. This involves positioning the store under study on a sting and obtaining

the force and moment coefficients at several Mach numbers and aircraft angles as the store is traversed along selected aircraft waterlines and buttlines at several store pitch and yaw angles. The data thus obtained are input to a computer program where, utilizing the general equations of motion, the separation characteristics may be computed at the desired release conditions.

(U) This procedure allows large parametric analyses to be conducted and eliminates the need to return to the tunnel for new conditions, etc. As a case in point, grid data for the Sparrow III missile obtained in 1958 is still being used to evaluate new launch parameters.

(U) Only a minimum of experience has been obtained by McDonnell using the "free fall" technique and that was qualitative, i.e., the data was not reduced to time history form for comparison with reduced flight data. Much work in this area has been done at the Naval Ship Research and Development Center but direct comparisons with flight data were not obtained. MCAIR has plans for future testing of this nature to establish correlation between flight and tunnel data. Reference (19) illustrates the use of this test technique to evaluate various partial loadings for jettison.

(U) The significance of establishing a means of simulating separation, launch or jettison characteristics by analytical and/or wind tunnel techniques that agrees with flight data cannot be over emphasized.

CONCLUSIONS

(U) The separation/jettison test programs conducted on the F-4 have been very successful using the semi-empirical method outlined herein. The technique utilizes previously obtained flight data to define "flow field" effects to predict separation characteristics of new stores. Three significant results can be concluded from the large bulk of flight test data accumulated on the F-4: (1) store separation characteristics from an aircraft do follow predictable trends as indicated by the plots of θ versus V_{KEAS} obtained from flight data. (2) A correlation can be established between the physical characteristics of the store and its trajectory from a given rack and aircraft station. (3) Mach number effects are small, i.e., the angle of attack and "q" effect are dominent and the Mach number effects are not noticeable at constant altitude conditions.

(U) The proper use of a wind tunnel simulation technique and/or analytical techniques to establish the tables of correlation is of great value in flight test certification of weapons on the F-4.

(U) The analysis techniques and methods established during the F-4 program have direct application to similar programs on future aircraft.

REFERENCES

1. Alford, William J., Jr., Theoretical and Experimental Investigation of the Subsonic Flow Fields Beneath Swept and Unswept Wings with Tables of Vortex-Induced Velocities, NACA Report 1327, 1957.

2. Anonymous, Satisfactory Separation of Airborne External Stores; General Design Procedure for, Aerial Measurements Laboratory, Northwestern University, Memo No. M-409, October 1964.

3. Bamber, Millard J. and Davidson, H. D., Equations for Computing Trajectories of a Store Launched from an Airplane, David Taylor Model Basin Aero. Report 981, September 1960.

4. Bamber, Millard J., Store Separation Investigation by Grid Method Using Wind Tunnel Data, David Taylor Model Basin Report 2202, April 1966.

5. Beechum, L. J., A Technique for the Simulation of Store Release At High Speeds, British (RAE) TN Aero. 2964, May 1964.

6. Blacis, Robert L., High Speed Store Separation-Correlation Between Wind Tunnel and Flight Test Data, AIAA 68-361.

7. Geier, Douglas, and Carlson, Harry W., Measurements of Static Forces On Externally Carried Bombs of Fineness Ratios 7.1 and 10.5 in the Flow Field of a Swept-Wing Fighter, Bomber Configuration at a Mach Number of 1.6, NACA RM L56K30, January 1967.

8. Hess, John L. and Smith, A. M. O., Calculation of Non-Lifting Potential Flow About Arbitrary Three-Dimensional Bodies, Report No. E.S. 40622, 15 March 1962.

9. Galigher, Lawrence L., Separation Characteristics of the SUU-41 Dispenser from the F-4C Aircraft at Mach Number from .5 to .9, AEDC TR-68-191, September 1968.

10. Hess, John; Giesing, Joseph; Faulkner, Sue, Comparison of Experimental Pressure Distributions with Those Calculated by the Douglas Neumann Program, Report No. LB31831, 1 December 1964.

11. Jendras, Steve J., The Effect of Release Mechanics on the Separation of an External Store from a High Speed Aircraft, Saint Louis University, 1968.

12. Marantz, Charles S., Unsteady Aerodynamic Effects on External Store Separation Characteristics, Stanford University Department of Aeronautics, Memo No. M-409, October 1964.

13. Martin, Joseph C. and Hubai, Paul, III, "A Wind Tunnel Investigation of the Separation of Partially Loaded Racks from a 10-Percent Scale F-8 Crusader," Naval Ship Research and Development Center, Test Report AL-50, June 1968.

14. Moskowitz, Barry, Approximate Theory for Calculation of Lift of Bodies, Afterbodies, and Combinations of Bodies, NACA TN 2669, April 1952.

15. Reynolds, John H., A Stretch Computer Program for Determining the Effects of Launch Disturbance on the Initial Motion of a Bomb, USN Naval Weapons Laboratory Report TM-K-12/67, February 1967.

16. Sadler, R. and Wiley, M., External Stores Separation Under Subsonic Conditions, Northwestern U. A.M.L. Memo 432.

17. Solarski, A; Turner, R.; Doerr, F.; Dynamics of Separating Bodies Vol. I Theoretical Analysis, AF DSR-109 (Headquarters Office of Aerospace Research Technical Report) Office of Research Analysis; Hollman Air Force Base, New Mexico, November 1963.

18. Sowyrda, Alexander, Theoretical Aerodynamic Forces and Moments on a Bomb in the Vicinity of an Aircraft Wing at Subcritical Mach Numbers, Cornell Aerodynamic Laboratory Report GC-910-C-5, April 1956.

19. Trobaugh, Lynn A., Investigation of the Utility of Low Speed Dynamic Model Tests for Aircraft Store Launch Research, Aerodynamics Laboratory, David Taylor Model Basin, Department of the Navy Test Report AL-36, January 1967.

Figure 1 Basic F-4 Airplane

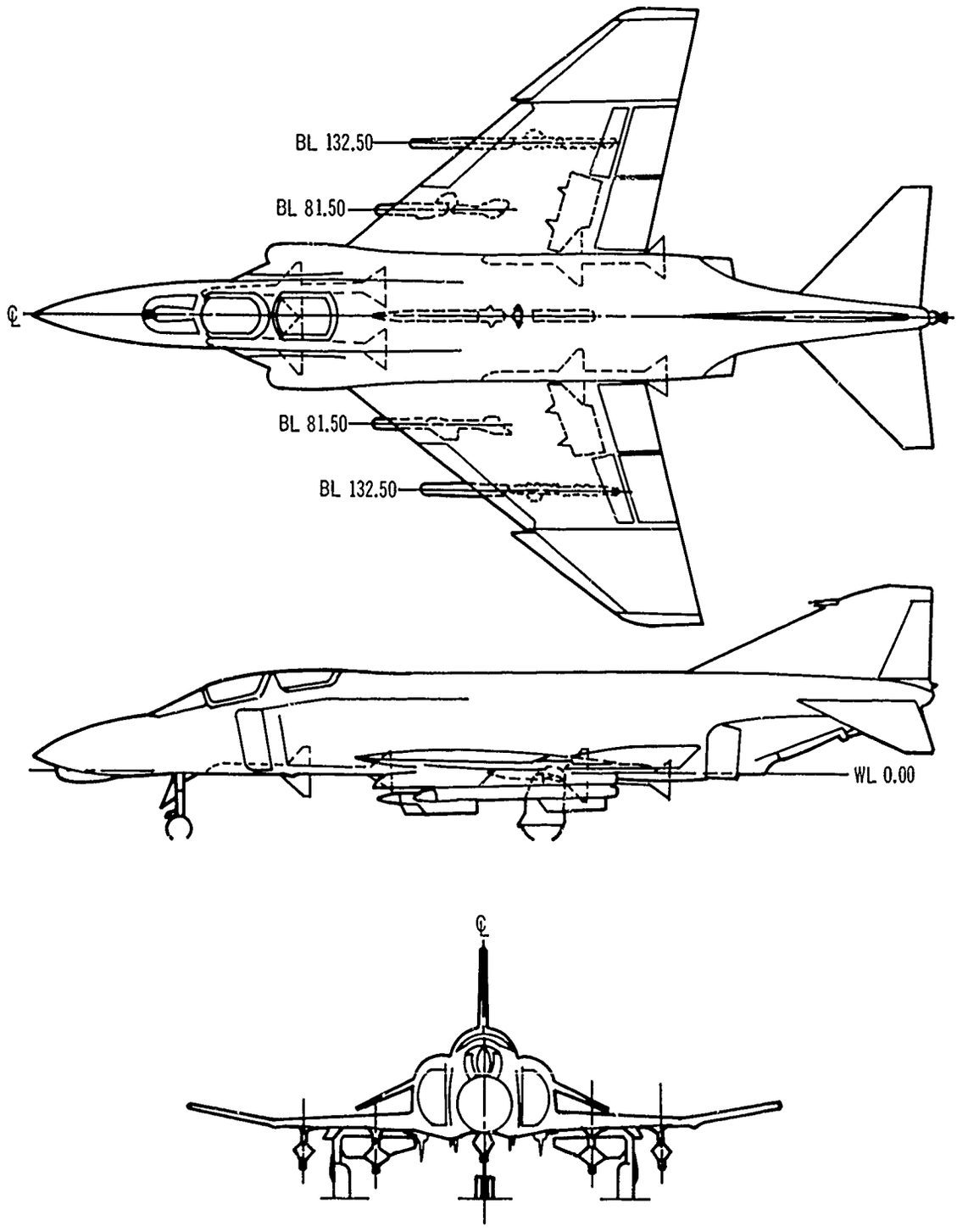

Figure 2 Multiple Ejector Rack (MER)

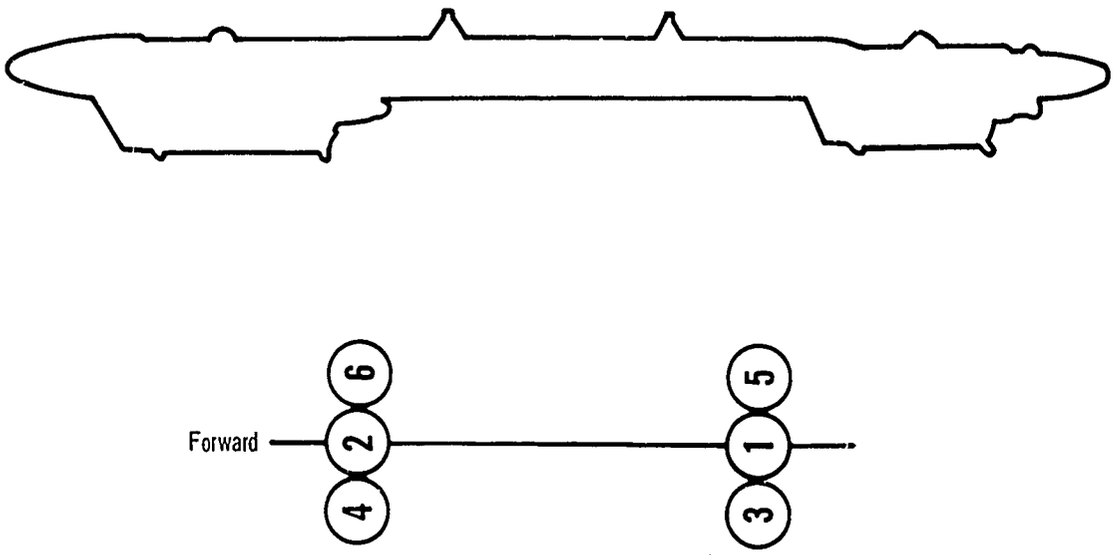

MER Station Numbering

Figure 3 Triple Ejector Rack (TER)

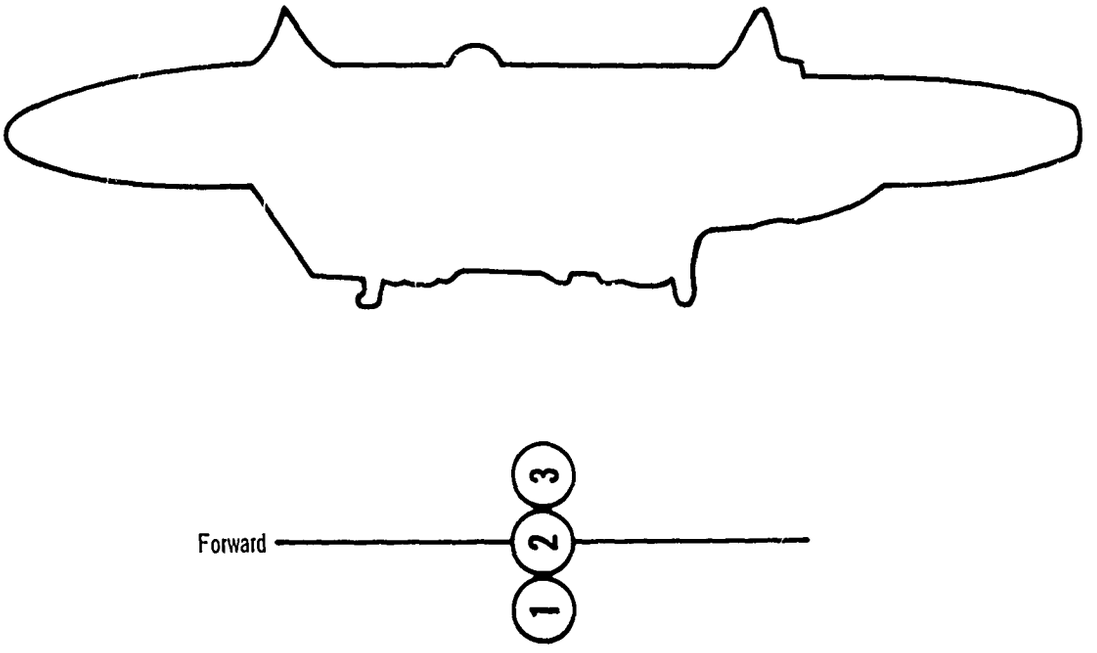

TER Station Numbering

Figure 4 CBU–28 Without Tail Cone

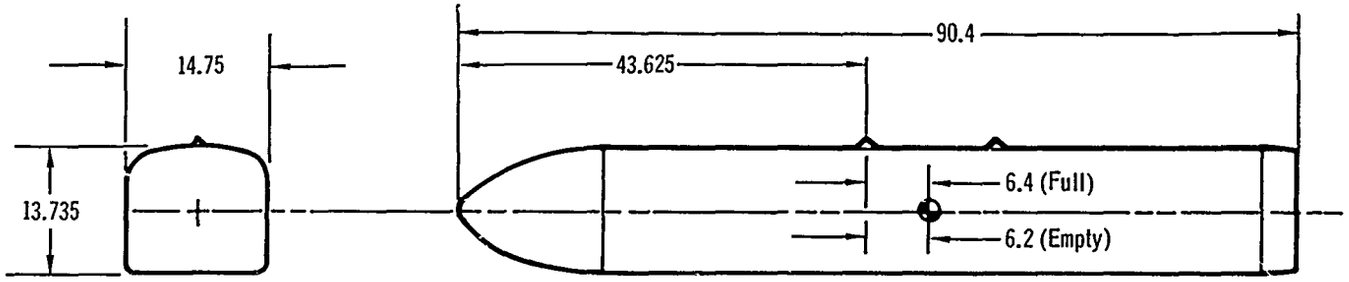

Weight	450 Lb
Reference area	1.465 Sq ft
Reference length	1.212 Ft

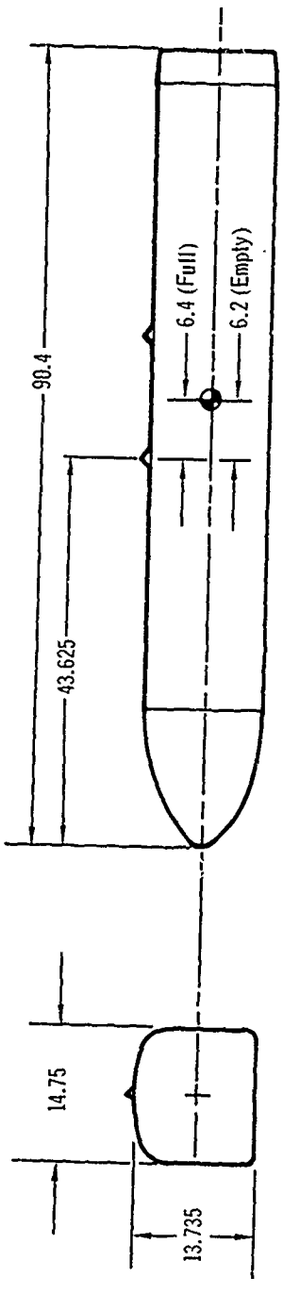

Figure 5 SUU-13/A Without Tail Cone

Weight	136 Lb
Reference area	1.465 Sq ft
Reference length	1.212 Ft

Figure 6 SUU–41 Without Tail Cone

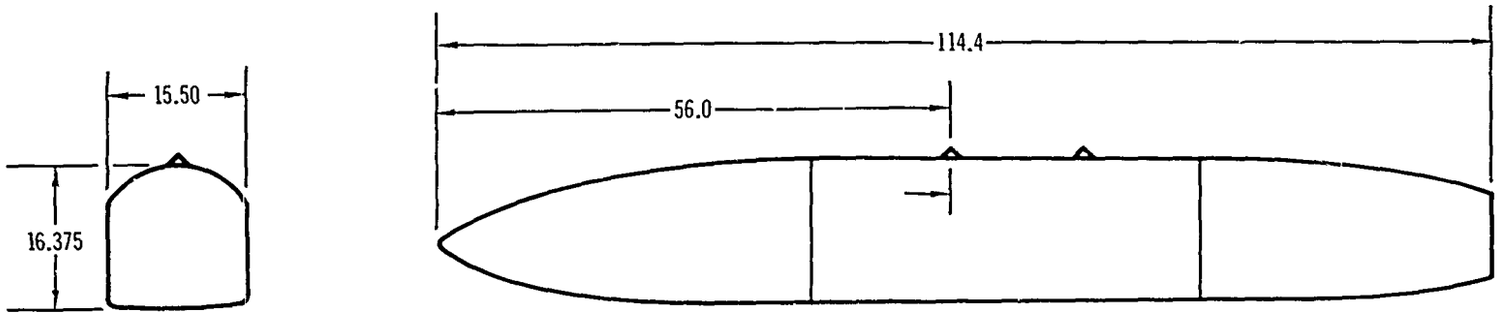

Weight	194 Lb
Reference area	1.50 Sq ft
Reference length	1.32 Ft

Figure 7 CBU-39 Without Tail Cone

Figure 8 BLU-1/B Fire Bomb

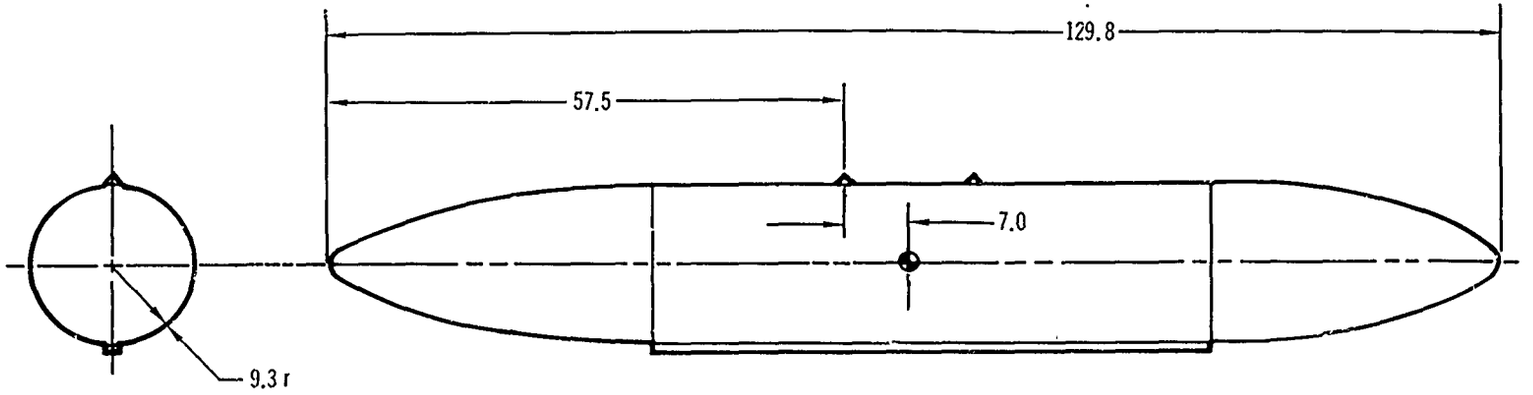

Weight	700 Lb
Reference area	1.886 Sq ft
Reference length	1.53 ft

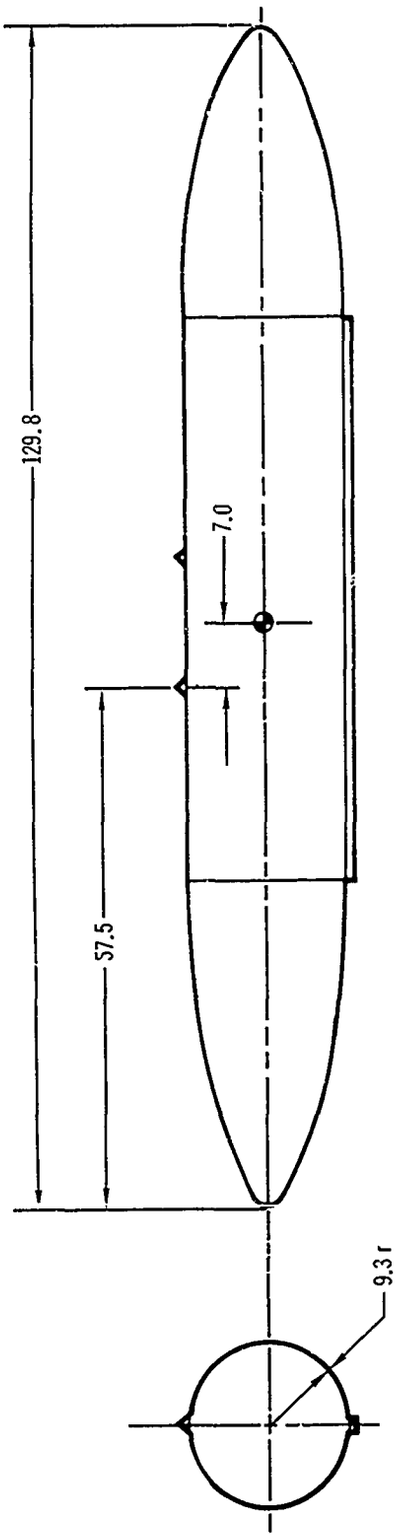

Weight	850 Lb
Reference area	1.886 Sq ft
Reference length	1.53 Ft

Figure 9 BLU-27/B

Figure 10 Model F–4E Flight Test Repeatability
Separation Trajectories for BLU–1/B from Aircraft Centerline Station and MER Station One

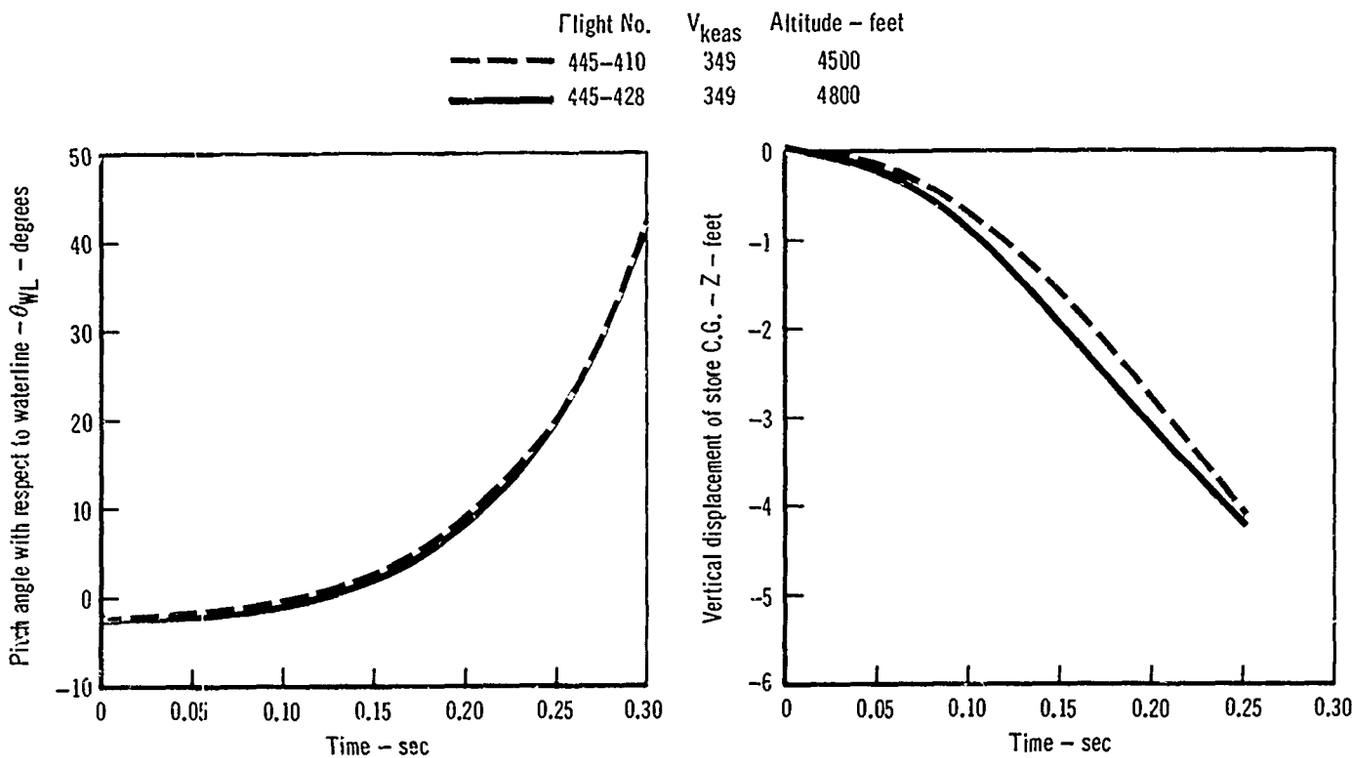

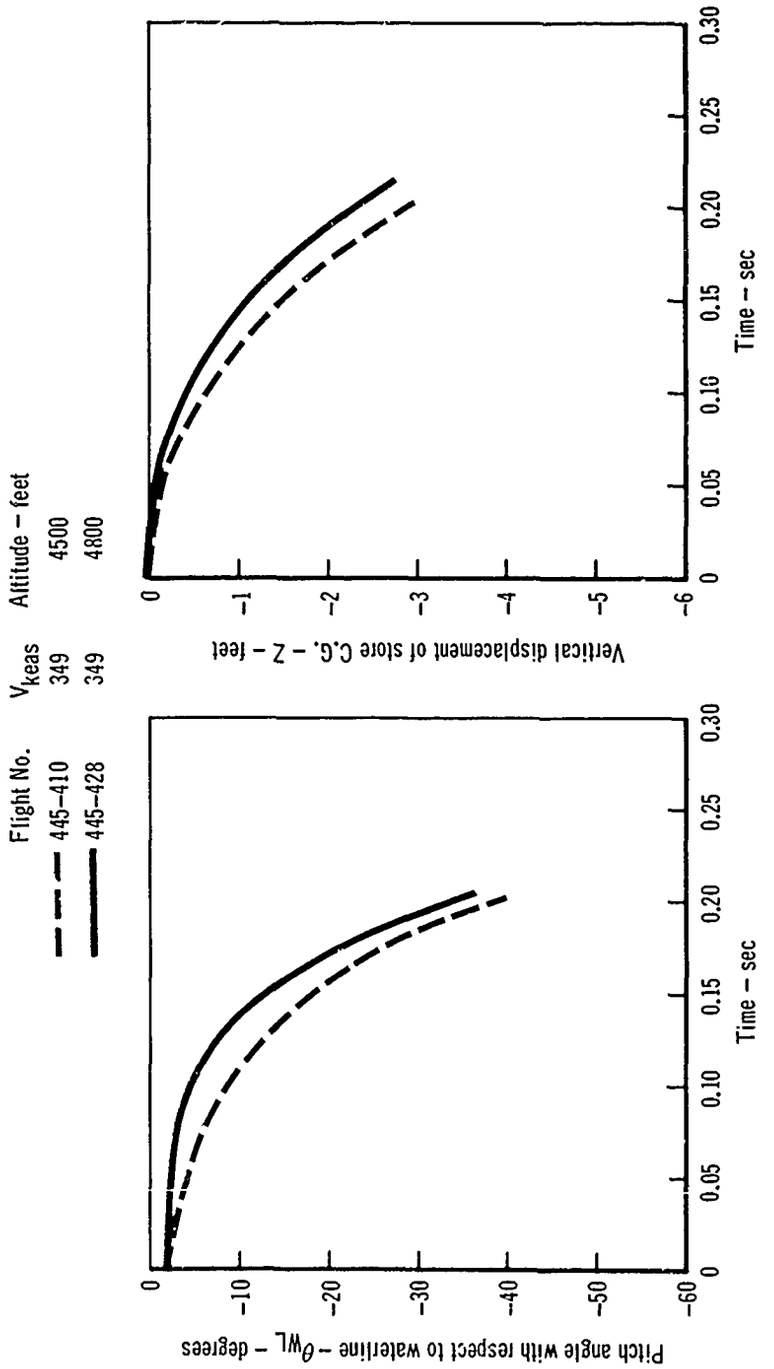

Figure 11 Model F–4E Flight Test Repeatability
Separation Trajectories for BLU–1/B from Aircraft Centerline Station and MER Station Four

Figure 12 Model F–4E Flight Test Repeatability
Separation Trajectories for BLU–1/B from Aircraft Centerline Station and MER Station Six

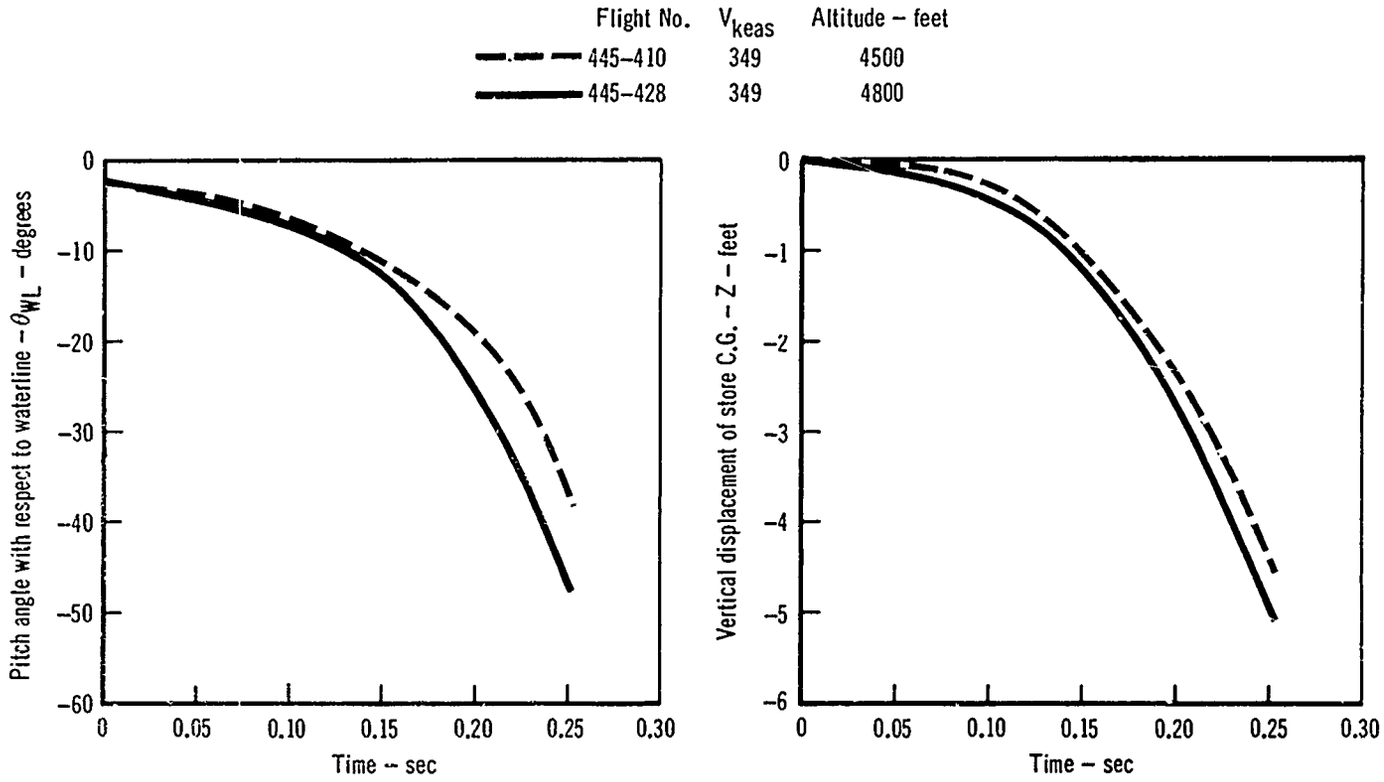

Figure 13 Model F–4D Flight Test Repeatability
Trajectories of Jettison of (3) CBU–39's and TER from the Aircraft BL 81.50 Station

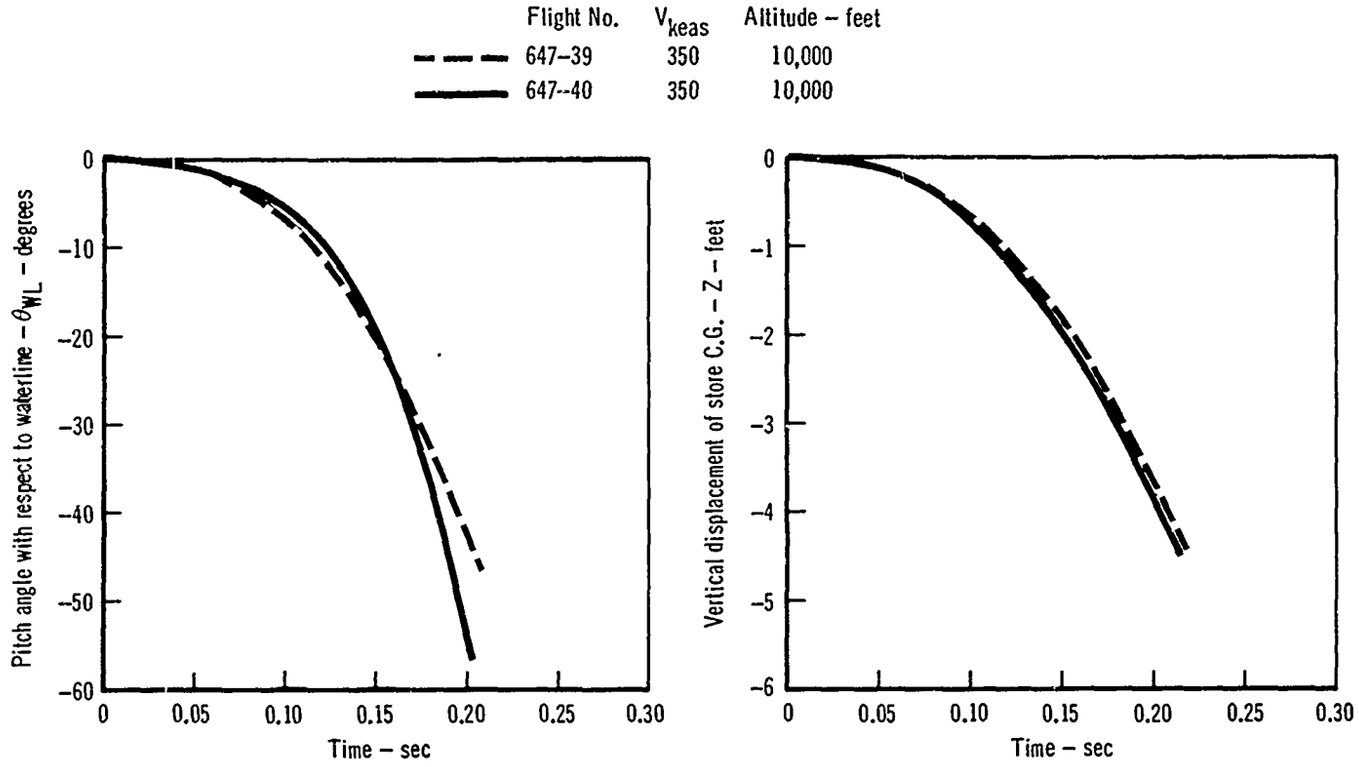

Figure 14 Model F–4D Flight Test Repeatability
Trajectories of Jettison of (3) SUU–41's and TER from the Aircraft BL 81.50 Station

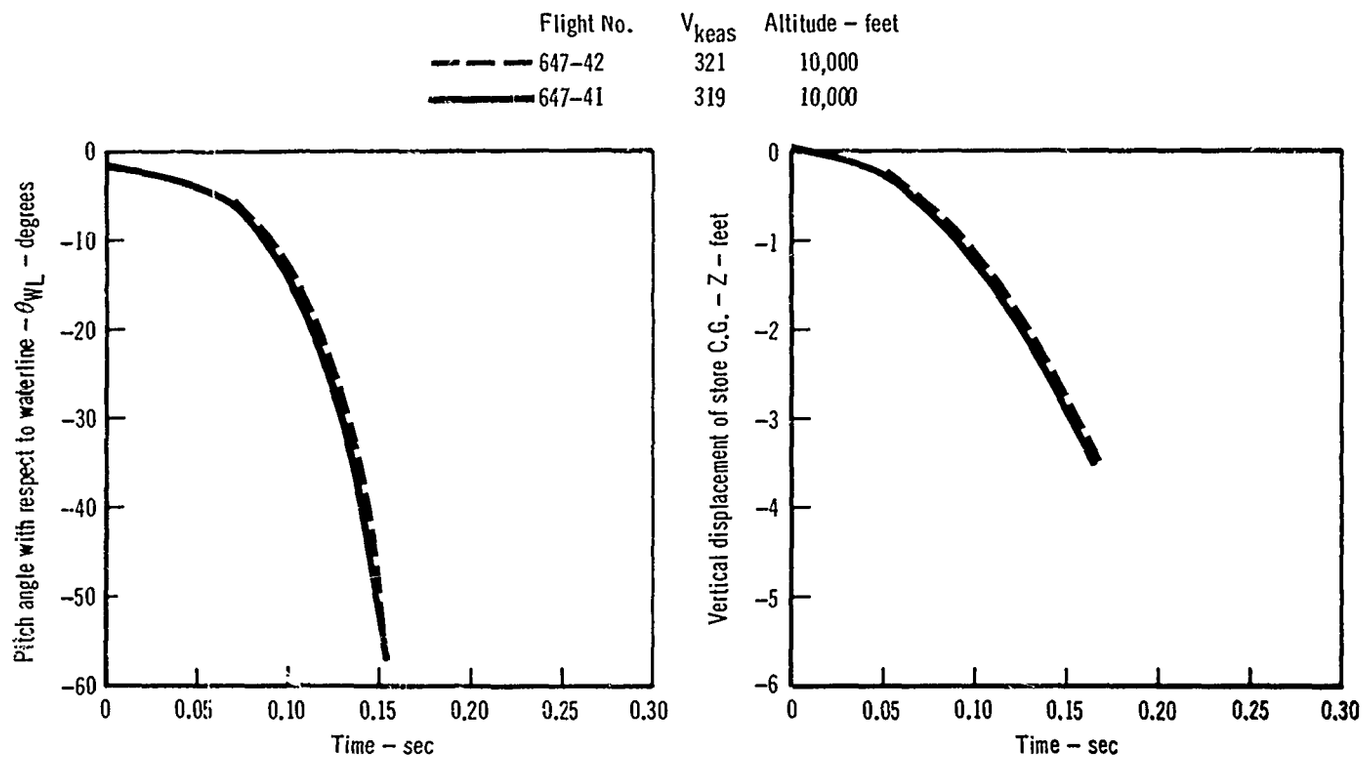

Figure 15 Collision Boundaries

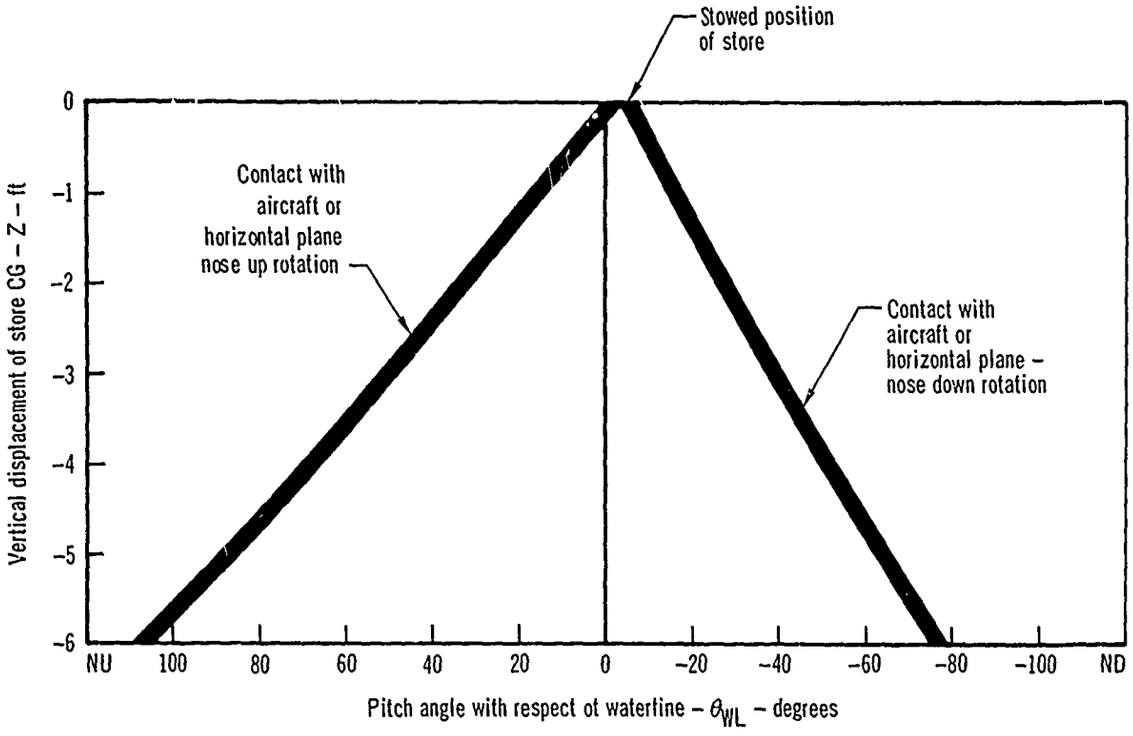

Figure 16 Effect of Speed on Separation Characteristics

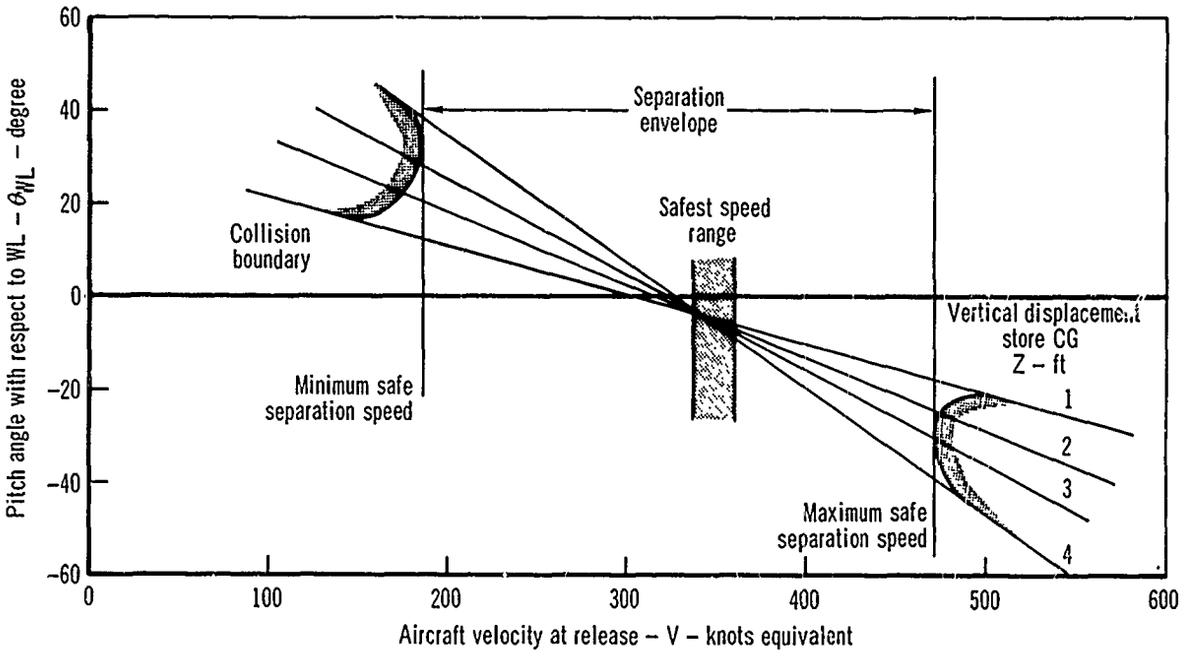

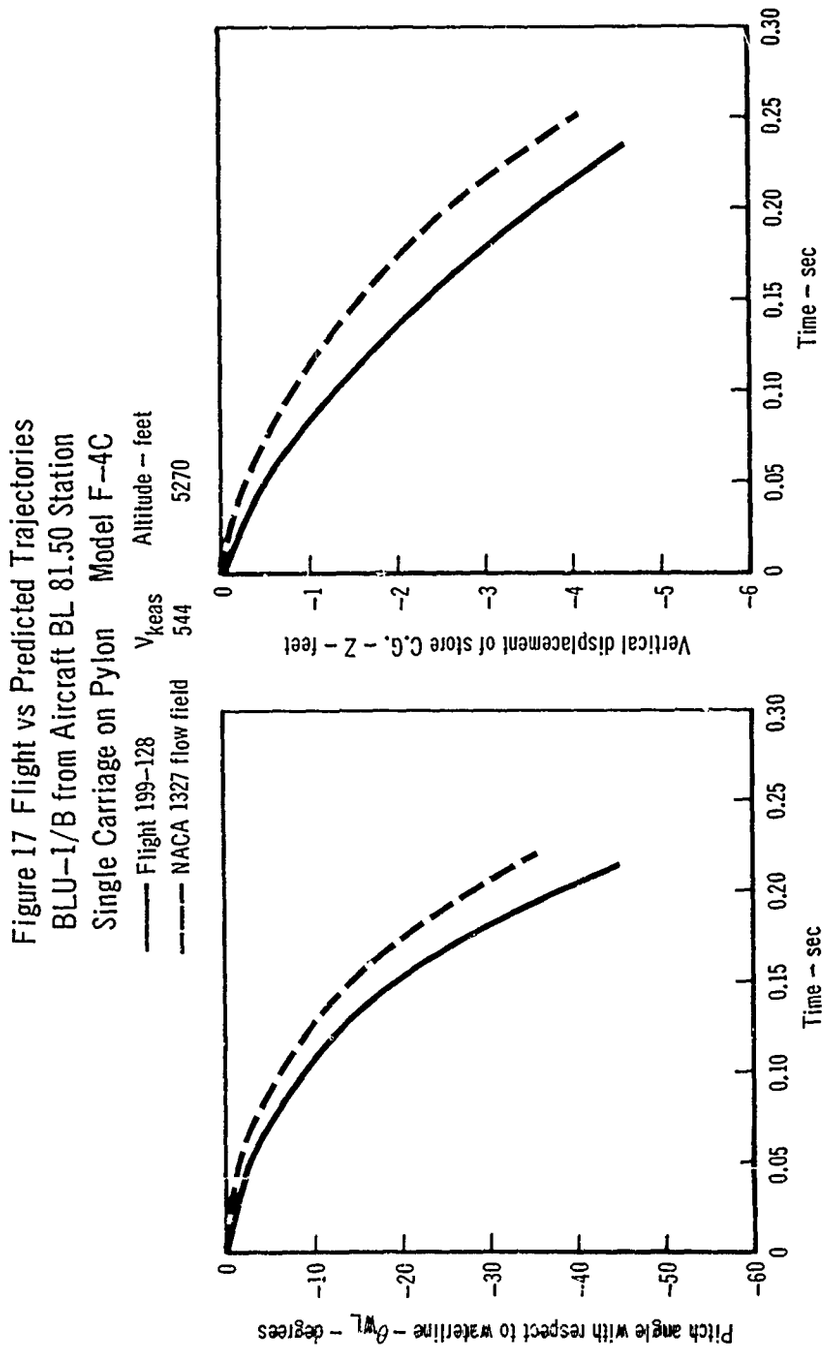

Figure 17 Flight vs Predicted Trajectories
BLU–1/B from Aircraft BL 81.50 Station
Single Carriage on Pylon Model F–4C

—— Flight 199–128 V_{keas} 544 Altitude – feet 5270
– – – NACA 1327 flow field

Figure 18 Flight vs Predicted Trajectories
BLU–1/B from Aircraft L/H BL 81.50 Station
TER Station Three Model F–4C

—— Flight 199–131 v_{keas} Altitude – feet
– – – NACA 1327 flow field 544 5060

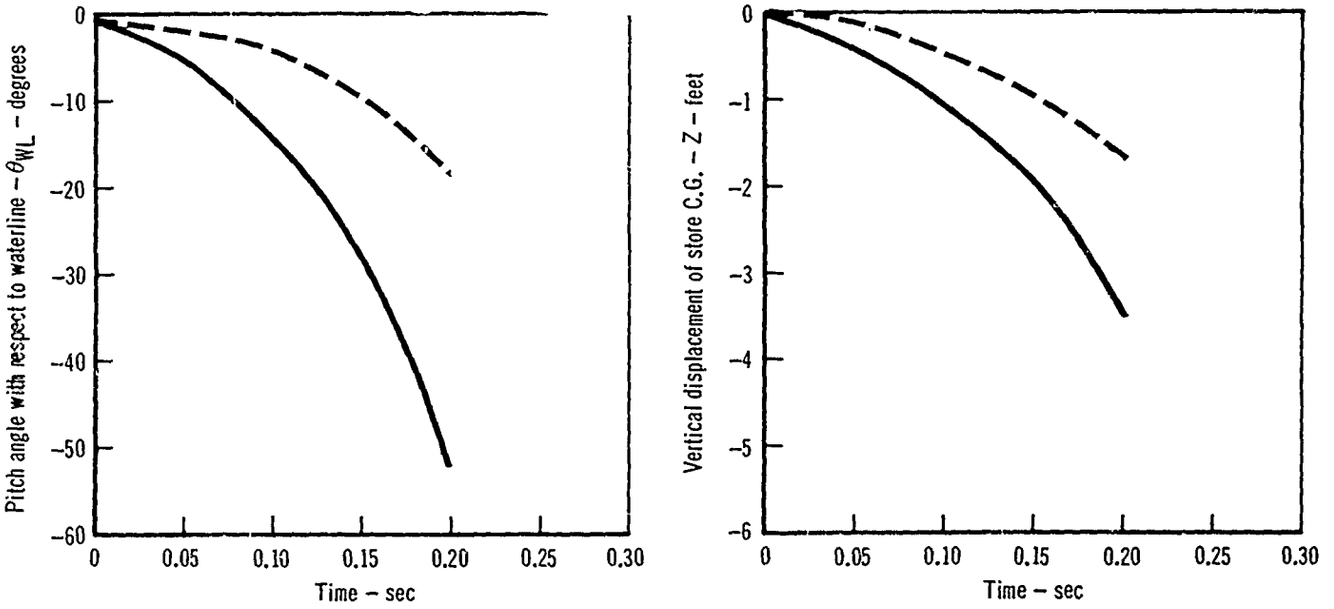

Figure 19 Flight vs Predicted Trajectories
CBU–39/A from Aircraft L/H BL 81.50 Station
TER Station Three Model F–4C

—— Flight 647–50
– – – Stowed loads varied per NACA 1327 flow field

V_{keas}	Altitude – feet
344	9980

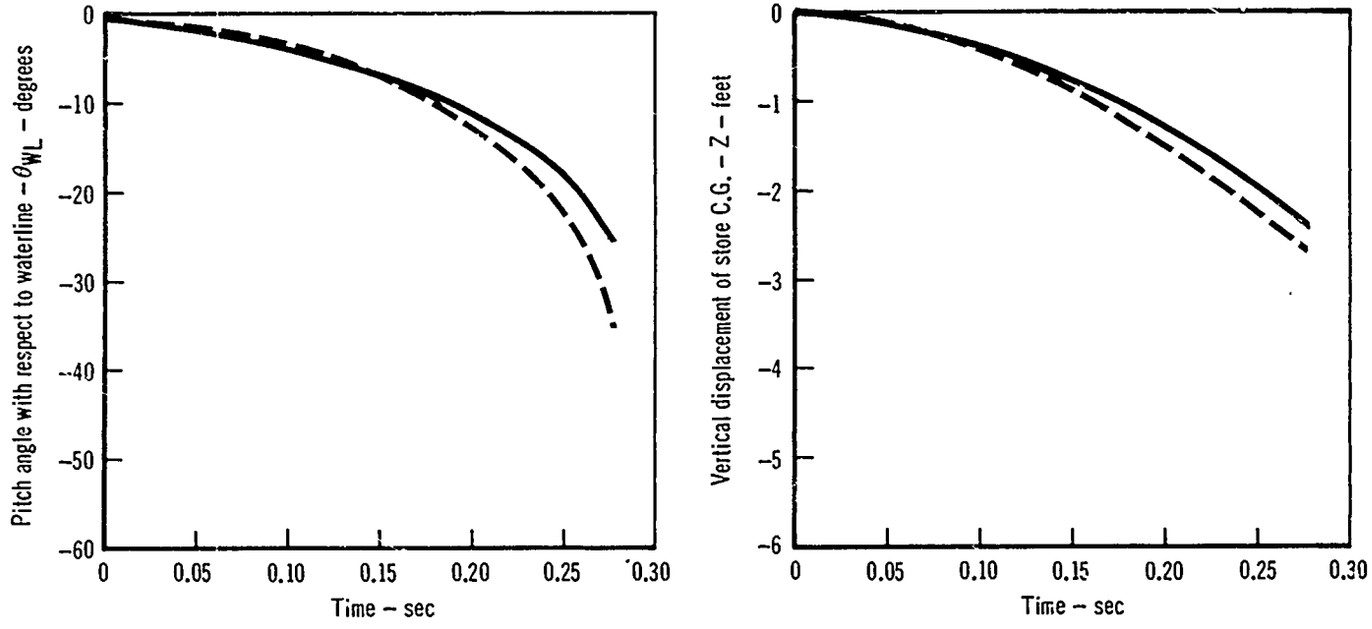

Figure 20 Comparison F-4C vs F-4E
External Moldline

Figure 21 Effect of Moldline Change on Store Separation Characteristics

F–4C vs F–4E

Trajectories for BLU–1/B from Aircraft Centerline Station and MER Station One

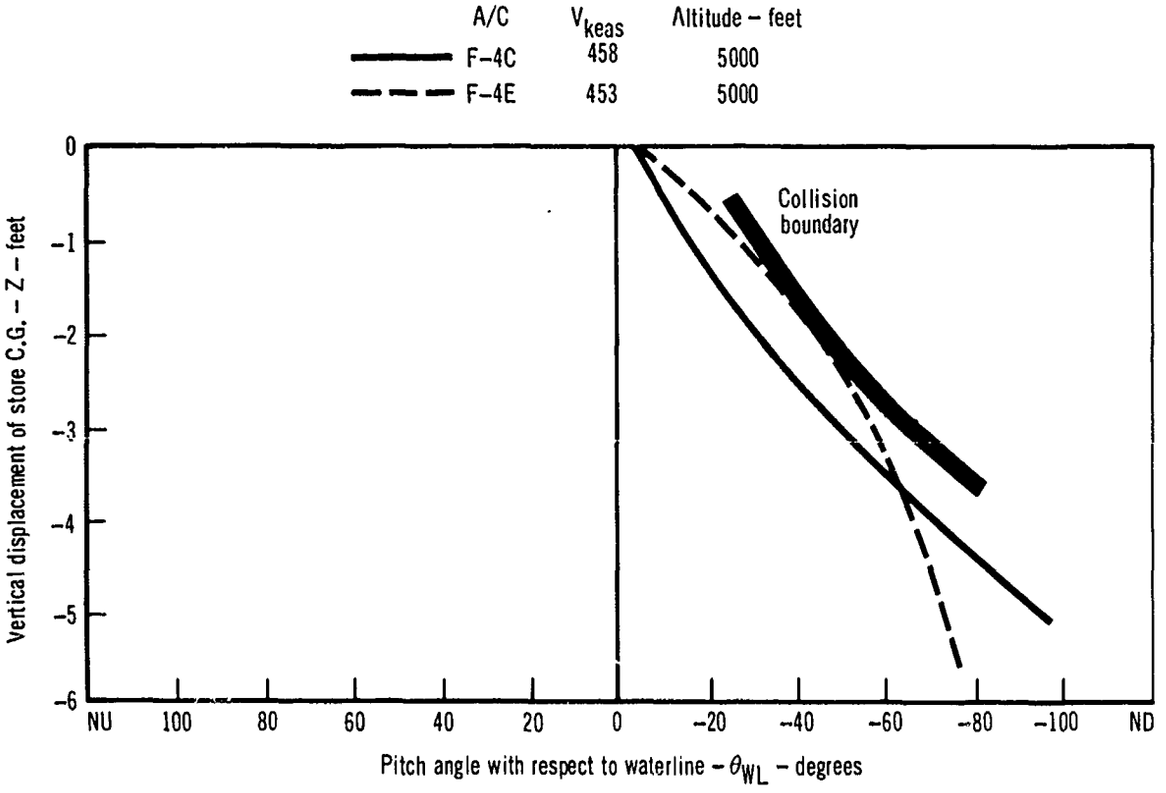

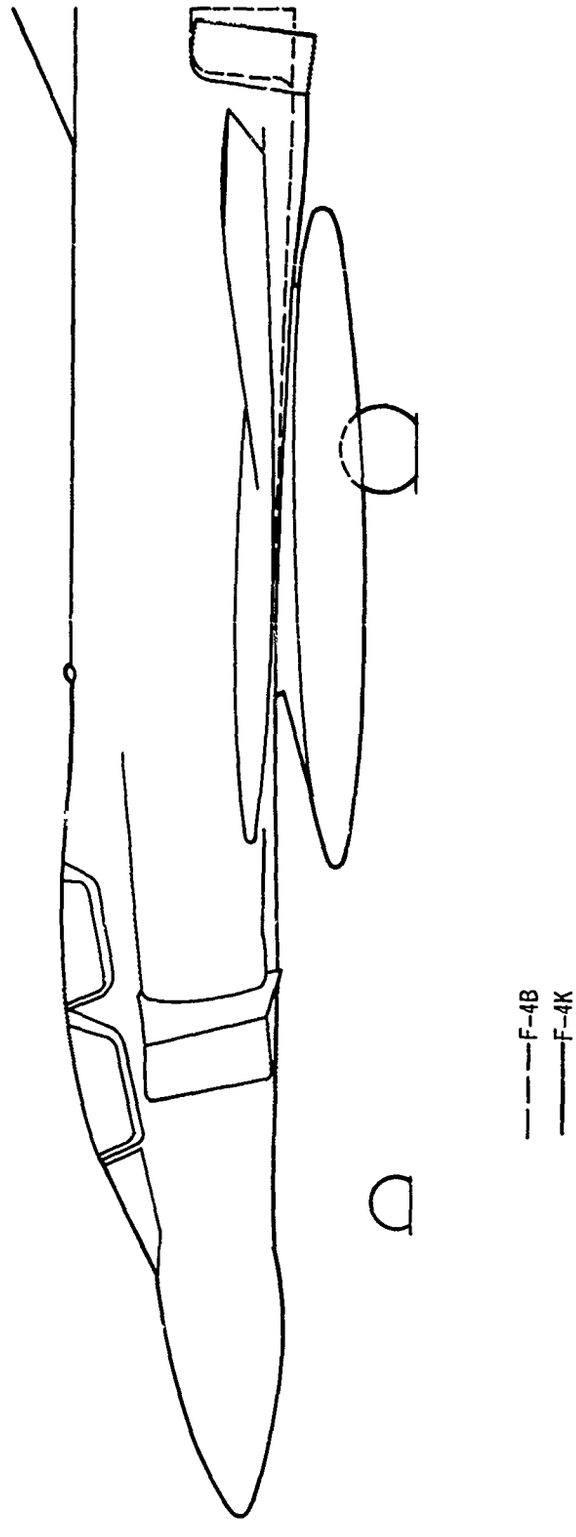

Figure 22 Comparison F-4B vs F-4K
External Moldline

Figure 23 Effect of Moldline Change on Store Separation Characteristics
F-4B vs F-4K
Trajectories for MK-21 from Aircraft Centerline Station and TER Station Two

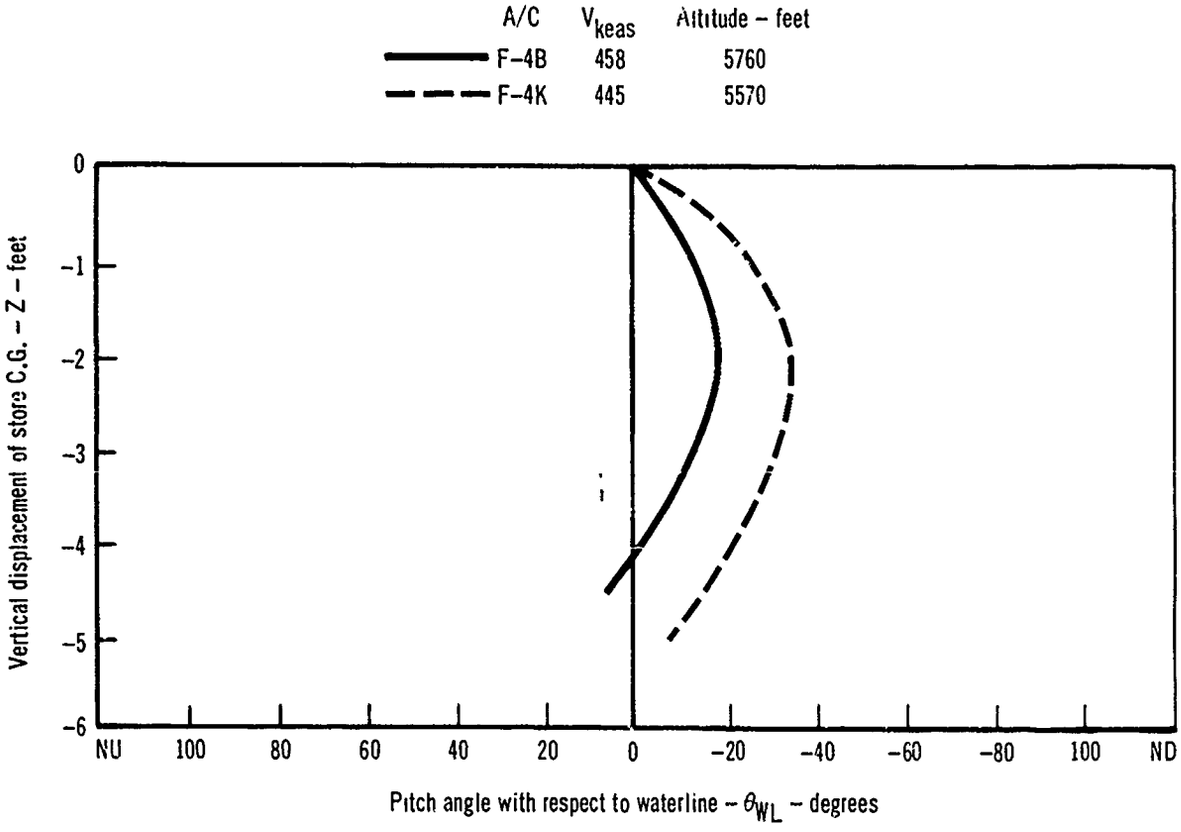

Figure 24 Effect of Flow Field on Store Separation
Model F-4D
Trajectories for CBU-39 from Aircraft BL 81.50 Station

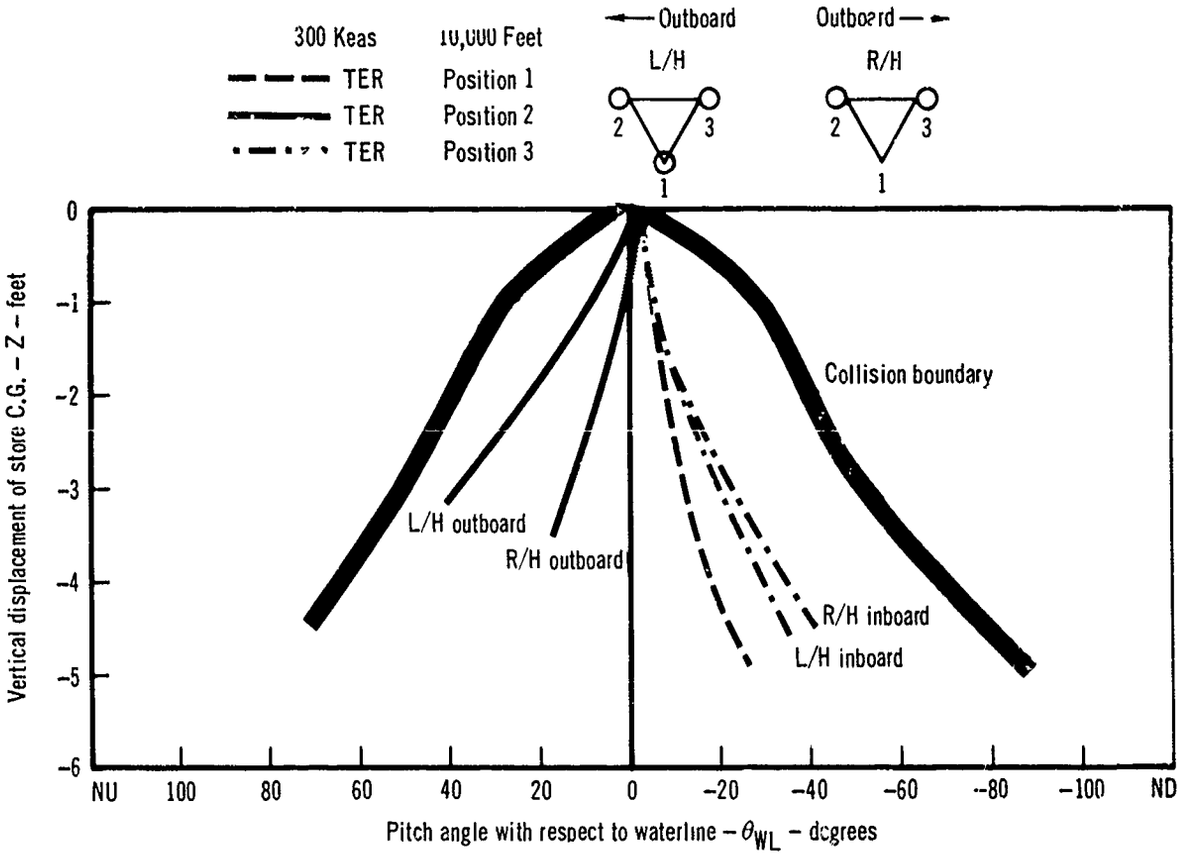

Figure 25 Model F-4D Predicted Trajectories
LH BL 81.50 Aircraft Station
TER Station Three

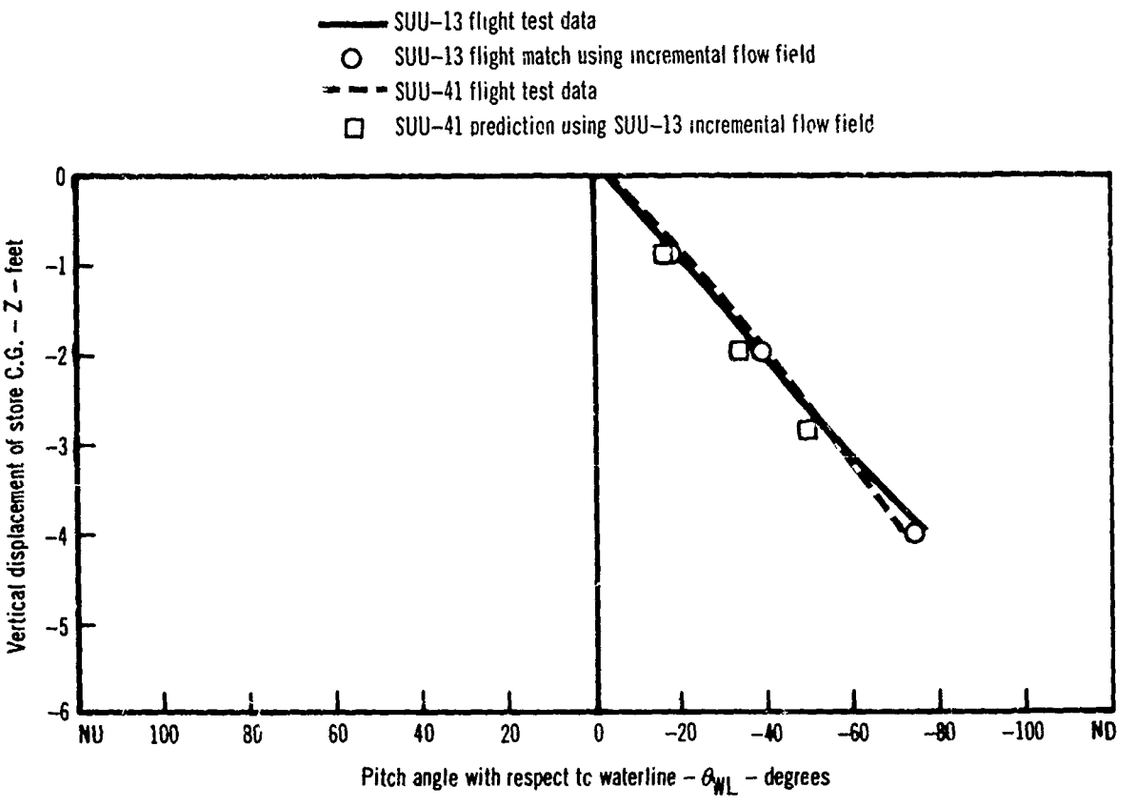

Figure 26 Model F-4D Predicted Trajectories
LH BL 132.50 Aircraft Station
MER Station Three

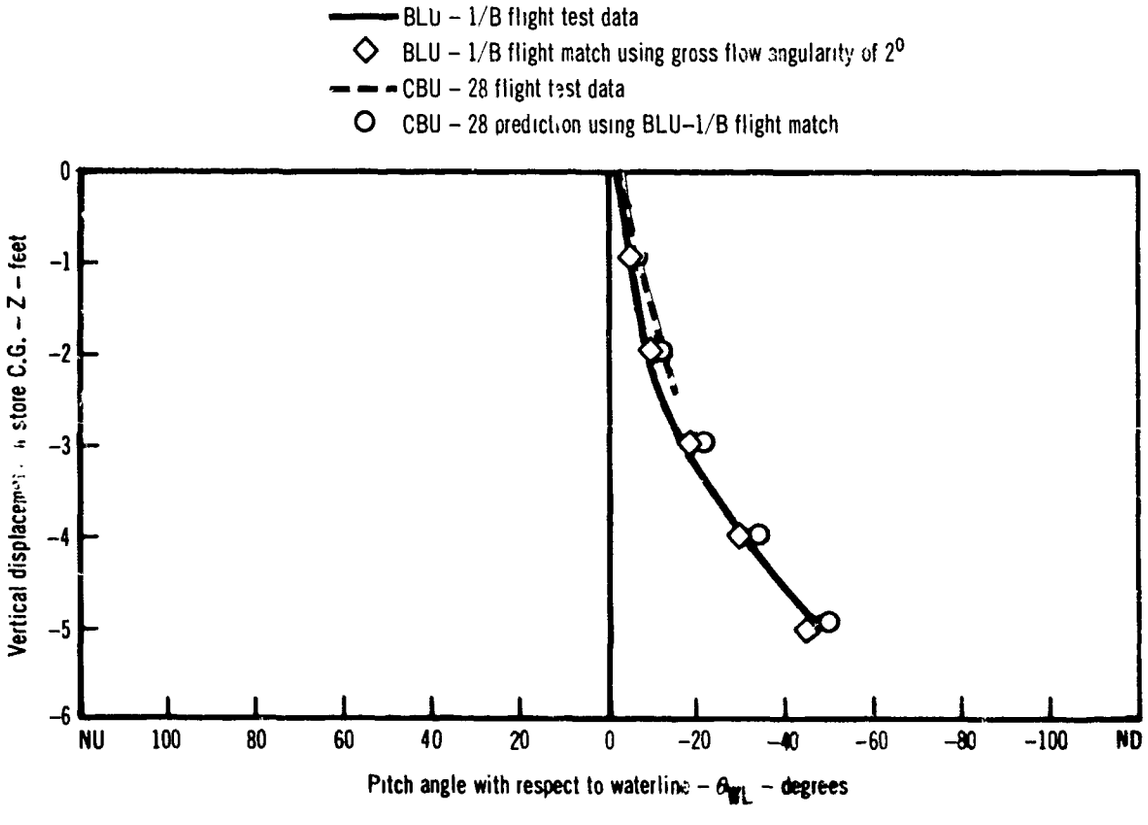

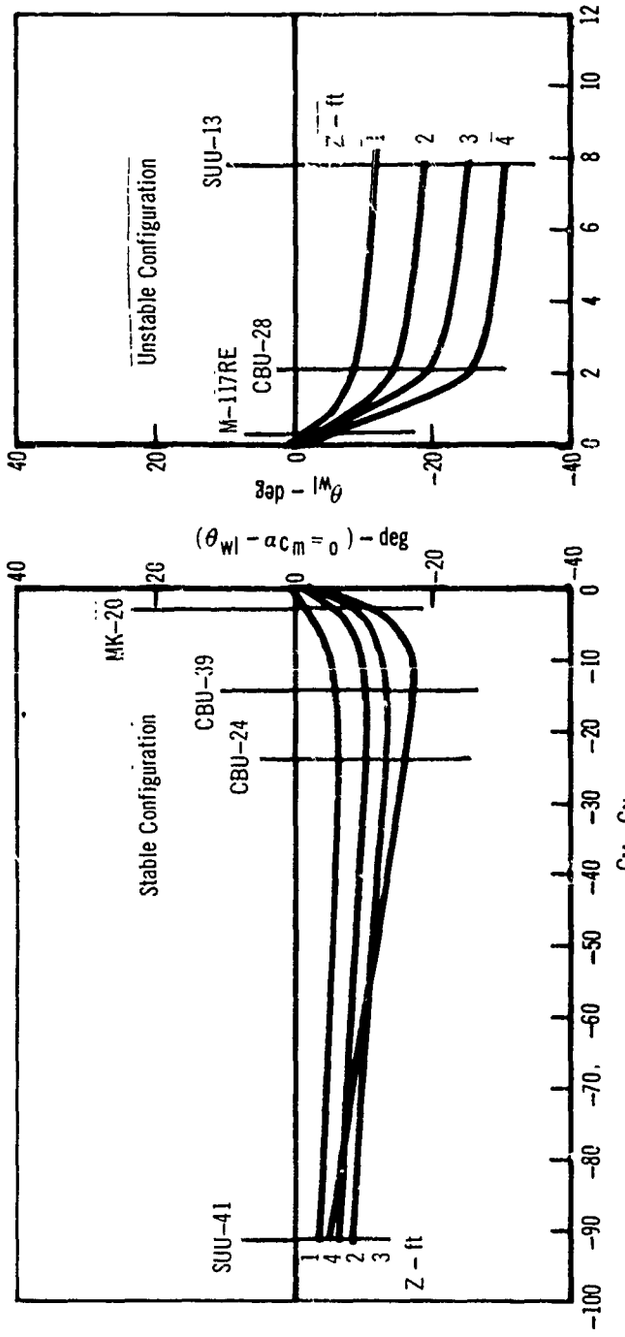

Figure 27 Model F-4D Jettison Characteristics Chart
Centerline Aircraft Station

Configuration V_{keas} 400 Altitude – feet 10,000

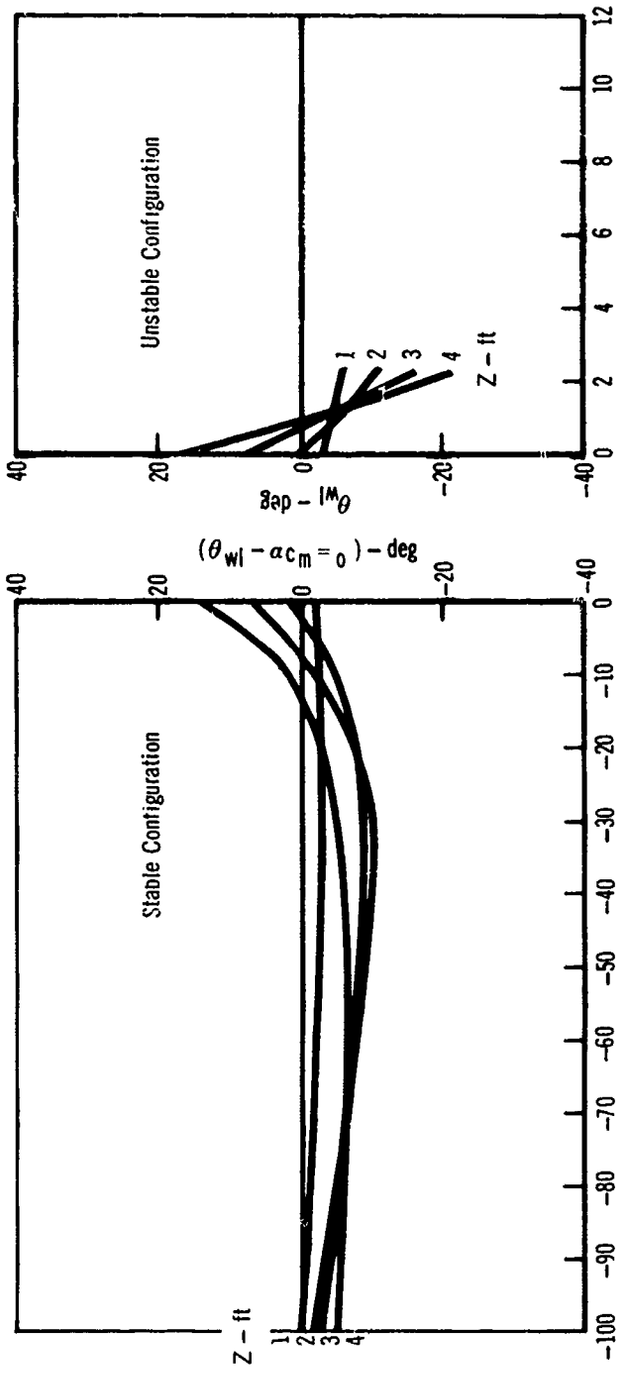

Figure 28 Model F–4D Jettison Characteristics Chart
Centerline Aircraft Station

Configuration ▽ ◁

V_{keas} 350

Altitude – feet 10,000

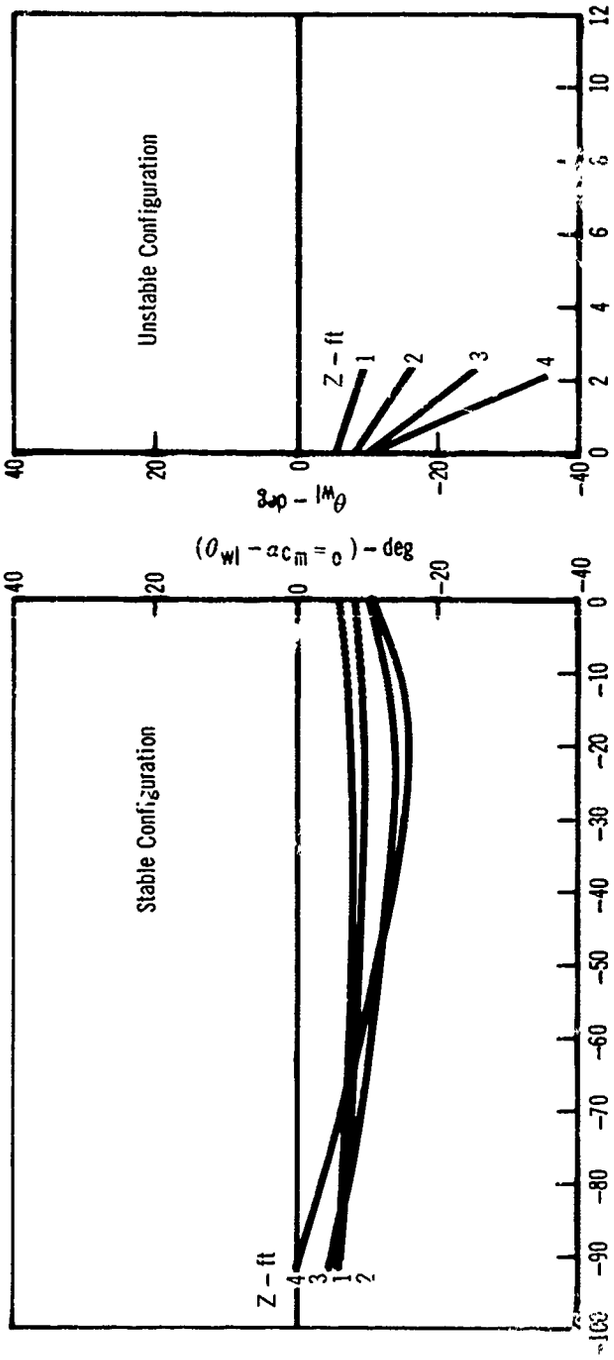

Figure 29 Model F-4D Jettison Characteristics Chart
Centerline Aircraft Station

Configuration V_{keas} 450 Altitude – feet 10,000

Figure 30 Model F-4D Separation Characteristics Chart
RH BL 81.50 Aircraft Station
TER Station Two
Zero Arm Between Ejector and C.G.

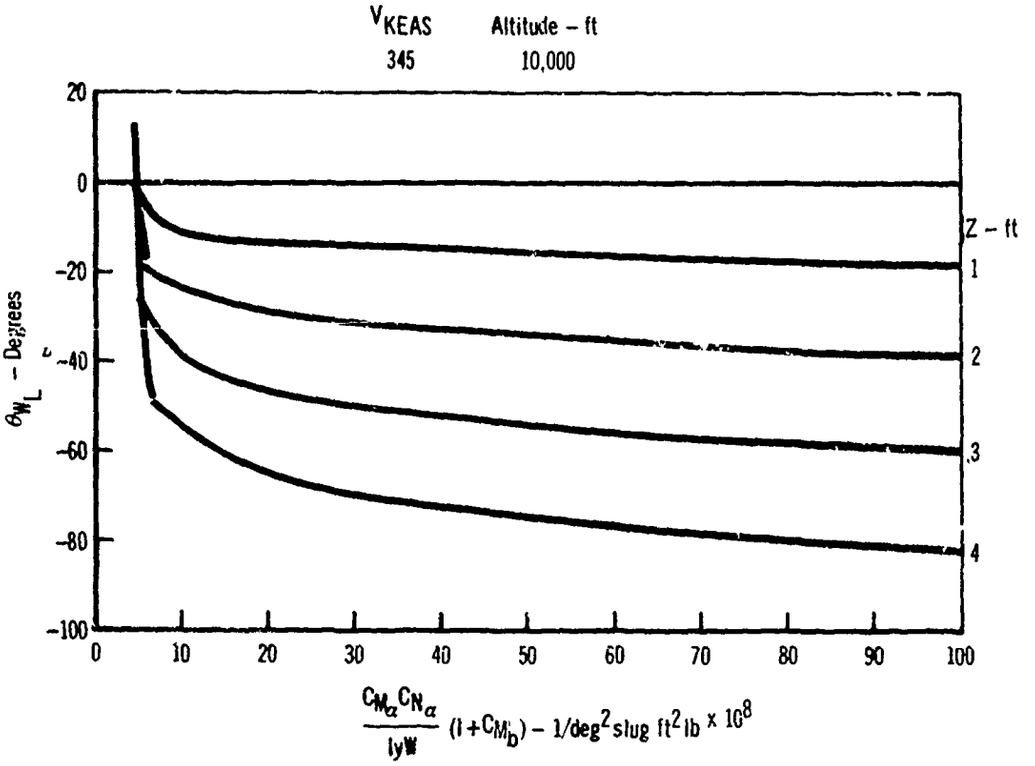

Figure 31 Model F-4D Separation Cnaracteristics Chart
RH BL 81.50 Aircraft Station
TER Station Two
Positive Two Inch Arm Between Ejector and C.G.

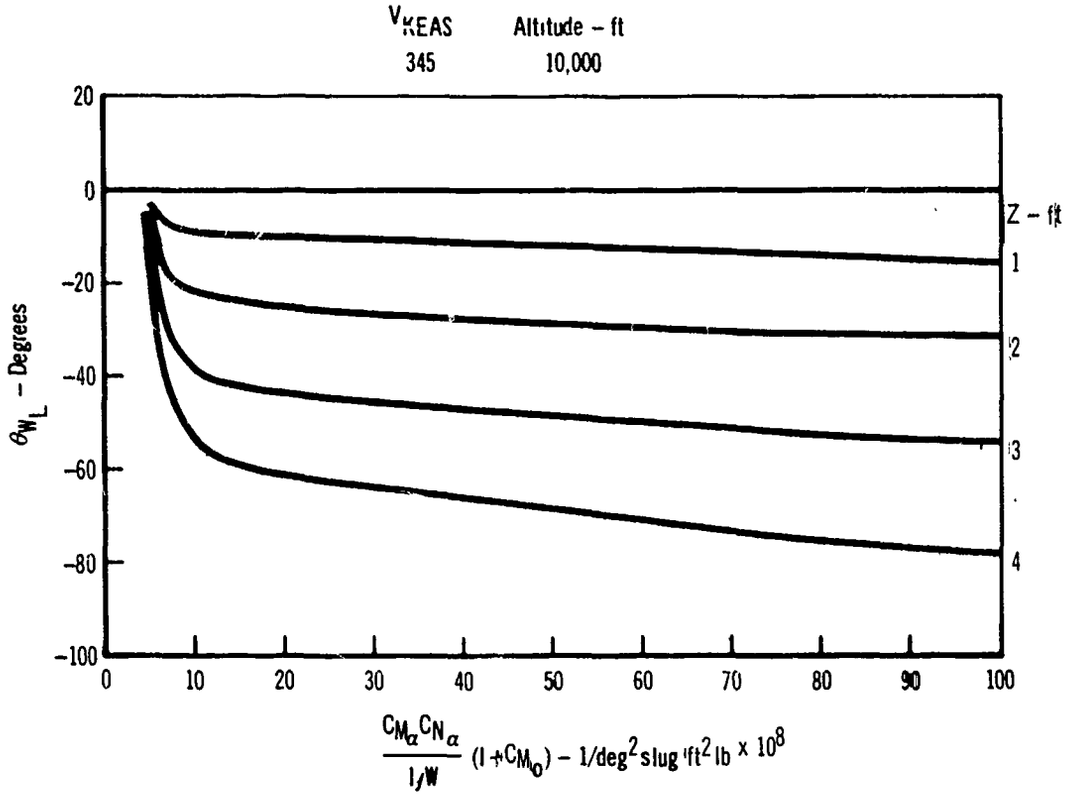

Figure 32 Model F-4D Separation Cnaracteristics Chart
RH BL 81.50 Aircraft Station
TER Station Two
Negative Two Inch Arm Between Ejector and C.G.

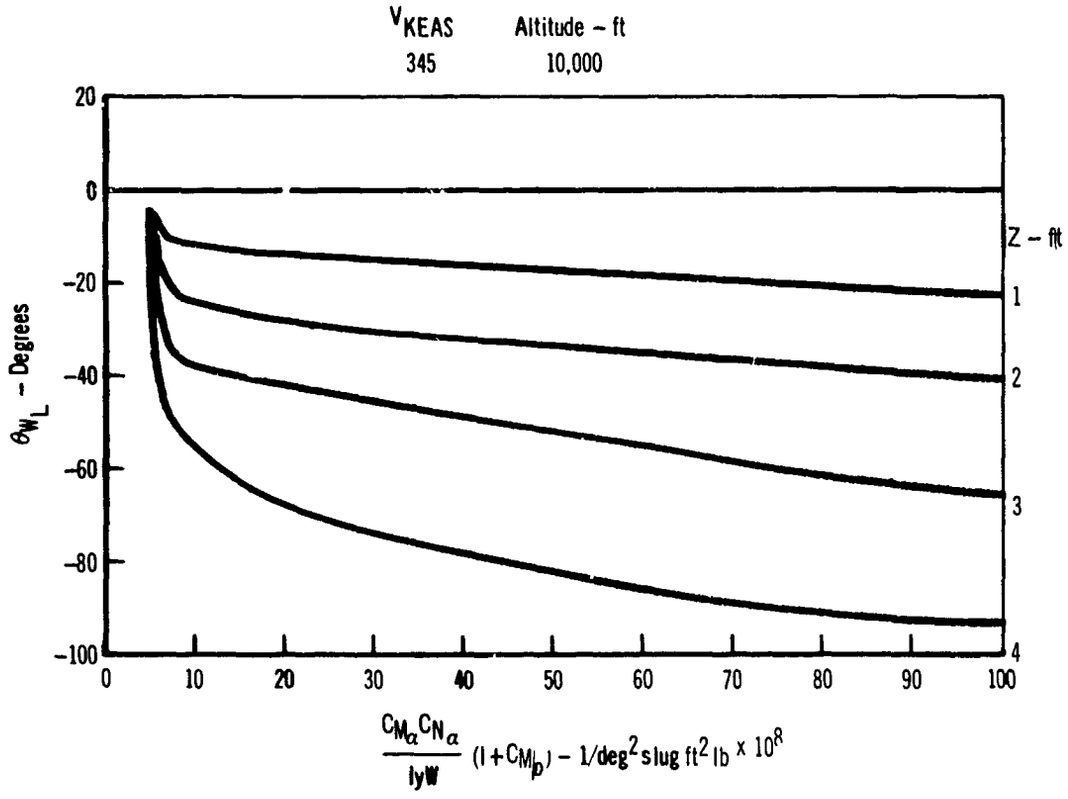

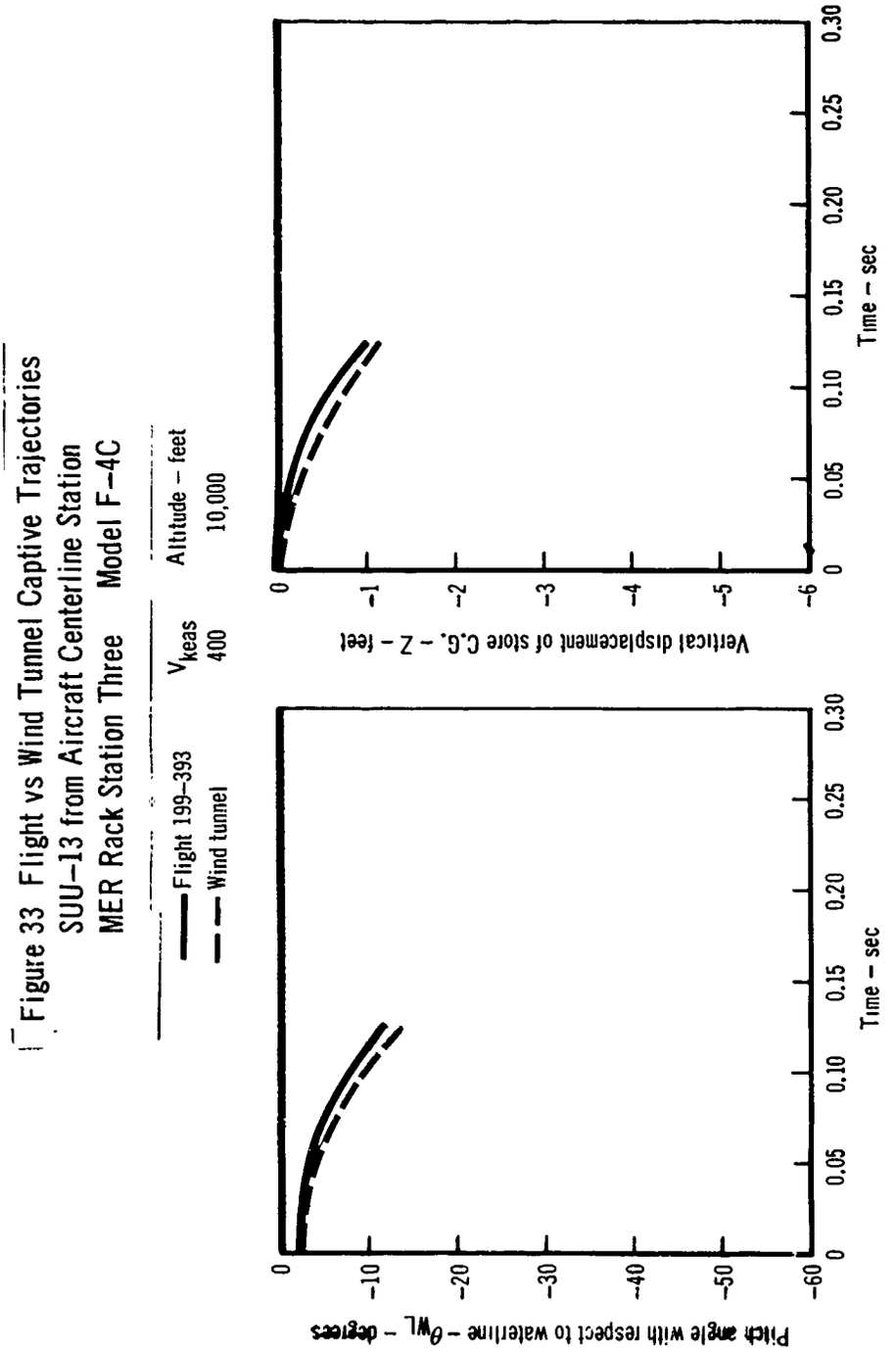

Figure 33 Flight vs Wind Tunnel Captive Trajectories
SUU–13 from Aircraft Centerline Station
MER Rack Station Three Model F–4C

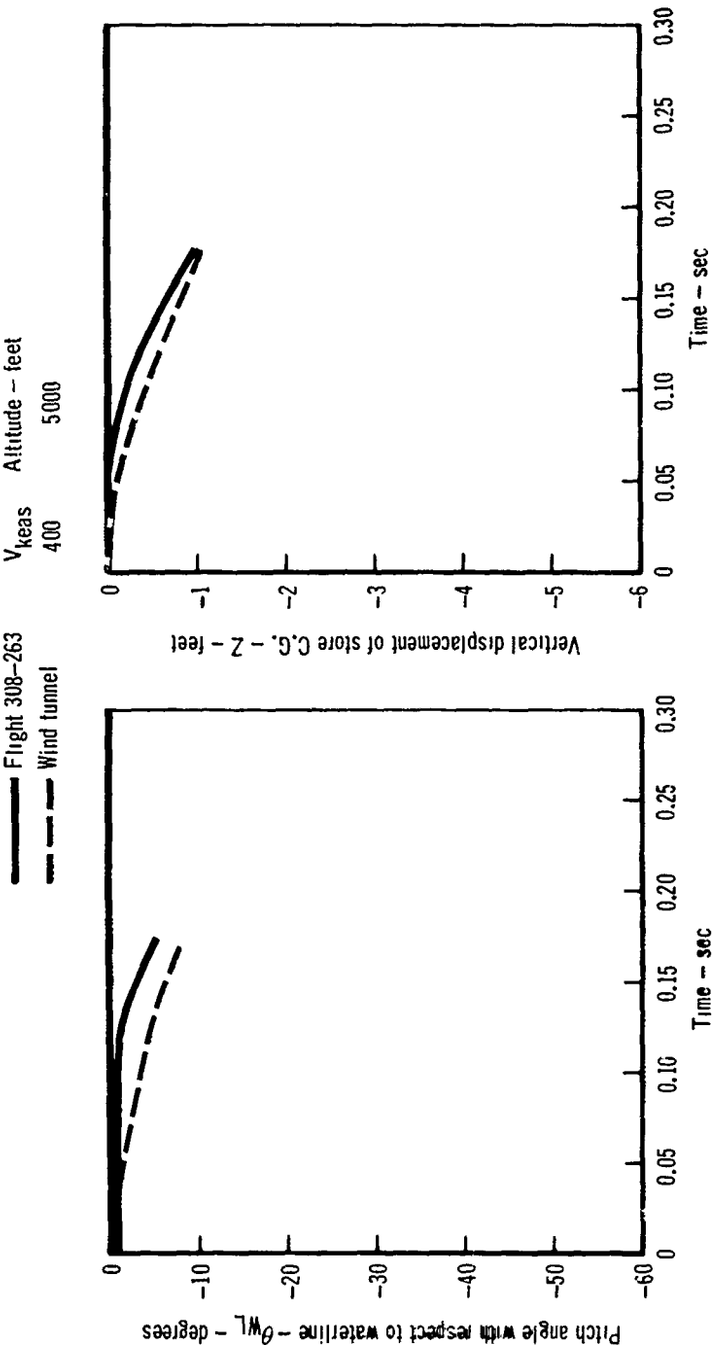

Figure 34 Flight vs Wind Tunnel Captive Trajectories
BLU–1/B from Aircraft L/H BL 81.50 Station
TER Rack Station Three Model F–4C

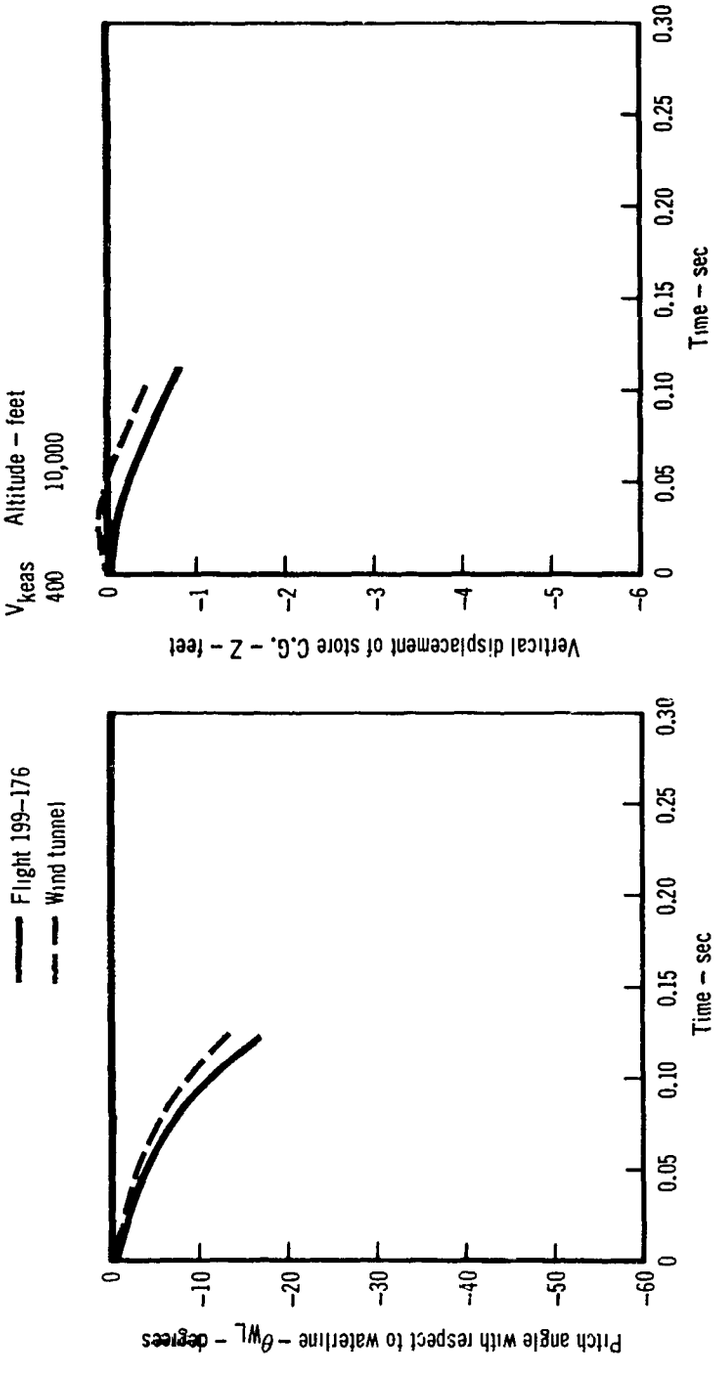

Figure 35 Flight vs Wind Tunnel Captive Trajectories
SUU–13/A from Aircraft L/H BL 81.50 Station
TER Station Two Model F–4D

Figure 36 Flight vs Wind Tunnel Captive Trajectories
BLU–1/B from Aircraft R/H BL 81.50 Station
TER Station Three Model F–4D

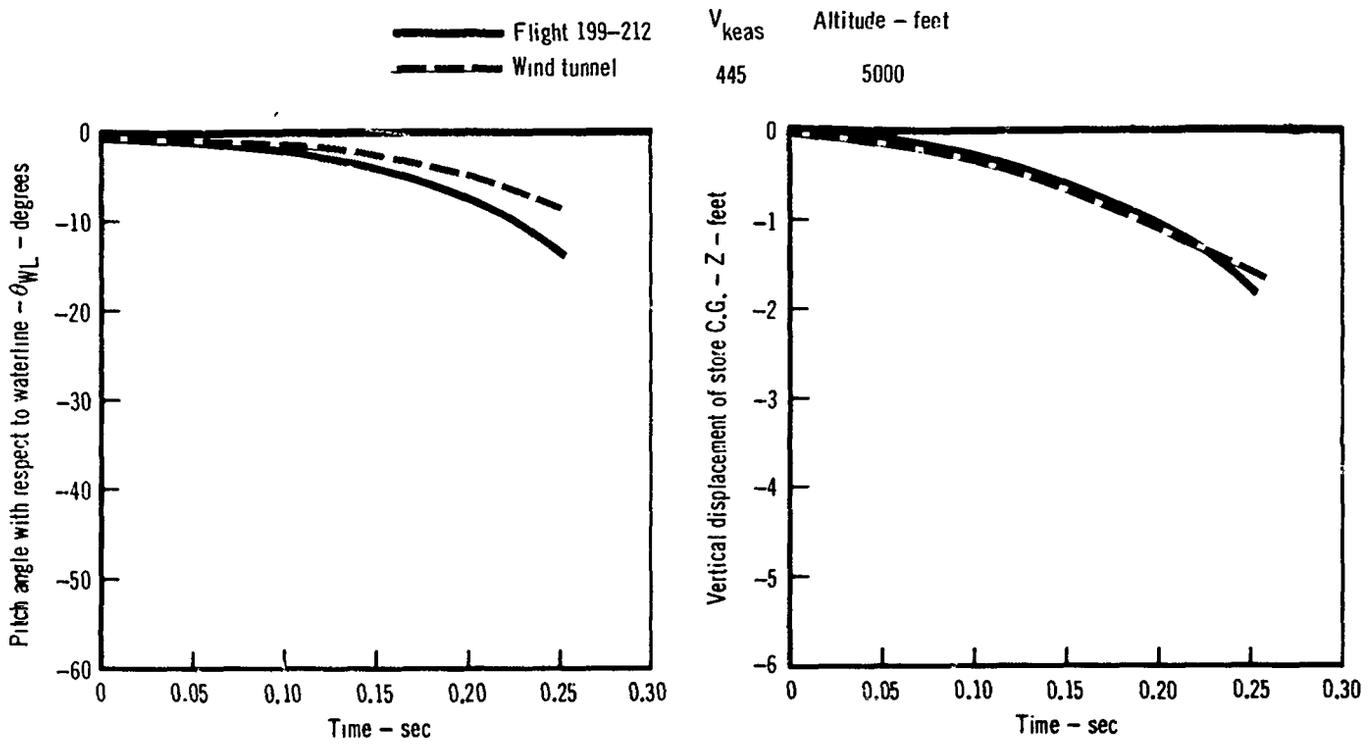

BLANK PAGE

Paper No. 43

AIRCRAFT/MUNITIONS COMPATIBILITY—U.S. AIR FORCE PROJECT "SEEK EAGLE" (U)

(Paper UNCLASSIFIED)

by

Charles S. Epstein
Armament Development and Test Center
Eglin Air Force Base Fla. 32542

ABSTRACT. (U) The qualification of external stores on modern high speed aircraft is an extremely complex problem to which little attention has been given in the past. In 1966 the USAF initiated Project SEEK EAGLE - a management tool whereby aircraft/munitions compatibility is recognized as a distinctly separate requirement and only those aircraft/munitions combinations deemed necessary by Headquarters, USAF, to maintain a balanced tactical and strategic strike capability would be certified. The purpose of this paper is to present Air Force weapons separation techniques and instrumentation; to discuss test results gained to the present and the correlation of this data to wind tunnel predictions; and to show the value of weapons separation technology in planning for future development of munitions and aircraft.

INTRODUCTION

(U) Separation of weapons from aircraft is a problem as old as the aircraft itself. It gained recognition, perhaps, when in the early days of World War I, aeronauts on both sides began throwing stones or bricks at each other. Since that time, regardless of the size or speed of the aircraft, or whether the weapons were carried internally or externally, weapon separation problems have continued to plague us. Not until the advent of modern, high speed jet aircraft, however, have the problems become of significant magnitude. It would be of interest, I think, to discuss for a few moments, the evolution of the problem since World War II.

WORLD WAR II AIRCRAFT

(U) At the conclusion of World War II, the U. S. Air Force tactical arsenal consisted primarily of three types of aircraft - the pursuit (or fighter), the light or medium bomber, and the heavy strategic bomber.

Pursuit (Fighter) Aircraft

(U) The pursuit aircraft was - as its name indicates - an air superiority vehicle with a very limited air-to-ground weapon delivery capability. It was generally armed with fixed machine guns or cannon for aerial combat and strafing. Some aircraft could carry one bomb on each wing, mounted on simple pylons. The bombs were gravity released; that is, not force ejected. Typical of this type aircraft was the propeller driven F-51.

Light or Medium Bombers

(U) Light or medium bombers were propeller driven aircraft - usually multi-engined. These aircraft were armed with guns, rockets and bombs. The bombs were generally carried internally in a bomb bay and were gravity released. The bomb load was usually six to eight medium sized bombs. Typical of this type aircraft was the twin-engined B-25.

Heavy Bombers

(U) Heavy strategic bombers, such as the B-17 or B-29, were large, multi-engined propeller driven aircraft. Their weapon delivery capability consisted entirely of a large load (8,000 to 16,000 pounds) of internally carried, gravity released bombs.

KOREAN WAR AIRCRAFT

(U) By the early 1950's, jet aircraft had all but supplanted the propeller driven aircraft in the fighter and light bomber types. Propeller driven heavy bombers were still abundant, however.

(U) Most of these early jet fighter aircraft (such as the F-86) did not differ significantly from their predecessor pursuit aircraft except in power plant and speed. A few, such as the F-84, were capable of carrying and dropping two to four medium sized bombs. The F-84 was equipped with a pneumatic bomb ejector system. The U. S. Navy maintained its fleet of propeller driven attack aircraft, such as the AD (AIE) which carried large loads of external bombs and delivered them accurately at much slower speeds.

THE FIGHTER-BOMBER

(U) During the time period from World War II to the late 1950's, the brunt of the delivery of conventional weapons in a tactical role was met by the Navy attack aircraft. Little interest was shown by the USAF, although some new medium bombers did appear (such as the B-57 and the supersonic B-58). Primarily, this was due to the heavy emphasis given to the delivery of nuclear weapons.

(U) In the early 1960's, however, the U. S. defensive strategy changed by shifting the emphasis from nuclear war back to conventional war. Almost overnight, a new breed of aircraft emerged - the fighter-bomber. The fighter-bomber evolved from the necessity to utilize the large existant inventory of jet fighter aircraft and, by whatever modifications were necessary, to develop for these aircraft a capability for delivering conventional munitions. What ultimately evolved from this "shotgun marriage" is a high speed, highly complex multi-million dollar weapons system (such as the F-105 or F-4) capable of more destruction than a fleet of heavy bombers in previous wars.

COORDINATION OF MUNITION AND AIRCRAFT DEVELOPMENT

(U) During the past twenty years, evolution of the fighter aircraft has been spectacular, measured by almost any yardstick. Our fighter aircraft have evolved into superb flying machines, but their design specifications too often include speed, rate of climb, maneuverability, etc., - not air-to-ground weapons delivery capabilities. The F-4, our best current tactical air-to-ground weapon

delivery aircraft, was originally designed as a Navy interceptor. Weapon suspension racks and release equipment used today (such as the multiple ejector rack) were designed to meet the "crash" requirement to develop as large a conventional munition delivery capability on existing fighters as possible. As a result, this equipment is not optimized for tactical missions.

(U) The recent emphasis on conventional munitions has produced a rapidly mushrooming family of new weapons. These weapons were developed to produce a limited war capability. Each munition was designed to provide a certain tactical effect or to "kill" a certain type target. Little emphasis was given to designing the weapon to mate with any specific aircraft. Rather, the weapon was required to fit and be released from all current aircraft.

(U) This separate, or uncoordinated, development of aircraft and munitions has resulted in:

1. An increase in logistical problems.
2. Aircraft performance degradation.
3. Dangerous store separation.
4. Reduced weapon accuracy.

U. S. AIR FORCE PROJECT "SEEK EAGLE"

(U) By 1966, literally dozens of newly developed conventional munitions had been added to the existing USAF inventory of World War II type weapons. It was apparent that testing resources required to certify every weapon on every station of every aircraft would be astronomical.

(U) As an example, if on the F-4, every weapon (both alone and in "mixed" loads with other weapons) were carried on every station, over four million possible configurations would result.

(U) Recognizing these problems, Headquarters, USAF, in 1966 initiated project "SEEK EAGLE". This project is a management tool whereby aircraft/munition compatibility is recognized as a distinctly separate requirement and only those aircraft/munition combinations deemed necessary by Headquarters, USAF, to maintain a balanced tactical strike capability would be certified. This narrowed the scope of the problem. A task force was formed, consisting of representatives from CSAF, AFSC, AFLC, TAC, SAC, and the using commands overseas in SE Asia and Europe. This task force (of which I am a member) advises CSAF on configuration requirements and assists CSAF

in decision making. Periodically, this group meets and discusses test results, problems, and new certification requirements. Shortly thereafter, a Requirement Action Directive (RAD) is published by CSAF which shows, for all USAF aircraft, the current aircraft/munition certification requirements and their relative priorities. As new weapons and new aircraft are added to the USAF inventory, the RAD is amended.

(U) Seek Eagle also established a method and responsible agencies for accomplishing aircraft/munition certification testing.

(U) Most of the aircraft/munition certification testing on U. S. Air Force aircraft since 1966 has been done at Eglin AFB by a team from the Armament Development and Test Center (ADTC) and the Air Force Armament Laboratory (AFATL).

EXTERNAL STORE CERTIFICATION

(U) The certification of external stores on modern high speed jet aircraft is an extremely complex problem. It involves many separate tasks and types of testing.

DEFINITIONS

(U) Prior to further discussion, it would be of value to define certain terms, as they are currently used by the Air Force.

Compatibility

(U) The establishment through analyses, ground, and flight tests of the flight envelope limits for loading, carrying, operating, releasing (employing), and jettisoning of an external stores configuration intended for tactical employment. A particular store may be compatible with the airplane in a specific external stores configuration, although not necessarily so with all pylons or under all conditions.

Certification

(U) The publication, for the particular store or configuration, the necessary supplements to the aircraft flight handbook, the loading manual and the weapons delivery manual. These are referred to as the aircraft -1, -33, and -34 Technical Orders.

Release

(U) Release or ejection of a store from its suspension equipment.

Employment

(U) The dispensing of CBU, the firing of guns, the launching of rockets/missiles or dispensing of flares.

Jettison

(U) The release from the aircraft of the store and its suspension equipment (for example, the jettison of bombs and TER or bomb and pylon).

COMPATIBILITY TESTING

(U) The determination of compatibility of a particular store with a specific aircraft is an involved process. On present day aircraft, with multiple external store stations and multiple store carriage at each station (MER, TER, etc.), many loading combinations can lead to serious aircraft stability and control, structural or flutter problems. Keeping track of the approved and not approved (and reasons for non-approval) configurations is a monumental task for even one type aircraft.

(U) Compatibility testing in general consists of many parts. The most important of these parts are discussed below.

Pre-flight Analyses

(U) This includes the necessary tasks and analyses which must be performed prior to flight testing the store. Testing configuration (or configurations) is identified, physical clearances are checked analytically, flutter and stability and control analyses are made, and wind tunnel tests (drop and/or captive trajectory tunnels) are made. Predicted captive and separation envelopes for the store/aircraft combination are developed. A test design is then formulated which calls for certain points to be demonstrated in flight to clear the entire envelope.

Fit and Function Test

(U) The store is fitted on the aircraft in the desired configuration to insure adequate clearances and physical and electrical compatibility. In order to accomplish these fit tests properly and determine the required clearances, I have written a local instruction which compiles all the design and military specification requirements. Copies of this instruction are available on request.

Flutter Flights

(U) Flutter analyses may require confirmation in flight using an

instrumented aircraft prior to issuing captive flight envelopes. If so, the aircraft manufacturer performs them since the USAF has no flutter capability in-house at Eglin.

Captive Structural Integrity Flights

(U) A series of one or two captive flights are conducted wherein the store, loaded on the aircraft in the desired configuration, is subjected to various maneuvers (such as pushovers, pullups, stick pulses, etc.) at various speeds up to the maximum predicted allowable. The store is flown for a period which is the time equivalent of combat radius of the aircraft plus 50%. A total of 30 minutes of this flight time must be at maximum allowable airspeed. This long flight may be accomplished in one or two sorties, as necessary. In between missions, the store is not downloaded, or otherwise disturbed.

(U) This long mission (or missions) is a direct result of the war in Vietnam. Many times stores are loaded on aircraft in Vietnam and flown, but not dropped due to lack of a target or other operational reasons. Stores sometimes make as many as three or four flights before being dropped. Also, many of the missions to North Vietnam required one or more inflight refuelings enroute. A store, then, might be subjected to as much as two or three hours of evasive maneuvering prior to drop. As a result, failures of the stores themselves were being experienced. These long back-to-back flights initiated at Eglin have unearthed a number of munition deficiencies which would not have been found otherwise.

Weapon Separation Tests

(U) Separation testing involves releasing (or employing) stores loaded in realistic combat configurations at various airspeeds, attitudes (level, dives), and release modes (single, pair, ripple) in sufficient quantity to demonstrate that an operational envelope may be cleared.

Bomb Ballistics

(U) The flow field and ejection characteristics of each type aircraft affect somewhat the initial trajectory of a bomb; therefore, testing on an instrumented range may be required to evaluate bomb ballistics.

Determination of HERO Effects

(U) Hazard of Electromagnetic Radiation to Ordnance testing involves determining if any electrical or electronic equipment on

the aircraft or on the ground support equipment nearby might produce an electrical potential in the weapon, causing an explosion, abnormal operation, or other undesirable side effect.

INITIAL USAF CERTIFICATION EFFORTS

(U) In 1966, very little constructive information on weapon separation testing procedures or technology existed. There were practically no manpower or facilities available to accomplish the necessary preflight analyses and wind tunnel tests prior to flight test. Due to the urgency of the limited war requirement and the magnitude of the compatibility testing necessary, flight testing was initiated on a "brute force" routine. That is, based on whatever information we had, an initial flight test point was determined. Weapon drops were then made in increasing (or decreasing) speed increments, usually 25 to 50 knots, until the maximum predicted envelope was demonstrated. Onboard and photochase motion pictures were taken of each drop. Decisions to proceed to the next point were normally based on review of this film.

(U) Obviously, overriding precedence had to be given to establishing flight safety standards. For this, a relatively simple table of relative risk factors was developed. This risk factor was used as a guide to the formulation of the test plan. I should stress that the factors were assigned by me, based solely on my experience and the information available to me at that time. The table and its explanation is included in this report as Appendix I.

(U) Examination of the Table of Risks brings out a few pertinent points:

1. Low density stores are the most hazardous to test - particularly if they are also unstable.

2. There are very few instances where a Category 3 (stable or unstable - c.g. not within limits) can be tested as such. The item should be modified into another category.

3. Two alternatives appear for high risk tests - modify the store to another category, or change the test objectives to a type test with less stringent requirements. Either alternative allows the item to be flight tested without further preliminary analyses or tests.

(U) In addition to using the Table of Risks, other actions were taken to minimize flight safety hazards in compatibility testing.

1. The store was flown and released first from an aircraft with the most stable airflow for external stores commensurate with test requirements.

2. The store was flown initially on an external store station which, in the past, had given the least trouble in releasing stores similar in size, shape, weight, and moments of inertia.

3. Where possible, the store c.g. was controlled to keep it in the most favorable position for a particular pylon ejector, so that no undue rotation was imparted to the store by the ejector foot.

4. As a first estimate as to the initial store release point, the following familiar equation was sometimes used:

$$C_{L_\alpha} \cdot \alpha \cdot q \cdot S = L \qquad (1)$$

If testing is begun at a point where the total store lift cannot exceed its weight (released at one "g"), we can enhance the safety of the test. By using extremely conservative numbers, such as

$$C_{L_\alpha} = 2.0 \,, \quad \alpha = 0.2 \text{ radians}$$

and knowing the store frontal area(s), we can solve for the dynamic pressure that produces lift equal to the store weight. Since dynamic pressure is constant with altitude for a particular equivalent airspeed, we may then establish an initial test point.

CURRENT USAF CERTIFICATION TECHNIQUES

(U) Using the procedures outlined above, over 300 separate compatibility tests have been completed at Eglin involving 14 types of aircraft and nearly 75 different types of munitions. A prestigious amount of compatibility analysis and testing experience has been built up within AFATL and ADTC. As this experience was being gained, improved prediction techniques and aircraft instrumentation were developed.

CAPTIVE TRAJECTORY WIND TUNNEL (4T)

(U) Recently a four-foot transonic wind tunnel was activated at Arnold Engineering Development Center, Tullahoma, Tennessee, (see Figure 1).

(U) The 4T tunnel is a closed-loop, continuous flow, variable-density tunnel with a Mach number range from 0.1 to 1.4. Simulation of flight speeds from 100 to 1,050 miles per hour at altitudes up to 60,000 feet are possible. Its unusual combination of continuous flow, variable porosity walls (0.5 to 6.0%) and a captive trajectory system

make it the only tunnel of its kind in the country. A complete description of the tunnel may be found in The Arnold Engineering Development Center Test Facilities Handbook, 7th Edition, dated July 1968.

(U) The aircraft model is mounted upside down in the tunnel on a sting. The store model is mounted on another sting. The two models are then mated as they would be in flight. (The inversion of models is an expedient to minimize equipment handling problems associated with the use of two sting support systems.) When the desired simulated flight test flow conditions are established, control of the model is given to an on-line computer which moves the store a small distance away from the aircraft as it would during release. Forces acting on the store are measured through instrumentation, examined by the computer, and a prediction made as to the next store position. The computer then activates the control system and places the store at the new position. This entire process is repeated until the trajectory is completed.

(U) In making its predictions, the computer takes into consideration the speed and attitude of the parent aircraft, the aerodynamic flow field around the aircraft and its effects on the store, and the bomb rack ejector force. If, upon reaching any point in the trajectory, the measured forces on the store do not agree with the computer's predictions, the computer automatically returns the store back half the time interval from the past previously predicted good point for additional measurements.

(U) Once flow conditions have been established and repetitive runs are commenced, the tunnel is capable of producing up to five runs per hour, making it considerably faster than any other tunnel of its kind. Additional flexibility is added through the computer program, which can mathematically simulate a variety of flight conditions not actually created in the tunnel.

(U) During the tunnel runs, the operator and engineers are provided with a continuous closed circuit TV picture of the model from above and from the side. As the on-line computer printout of the trajectory is being made, six parameters (X, Y, and Z displacements and pitch, yaw and roll angles) are concurrently displayed on separate graphs on another CRT monitor, located in the control room.

THE STORES RELEASE EVALUATION SYSTEM (STRES)

(U) STRES is a program for obtaining store separation information through the use of airborne photogrammetric data gathering and computerized data reduction.

Airborne Data Gathering

(U) High speed, 16 mm cameras, operating at 200 frames/sec and having time annotation on each frame, are mounted on the aircraft, viewing both the store to be released and part of the aircraft or pylon (for reference). Both the store and the pylon are painted with a pattern of crosses and dots whose positions are accurately known. Size and color of the dots or crosses are optimized for accuracy and ease of film reading. As the store is released, its initial trajectory is filmed by one or more cameras with as large a field of view as is possible without introducing massive distortion errors.

(U) A small electronic device known as the Airborne Digital Instrumentation System (ADIS) is installed in the drop aircraft. The ADIS records exact aircraft parameters (airspeed, altitude, roll, pitch, yaw and, in some cases, angle of attack) at the time of drop.

Data Reduction

(U) Each frame of the onboard film is read manually, noting the location of each dot or cross on the store and the pylon. This data, along with various physical relationships and measurements, is input to a computer. Two alternate computer solutions are available. The first is a one-camera photogrammetric solution, where data from only one onboard camera is used to determine trajectory. The other solution is the two-camera, or classic triangulation solution. In the second method, the computer utilizes data taken simultaneously from two cameras viewing the store from different angles. By knowing the spatial orientation of the store with reference to two separate, time-correlated cameras, the computer can make a more reliable solution. The one-camera solution provides accuracies of no greater than $\pm$ 3 inches for displacements and + 4° for angular measurements. The two-camera solution provides $\pm$ 2 inches and $\pm$ 2° accuracies.

(U) Installation of data gathering cameras on test aircraft in positions widely enough separated to be of value for the two-camera solution is very difficult. For this reason, most tests to date have utilized the one-camera solution. It is expected that 90% of future tests will also utilize the one-camera solution.

CORRELATION OF DATA

(U) Several compatibility tests have been run at Eglin since acquisition of the 4T wind tunnel and the STRES system. In these tests, the 4T tunnel was used to run a parametric survey with a particular aircraft/munition configuration to determine a safe store separation envelope. The tunnel runs were then analyzed and points were picked for flight test verification. These drops were made, data gathered utilizing the STRES system, and the results plotted and compared against the identical plots obtained from the tunnel.

Results of the first of these comparison tests will serve to illustrate the degree of correlation, and is especially interesting since part of the flight test was performed prior to getting the wind tunnel data. Details of this test are given below.

Compatibility Test of the SUU-23/A Gun Pod on the F-4

(U) Recently, a high priority requirement existed to certify the SUU-23/A gun pod on the inboard pylon of the F-4 aircraft. At the time, the STRES system was available, but the 4T tunnel was just being activated, and there was insufficient time to get predicted wind tunnel runs prior to the required certification date.

(U) The only compatibility aspect of the test imposing problems was the safe jettison of the full and empty pod from the pylon. An analytically predicted safe jettison envelope was developed. The initial test point for flight test was established at 275 KCAS at 5,000 feet. An empty gun pod (weighing 1038 pounds) was painted to allow STRES system data gathering and jettisoned. Immediately after release the pod rotated nose upward, yawed outboard slightly, and cartwheeled just under the aircraft, narrowly missing the pylon.

(U) Due to this unexpected, dangerous result further testing was suspended until a complete wind tunnel survey could be run in the 4T tunnel. To establish the veracity of the tunnel, runs were first made at the conditions of the previous flight test. Then, the data from the tunnel was compared to the data obtained from the STRES system. The degree of correlation was remarkable (see figures 2 and 3).

(U) Next, tunnel runs were made at various speeds and flight conditions to determine if there were any safe jettison points. The tunnel indicated that a safe jettison could be made at higher Mach numbers. Based on this, another empty gun pod was jettisoned from the F-4 at 0.86M at 5,000 feet. Separation from the aircraft was excellent and data correlation was again amazingly good. (See figures 4 and 5.)

Subsequent Compatibility Tests

(U) The SUU-23/F-4 test was run in September 1968. Since then, several other tests have been completed wherein 4T tunnel data was used to establish flight verification points, flight tests were made, and the data was compared.

(U) Results of these tests have been very encouraging where stores were released directly from a pylon (single carriage). The first test wherein a store was released from a MER has recently been completed. This test involved releasing a low density, unstable, flare dispensing

pod from the shoulder station of the F-4 centerline MER. The data correlation was poor.

(U) It should be pointed out that this test - separation of a low density, low inertia, unstable store - imposes the severest possible test to both the onboard data gathering system and the captive trajectory tunnel system. Normally, this type of store would be tested only in a drop tunnel. Poor correlation of data could be caused by errors in the onboard data gathering and data reduction system, or in the wind tunnel data, or in both systems. Programs are now underway designed to "de-bug" and verify the data from both systems.

(U) Verifying STRES Data. One reason for doubting the validity of the flight test data is the close proximity of the F-4 centerline MER to the aircraft (there is no pylon). This close proximity results in a scarcity of aircraft reference spots which must be visible in each frame of film for input to the computer. Because of this, AFATL compatibility engineers have undertaken a very comprehensive ground test program to verify the entire data reduction technique and computer program. The test will also determine which parameters affect the photogrammetric solution and how much error each parameter contributes. A simulated store was painted with the standard STRES pattern and placed on an adjustable wooden framework. Using precision measuring and alignment devices and three 35 mm cameras located at different viewing angles, still pictures were taken of the store in a series of positions and attitudes, simulating trajectories. Trajectories were run by varying each degree of freedom separately and also in combination. Each store position was accurately measured relative to a known reference. By processing each picture through the film reader and the computer program as if it were an actual drop, an accurate check of the entire program can be made. Trajectories were also run wherein the camera positions were changed slightly, simulating camera movement in flight due to aircraft aeroelasticity, to determine if the camera position relative to the aircraft pylon must be read in each film frame. If not, film reading time could be cut almost in half. This ground test being done by AFATL will provide a positive check on the data reduction technique and valuable information on the importance in the solution of such things as camera look angle, reference points, and film reading errors. The results of this test will be published as an AFATL Technical Report within six months.

(U) Wind Tunnel Verification. In observing the 4T wind tunnel runs, it is apparent that one of the most important inputs is rack ejector force. Some ground static test data are available, for a few racks, of ejector force versus time for different cartridges and different store weights. Practically no data are available, however, from airborne drops where airloads and aircraft and rack dynamic response may vary effective ejector force significantly. A program is

currently underway at Eglin in which an F-4 inboard MAU-12B/A pylon is being instrumented to measure various events and ejector piston forces during airborne store releases. If this initial program is successful and provides significant data, it will be expanded to include a MER or TER, where dynamic response would be at a maximum. The MAU-12B/A pylon was chosen as the initial test bed because the best available rack ground test data is for this pylon, providing an opportunity for direct comparison of ground versus flight data.

(U) Summary. If we are successful in correlating the flight test data with wind tunnel data on the low density store test by verifying or improving either or both systems, a significant contribution to the state of the art will have been achieved, and testing costs will have been cut drastically.

THE A7D CERTIFICATION PROGRAM

(U) Preparations are now being made to begin A7D compatibility testing at Eglin. Approximately 325 configurations will be certified initially. The A7D program represents a giant step forward for the Air Force. All of the separation wind tunnel tests and flight tests will be done by the AFATL/ADTC team instead of the aircraft manufacturer. Utilizing the capabilities and experience of the Eglin team instead of doing the job exclusively under contract has saved approximately 16.5 million dollars. This project will be the first large scale use of the Air Force in-house compatibility testing capabilities, facilities and techniques described above.

NEAR TERM FUTURE PLANS

(U) Both the ADTC and AFATL are now active in assisting the AMSA (B-1A) and the F-15 SPO's in planning the weapons integration for these aircraft. We have offered to accomplish both of these weapons certification programs at Eglin. We feel that the in-house capability now in being at Eglin can be of great value.

4T TUNNEL MODIFICATION

(U) The 4T tunnel is now being modified to provide a drop model capability. Compatibility testing on the F-111A, using drop models, is scheduled to begin soon.

(U) A study is underway to redesign the store model sting with a "dog-leg," or offset, to prevent the sting from striking the aircraft model on some tests.

FUEL TANK CAMERA PODS

(U) Combat configurations for most USAF aircraft today include external fuel tanks. These tanks must be present during flight tests to provide the proper aircraft aerodynamic flow field. Several of these tanks are now being modified to provide camera mounts and viewing windows. The long length of the tanks makes it possible to photograph store separation simultaneously from two or more widely separated cameras. This will allow two-camera computer solutions. Cameras will be time correlated, with time annotation on each frame.

AIRBORNE TV SYSTEM

(U) An Eglin F-4 aircraft will soon be instrumented with a TV camera for observing weapon separations. The camera will be mounted in one of the standard ADTC camera pods. The pilot will be provided a monitor in the cockpit (in this case, the Walleye weapon display) so that he can observe the test item during separation. The TV picture may be telemetered back to the range control for real time observation by engineers, or it may be recorded by an onboard video tape recorder.

STORE MASS TOLERANCE MEASUREMENT

(U) One of the most important problems now being faced by aircraft manufacturers in the analysis of flutter and aircraft structure is the lack of accurate store mass properties information and their production tolerances. The AFATL has recently acquired a large machine (called the Big I) which can determine store weight, c.g. and moments of inertia to very precise accuracies. A program has begun to lot-sample many of the current stores to determine how much tolerance exists in their mass properties. This facility, costing several hundred thousand dollars, represents a unique Air Force testing capability at Eglin. Inert or live munitions weighing up to 3500 pounds can be "swung" on the machine.

ULTIMATE GOALS

(U) Although U. S. aircraft and weapons have reached new heights in sophistication, the simple truth is that we are not much better at hitting a specific target than we were in World War I. Improving weapons delivery accuracy is a topic much in discussion today at all levels throughout the military establishment. Erratic store behavior during separation or afterwards, of course, leads to inaccurate deliveries, and so do malfunctions and errors in the weapon release system.

(U) One of the biggest reasons for the problems we encounter today in weapon separation and delivery accuracy is the method used to design and produce the aircraft itself. All of the tactical aircraft procured in recent years for the Air Force and the Navy have been designed primarily around performance specifications based on the clean aircraft. Nearly all the mandatory stability, performance, and handling characteristics demonstrations require a clean aircraft configuration. The aircraft, in other words, is thought of as an airplane on which bombs may be hung, rather than as a weapons platform.

(U) Recently, one of the large manufacturers of aircraft flight control systems has come upon an interesting discovery. General Electric, in trying to improve the accuracy of the M61 gun in the F-4E, discovered that small changes in relays and damper ratios in the flight control system made large increases in gun accuracy. A flight control simulator was built and tested by pilots, who confirmed that the simulator did indeed duplicate problems encountered in combat. From this has come the possibility of multi-mode flight control systems and a reexamination of the military specifications on flight control systems.

(U) We in the Air Force hope that we can take advantage of the interest generated - at all levels - in recent years on weapon separation to cause a reexamination of current aircraft design and procurement methods. We are working with the other services now to increase the interchange of technical information and hope soon to establish a joint Technical Coordinating Group subcommittee on weapons separation. We are making plans now to conduct an Air Force sponsored symposium, such as this, at Eglin AFB in the fall of this year.

(U) Perhaps, if all these things actually materialize, we may even, one of these days, cause an aircraft to be designed from the ground up as a true weapons delivery platform - not a rapid transit system for transporting munitions from a friendly air base to an enemy target.

Appendix I

CLASSIFICATION OF EXTERNAL STORES

(U) The mission of ADTC requires the use, or test, of a great variety of external stores, some of which are never intended to be fully qualified on any type of aircraft. These stores must be qualified to a varying degree, dependent on the type store, the test requirement, and the intended use of the store.

(U) No flight testing of a newly developed external store should be undertaken without first having accomplished all the necessary preliminary tests (wind tunnel, computer studies, etc.). It is a fact of life, however, that there is rarely the time, the money, or the test items available to do all the preliminary tests. Obviously, there is a need to flight test these items and, just as obviously, some compromises are required if flight testing is going to be accomplished. In making such compromises, past experience plays a large role. Based on past experience in external stores testing, and the classification of the types of stores and tests required, a table may be established. This table will show the relative risk involved in flight testing each class and category store for each type test requirement without having previously accomplished all the necessary preliminary tests (such as computer studies, wind tunnel tests, etc.). For the purpose of discussion, the various types of stores that ADTC is called upon to test can be categorized as follows:

CLASS "A": Low density stores which undergo a change of weight and/or C.G. in flight due to expenditure of munitions or operation of an internal system. Item is intended to be retained and re-used -- jettison under emergency conditions is required (fuel tanks, gun pods, dispensers, etc.).

CLASS "B": Low density stores which have fixed equipment installed such that no weight or C.G. change occurs in flight. Item is intended to be retained and re-used -- jettison under emergency conditions is required (camera pods, radar pods, modified fuel tanks, instrumentation pods, etc.).

CLASS "C": Low density stores which may or may not undergo a weight or C.G. change in flight, but which are intended to be dropped and not brought back in an operational environment (CB spray tanks, napalm tanks, fire bombs, etc.).

CLASS "D": High density stores which undergo no weight or C.G. change in flight and are intended to be dropped (bombs, mines, missiles, etc.).

NOTE: "Inflight" refers to period of time item is airborne but still attached to carriage aircraft.

These stores may be further categorized as follows:

CATEGORY 1: Stable store, C.G. within the MIL SPEC limits.

CATEGORY 2: Unstable store, C.G. within MIL SPEC limits.

CATEGORY 3: Stable or unstable store, C.G. not within MIL SPEC limits.

Where: "Stable" means the item has a static margin of at least one body diameter in pitch and yaw at the most aft C.G.

"Unstable" means the item has a static margin of less than one body diameter in either pitch or yaw at the most aft C.G.

"C.G. within limits" refers to limits specified in MIL-A-8591C. C.G. must be within $\pm$ 3.0" of center point between attachment lugs.

(U) In addition to categorizing the stores themselves, the types of tests that ADTC is called upon to conduct can be categorized as follows:

TYPE 1: Full scale compatibility tests and qualification of a new item on one or more types of aircraft, including determination of carriage and ejection envelopes and allowable loading configurations both for the item alone and in combination with other stores.

TYPE II: Limited compatibility testing of a new item on one or more types of aircraft, but not determination of carriage envelope or allowable loadings in combination with other stores (engineering evaluation of item itself).

TYPE III: Limited flight tests of a new or standard item on one or more types of aircraft for the purpose of investigating or demonstrating feasibility or concepts of operation.

TYPE IV: Full scale compatibility tests and qualification of a standard or already developed item on a different aircraft or station from that on which it is currently cleared for carriage. Test will include determination of carriage and ejection envelopes and allowable loading configurations both for the store alone and in combination with other stores.

TYPE V: Limited compatibility testing of a standard or already developed store on a different aircraft or station from that on which it is currently cleared for carriage. No determination of carriage envelope or allowable loadings in combination with other stores.

TYPE VI: Limited flight testing of a store which is standard for another service, or foreign government, on one or more USAF aircraft for the purpose of investigating or demonstrating the feasibility of its use as an Air Force weapon.

Category I - Stable - C. G. Okay
Category II - Unstable - C. G. Okay
Category III - Stable or Unstable - C.G. out of limits

AIRCRAFT/STORES COMPATIBILITY TESTING

TABLE OF RELATIVE RISK FACTORS

TYPES OF STORES			TYPES OF TESTS					
CLASS		CATE-GORY	FULL SCALE COMPATI-BILITY NEW OR DEVELOP-MENT ITEM	LIMITED COMPAT-IBILITY NEW OR DEVELOP-MENT ITEM	FEASIBILITY TEST - NEW OR STAND-ARD ITEM	FULL SCALE COMPAT-IBILITY, STANDARD ITEM, DIFFERENT A/C	LIMITED COMPAT-IBILITY, STANDARD ITEM, DIFFERENT AIRCRAFT	FLIGHT TEST OF OTHER SERVICE OR FOREIGN ITEMS
			TYPE I	TYPE II	TYPE III	TYPE IV	TYPE V	TYPE VI
A	Lo-Density, C.G. change, reusable emerg. jett. only	1 2 3	High V. High V. High	Med High V. High	Low * Med* High*	High V. High V. High	Med High V. High	Low* Med* High*
B	Lo-Density, fixed C.G., reusable, emerg. jett. only	1 2 3	High V. High Unaccep	Med High Unaccep	Low* Med* Unaccep	High V. High Unaccep	Med. High Unaccep	Low* Med* High*
C	Lo-Density, C.G. variable, intended to be dropped.	1 2 3	High V. High Unaccep	Med High Unaccep	Med * High * Unaccep	High V. High Unaccep	Med High Unaccep	Med High Unaccep
D	Hi-density, fixed C.G., intended to be dropped.	1 2 3	Med Unaccep Unaccep	Low Unaccep Unaccep	Low Unaccep Unaccep	Med Unaccep Unaccep	Low Unaccep Unaccep	Med Unaccep Unaccep

EXPLANATION OF RATINGS:

LOW -- Low risk item. Can be flight tested with minimum risk after a few preliminary tests and use of conservative flight limits.

MED -- Medium risk item. Can be flight tested with medium risk by using experience factor and performing only some preliminary tests. Results to be gained are usually worth the risk involved.

HIGH -- High risk item. Can be flight tested with high risk by using experience factor and performing only some preliminary tests. Results to be gained probably not worth risk involved.

V. HIGH -- Very high risk item. Some limited flight testing could be done by using experience factor and performing some preliminary tests. Entire flight test program should not be accomplished unless all ground tests have been performed (wind tunnel, computer, etc.). Results gained are definitely not worth full flight test without full preliminary testing.

UNACCEP -- These items should not be flight tested in their present form under any circumstances. In most cases, the "Unaccep" classification imposed because it is not logical to have an item of the particular class in a particular category. The item itself could be altered to place it in a safer category and, therefore, testable.

* Rating assumes that no intentional jettisoning will be accomplished during test. If jettisoning is to be done, rating should be increased at least one level.

(U) FIG. 1. Technician Adjusting Model in AEDC 4T Transonic Wind Tunnel (4T).

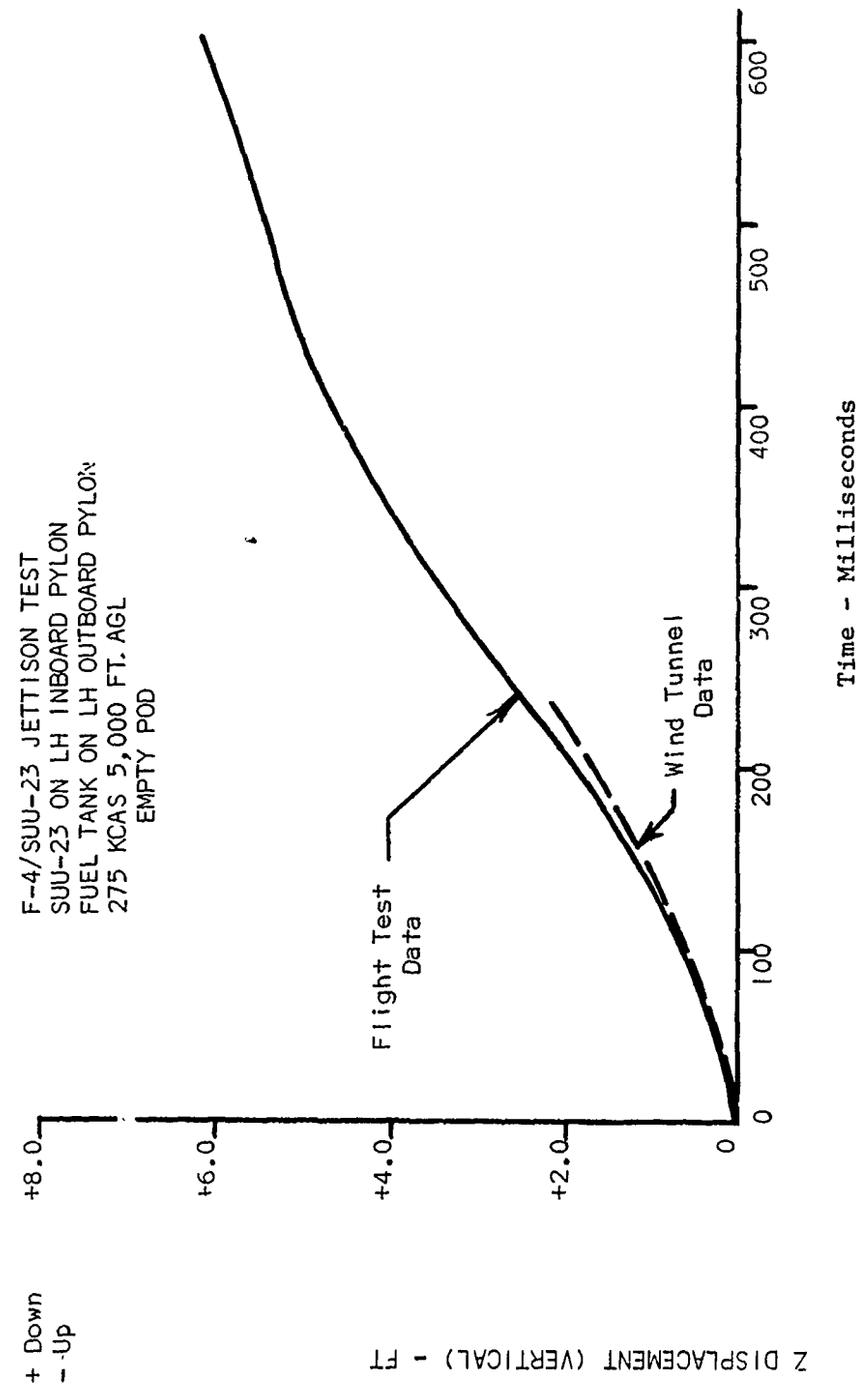
F-4/SUU-23 JETTISON TEST
SUU-23 ON LH INBOARD PYLON
FUEL TANK ON LH OUTBOARD PYLON
275 KCAS 5,000 FT. AGL
EMPTY POD
Flight Test Data
Wind Tunnel Data
+ Down
- Up
+8.0
+6.0
+4.0
+2.0
0
0
100
200
300
400
500
600
Z DISPLACEMENT (VERTICAL) - FT
Time - Milliseconds

(U) FIG. 2

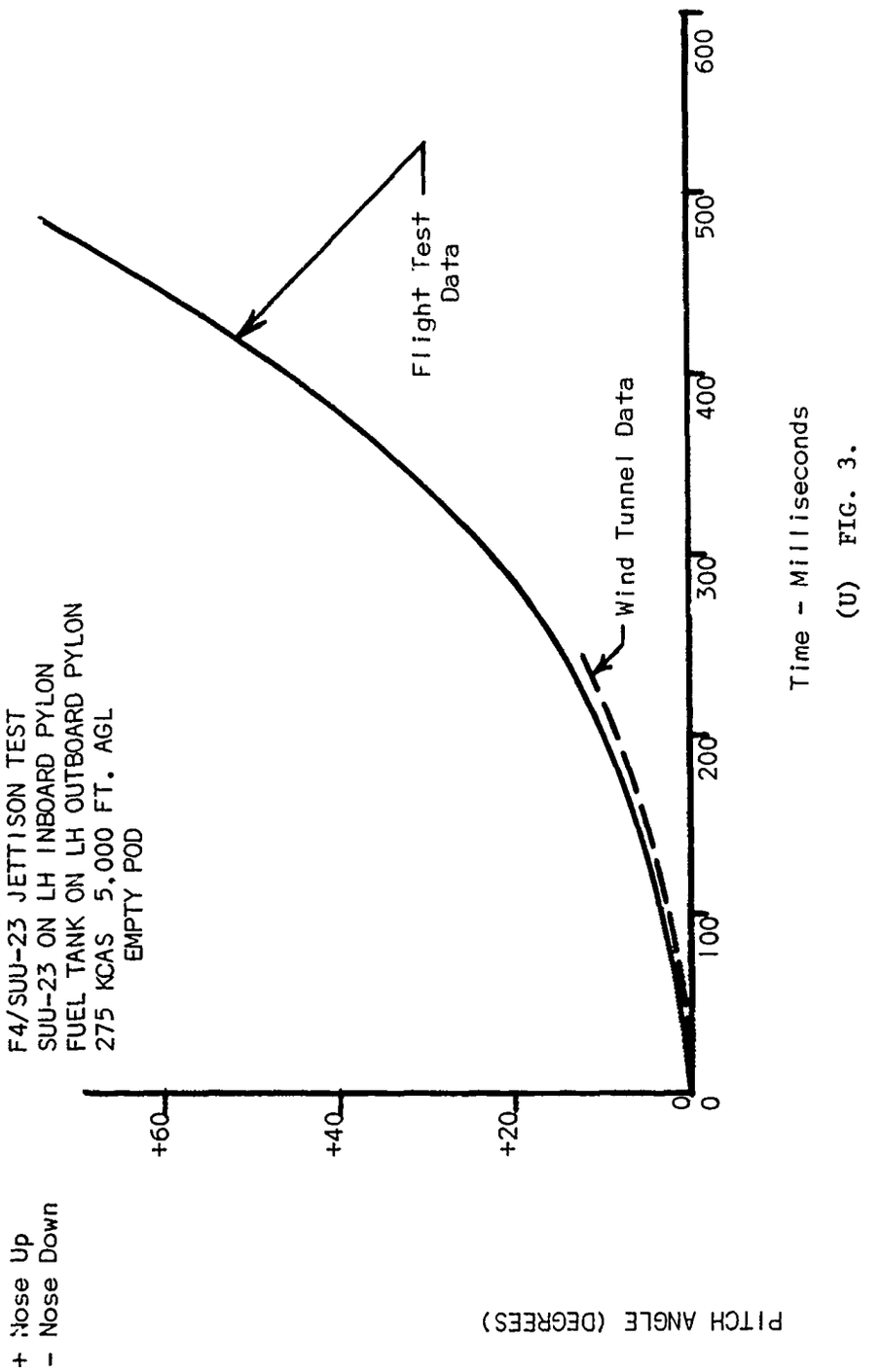
F4/SUU-23 JETTISON TEST
SUU-23 ON LH INBOARD PYLON
FUEL TANK ON LH OUTBOARD PYLON
275 KCAS 5,000 FT. AGL
EMPTY POD
+ Nose Up
- Nose Down
+60
+40
+20
0
0
100
200
300
400
500
600
Flight Test Data
Wind Tunnel Data
PITCH ANGLE (DEGREES)
Time - Milliseconds

(U) FIG. 3.

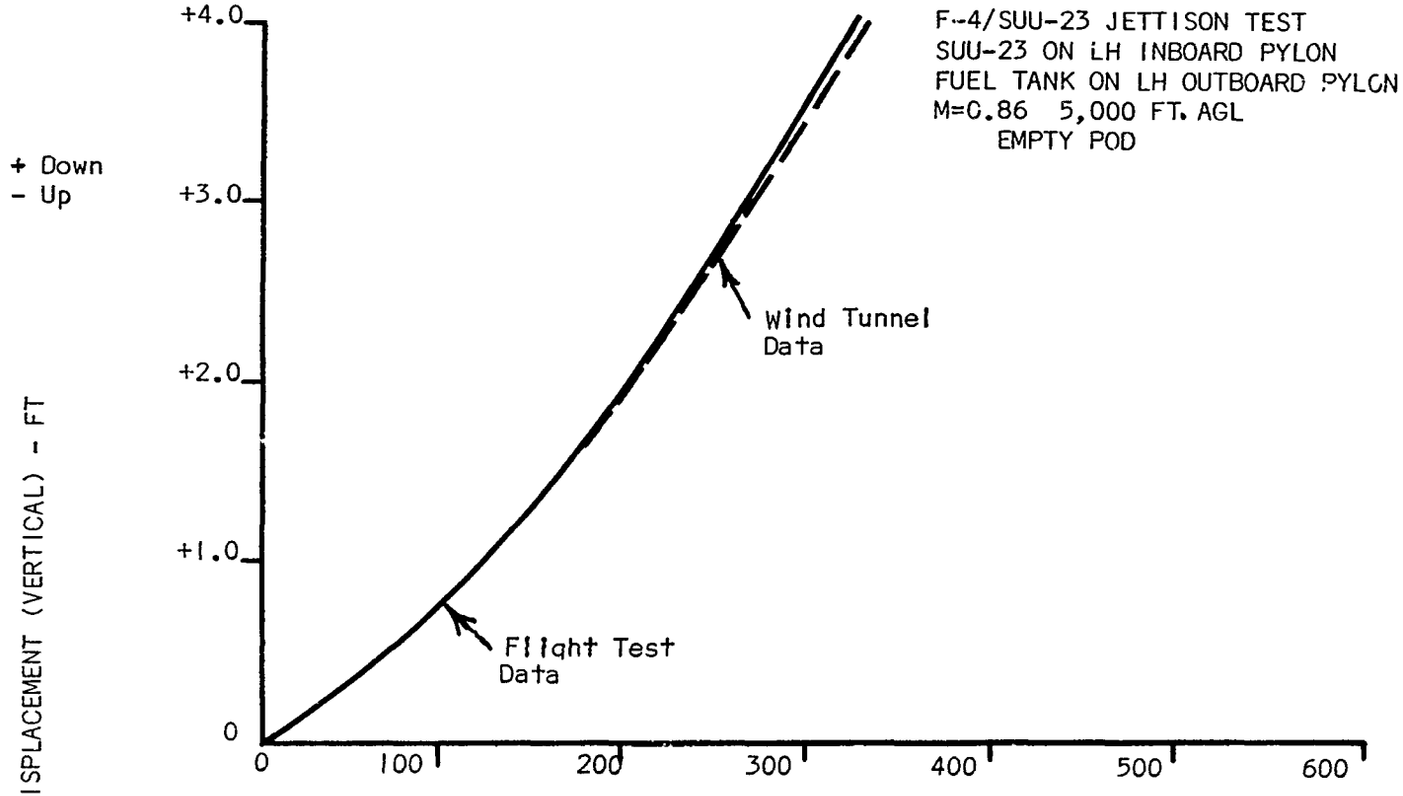
F-4/SUU-23 JETTISON TEST
SUU-23 ON LH INBOARD PYLON
FUEL TANK ON LH OUTBOARD PYLON
M=0.86 5,000 FT. AGL
EMPTY POD
+ Down
- Up
Z DISPLACEMENT (VERTICAL) - FT
+4.0
+3.0
+2.0
+1.0
0
0
100
200
300
400
500
600
Wind Tunnel Data
Flight Test Data
Time - Milliseconds

(U) FIG. 4

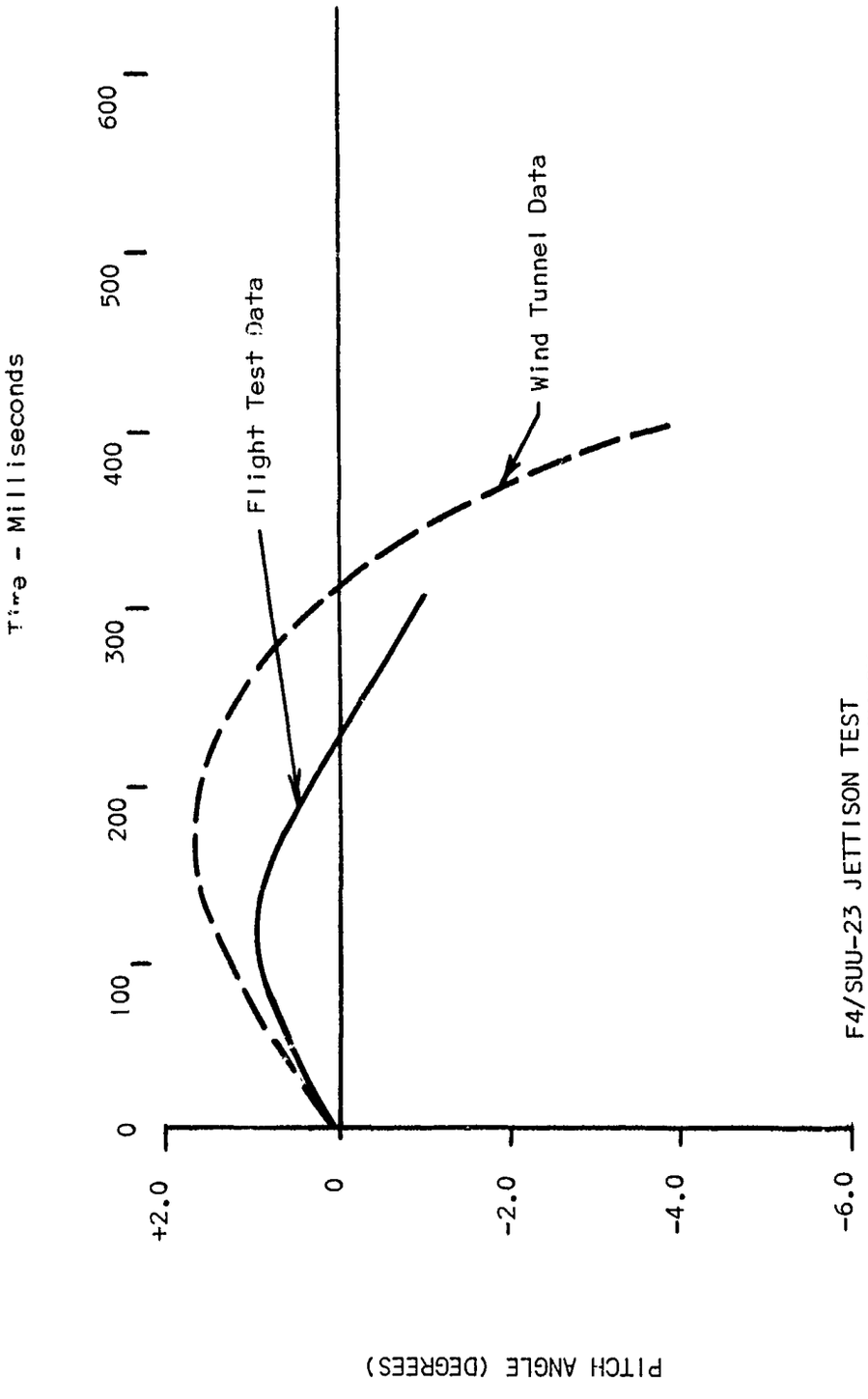
Time - Milliseconds
0
100
200
300
400
500
600
Flight Test Data
Wind Tunnel Data
+2.0
0
-2.0
-4.0
-6.0
PITCH ANGLE (DEGREES)
F4/SUU-23 JETTISON TEST
SUU-23 ON LH INBOARD PYLON
FUEL TANK ON LH OUTBOARD PYLON
M=0.86 5,000 FT.AGL
EMPTY POD
+ Nose Up
- Nose Down

(U) FIG. 5.

Paper No. 44

PREDICTION OF STORE LAUNCH CHARACTERISTICS THROUGH STATISTICAL METHODS (U)

(Paper UNCLASSIFIED)

by

Michael A. Sekellick
Naval Ship Research and Development Center
Washington, D.C. 20007

ABSTRACT. (U) Two statistical methods, a multiple regression and a discriminant function analysis, were applied to store launch data in order to establish the feasibility of their application in the prediction of store separation characteristics. With the aid of the computer, these analyses were applied to trajectory data from wind tunnel dynamic model store drops. Regression equations for the initial maximum pitch angle and time integral of store nose distance from its original position were evolved. These equations contained as independent variables those statistically important parameters and parameter combinations which describe flow conditions and store/aircraft geometry. Through the discriminant function analysis, a linear function of the launch parameters was formed which categorized the launches into two groups, satisfactory and unsatisfactory.

SYMBOLS

c	local wing chord, inches
e	δ/w
M	Mach number
R_N	distance from store C.G. to tip of store nose, inches
R_T	distance from store C.G. along axis of symmetric to tip of tail, inches
TLIM	integration limit for time integral of z_N, z_T, seconds
w	distance in x-z plane of store C.G. from leading edge of wing, inches
x	longitudinal coordinate
z	vertical coordinate
z_N	vertical distance of store nose from its launch position, inches
z_T	vertical distance of store tail from its launch position, inches
α_w	angle of attack of wing, radians
β	$\sqrt{1-(\text{Mach no.})^2}$
δ	distance of store C.G. from wing undersurface, inches
θ	store pitch angle, radians
θ_o	reference pitch angle (=0 at t=0), radians
θ_1	initial pitch maximum angle, radians
Λ	leading edge sweep angle, radians
τ	maximum wing thickness at pylon station, inches

NOTE: Full-scale aircraft and store dimensions were used throughout the calculations.

INTRODUCTION

(U) It is now possible, utilizing new experimental and analytical techniques, to generate a large number of launch events describing store separation behavior for a variety of launch conditions and store parameters. It appears profitable to quantify the relationship between the results obtained and parameters describing the configurations and launch conditions in order to attain a capability for predicting the separation characteristics of an untried aircraft/store combination. Insufficient knowledge of the complex interference flow field about a launched store near the parent aircraft has limited the use of purely theoretical methods, but it is reasonable to attempt to deal with the problem on a statistical basis. Below are presented two statistical methods to be employed in such an approach and examples of their application to a limited number of launch events.

(U) A mathematical relation must be found between an aircraft/store configuration, the launch conditions, and the nature of the associated trajectory. In order to describe an aircraft/store combination adequately, it must be characterized by parameters representing the important geometric and physical features which affect separation behavior. Some typical geometric parameters are illustrated in Figure 1. Launch events or trajectory characteristics can be catalogued in terms of such parameters, and statistical methods, in the form of computer programs, can be utilized to predict the outcome of an untried launch situation.

(U) Reference 1 provides separation characteristics of various weapons carried by the F-111 airplane. These data were obtained from wind tunnel dynamic model drops of model stores at a variety of launch conditions and mounting locations. The trajectories were recorded by high speed motion picture cameras, and this information was transformed by computer into tabulated data describing the time history of each store's pitch, yaw, and c.g. position during separation. A subset of the data, sixty-one drops of the M 117 bomb from four wing pylons and various rack configurations, was chosen for analysis. An outline of the mounting locations and launch conditions is also given in Reference 1.

(U) As an aid in assessing how well the statistical methods distinguished between safe and hazardous launches, the sixty-one dynamic drops were classified into two groups, satisfactory and unsatisfactory. Any separation which possessed an initial pitch maximum angle greater than fifteen degrees was called unsatisfactory, as were those with

erratic z(t) and θ(z) curves. Also, launched stores which made contact with adjacent mounted stores or the aircraft during launch were said to have an unsatisfactory separation. All other launches were called satisfactory. A listing of the separations is given in Table 1, along with appropriate remarks.

(U) Two characteristics of store behavior, pitch, and the time integral of store nose distance from its launch position, have been chosen to portray the nature of the separation and act as indices of the degree of hazard. By using the technique of multiple linear regression, an empirical relation was found between each index and parameters expressing configuration geometry and flow conditions. Each index was a dependent or response variable in a separate regression analysis.

(U) The general approach was as follows. A regression analysis was performed to construct a linear fit between the dependent variable and the basic group of k - 1 parameters:

$$x_1 = f(x_2, x_3, \ldots x_k) \tag{1}$$

(U) The fit was improved by modifying members of the basic group and including as new parameters:

$$x_1 = f(x_2, x_3, \ldots x_k, x_{k+1}\, x_{k+2}, \ldots) \tag{2}$$

where $x_{k+1} = x_2^2$

$x_{k+2} = x_2 x_3$, for example.

Also functions of members of the basic group were formed. During the construction of these functions, there was heavy reliance on geometric intuition:

$$x_1 = f(x_2, x_3 \ldots x_{k+1}, x_{k+2}, \underbrace{x_{k+3}}_{\sin x_5}, \underbrace{x_{k+4}}_{\tan^{-1} \frac{x_3}{x_6}}) \tag{3}$$

, for example.

(U) Because of limited computer storage space, these calculations were under the constraint that the regression equation have a maximum of nineteen independent parameters.

(U) As a measure of goodness of fit, the multiple correlation coefficient was computed for each regression equation. The influence of the i^{th} parameter in an equation was reflected in the parameter's partial correlation coefficient and magnitude of the co-factor of the $(1,i)^{th}$ term of the covariance matrix.

(U) Several series of regression analyses were performed. As is seen above, the first mathematical model in each series was nested within all succeeding models in that series. The effectiveness of the

additional parameters in a particular model was measured by the F-test, a statistical device which compares the estimates of error variance between the given model and the first. For a further discussion of these terms see Appendix A and Reference 2.

REGRESSION ANALYSIS OF INITIAL PITCH MAXIMUM ANGLE

(U) Usually the $\theta(z)$ curve for a stable store exhibits a damped sinusoidal oscillation, and one of the outstanding features of such motion is its first pitch maximum angle. This first maximum might be regarded as a rough gauge of the extent of flow field distortion present during the store's separation from the parent aircraft, assuming that the $\theta(z)$ curve is single-valued and does not diverge.

(U) There were two main subgroups of the data - those trajectories which fit the above description, and those which did not. About ten percent of the observations exhibited diverging $\theta(z)$ curves, and another ten percent showed $\theta(z)$ not single-valued. It might be argued that this twenty percent should not have been included in the analysis, since prediction of initial pitch maximum is of little value in portraying the hazard in these cases. However, it was felt that if the initial maximum could be predicted accurately even for these, then other aspects of the trajectory might also be correlated with configuration and flow field parameters.

(U) From the regression analysis of initial pitch maximum a set of parameter combinations was built which defined a regression surface with a multiple correlation coefficient of 0.92. According to a method discussed in Reference 2, bounds on this coefficient should be placed at 0.86 and 0.95. One interpretation given to this number is a measure of the usefulness of the relation between the independent variables and initial maximum. It can be shown that the square of the multiple correlation coefficient represents the percentage of the variance of the initial maximum attributable to the independent variables. Thus, about 80% of the variance in the initial maximum is accounted for by the combinations of values of the given parameters, and 20% is ascribed to error.

(U) The set of parameters along with their coefficients is presented in Table 2. When a prediction of the values of initial maxima in the data was attempted, the error distribution shown in Figure 2 resulted. To illustrate its utility as a means of scoring, predictions of the regression equation were compared in Table 4 with segregation by the 15° criterion and the original satisfactory—unsatisfactory grouping ("reality"). The 15° rule errs in nine cases, or 15% of the total with respect to reality. The regression equation errs in five cases (8%) with respect to the 15° rule, and 15 cases (23%) with regard to reality.

REGRESSION ANALYSIS OF NOSE DISTANCE INTEGRAL

(U) As another method of scoring separations the following was used: Two extreme points on the store - the nose tip and tail end - were chosen as reference points. Graphs of the distance of these points from their original positions are approximately given as a function of time by:

$$z_N(t) = z(t) - R_N\,\theta(t)$$
$$z_T(t) = z(t) + R_T\,\theta(t) \qquad (4)$$

(U) An example of the construction of the $z_N(t)$ and $z_T(t)$ curves is presented in Figures 3 and 4. Shown are the resultant curves corresponding to graphs of $z(t)$ and $\theta(t)$ for a typical trajectory.

(U) The integrals of the $z_N(t)$ and $z_T(t)$ curves of each of the model dynamic drops were calculated by computer program. Limits of integration of 0.04, 0.06, and 0.07 seconds were tested. At 0.04 seconds the integrals did not allow a segregation of the launches. That is, values of the integrals of satisfactory and unsatisfactory launches fell together in a random fashion with no apparent pattern and thus, had no value in scoring. However, at 0.06 and 0.07 seconds, significant separation of the $\int_o^{TLIM} z_N dt$ populations was achieved. (See Appendix B). It was impossible to use a limit of integration above TLIM = 0.07 since data was not recorded for many trajectories beyond this time. Figure 5 illustrates the distribution of $\int_o^{TLIM} z_N dt$ values. No similar separation of $\int_o^{TLIM} z_T dt$ values was found; hence, it was not used as a separation scoring device.

(U) In Figure 5, upper and lower bounds (U.B.,L.B.) were erected on the $\int_o^{TLIM} z_N dt$ scale in order to separate the satisfactory population from the unsatisfactory. The lower branch of the unsatisfactory group represents only stores which floated, having experienced high lift and remained near the aircraft, while those in the upper branch possessed large initial values in pitch. All satisfactory separations fell between these two groups, and there was little overlap. Thus, the integral of nose distance from launch position with time appears to be an effective means of scoring separations.

(U) Use of the nose integral as a dependent variable in a regression analysis was fruitful in the following sense: A set of parameter combinations was found which, when used as a set of independent variables, predicted the outcomes of the data launches correctly in 50 out of the 61 cases (18% error). The bounds erred in five cases (8%) because of the slight overlap in the distributions, and the regression equation erred in nine cases (15%) with respect to the bounds. Table 5 presents a three-way comparison of the outcome for each trajectory for an integration limit of 0.07 seconds. In the Table reality

is matched with the $\int_0^{TLIM} z_N dt$ scoring scale, and both of these with the prediction of the regression equation. Results are similar for 0.06 seconds.

(U) Consider Table 6, which is a comparison of the unsatisfactory outcomes forecast by applying the two regression equations to the input data. This suggests the possibility of utilizing additional indices and assigning a weight to each regression equation to produce a composite prediction. Such a scheme may overcome some of the shortcomings of using each index individually. With more indices, proper weights, and more meaningful parameter combinations, perhaps a dependable forecast of unsafe separations will result.

DISCRIMINANT FUNCTION ANALYSIS

(U) One of the simplest methods of making the separation data statistically useful was to classify the launches into two categories: satisfactory and unsatisfactory. The information in this form can also be operated on by a discriminant function analysis, a technique for finding a function which will discriminate between the categories.

(U) For each launch the configuration and flow conditions were represented as k parameters X_i, i = 1, ...k. A linear function Z (X_i) was formed for which coefficients of the X_i's were determined so as to maximize the distance between the Z-means of the two categories while minimizing the separation between Z-values within each category.

(U) A good discriminant function is useful to the study of store separation in several ways. Given information describing a proposed launch (in the form of a set of parameter values describing the launch conditions) the function provides a means of determining the launch's acceptability by predicting into which category it will most likely fall. If both categories produce populations of Z-values with roughly equal variances, a scale may be established from the Z-mean of one category's population to that of the other. The mid-point of this distance is defined as a zero-point. Thus if the Z-function of a given drop is computed and referenced to this scale, one can relate the drop to a number representing its degree of acceptability.

(U) Through another F-test (Appendix A) one is able to gauge the goodness of discrimination of a particular Z-function by measuring the separation between the means of the populations in relation to their variances. This is necessary since some functions may be much better than others in distinguishing between the groups. That is, some sets of parameters may be more physically meaningful in the sense that their interrelationships express the two-category classification of the data more fully. An offshoot of such a comparison of functions is the ability to distinguish a relatively unimportant parameter by comparing F-numbers of a set containing the parameter and one without.

(U) The same set of parameter combinations from the multiple linear regression analysis of θ_1 was adopted as the set of independent variables. Since this set had met with some success in prediction of the initial pitch maximum angle, it was probable these combinations would also be helpful in differentiating between good and bad launch groups.

(U) A representative launch was chosen from each category and excluded from the construction of the discriminant functions. One launch, T_1, exhibited satisfactory separation, while the other T_2, was clearly hazardous. These were employed as tests on the power of the functions generated, and the positions of their Z-values with respect to the distributions of the categories were noted.

(U) Two discriminant functions were built, the second being formed by deletion of the last independent variable from the first equation. These functions are given in Table 7, and their statistical information is listed in Table 8.

(U) In order to illustrate the form of the Z distributions the discriminant functions were applied to the input data in order to help visualize the separation of the two groupings. These are illustrated as frequency distributions in Figures 6(a) and 6(b). The scale upon which each distribution is represented has been manufactured by the analysis and depends only upon the aggregate of index values and not upon launch parameters.

(U) Because of the large overlap in these distributions, the parameter Set #1 apparently is not the best choice for the independent variables, although the F-test indicates a significant difference in the two groups at the 5% level. Prediction of the test cases was conservative; both launches were placed well into the unsatisfactory grouping, and their order was preserved with respect to the scale. It is believed that a careful choice of independent variables will lead to a more powerful function.

(U) It is interesting to note how the deletion of an important parameter affects the distributions. Set #2 is even less efficient than #1. The groups merge and the order of the test cases is reversed on the scale.

CONCLUDING REMARKS

(U) Two statistical methods, a multiple regression and a discriminant function analysis, were performed on store launch data. Relationships between launch behavior and parameters describing aircraft/store geometry and launch conditions were shown to be accessible through these techniques. It is believed that they may be extended to a composite scoring method composed of several regression and discriminant equations to predict hazardous store separations.

REFERENCES

1. 1/24-Scale F-111A and F-111B Trajectory (Drop) Model Wind Tunnel Data Report (U), by J. R. Johnson. Ft. Worth, Texas, June 1966. 24 illus. (GD/Fort Worth Rpt. FZT-12-142, publication UNCLASSIFIED.)

2. Introduction to Mathematical Statistics (U), by Paul C. Hoel. N.Y., Wiley, 1947. 258 p. illus.

3. The Statistical Analysis of Experimental Data (U), by John Mandel. N.Y., Interscience Publishers, 1964. 410 p. illus.

4. Statistical Methods in Research (U), by Palmer O. Johnson. N.Y., Prentice-Hall, 1949. 377 p. illus.

APPENDIX A

USING THE F-DISTRIBUTION

Application of the F-Distribution to Nested Mathematical Models in the Regression Analysis

(U) Consider the general linear model:

$$(I) \quad X_1 = B_o + B_2 X_2 + \ldots + B_k X_k + \epsilon$$

where ϵ denotes an experimental error. Suppose it is desired to add more independent variables to this equation either by constructing them from the original set (e.g., $X_{k+1} = X_2 X^2_3$) or choosing additional parameters. Then the model becomes:

$$(II) \quad X_1 = (B_o + B_2 X_2 + \ldots + B_k X_k) + \beta_1 Y_1 + \ldots \beta_q Y_q + \epsilon$$

(U) One method of finding whether these additional parameters aid in estimating X_1 is through the F-test, which compares the estimates of error variance associated with each model.

(U) Suppose regression analyses are performed on both models I and II and the estimates of their coefficients are:

$$(I) \quad B_o, B_2 \ldots B_k$$

$$(II) \quad B_o', B_2' \ldots B_k', \ldots \beta_q$$

where primes indicate that coefficients of the first k terms are probably different for each model. The hypothesis to be tested is that the additional q parameters add nothing to the model; i.e., $\beta_1 = \beta_2 = \ldots \beta_q = 0$.

(U) Given n sets of data, the estimates of error variance are:

$$V_I(\epsilon) = \frac{\sum_I (X_1 - X_1')^2}{n - k} \equiv \frac{SS_I}{n-k}$$

$$V_{II}(\epsilon) = \frac{\sum_{II} (X_1 - X_1')^2}{n - (k+q)} \equiv \frac{SS_{II}}{n-(k+q)}$$

Let $M_\Delta = (SS_I - SS_{II})/q$

The F-test here is defined as:

$$F = \frac{M_\Delta}{V_{II}(\epsilon)} = \frac{(SS_I - SS_{II})/q}{SS_{II}[n-(k+q)]}$$

(U) This ratio is said to have q degrees of freedom in the numerator and $[n-(k+q)]$ in the denominator.

(U) Note that if the given hypothesis is false, then the F-ratio will be close to unity, while if model II is a more accurate representation of the data, then F will tend to exceed unity. In most sets of mathematical tables, values of F for various combinations of degrees of freedom have been given for regions of low probability (high significance). Thus, model I can be considered inadequate if the numerical value of F falls within the chosen critical region of F defined by q and n - k - q degrees of freedom.

Application of the F-Distribution to Discriminant Function Analysis

(U) Given a discriminant function $Z(x_i)$ define the means of the two groups as:

$$\bar{Z}_1 = \sum_i \lambda_i \bar{x}_{1i} \quad (i = 1, \ldots k)$$

$$\bar{Z}_2 = \sum_i \lambda_i \bar{x}_{2i} \quad (i = 1, \ldots k)$$

where $\bar{x}_{ji}$ is the mean value of x_i for the j^{th} group, and N_j is the number of members of group j. The hypothesis to be tested is that the expectations of mean value for both groups are equal. In other words, there is no significant difference between the groups for the function Z.

(U) The sum of squares due to "within groups" variation is:

$\sum_i \lambda_i (\bar{x}_{1i} - \bar{x}_{2i})$ with $N_1 + N_2 - k - 1$ degrees of freedom.

(U) The sum of squares due to "between groups" variation is:

$$\frac{N_1 N_2}{N_1+N_2} \sum_i \lambda_i (\bar{x}_{1i} - \bar{x}_{2i})^2$$ with the degrees of freedom.

(U) The test of the hypothesis is given by:

$$F = \frac{N_1 + N_2 - k - 1}{k} \cdot \frac{N_1 N_2}{N_1+N_2} \sum_i \lambda_i (\bar{x}_{1i} - \bar{x}_{2i})$$

If this number falls within the region of low probability for the chosen level of significance, then the hypothesis is rejected.

APPENDIX B

CHI-SQUARE TEST OF A SIGNIFICANT DIFFERENCE IN THE DISTRIBUTIONS OF $\int_o^{TLIM} z_n dt$ VALUES

Interval	Unsat. (α)	Sat. a'	$P = \frac{\alpha}{\alpha+\alpha'}$,	αP
-4 → 0	3	0	1.000000	3.000000
0 → 4	9	2	.818181	7.363629
4 → 8	1	17	.055556	0.055556
8 → 12	3	16	.157895	0.473685
12 → 16	7	0	1.000000	7.000000
16 → 20	0	0	0.000000	0.000000
20 → 24	2	0	1.000000	2.000000
24 → 28	1	0	1.000000	1.000000
	26	35	0.628954	20.892870

n_1 ↑ n_2 ↑ $\bar{P} = .628954$ $\sum \alpha P$

$$\chi_o^2 = \frac{1}{\bar{P}(1-\bar{P})} \sum \alpha P - n_1 \bar{P}$$

$$= \frac{1}{.628954(.371046)} \left[20.892870 - 26(.628954)\right]$$

$$\chi_o^2 = 19.4543$$

($\chi^2_{.01} = 18.475$ for $n = 7$)

(U) TABLE 1. A Listing of the Model Dynamic Drops

Case	Config.*	Remarks
1	54-1	
2	54-2	Unsatisfactory; $\theta_1 = 17.9^\circ$
3	55-1	
4	55-2	Unsatisfactory; $\theta_1 = 18.5^\circ$
5	58-1	
6	58-2	
7	59-2	
8	60	
9	61-1	
10	61-2	Unsatisfactory; flew over wing
11	62-1	
12	62-2	
13	63-1	Unsatisfactory; but adjacent store
14	63-2	Unsatisfactory; flew up over wing
15	64-1	Unsatisfactory; floated
16	64-2	Unsatisfactory; floated
17	65-1	Unsatisfactory; $\theta_1 = -16.1^\circ$
18	65-2	Unsatisfactory; floated
19	67-1	Unsatisfactory; $\theta_1 = -27.4^\circ$
20	67-2	
21	68-1	Unsatisfactory; $\theta_1 = -24.2^\circ$
22	68-2	
23	69-1	Unsatisfactory; $\theta_1 = -26.0^\circ$
24	69-2	Unsatisfactory; $\theta_1 = 19.6^\circ$, floated
25	70-1	Unsatisfactory; $\theta_1 = -33.4^\circ$
26	70-2	
27	71-1	Unsatisfactory; $\theta_1 = -35.4^\circ$
28	71-2	
29	72-2	
30	73-1	Unsatisfactory; $\theta_1 = -27.9^\circ$
31	73-2	

(U) TABLE 1. Concluded

Case	Config.*	Remarks
32	74-1	
33	74-2	Unsatisfactory; $\theta_1 = -27.1^\circ$
34	75	
35	76	
36	77-1	Unsatisfactory; $\theta_1 = -28.3^\circ$
37	77-2	
38	78-1	
39	78-2	
40	79-1	
41	79-2	Unsatisfactory; floated
42	80-1	
43	80-2	
44	95-1	
45	95-2	
46	96-1	
47	96-2	Unsatisfactory; floated
48	97-1	
49	97-2	Unsatisfactory; floated
50	98-1	
51	98-2	
52	99-1	Unsatisfactory; $\theta_1 = -15.0^\circ$
53	99-2	
54	100-1	Unsatisfactory; $\theta_1 = -46.8^\circ$
55	100-2	Unsatisfactory; $\theta_1 = -15.6^\circ$
56	101	
57	102-1	Unsatisfactory; $\theta_1 = -28.3^\circ$
58	102-2	Unsatisfactory; $\theta_1 = -19.7^\circ$
59	103	Unsatisfactory; $\theta_1 = -27.9^\circ$
60	104	
61	105	

*Configuration denoted in Reference 1.

(U) TABLE 2. Independent Variables and Coefficients in the θ_1 Regression Equation

I	X(I)	B(I)
2	θ_o	$.17519727 \times 10^{3}$
3	$\sin \theta_o$	$-.10059459 \times 10^{5}$
4	$1/\tan(\alpha_w - \theta_o)$	$-.22774532 \times 10^{-1}$
5	τ	$.23990683 \times 10^{2}$
6	$\tau^{\frac{1}{3}}$	$-.40848063 \times 10^{3}$
7	w	.23065255
8	$[\sin(\tan^{-1}e]/\beta$	$.17418278 \times 10^{2}$
9	$[\sin^3(\tan^{-1}e]/\beta^3$	$-.3+984380 \times 10'$
10	e	$.16499741 \times 10^{2}$
11	δ/c	$-.52255057 \times 10^{2}$
12	w/c	$-.10066301 \times 10^{2}$
13	$\cos(\tan^{-1}e)$	$-.79576607 \times 10'$
14	$\cos^2(\tan^{-1}e)$	$.346158\&4 \times 10^{2}$
15	$e\sqrt{\delta^2+w^2}$	-.18584248
16	$(w/c) \sin \theta_o$	$-.17165529 \times 10^{3}$
17	$\tan \alpha_w$	$.30918152 \times 10^{3}$
18	$w/\tan(\alpha_w - \theta_o)$	$-.78866332 \times 10^{-3}$
19	$\sin \Lambda$	$-.95135783 \times 10'$
20	$e \sin \Lambda$	$-.13564768 \times 10^{2}$

$B_o = .64518888 \times 10^{3}$

(U) TABLE 3. Independent Variables and Coefficients in the $\int z_N dt$ Regression Equation

I	X(I)	B(I)
2	τ	$-.67242439 \times 10^{1}$
3	$\tau^{\frac{1}{3}}$	$.11909168 \times 10^{3}$
4	w	$-.15974839$
5	$[\sin(\tan^{-1}e)]/\beta$	$-.56260789 \times 10^{1}$
6	$[\sin^3(\tan^{-1}e)]/\beta^3$	.80241813
7	e	$-.25115754 \times 10^{1}$
8	δ/c	$.21690757 \times 10^{2}$
9	w/c	$.60037019 \times 10^{1}$
10	$\cos(\tan^{-1}e)$	$.17734324 \times 10^{3}$
11	$\cos^2(\tan^{-1}e)$	$-.84805473 \times 10^{2}$
12	$e\sqrt{\delta^2+w^2}$	.12972364
13	$(w/c)\tan\alpha_w$	$.22002563 \times 10^{2}$
14	$\tan\alpha_w$	$-.20050523 \times 10^{2}$
15	$\sin\Lambda$	$-.55508767 \times 10^{1}$
16	$e\sin\Lambda$	$-.34636859$
17	M^2	$.12506348 \times 10^{3}$
18	$M^2\cos(\tan^{-1}e)$	$.11017809 \times 10^{3}$

$B_o = -.30024542 \times 10^{3}$

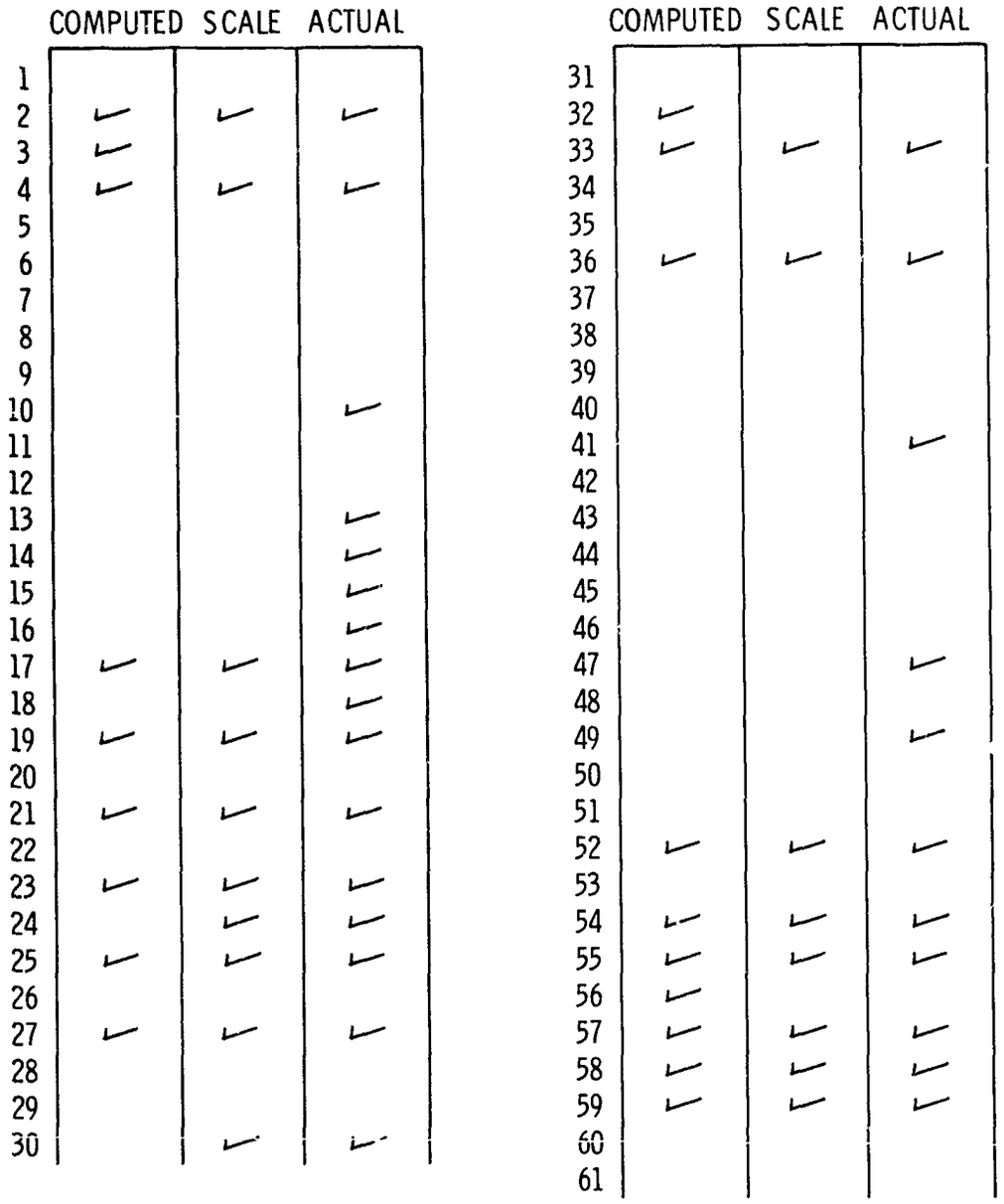

⌐ INDICATES UNSATISFACTORY SEPARATION

TABLE 4 - COMPARISON OF θ_1-PREDICTED, θ_1-SCALE, AND ACTUAL UNSATISFACTORY LAUNCHES.

	COMPUTED	SCALE	ACTUAL
1			
2	✓	✓	✓
3			
4	✓	✓	✓
5			
6	✓		
7			
8			
9			
10	✓	✓	✓
11			
12			
13	✓	✓	✓
14	✓	✓	✓
15	✓	✓	✓
16	✓	✓	✓
17			✓
18	✓	✓	✓
19	✓	✓	✓
20			
21	✓	✓	✓
22			
23		✓	✓
24	✓	✓	✓
25	✓	✓	✓
26			
27	✓	✓	✓
28			
29			
30		✓	✓

	COMPUTED	SCALE	ACTUAL
31			
32	✓		
33	✓	✓	✓
34	✓		
35			
36	✓	✓	✓
37			
38			
39			
40			
41		✓	✓
42	✓	✓	✓
43			
44			
45		✓	
46			
47			✓
48			
49	✓	✓	✓
50			
51	✓	✓	
52	✓		✓
53	✓		
54	✓	✓	✓
55	✓	✓	✓
56	✓	✓	
57	✓	✓	✓
58	✓	✓	✓
59	✓	✓	✓
60			
61			

✓ INDICATES UNSATISFACTORY SEPARATION

TABLE 5 - COMPARISON OF $\int z_n\,dt$-PREDICTED, $\int z_n\,dt$-SCALE, AND ACTUAL UNSATISFACTORY LAUNCHES.

	θ_1	$\int z_n dt$	ACTUAL
1			
2	✓	✓	✓
3	✓		
4	✓	✓	✓
5			
6		✓	
7			
8			
9			
10		✓	✓
11			
12			
13		✓	✓
14		✓	✓
15		✓	✓
16		✓	✓
17	✓		✓
18		✓	✓
19	✓	✓	✓
20			
21	✓	✓	✓
22			
23	✓		✓
24		✓	✓
25	✓	✓	✓
26			
27	✓	✓	✓
28			
29			
30			✓

	θ_1	$\int z_n dt$	ACTUAL
31			
32	✓	✓	
33	✓	✓	✓
34		✓	
35			
36	✓	✓	✓
37			
38			
39			
40			
41			✓
42		✓	
43			
44			
45			
46			
47			✓
48			
49		✓	✓
50			
51		✓	
52	✓	✓	✓
53		✓	
54	✓	✓	✓
55	✓	✓	✓
56	✓	✓	
57	✓	✓	✓
58	✓	✓	✓
59	✓	✓	✓
60			
61			

✓ INDICATES UNSATISFACTORY SEPARATION

TABLE 6 - COMPARISON OF θ_1-PREDICTED, $\int z_n dt$-PREDICTED, AND ACTUAL UNSATISFACTORY LAUNCHES.

(U) TABLE 7. Coefficients of the Discriminant Functions

I	Parameter Set #1 B(I)	Parameter Set #2 B(I)
1	3.0799506	2.2650513
2	-1.7718093×10^{2}	-1.3021588×10^{2}
3	$-1.1079103 \times 10^{-4}$	$-7.3211222 \times 10^{-5}$
4	$-5.7014278 \times 10^{-2}$	$-4.0619518 \times 10^{-2}$
5	1.0217454	7.6006846×10^{-1}
6	3.7133290×10^{-4}	$-4.4874456 \times 10^{-4}$
7	$-2.7026051 \times 10^{-2}$	1.4490428×10^{-2}
8	2.4840395×10^{-3}	$-1.1866090 \times 10^{-2}$
9	1.3476074×10^{-1}	$-4.4317095 \times 10^{-2}$
10	2.8728325×10^{-1}	1.9683863×10^{-1}
11	$-1.3648874 \times 10^{-1}$	$-4.2660372 \times 10^{-2}$
12	6.6828498×10^{-1}	5.9081963×10^{-1}
13	$-3.7811621 \times 10^{-1}$	$-3.7900272 \times 10^{-1}$
14	2.1590669×10^{-3}	2.2312982×10^{-3}
15	$-6.3146884 \times 10^{-1}$	$-4.1231731 \times 10^{-1}$
16	3.9234117×10^{-1}	2.8802868×10^{-1}
17	$-4.5151724 \times 10^{-6}$	$-2.8453368 \times 10^{-6}$
18	3.3274232×10^{-1}	2.3751831×10^{-1}
19	$-2.3190540 \times 10^{-1}$	

(U) TABLE 8. Statistics Related to the Discriminant Functions

Parameter Set #1

	Sums of Squares	Degrees of Freedom	Mean Square	
Within	.06216390	39	.00159395	F
Between	.05567285	19	.00293015	1.838

$\bar{Z}(1) = 2.289473$

$\bar{Z}(2) = 2.22730910$

Parameter Set #2

	Sums of Squares	Degrees of Freedom	Mean Square	
Within	.04305419	40	.00107635	F
Between	.02670532	18	.00148363	1.378

$\bar{Z}(1) = 1.72376255$

$\bar{Z}(2) = 1.68070836$

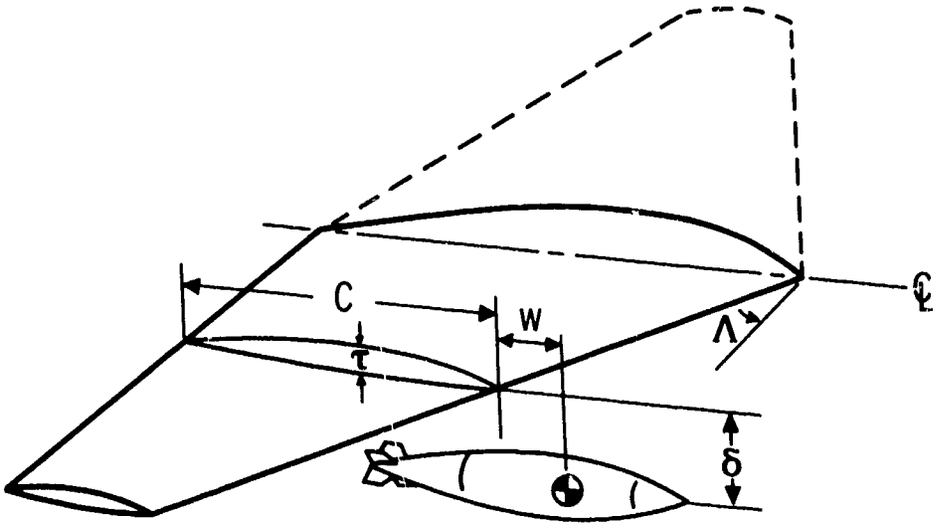

FIGURE 1 - TYPICAL GEOMETRIC PARAMETERS DESCRIBING AN AIRCRAFT/STORE COMBINATION

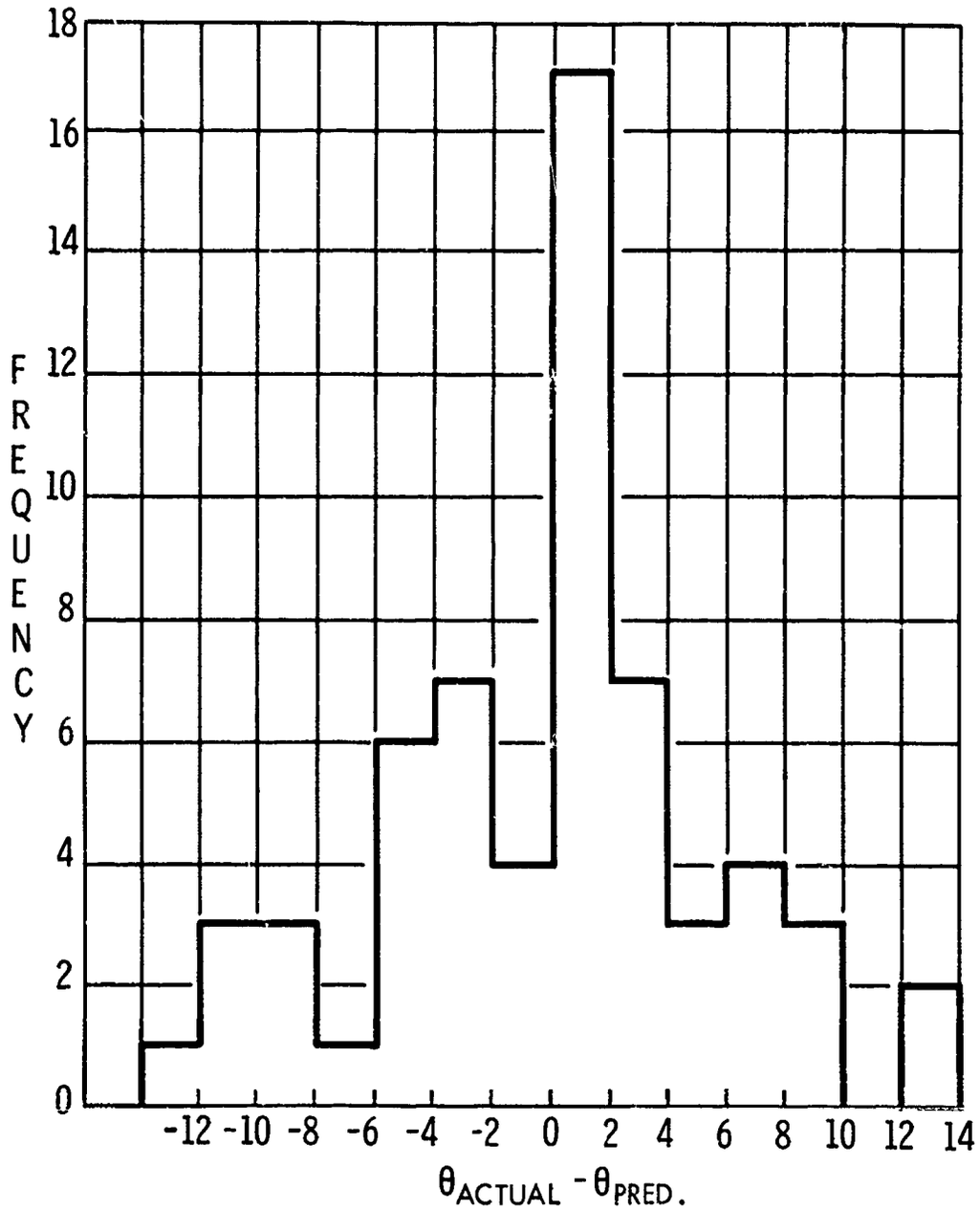

FIGURE 2 - DISTRIBUTION OF ERRORS FROM ESTIMATION OF INITIAL PITCH MAXIMUM ANGLE.

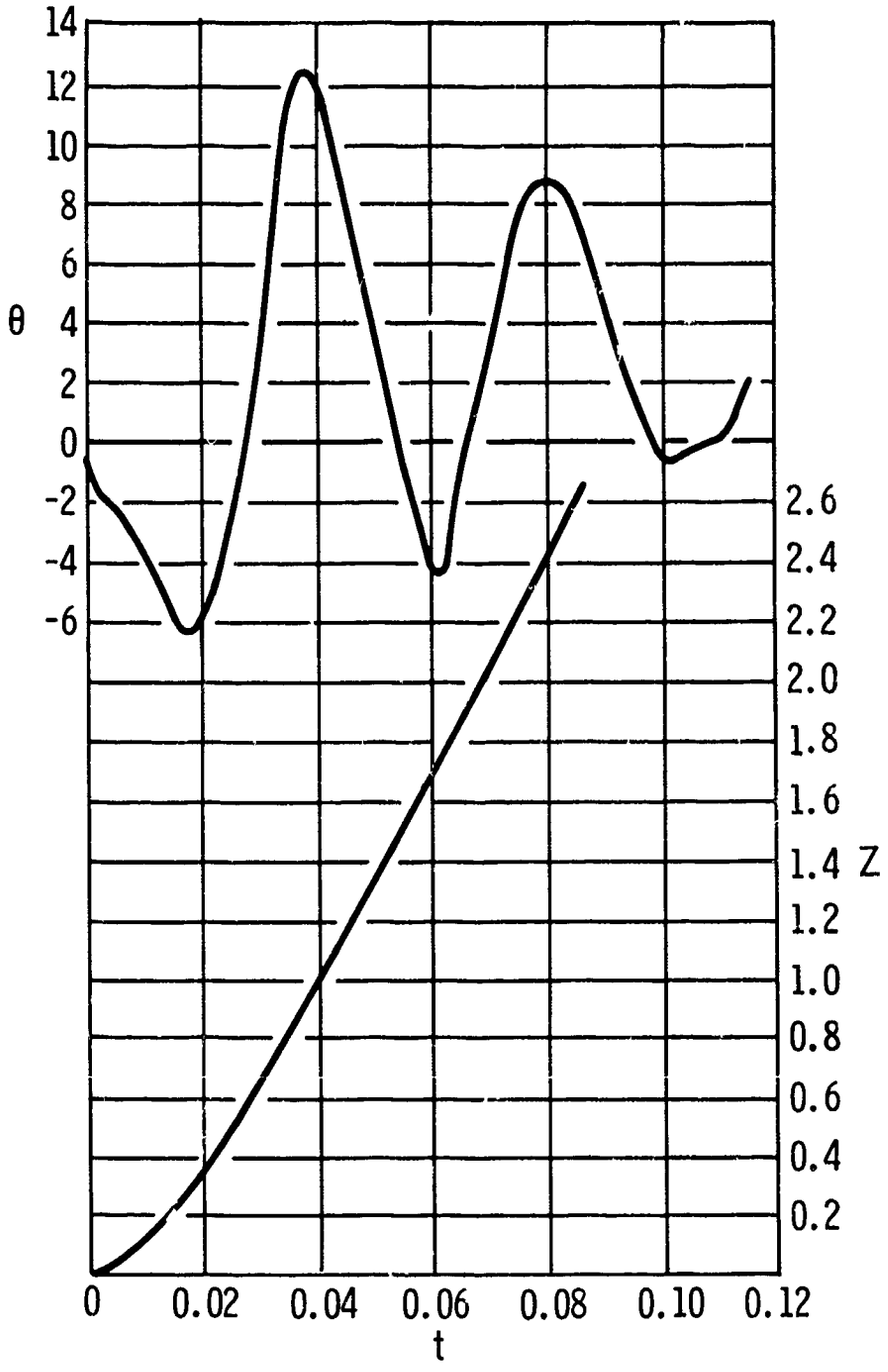

FIGURE 3 - VARIATION OF θ AND Z WITH TIME FOR A TYPICAL STORE SEPARATION.

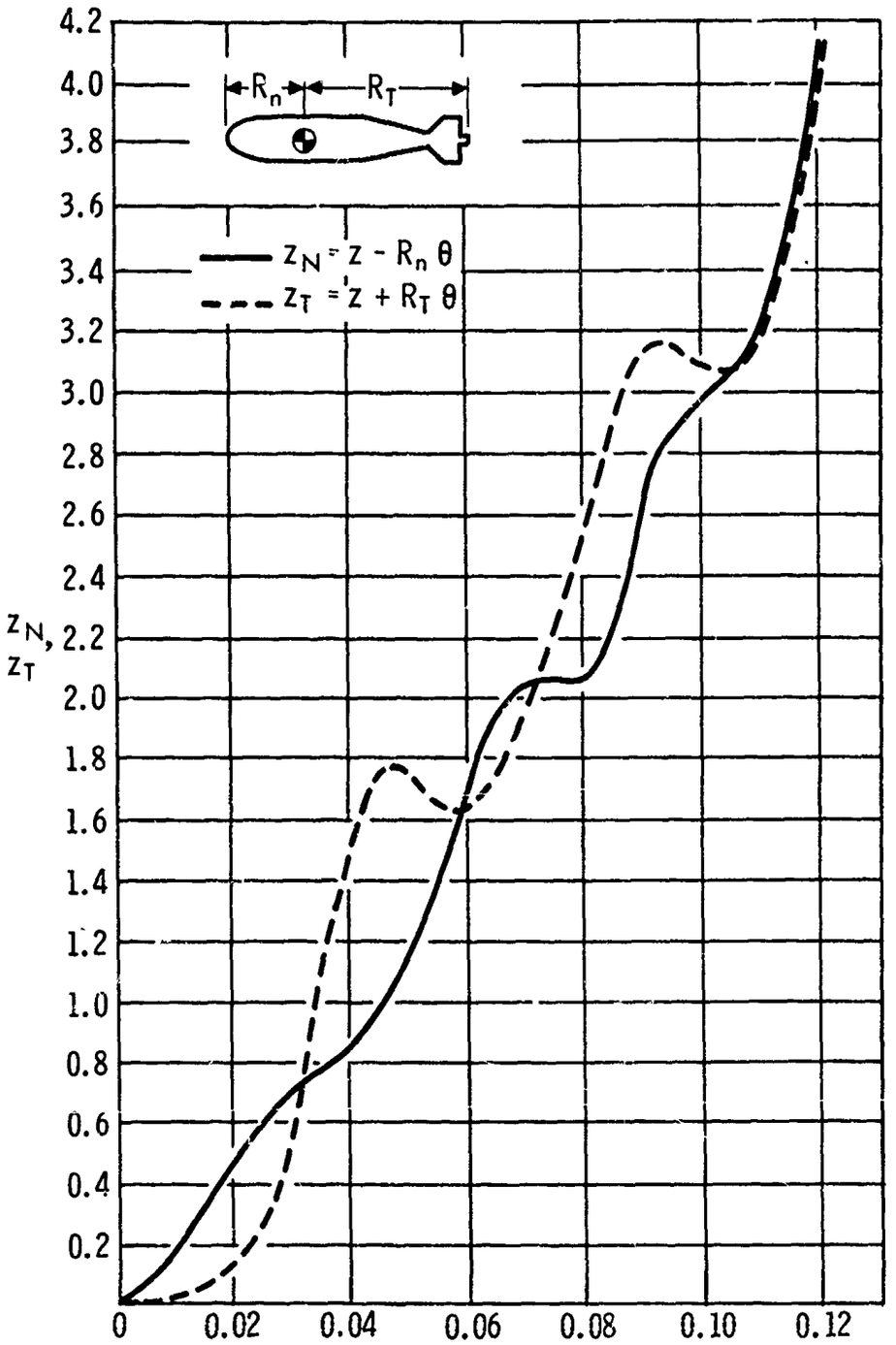

FIGURE 4 - VARIATION OF z_n AND z_t WITH TIME FOR A TYPICAL STORE SEPARATION.

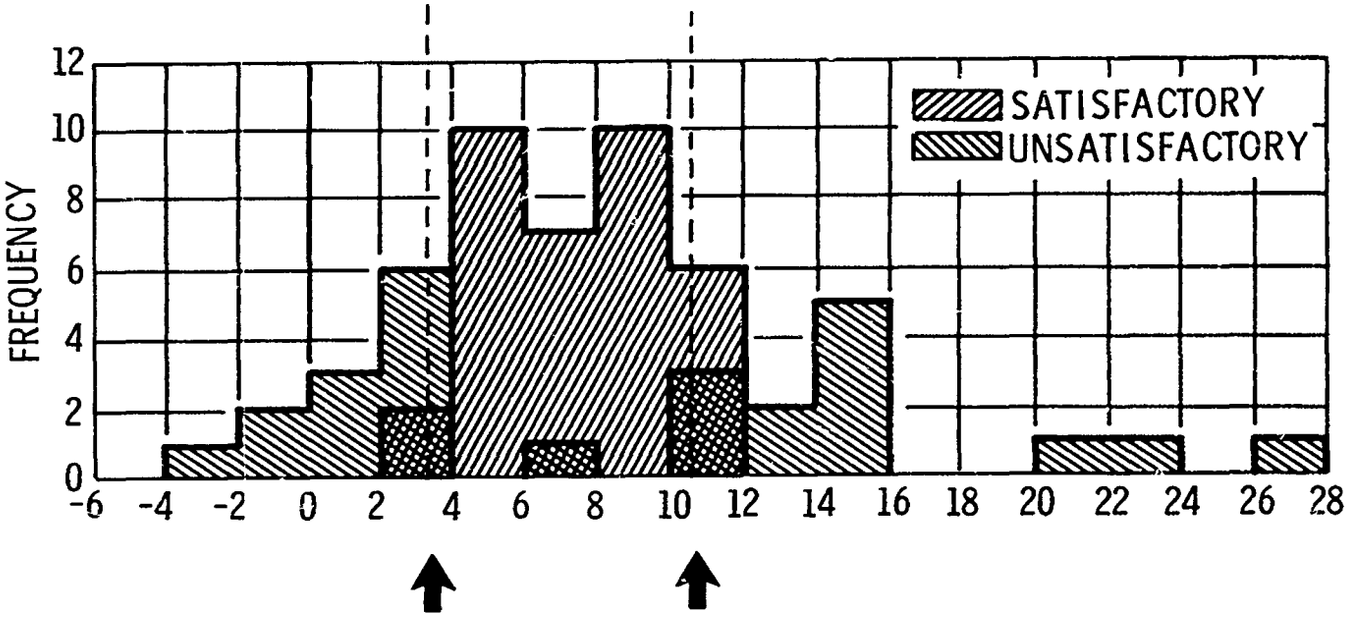

FIGURE 5 - DISTRIBUTION OF $\int_0^{TLIM} z_N dt$ VALUES FOR TLIM = 0.07 SEC.

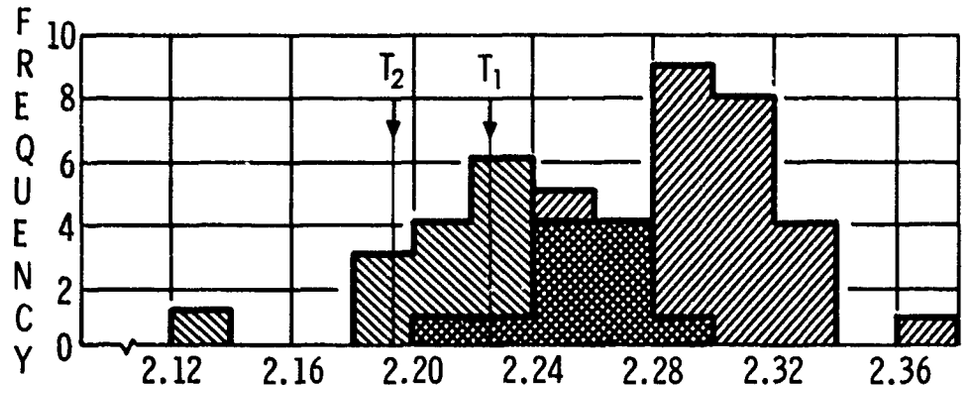

FIGURE 6a - DISTRIBUTION OF DISCRIMINANT FUNCTION VALUES FOR PARAMETER SET #1.

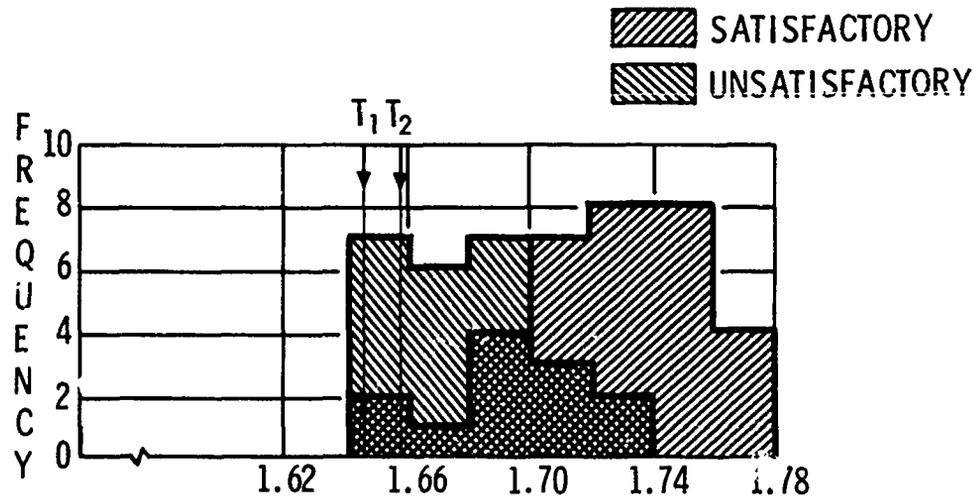

FIGURE 6b - DISTRIBUTION OF DISCRIMINANT FUNCTION VALUES FOR PARAMETER SET #2.

Paper No. 45

EXTERNAL STORE AIRLOADS PREDICTION (U)

(Paper UNCLASSIFIED)

by

R. D. Gallagher and P. E. Browne
Aeronautics Division
LTV Aerospace Corporation
Dallas, Tex. 75222

ABSTRACT. (U) An empirical technique for predicting the complex aerodynamic forces on aircraft wing-pylon store installations is described. The basis of the technique is a parametric correlation of extensive subsonic and transonic wind tunnel airloads data involving numerous store types and loading configurations. The correlation process involves an analysis to identify specific store installation geometric parameters which provide a mathematically describable relationship for each contributing airload term. Use of the technique involves solving the resulting empirical equations for the desired store configuration, flight attitude, Mach number, etc., to determine values for all individual contributing airload terms. Proper summation of the terms yields the net store installation airloads. The technique is presently most effective for predicting the design critical lateral airload components; however, vertical and axial component correlation is in development. The technique has been used on a limited basis in conjunction with two current aircraft-store development programs for subsonic and transonic airloads.

INTRODUCTION

(U) Today's increased usage of external stores and the high density of store loadings on combat aircraft is placing much more emphasis on aircraft-weapon compatibility considerations in the design of new aircraft systems. The early day installation of single stores on simple suspension systems would permit rather approximate aerodynamic analyses to assure safe carriage of the available stores. However, recent trends to such high density store loadings as shown in Fig. 1 for an A7A Airplane demand more sophisticated techniques for predicting the aerodynamics of such installations. Certainly, it would be highly desirable to analytically predict the external flow field accurately, including all interference effects, and to provide reliable estimates of the forces and moments on all components of the entire system. This would permit valid flight boundaries of the form shown in Fig. 2 to be developed with few requirements for flight test certification. However, the analytical technologies that would make this possible have not yet been achieved.

(U) Developing mathematical descriptions and achieving representative solutions for various segments of the external flow field about an airplane has intrigued and challenged the fundamental aerodynamicist for a long while. There are numerous technical documents describing noteworthy accomplishments in the fields of lifting surface and lifting body aerodynamics, particularly in recent years with the assistance of high speed electronic computers. Many of these are directly related to the aerodynamic technologies of external stores. Even the viscous flow field is recently becoming more submissive to limited analytical exploration. However, there remains many areas that yet defy the most aggressive mathematical efforts. We have yet to fully achieve mathematical solutions for mixed flow fields in transonic flight, interference effects between major aircraft components, boundary layer transition and separation, and many other attributes of compound flow fields. Until success is achieved in these areas, truly theoretical solutions for store airloads cannot be realized since all of these have their place in the definition of forces and moments on external stores. However, as in other engineering endeavors, such shortcomings in technology development frequently cause the aeronautical engineer to resort to empirical methods for achieving adequate design information.

(U) Some of the earlier analyses used wind tunnel flow field survey data from aircraft and models without stores. The aerodynamic environment of the captive store was analytically predicted by attempting to superimpose the store in the aircraft flow field by using the isolated store aerodynamic data. Unfortunately, the curvalinear nature of most local

flow environment, plus strong interference effects, invalidated most every analysis performed in this manner. Therefore, experimental data obtained with instrumented stores has been the most dependable but costly method for determining this information.

(U) While there must necessarily be a continuing effort to achieve every contribution possible from theoretical efforts, the most productive results for practical design guidance has thus far been derived from experimental and empirical solutions. This fact has been apparent to many investigators and has prompted several helpful programs intent on cataloging, summarizing, or correlating existing data and/or methods. While Ref. 1 suggests captive flight loads may be predicted theoretically for highly idealized configurations, this situation never seems to exist in the real world. Also, even though a single store installation is considered by first either measuring or predicting the wing-body flow field, the task is quite involved and has been reported in Ref. 2 to produce disappointing results. As the complexity of aircraft configurations and multiple store arrangements are increased, these attempts have been of less value. Therefore, the results of all known attempts to analytically insert typical store installations in the complex curvalinear flow fields near representative aircraft have been unsatisfactory.

(U) The point must be emphasized, however, that there are not many documents available that present formalized methods for predicting captive store loads. There is an even greater shortage of valid flight test data for use in verifying either predicted or wind tunnel determined airloads. There have been several programs such as that described in Ref. 3 which evaluate the incremental effects of locating stores in alternate locations and arrangements on specific aircraft configurations. Also, there are large quantities of test data related to store installations, much of which are identified in the bibliographies of Ref. 1 and Ref. 2. Yet, many attempts to correlate these data to provide a dependable means of predicting multiple store airloads have been inconsistent.

(U) This assessment of the situation may sound gloomy at this time but it certainly presented a dismal prospect to those of us at the Vought Aeronautics Division involved in A7 development programs. With some 120,000 logical store loading arrangements to consider in the certification program for store carriage and separation, some means of categorization and correlation was essential if the task was to be kept within reasonable bounds. Fortunately, a successful procedure for predicting captive flight airloads was developed and a description of the method forms the basis for this paper.

APPROACH

(U) During the early F8U and A7A aircraft development programs, external store airloads were predicted almost exclusively from wind tunnel data. Previous attempts to use aerodynamic data for isolated stores in predicting airloads gave results vastly different than wind tunnel data. Since careful assessment of test techniques and data strongly supported testing in lieu of analytical predictions as the more logical approach, numerous test programs were conducted. As the considerable quantities of instrumented store (metric) airload data involving a variety of store types and aircraft loading arrangements became available, the feasibility of correlating this data to develop a general airloads prediction technique was recognized. Furthermore, realizing that airloads prevalent on any body are at least a partial function of the physical area exposed to flow impingement, a beginning assumption in the correlation process was that geometric parameters describing the size and placement of a given store installation could offer a logical basis for predicting airloads. As an example, the store installation side force component (C_Y) could be expected to be a function of the side projected area (SPA) and the relative position of the installation below the aircraft wing.

(U) Development of the approach was initially quite tedious. However, through continued recognition of simplifying parameters and factors, the fruits of the approach slowly evolved. The normal difficulties of handling airload coefficient variance with aircraft angle of attack, sideslip, etc., were resolved by linearizing these relationships and expressing them as slope functions (i.e. C_{Y_α}, C_{Y_β}, etc.). Through observations that: (a) certain airloads vary almost linearly over the normal aircraft flight angle of attack range (0° to 10°), and (b) variation of certain airloads with Mach number is relatively constant with store type, numerous major problem areas were sidestepped. Finally, through semi-theoretical processes of multiplying, inverting, eliminating, and otherwise altering the geometric parameters selected for each airload component sub-term, a valid, mathematical description of the variance of each airload component sub-term with its respective geometric parameter combination was obtained which satisfied the variety of store types and configurations for which data were available. The technique essentially provides, through substitution of the geometric characteristics of any given store installation into the derived empirical relationships, a simple, effective method for establishing the principal, net airloads prevalent upon that installation.

TECHNICAL DISCUSSION

(U) To provide clarity in describing the tasks and procedure involved in deriving the airload prediction method, the discussion is divided into three categories. The first of these includes a brief description of store airload terminology. The second provides a brief explanation of the controlling variables considered in the technique development. Finally, a step-by-step description of the derivation process is explained.

TERMINOLOGY

(U) The difficulties associated with the prediction of external store installation airloads can be more clearly explained provided a common terminology for the airloads prevalent on a given installation is established. For illustration purposes, a store loading common to many current attack aircraft is used. The configuration, as depicted in Fig. 3, consists of a fully loaded multiple ejector rack (MER) mounted beneath a typical aircraft wing pylon. On an adjacent, more inboard wing pylon station is a single store installation shown here only to serve as a flow interference source. The primary flow prevalent about the subject installation, while largely a function of the aircraft flight attitude and velocity, generally originates from three sources: (a) the upwash prevalent at the wing leading edge, (b) the outboard sidewash along the lower, leading edge of the wing resulting from wing sweep and the flow interaction common to the fuselage/wing junction, and (c) the downwash at the wing trailing edge. In the case of suspending objects beneath a wing, such as a wing pylon or store installation, an additional inboard sidewash flow at the lower wing trailing edge is also common. The resultant store installation airload components (C_Y, C_N, C_A, C_η, C_m, and C_{RBM}) induced on the store installation by these general flow patterns are describable through use of the conventional, body-axis aircraft reference system, also shown in Fig. 3. The x, y, and z axes being positive forward, outboard, and upwards, respectively.

(U) Each airload component is necessarily comprised of a series of airload sub-terms describable by such relationships as:

$$C_Y = \Delta C_{Y_\alpha}\left(\alpha - \alpha_{C_Y=0}\right) + \left[\Delta C_{Y_\beta} + \left\{\Delta C_{Y_{\beta_\alpha}}(\alpha)\right\}\right]\beta + \Delta C_{Y_{\alpha=0_\theta}} + \Delta C_{Y_{\alpha_\theta}}(\alpha) + \left\{\Delta C_{Y_{\beta_\theta}}(\beta)\right\} + \Delta C_{Y_{\gamma=0_{INTF}}} + \Delta C_{Y_{\alpha_{INTF}}}(\alpha) + \left\{\Delta C_{Y_{\beta_{INTF}}}(\beta)\right\}$$

$\{\ \}$ These terms are either insignificant or small in comparison to other terms and are not considered in development of the C_Y and C_η components.

$$C_n = (\Delta C_{n_\alpha})_{NOSE}(\alpha) + (\Delta C_{n_{\alpha=0}})_{NOSE} + \left[\Delta C_Y - (\Delta C_{Y_{\beta_\theta}} + \Delta C_{Y_{\beta_{INTF}}} + \Delta C_{Y_\beta})(\beta)\right]\frac{PROJ}{b} + \left[\Delta C_{n_\beta} + \left\{\Delta C_{n_{\beta_\alpha}}(\alpha)\right\}\right]\beta + \Delta C_{n_{\alpha=0_\theta}} + \left\{\Delta C_{\alpha_\theta}(\alpha) + \Delta C_{n_{\beta_\theta}}(\beta)\right\} + \Delta C_{n_{\alpha=0_{INTF}}} + \Delta C_{n_{\alpha_{INTF}}}(\alpha) + \left\{\Delta C_{n_{\beta_{INTF}}}(\beta)\right\}$$

Similar mathematical expressions may be prepared for the other coefficients C_N, C_A, C_m, and C_{RBM}.

(U) Need for the numerous sub-terms required in expressing the above root equations is shown in Fig. 4, which illustrates the sub-term primary airload sources. Thus, for the sample store loading configuration previously described, the airload contributions for each of the following components must be considered:

a) the basic, rigid store installation as a function of angle of attack f(α),

b) the influence of the unsymmetrical rigid aircraft attitude ($\Delta\beta$),

c) the induced effects of rack/installation flexibility ($\Delta\theta$), and

d) the induced effects of adjacent installation interference (Δ INTF).

Of major importance is the frequent disparity that exists in the magnitude of the contribution that any single equation sub-term makes to the various airload components. Two prominent examples of this are revealed in Fig. 5. Realizing that side force (C_Y) is the predominant function that establishes yawing moment (C_n) and root bending moment (C_{RBM}), one might logically expect the magnitude of the contributions of the $\Delta\alpha$, $\Delta\beta$, $\Delta\theta$, and Δ INTF terms to be consistent for the three lateral airload components. As evidenced particularly by the differences in the $\Delta\theta$ and Δ INTF term contributions in Fig. 5 for each of the C_Y, C_n, and C_{RBM} components, this assumption can result in serious error. As a rule, such an assumption proves adequate for airload prediction at low subsonic flight conditions, but unacceptable error may result for most conditions beyond 0.6 MN.

LIMITING VARIABLES

(U) Some assessment of the variables considered in developing the technique is necessary as this criteria essentially defines the range of applicability of the technique. For example, the technique has been found to produce most valid predictions for angles of attack less than 10 degrees. Attempts to predict lateral airloads beyond these boundaries will result in progressively large errors. The influence of Mach number on store installation airloads is yet another important relationship to be considered in the prediction of airloads. Fig. 6 illustrates the variation of C_Y, C_η, and C_{RBM} with MN for the sample loading configuration. Similar non-linear and divergent trends are common to most single and multiple store, wing mounted installations, particularly in the transonic flight range. The Mach range over which wind tunnel data were correlated in developing the technique was 0.7 to 1.05. Programs are underway for extending both the useful Mach number and angle of attack prediction ranges.

(U) The technique to date has been developed exclusively from correlation of measured A-7 and F-8 store airloads data derived from wind tunnel programs. While the primary correlation data were obtained for multiple store installations mounted on the A-7 center wing pylon installation, methods have been established from correlations of data involving both single and multiple store loadings on more inboard and outboard pylon locations that permit extension of the prediction capabilities to other wing stations without inducing appreciable errors. A description of the methods for performing airload transfers between both pylon stations and single vs. multiple store installations is included in later paragraphs along with the technique deviation.

(U) The technique is presently most effective for predicting lateral airload components. These components are the most critical from the standpoint of store installation design as they act in the direction of the least structural strength of the supporting pylon. Efforts towards correlating the remaining normal force, pitching moment, and axial force components are underway but additional measured data are needed.

(U) The present technique certainly is not adequate to account for contributions from major aircraft components or airframe configuration changes strongly influencing the local flow field. With sufficient data for correlation purposes, the procedure would likely be extended for this purpose. However, such flow field contributors as engine inlets, deflected aircraft control surfaces, speedbrakes, gun/rocket blast impingement, locally separated boundary layer effects must be considered as part of the parent aircraft configuration. At present, these must either be evaluated as part of the basic flow field in the wind tunnel or incremental effects must be assessed by ground/or in flight test programs.

DERIVATION

(U) Realizing that a description of each individual sub-term would make the paper unnecessarily long, the following paragraphs trace only

the derivation of the empirical relationship for one typical airload coefficient sub-term, Cy_{α}. It should be understood that all remaining sub-terms are derived in an essentially similar manner. In addition to presenting the general empirical equations, the ensuing text also illustrates the accuracy of the **derived empirical relationships in describing the variance of each sub-term of the side force and yawing moment airload components.**

(U) After making the assumptions and observations defined previously, the remaining (and most difficult) effort in developing the technique involved describing the variation of the numerous airload equation sub-terms as a function of store installation geometry and Mach number (MN). The intent being to express the variation of these factors as simple, manageable slope and intercept relationships. As a beginning effort to achieve this, advantage was taken of the linear relationships found to be inherent in the wind tunnel airload coefficient data over the low angle of attack range ($\alpha \leq 10$ degrees). Next, after expressing these linear relationships in terms of slopes, the average slope values for each store type were computed to provide an indication of the airload variation among the stores without regard to Mach number. Table I, which is an abbreviated, sample tabulation of the measured slope values for the Cy_{α} sub-term provides an illustration of this essentially numerical-averaging process. In the table, "Store/MER Type" refers to a fully loaded pylon/store/multiple ejector rack (MER) installation, of each store type listed, for which Cy_{α} data was measured in the wind tunnel. As airloads prevalent upon these five installations constitute the primary data basis for the technique derivation, comparison of their relative physical differences are provided in Fig. 7.

TABLE I: Variation of Cy_{α} with Store/MER Type and Mach Number

Mach No. / Store/MER Type	MN = 0.7	MN = 0.9	MN = 1.05		$Cy_{\alpha_{AVG}}$ (Store/MER Type)
PYLON	.00033	.00040	.00033	⇒	.00035
MK-82/MER	.00120	.00130	.00136	⇒	.00134
WETEYE/MER	.00130	.00142	.00158	⇒	.00143
M-117/MER	.00130	.00159	.00180	⇒	.00156
TFDM/MER	.00144	.00142	.00157	⇒	.00148
	⇓	⇓	⇓		
$Cy_{\alpha_{AVG}}$ (MN VARIATION)	.00111	.00123	.00136	↘	
				↙	.00123
f(MN) MN CORRECTION FACTOR	0.90	1.00	1.10		

(U) In Table I, the average C_{Y_α} values have been computed by averaging the three horizontal terms for each store type, and are tabulated in the right hand column. The intent in computing these averages is to derive values, representative of the airload variation for each store/MER type, which can be plotted versus various arrays of store installation geometric parameters for the purpose of defining the geometric relationship most compatible with the following criteria:

a) Establishes a linear geometric parameter vs. C_{Y_α} relationship

b) Possesses a tendency to intercept zero

c) Establishes a relative order of magnitude between store types

d) Produces equivalent loads and parameters for the various store types

The slope and intercept of the mean straight line faired through the values of $C_{Y_{\alpha AVG}}$ (for each store/MER type), when plotted versus the "optimum" geometric parameter function, forms the basic portion of the general empirical equation describing C_{Y_α} variance.

(U) The process of selecting the store installation geometric parameters which might satisfy the above criteria for any airload sub-term is essentially iterative in nature. Until a satisfactory geometric combination is found, another is selected and tried. To date, various combinations of the geometric parameters illustrated in Fig. 8 have been found to be adequate for describing the "optimum" values for every airload sub-term. Initially, efforts were made to justify parameter selection on a purely theoretical basis. This was not always possible, but parameters contradictory to theory were definitely avoided. If several parameter combinations were found to yield acceptable results, the arrangement inducing the least error and revealing the most intuitive relationship to the respective airload sub-term was selected. As an example, the store installation geometric parameters of SPA, $D^2/(AR + 2)$, and SPA(AR) were earnestly evaluated prior to the selection of $D^2/(AR + 2)$ as being most representative of C_{Y_α} variance.

(U) Figures 9 and 10 present the derived plots of coefficient slope versus "optimum" geometric parameter for establishing the slope and intercept mathematical relationships of all contributing airload sub-terms involved in computing the net side force and yawing moment components, respectively. Upon examination of the plots in general, it is observed that rather remarkable compliance with the previously stated criteria has been achieved. In particular, few situations exist where the plotted average coefficient slope values (for each store/MER type) lie other than along or closely adjacent to the mean faired line, which forms the description of each respective sub-term variance. A unique approach which permitted resolution of a coefficient sub-term that seemingly defied correlation is demonstrated in the two center (ΔC_η, (ΔC_η)$_{NOSE}$ vs. α) plots of Fig. 10. Here, by simply resolving the yawing moment about the store installation nose (bottom plot) instead of the

mid-section (top plot), an essentially linear function was obtained instead of the decidedly non-linear function generated by other correlation procedures.

(U) Another item in the derivation process that needs explanation is the manner of compensating for airloads variation due to Mach number (MN). This is also achieved through a numerical-averaging process and is revealed by further examination of Table I. First, by summing the C_{Y_α} values tabulated in each column, the average C_{Y_α} value for each Mach condition can be computed. Next, by averaging these computed values, a value (shown in the lower, right-hand corner of Table I) describable as the average mean of the MN variance is obtainable. Finally, by computing $C_{Y_\alpha\,(MN\ variation)}$ /average mean of $C_{Y_\alpha\,(MN\ variation)}$, a ratio which can be appropriately applied to the previously derived slope and intercept empirical functions to compensate for airload variance with MN can be obtained. These values, shown on the bottom row of Table I for each respective MN condition, will be referred to as MN correction factors, f(MN).

(U) Figure 11 presents a summary of all general sub-term equations, derived by the previously described airload data correlation process, necessary for computing the side force and yawing moment coefficients on any given A-7 aircraft, center wing pylon store installation. The method of using these equations to establish the airloads on a given installation consists of the following sequence:

1. Solve for the incremental contribution of each applicable airload component sub-term by:
   a) Substituting the prescribed store installation geometric parameters into the base equations provided in Fig. 11 and then
   b) Multiplying the resultant equation solutions (from item (a)) by the respective Mach No. correction factor, f(MN).
2. Substitute the values derived from (item 1) above, along with the required aircraft flight criteria, into the respective C_Y or C_n component equations (described in the "Terminology" section of this document) and solve for the net airload component coefficients.

(U) While the equations presented in Fig. 11 were derived solely from data measured on MER-store installations on the A-7 center wing pylon, preliminary attempts to extrapolate the existing airload prediction capabilities to other wing installations appear to offer some promise of success. Furthermore, attempts to predict single store airloads using the derived technique have been investigated. The approach used to achieve these correlations was through comparisons of measured airloads data on different A-7 wing-pylon stations involving identical store installations. While presented only to suggest airload trends, the highly preliminary results of this extended correlation approach are presented in Table II in the form of ratios which may be applied to the equations

presented in Fig. 11. Table II is in no way intended for design usage at this time because there are insufficient data available to provide the desired confidence in the values presented.

Table II: Transfer Ratios for Predicting Store Airload Variations Between A-7 Aircraft Pylon-Pylon and Multiple-Single Store Installations

Store Installation	Coef.	$\Delta\alpha$ Ratio*	$\Delta\beta$ Ratio*	$\Delta\theta$ Ratio*	Δ INTF Ratio*
MER: To obtain A-7 outboard pylon/MER/store values	C_Y	1.00	1.00	1.00	1.00
	C_n	$\frac{b^2/AR+2}{1500}$ @ Subsonic 1.0 @ Supersonic	1.00	1.00	.60
MER: To obtain A-7 inboard pylon/MER/store values	C_Y	.50	.75	1.00	N/A
	C_n	1.70	.50	1.00	1.00
SINGLE: To obtain A-7 center pylon/store values	C_Y	1.25	.80	N/A	1.00
	C_n	$C_{n_\alpha} = 1.25$ $C_{n_{\alpha=0}} = 1.00$	1.00	N/A	1.00

* The equations of Fig. 11 are to be multiplied by these ratios.

(U) An estimation of the overall technique accuracy for predicting airloads must come from a consideration of various factors. In general these can be isolated into two categories: (a) the accuracies of the wind tunnel models, instrumentation devices, recording equipment, and data reduction processes inherent in obtaining the base airloads data and (b) the accuracies peculiar to the airload correlation process and the descriptive mathematical relationships. Based on considerable wind tunnel airloads testing experience, the established error for the first category is approximately $\pm 5\%$. The errors peculiar to the latter category are not as straight forward as they may vary appreciably for different airload components and sub-terms. Certainly, a degree of error must be attributed to the linearized data assumptions used in the correlation process. Furthermore, when deriving the "optimum" geometric parameter relationships, attempts to maintain all values within $\pm 5\%$ were generally successful. In order to approximate the magnitude of the latter category error, random comparisons of measured airloads data with values computed using the described analytical method were conducted. An average error of $\pm 5\%$ and a maximum error of 9% was revealed.

DATA, MODELS, AND INSTRUMENTATION

(U) The measured airloads data, which were correlated to serve as the basis of the prediction technique, were obtained during various test programs conducted in the 4 x 4 ft. transonic section of the LTV Vought

Aeronautics Division High Speed Wind Tunnel. The test model was an .05 scale A-7 aircraft parent model incorporating instrumented (metric) wing pylons upon which the various scaled store installations were mounted. Figure 12 illustrates a typical metric test installation in the tunnel test section. Each wing pylon was capable of being equipped with an internal three or six-component strain gage balance designed to accurately measure airloads prevalent upon the attached single or multiple store installation throughout the range of test conditions. The cutaway view of a typical instrumented pylon presented in Fig. 13 reveals the general internal balance design.

(U) Airload data were obtained over a parent model angle of attack range of -4° to $+16^{\circ}$ and a sideslip range of -8° to $+8^{\circ}$ at Mach numbers ranging from 0.7 to 1.1.

CONCLUSIONS

(U) The empirical technique described herein has been a valuable asset in predicting external store airloads for the design of two present day aircraft. The fact that both of these airplanes are high winged should add to the complexity of flow about external stores suspended under the swept wings and was expected to increase the difficulty of predicting store airloads. Therefore, the success achieved on these programs increases the hope that such an approach can be successful on other aircraft configurations.

(U) Without dependable inflight airloads data, verification of this approach is impossible. Even the fact that structural designs based on these results have been flight tested to all the critical maneuvering conditions without indications of structural inadequacy is not sufficient verification of the accuracy of the technique. However, there are sufficient benefits and success with the technique to recommend its extension to other aircraft in an attempt to develop a universal technique. There will undoubtedly be a continuing need for much wind tunnel testing for design purposes. Many basic aircraft configuration related effects must necessarily be determined in the forseeable future by wind tunnel testing. Yet, development of such an empirical solution would drastically reduce the amount of testing needed and permit predictions of store configuration and loading arrangement related effects.

(U) Two important factors are yet to be evaluated before broad applicability can be claimed for this technique as a precise design tool. First, correlation of data for other aircraft configurations obviously must be completed. In the meanwhile, flight test data from well instrumented aircraft are needed to establish the direct relationship between wind tunnel and inflight airloads data. Certainly, such test programs are strongly recommended for the benefit those data would provide to many aspects of external stores carriage and separation technologies. However, coordinated efforts within industry and government organizations are also strongly recommended to establish the suitability of this or a similar technique for empirically predicting external store airloads.

SYMBOLS

C_Y = Side-Force Coefficient, (Side-Force)/(qS)

C_A = Axial-Force Coefficient, (Axial-Force)/(qS)

C_N = Normal-Force Coefficient, (Normal-Force)/(qS)

C_η = Yawing-Moment Coefficient, (Yawing-Moment)/(qSb)

C_m = Pitching-Moment, (Pitching-Moment)/(qS$\bar{c}$)

C_{RBM} = Root-Bending-Moment Coefficient, (Root-Bending-Moment)/(qSb)

$\Delta C_{(\ )}$ = Increment of Any Coefficient of Force or Moment

$C_{(\ )_{\alpha=0}}$ = Value of $C_{(\ )}$ at $\alpha = 0$

$C_{(\ )_\alpha}$ = Rate of Change of $C_{(\ )}$ with Angle of Attack, α

$C_{(\ )_\beta}$ = Rate of Change of $C_{(\ )}$ with Angle of Sideslip, β

$C_{(\ )_{\beta_\alpha}}$ = Rate of Change of $C_{(\ )_\beta}$ with Angle of Attack, α

q = Free Stream Dynamic Pressure, Lb./Ft.^{2}

S = Aircraft Wing Area, Ft.

b = Aircraft Wing Span, Ft.

$\bar{c}$ = Aircraft Mean Geometric Chord, Ft.

PROJ = Distance from Nose of Store Installation of Moment Reference Point, Ft.

α = Fuselage Angle of Attack, Deg.

β = Fuselage Angle of Sideslip, Deg. ($\beta_{\text{RIGHT WING}} = -\beta_{\text{LEFT WING}}$)

$\alpha_{C_{Y=0}}$ = Fuselage Angle of Attack for Zero Side Force, Deg.

SUBSCRIPTS:

θ = Flexibility Effects

INTF = Interference Effects

REFERENCES

1. U. S. Naval Ordnance Test Station. Determination of Captive Flight Loads and Separation Trajectories of Airborne Stores (U), by Dale B. Knutson. China Lake, Calif., NWC, March 1967. 78 pp. NOTS IDP 2677, publication UNCLASSIFIED)

2. Aircraft Research Association Ltd. Aerodynamic Loads on External Stores: A Review of Experimental Data and Methods of Prediction (U), by P. Marsden and A. B. Haines. Great Britain, November 1962. Vol. I 131 pp., Vol. II 60 pp. (A.R.A. Report No. 5 (or R. & M. Report No. 3503), publication CONFIDENTIAL)

3. David Taylor Model Basin. The Effects of Store Location, Store Incidence, and Wing Leading-Edge Geometry on the Incremental Lift and Drag of a Typical Missile-Type External Store (U), by Peter T. Eaton and Charles S. Swinney. Washington., Sept. 1966. 60 pp. (Report 2224, publication UNCLASSIFIED)

(U) FIG. 1. High Density Weapons Loading.

A/C STORE LOADING CONFIG.

STORE TYPE*	STATION LOADINGS							
	1	2	3	4	5	6	7	8
LAU-13A/A ROCKET POD MK 197 LDGP BOMB	L-13							L-13
MK 197 LDGP BOMB								

VELOCITY ENVELOPES:

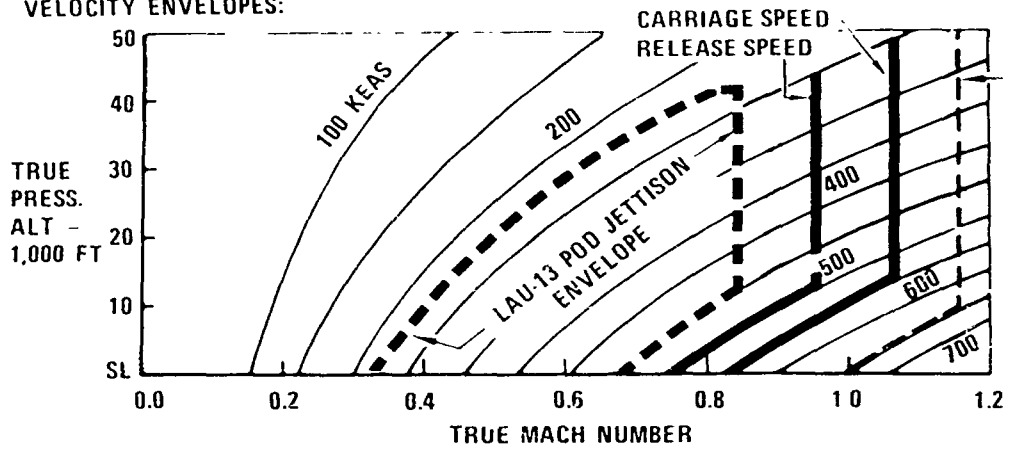

NORMAL ACCELERATIONS/DIVE ANGLE

(1) Carriage
- LAU 13A/A — 2.0g to 7.0g
- MK 197. — 3.0g to 8.0g

(2) Launch/Release
- LAU 13A/A — 0.2g to 4.5g, 70 Deg
- MK 197 — 0.1g to 8.0g, 70 Deg

(3) Jettison
- LAU 13A/A — 1.0g Level Flight

RELEASE INTERVAL

(1) Pylon to Pylon
- LAU 13A/A — Firing or Pod Jettison Not Restricted
- MK 197 — 130 ms

(2) Station to Station (MER and TER)
- LAU 13 A/A — Firing or Pod Jettison Not Restricted
- MK 197 — 80 ms

MAX L-13 CARRIAGE SPEED

REMARKS:

(1) Initiate mild pullup after firing rockets to avoid debris

(2) MAU-108 fins on MK 197 restricted to 475 KN

(3) MK 197 bombs should be released sequentially moving from the more outboard pylon stations inboard

*Fictitious Stores

(U) FIG. 2. Aircraft Flight Boundaries With External Stores.

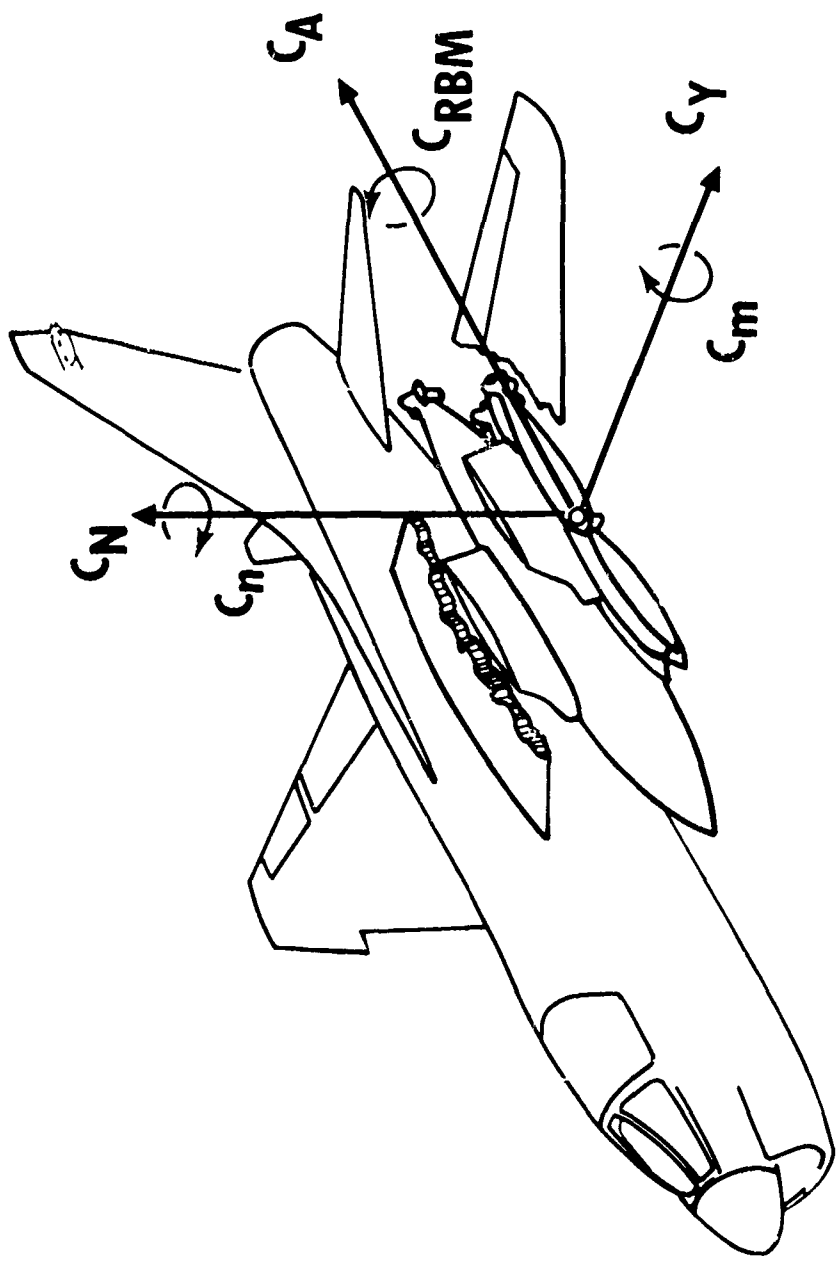

(U) FIG. 3. Store Installation Airload Terminology

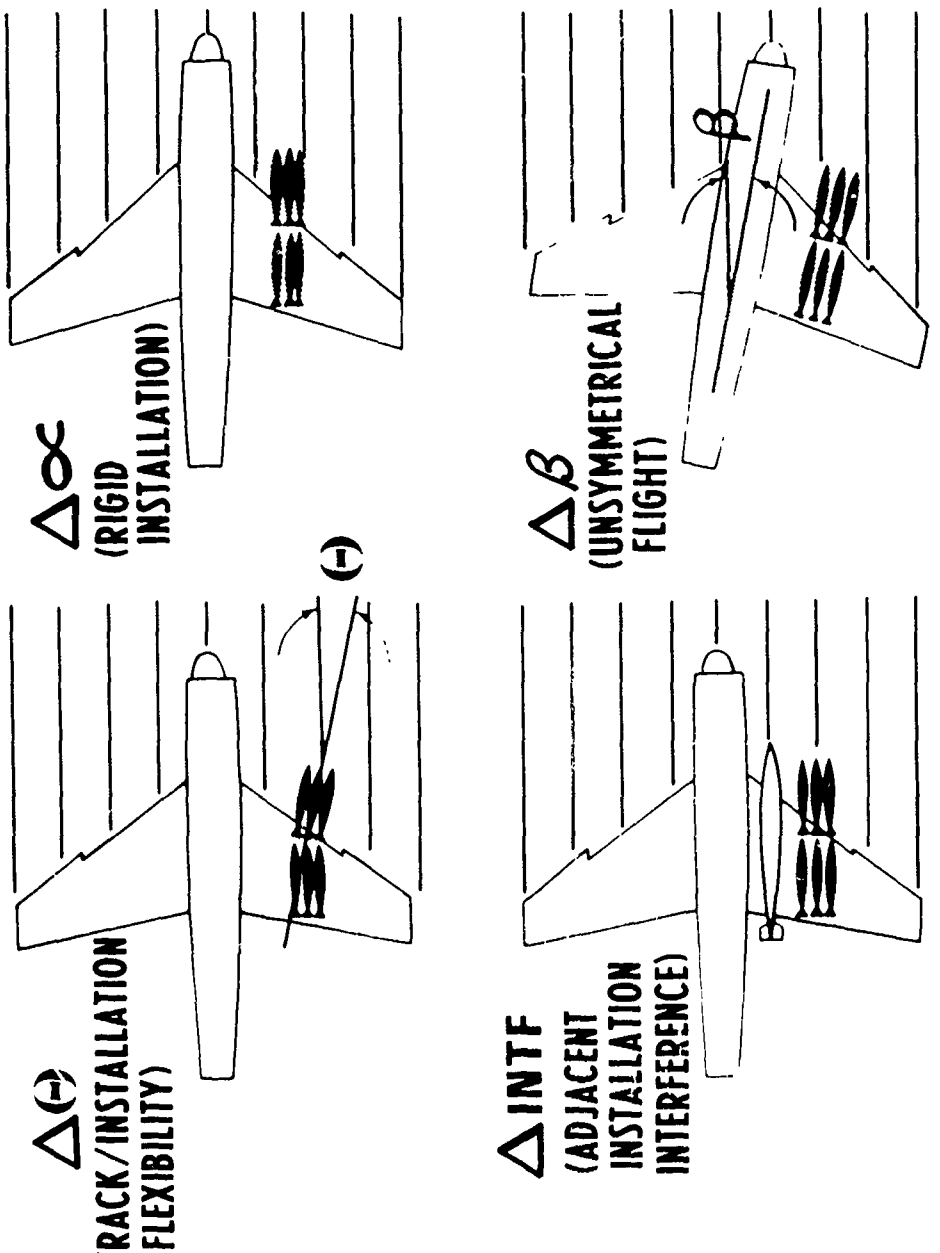

(U) FIG. 4. Airload Contributions

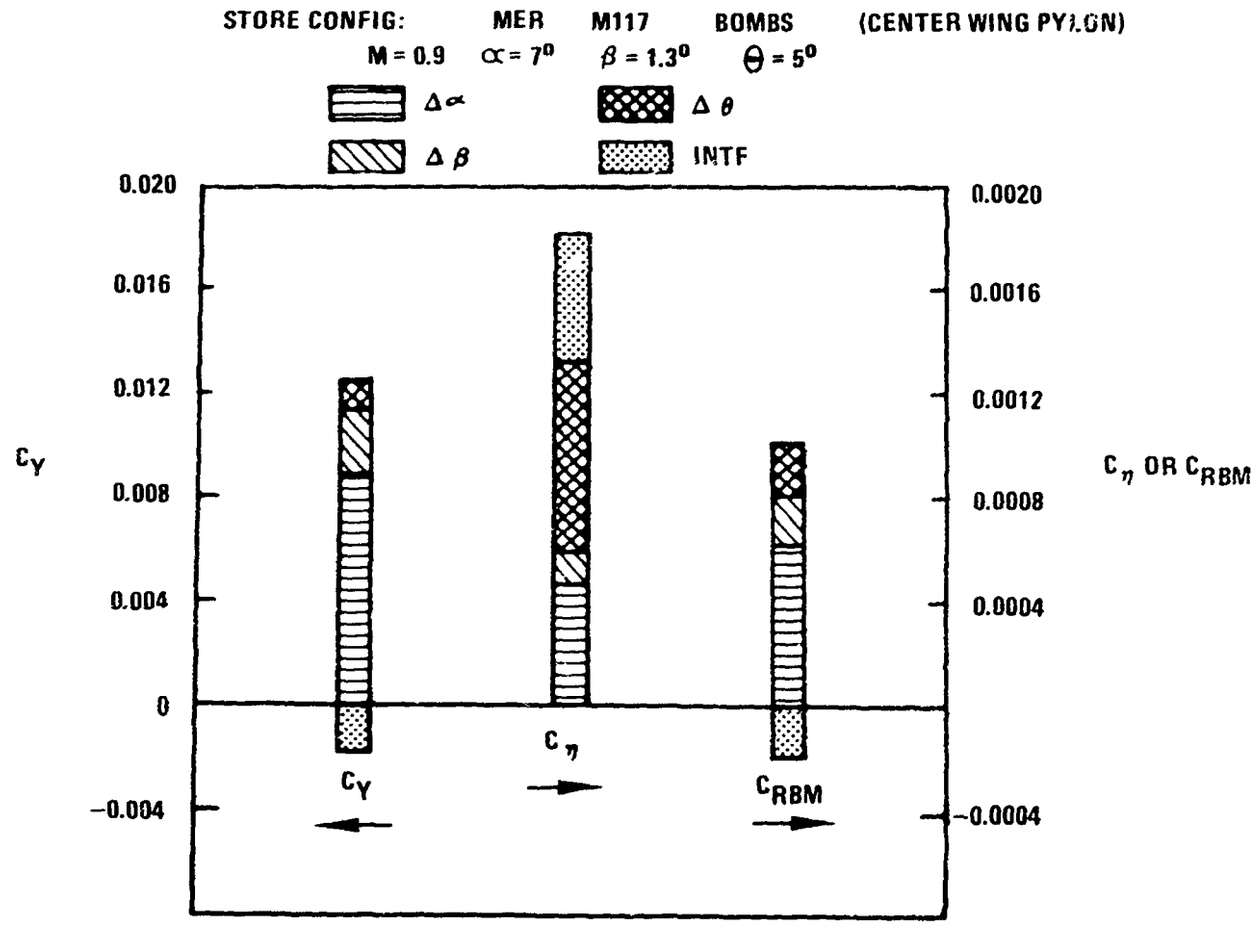

(U) FIG. 5. Typical Contributions to Installation Airloads

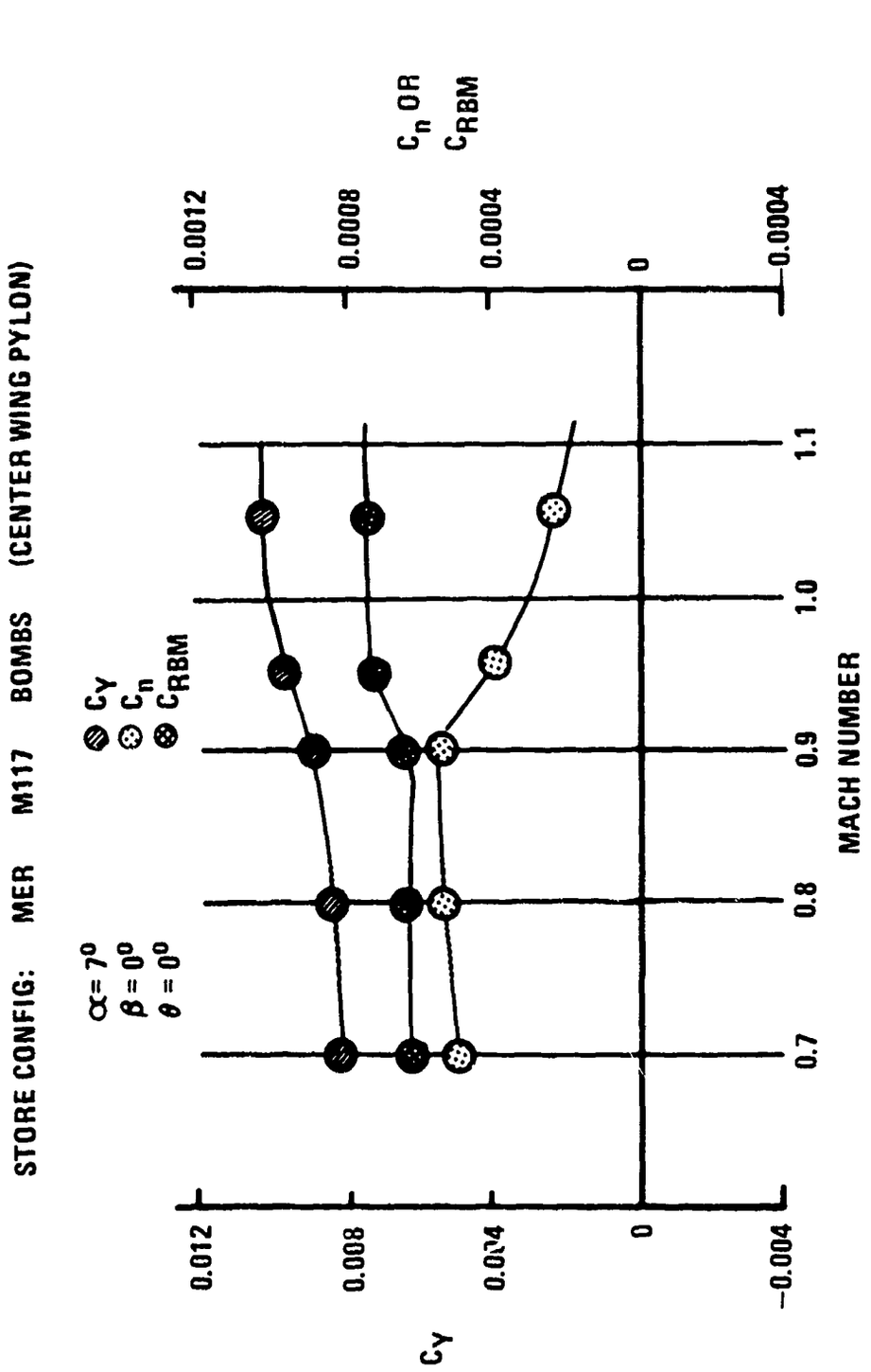

(U) FIG. 6. Typical Variation of Rigid Installation Airloads with Mach Number

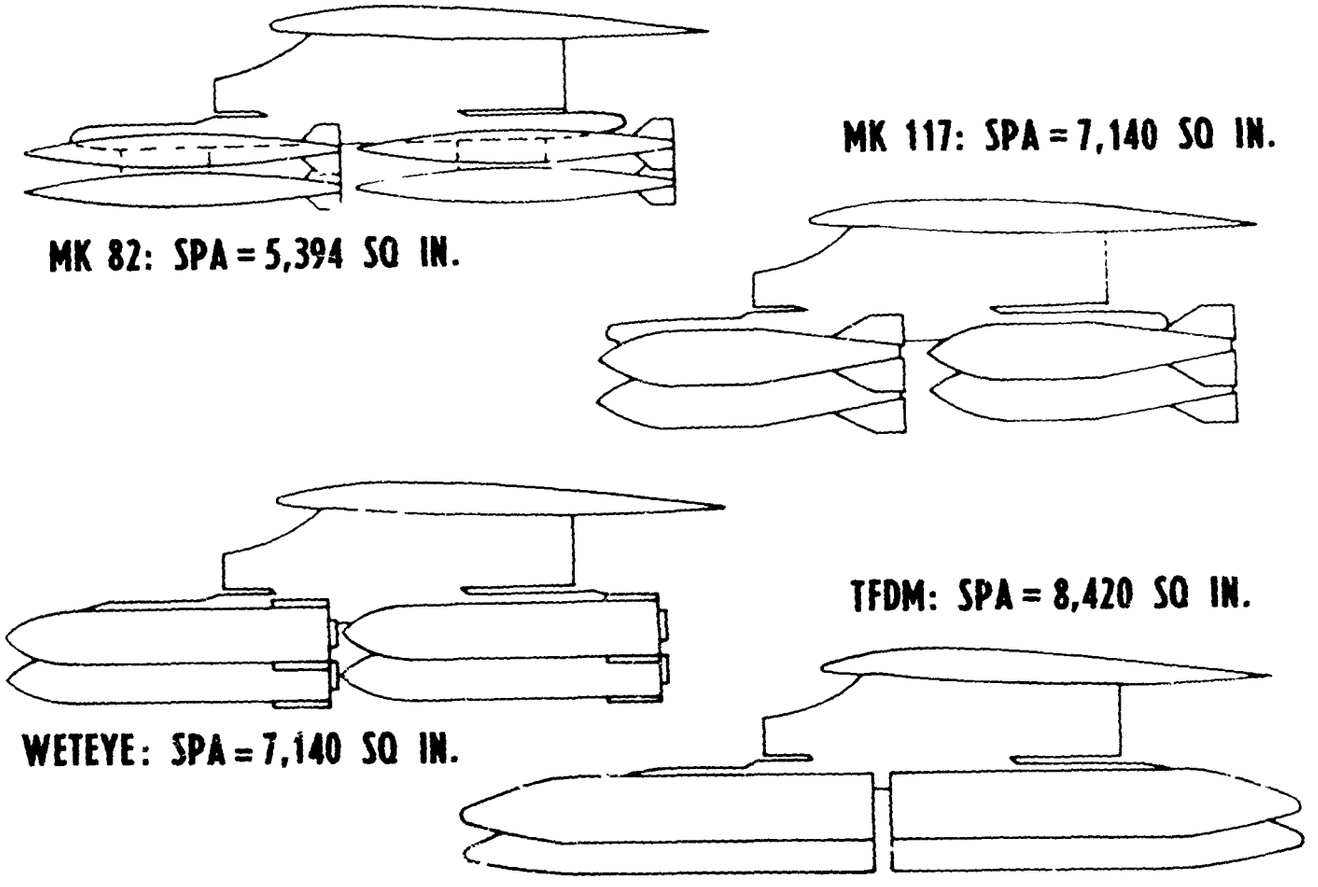

(U) FIG. 7. Comparison of Metric Test Store Configurations

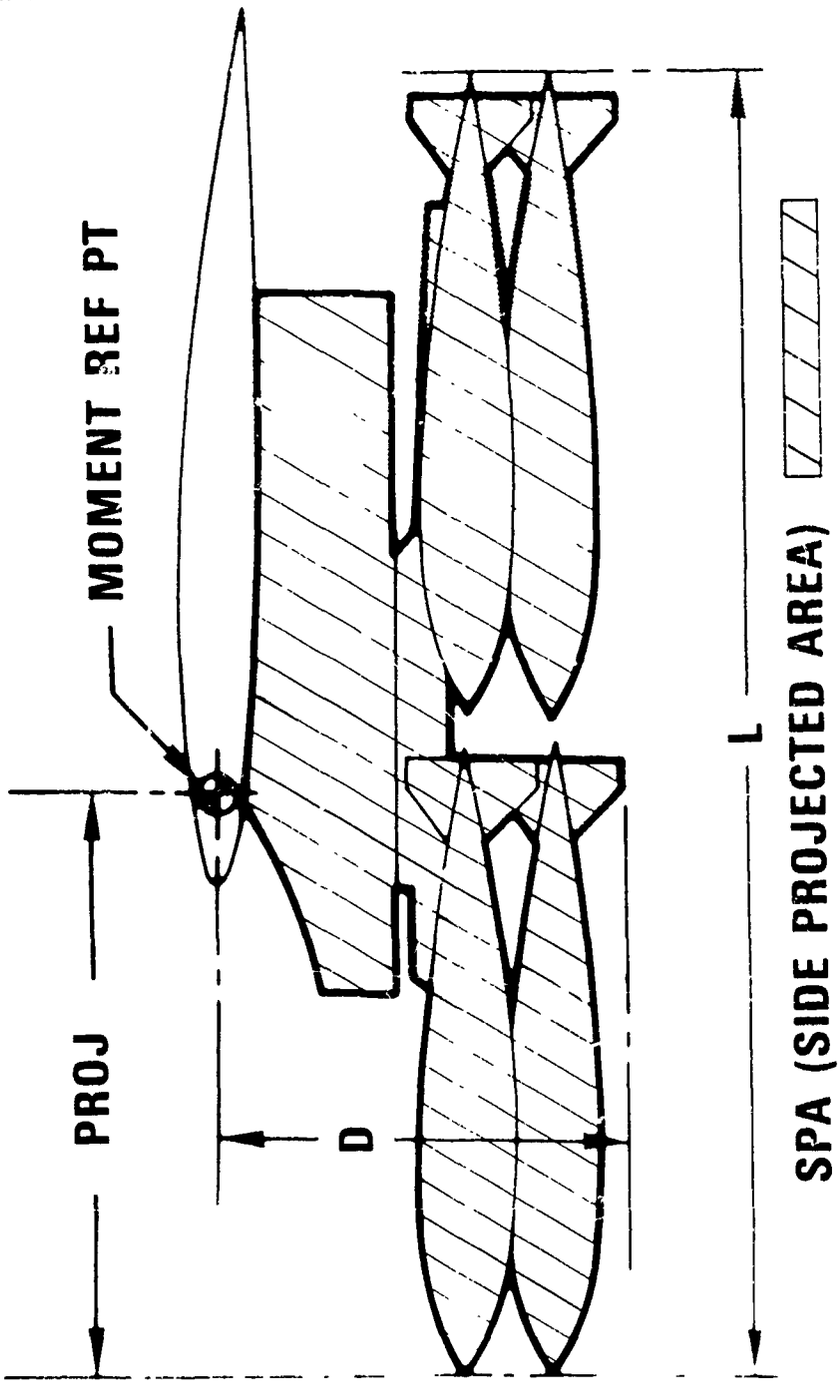

(U) FIG. 8. Geometric Parameters Used in Airloads Correlation

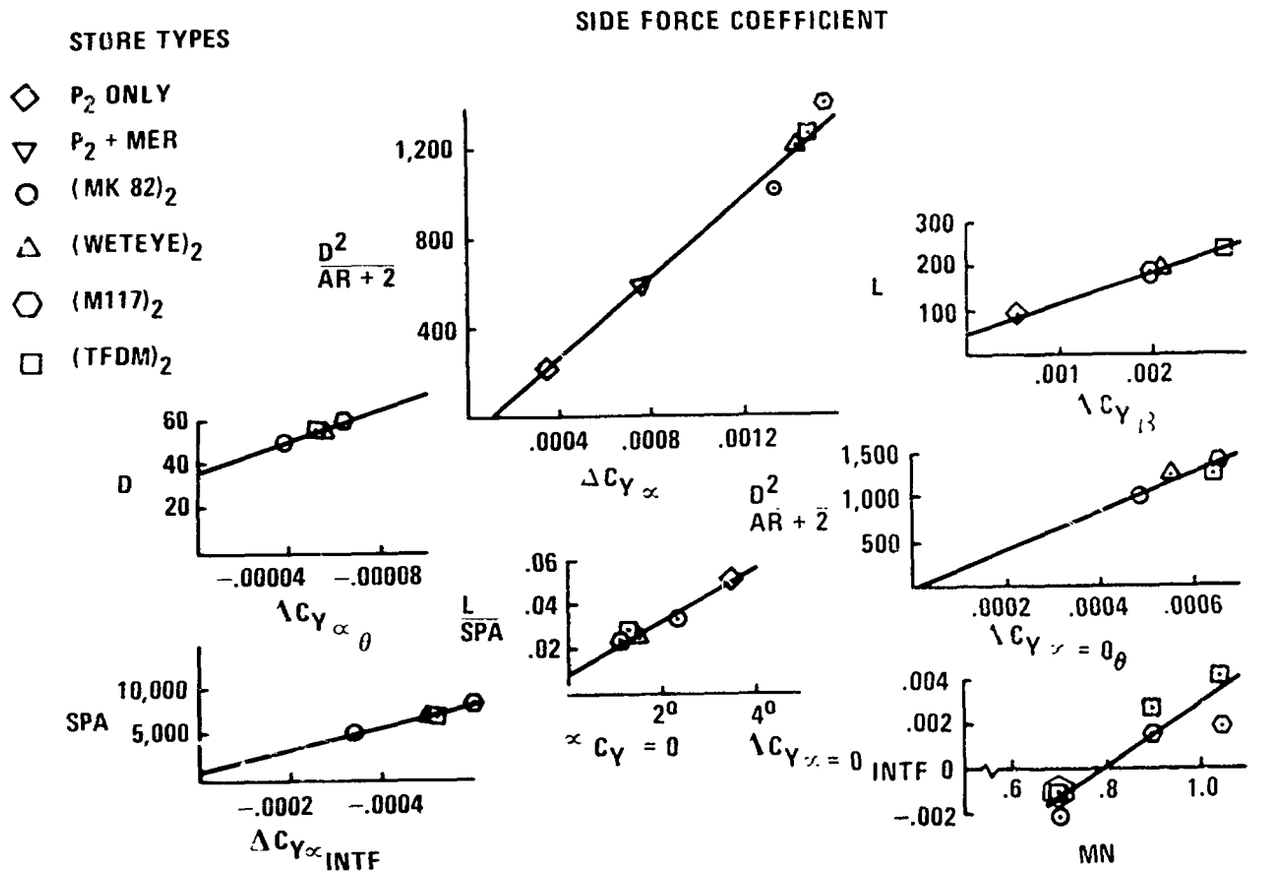

(U) FIG. 9. Airload Contribution Correlation Parameters

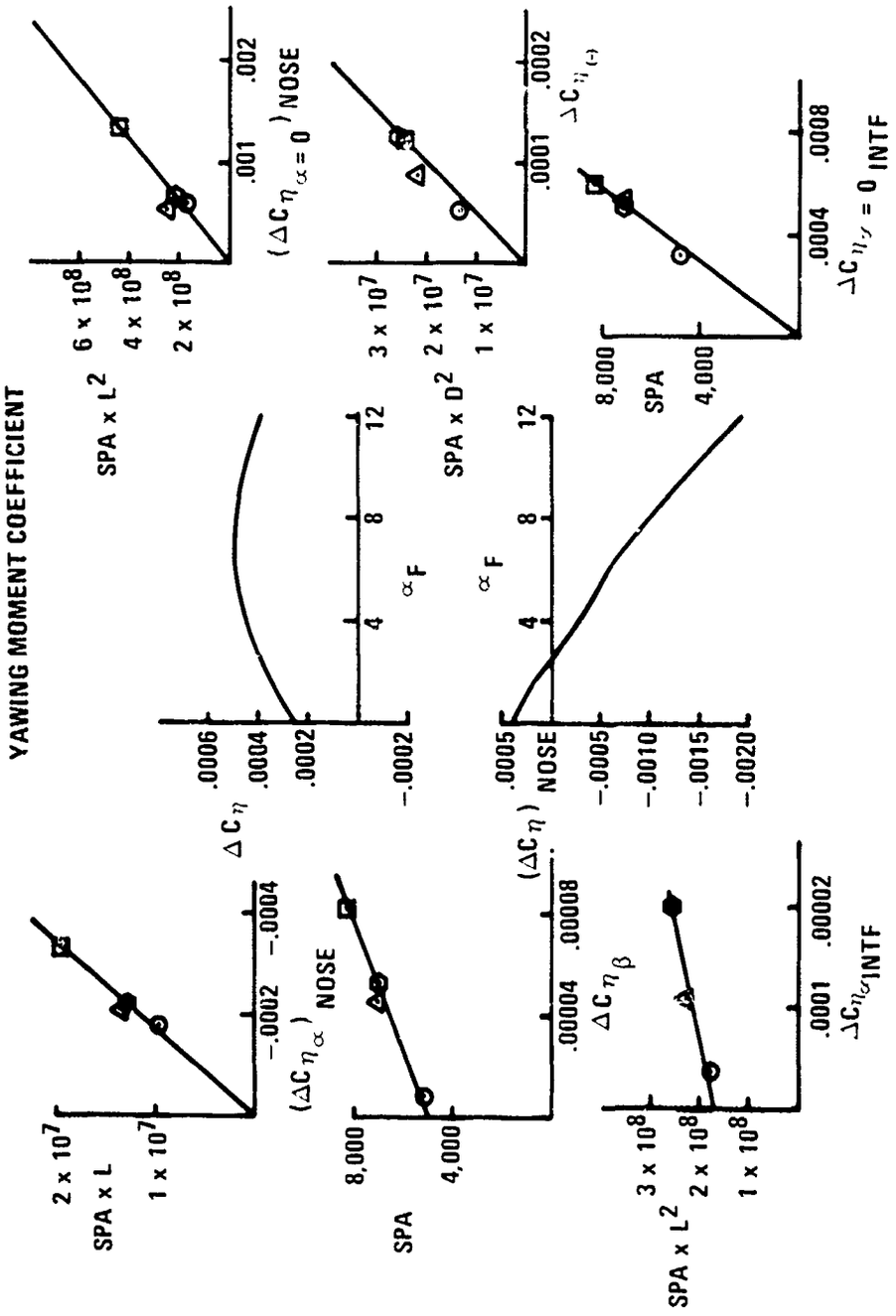

(U) FIG. 10. Airload Contribution Correlation Parameters (Cont.)

VAR	PARAMETER (DEFINED IN FIG. 8)	EQUATION (DIMENSIONS IN INCHES)	f(MN)		
			.7	.9	1.05
ΔC_{Y_α}	$D^2/(AR + 2)$	$.00010 + .0000011\ D^2/(AR + 2)$	.90	1.00	1.10
$^{\alpha}C_{Y=0}$	L/SPA	(100 L/SPA) − 1	.86	.96	1.16
ΔC_{Y_β} *	L	.00016 L − .0008	.91	1.00	1.14
$\Delta C_{Y_{\alpha_\theta}}$	D	$(D - 38)\ (-3.0 \times 10^{-6})$	.65	1.22	1.14
$\Delta C_{Y_{\alpha=0_\theta}}$	$D^2/(AR + 2)$	$(4.9 \times 10^{-7})\ (D^2/(AR + 2)$	.75	1.20	1.07
$\Delta C_{Y_{\alpha\ INTF}}$	SPA	(-8.0×10^{-8}) (SPA − 1,000)	.80	1.04	1.14
$\Delta C_{Y_{\alpha=0\ INTF}}$	PROJ, MN	−.0020 + PROJ/75 (MN − .6) (.0110)			
$(\Delta C\ \eta_\alpha)_{NOSE}$	SPA · L	(-1.74×10^{-10}) (SPA · L)	.90	.92	1.17
$(\Delta C\ \eta_{\alpha=0})_{NOSE}$	SPA · L^2	(2.94×10^{-12}) (SPA · L^2)	.86	.87	1.28
ΔC_{η_θ}*	SPA · D^2	(5.00×10^{-12}) (SPA · D^2)	1.06	1.04	.91
ΔC_{η_β}*	SPA	(2.42×10^{-8}) (SPA − 5,000)	1.00	1.00	*
$\Delta C_{\eta_{\alpha\ INTF}}$	SPA · L^2	$(SPA \cdot L^2 - 1.7 \times 10^8)\ /4.5 \times 10^{+12}$	.82	.73	1.27
$\Delta C_{\eta_{\alpha=0\ INTF}}$	SPA	(7.15×10^{-8}) (SPA)	.92	1.08	.84

* DOES NOT VARY SIGNIFICANTLY WITH α

* 0 5 FOR FINLESS STORES, −0.5 FOR FINNED STORES

(U) FIG. 11. MER Installation Airloads Correlation Parameters and Equations

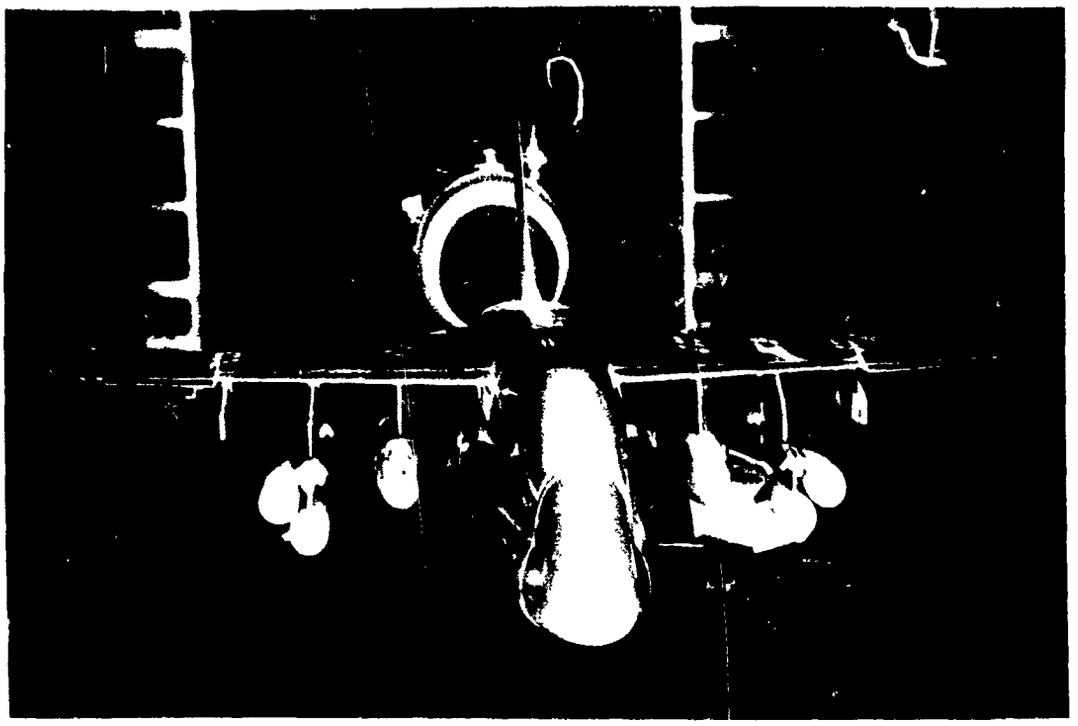

(U) FIG. 12. Wind Tunnel Metric Model Installation.

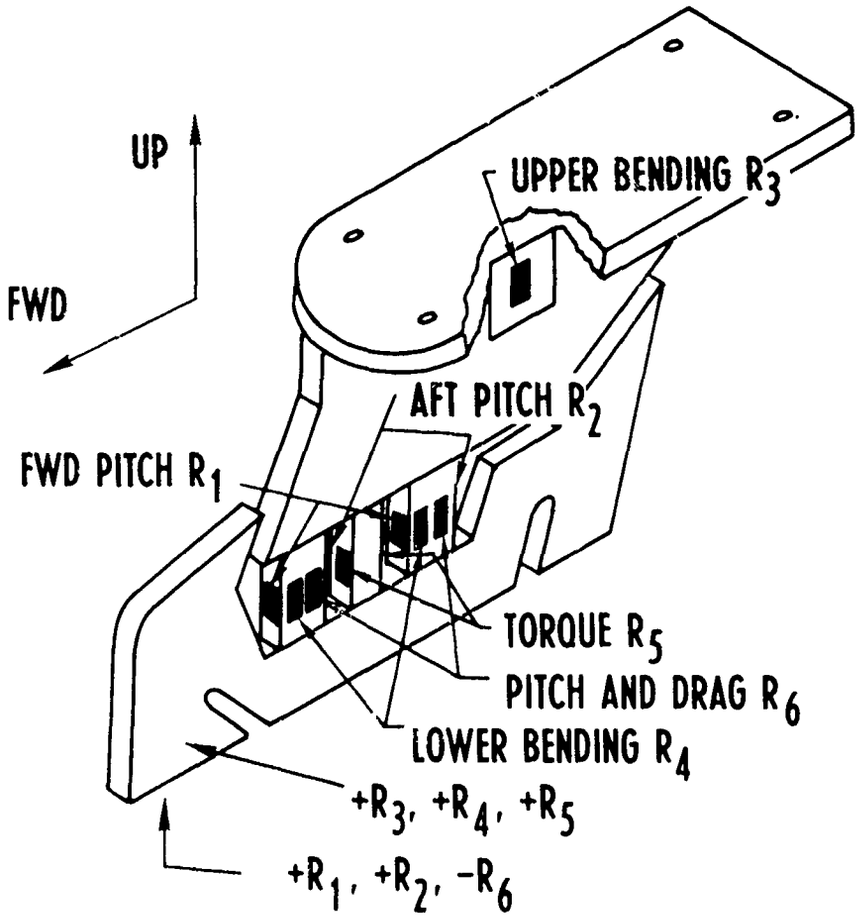

(U) FIG. 13. Pylon Metric Balance

BLANK PAGE

Paper No. 46

ESTIMATION OF AIRCRAFT STORE SEPARATION BEHAVIOR ON THE BASIS OF CAPTIVE LOAD DATA (U)

(Paper UNCLASSIFIED)

by

D. A. Jones
Naval Weapons Laboratory
Dahlgren, Va. 22448

ABSTRACT. (U) A simple dynamic model for estimating store separation behavior in the pitch plane is presented, based on the captive or initial values of the aircraft interference loads. Important parametric effects are illustrated through application of the model to a typical configuration, and safe-launch boundaries are defined in terms of release airspeed and normal "g". Approximate analytical solutions are obtained for the cases of constant interference loads and linear decay of the loads with distance below the launch point. These solutions, together with an approximate first integral of the motion equations, lead to closed-form expressions for the safe-launch boundary. The results of the study indicate that marginal separation behavior can be avoided by imposing suitable lower limits on store static stability and release ejection velocity.

INTRODUCTION

(U) Knowledge of aircraft store separation behavior is required in order to prevent or alleviate the occurrence of large release disturbances, which can lead to store-aircraft or store-store collisions, weapon flight instabilities and unacceptable degradation of ballistic aiming data. This paper outlines some approximate but simple techniques for quickly estimating separation behavior on the basis of captive or initial store load data. The approach is directed toward a particular class of stores, namely freefall statically stable weapons such as low-drag bombs, with the objective of understanding the gross effects rather than precise details of initial store motion.

(U) The following paragraphs focus upon the dynamic model, its application to a configuration of current interest and some analytical results which highlight the importance of various parameters.

DYNAMIC MODEL

(U) Usually, store-aircraft collisions are observed to result primarily from the store's initial motion in the pitch plane. Therefore, as shown in Figure 1, only pitching motion relative to the velocity vector at release and c.g. heaving motion relative to the aircraft will be examined.

(U) The aircraft is considered to be flying at dive angle ϕ, or more generally, to be flying a slightly curvilinear profile during and after store release. Assuming the aircraft normal acceleration g_N remains constant, the effective gravitational acceleration of the store relative to the aircraft (in the z-direction) is approximately equal to g_N.

(U) The aerodynamic forces are considered as follows: in the captive launch position, the distribution of local angle of attack and vertical pressure gradient along the length of the store will result in a normal force Z_0 and pitching moment M_0. These initial interference loads are assumed to be known experimentally or otherwise. If the store then pitches through an angle α, it is assumed that the free-stream contribution can be linearly superimposed onto the interference loads, to yield new loads $Z_0 + Z_\alpha\alpha$ and $M_0 + M_\alpha\alpha$ (no distinction is made between lift and normal force). Here, Z_α and M_α denote normal force and pitching moment derivatives, respectively, for the store in isolation.

Figure 2, obtained by combining store free-stream static stability data with data contained in reference 1, indicates that the assumption holds quite well at small store incidence. It can be reasonably extended to larger incidence angles, provided the store in question has good static stability, say at least a caliber of static margin. It is also assumed that the initial interference loads decay linearly with distance below the launch point, and vanish at some point z_1 (usually taken to be a wing chord length) where free-stream conditions exist. The assumption of linear load decay is mainly for convenience; load measurements might reveal that some other form of load decay is more generally applicable. However, the results obtained later suggest that the magnitude and direction of the initial loads are likely to be more important than the manner in which they decay.

(U) Finally, it is assumed that the effect of an initial ejection force and moment can be adequately represented by translational velocity v_e and rotational velocity w_e introduced at release.

(U) In accordance with the above assumptions, the store equations of motion are given in Figure 1.

AIRCRAFT INTERFERENCE LOADS

(U) Before discussing parametric effects, let us briefly consider the nature of the captive store loads due to aircraft interference - in particular, the distinctions between single and multiple store carriage configurations (Figures 3 and 4).

(U) In single carriage, the store c.g. is typically positioned near the wing section center of pressure, i.e. quarter or mid-chord point (Figure 3). Then, as shown in Figure 5, the flow pattern over a wing-pylon (in the low aircraft incidence region of primary interest) indicates downwash over the store nose and upwash over the tail fins, and a negative pressure region between the store and wing, which tends to concentrate slightly aft of the store c.g. This flow pattern results in a normal force directed upward toward the wing and a nose-down pitching moment, as shown in Figure 6. This is consistent with the results of full-scale flight tests of stores in single carriage, in which the initial pitching motion is almost invariably nose-down.

(U) In contrast, stores in multiple carriage arrangements are located in extreme forward and aft chordwise positions (Figure 4), and the initial pitching motion may be either nose-down or nose-up, apparently depending upon the precise flight conditions at release. This, as will be seen in the following section, has important consequences for the separation behavior of stores in multiple carriage.

PARAMETRIC EFFECTS

(U) Use of multiple carriage racks in steep dive, low-g tactical maneuvers has frequently led to serious store separation problems. It has sometimes been conjectured that these problems are associated with rack deficiencies which lead to store shackle hang-up and/or rack flexure and non-rigidities which lead to reduced ejection velocities. Indeed, computer studies indicate that ejection velocities developed by the multiple ejection rack (MER) can vary by ±30% due to relative motion between store and rack during ejection.* However, it will be shown that for more basic reasons, store-aircraft collisions are possible even if the ejection force developed by the MER is entirely effective.

(U) Based on the dynamic model previously described and best available estimates of initial store loads, computer studies have been performed in order to examine the effects of various parameters on initial store motion. Results are presented for a typical multiple carriage configuration, the 500 lb low drag bomb ejected from the MER (see Figure 4). Pitching and heaving motions have been combined to obtain the motion of the store nose or tail tip (whichever is closer) relative to the aircraft. The range of initial pitching moment coefficients considered varies from -1.5 (corresponding to a maximum pitch amplitude of approximately 30 degrees nose-down) to +1.0 (20 degrees nose-up). This range appears representative of release behavior observed in full-scale flight tests.

(U) The most striking result from the studies is that under high-speed, low-g flight conditions, separation behavior becomes extremely dependent upon the nature of the initial pitching motion. This dependence is essentially unaffected by the relatively small ejection velocities provided by current multiple ejection racks. Much higher ejection velocities, of the order of those provided by aircraft parent racks, are necessary to significantly reduce pitching motion influence.

(U) Figure 7 presents the effect of aircraft normal g factor on separation behavior. Even at 1 g (level flight), the contrast between the effect of positive (nose-up) and negative (nose-down) pitching moments is significant. Although no store-aircraft collisions are indicated, the results (not shown in figure) displayed a 40 ft/sec spread in c.g. velocities two seconds after release. In level flight, this could easily lead to considerable ballistic dispersion. As normal g is reduced to 0.5 (60 degree dive, say), intercepts with the aircraft are indicated for stores acted upon by small positive pitching moments. As normal g is further reduced to 0.2 (60 degree dive in combination with a slightly nose-over curvilinear profile at release), a store with zero captive pitching moment is unable to

*Undocumented study performed at NWL by author.

separate, and lingers with the aircraft. Finally, under a negative g condition of -0.2 (steep-dive, strongly nose-over), only a store which experiences a sizeable nose-down moment is able to separate cleanly. Even this store is likely to incur a grazing collision with the aircraft, since the motion indicated on the graph does not account for the physical clearance needed for the span of the tail fins.

(U) Thus, the positive lift generated by small nose-up pitching moments can easily be sufficient to cause a collision, while the negative lift associated with nose-down moments can exert a very favorable influence in achieving separation. There is good qualitative agreement between the motions of Figure 7 and the motions observed during weapon separation tests. This suggests that the main reason store separations under low-g conditions are as good as they are, is that the majority of stores pitch nose-down at release.

(U) The substantial effect of dynamic pressure is indicated in Figure 8, where releases at 500 knots and at 300 knots are compared. At the lower airspeed, distinctions between positive and negative pitching moments tend to vanish. The spread of c.g. velocities after two seconds was 15 ft/sec, which at .5g (60 degree dive) is more acceptable in terms of ballistic dispersion.

(U) In Figure 9, the effect of ejection velocity is considered. Ejection from a shoulder MER station (which provides an effective downward velocity of only 4 ft/sec) is compared with ejection from an AERO-20A aircraft parent rack (which provides 18 ft/sec ejection velocity). The results indicate the substantial increase in ejection velocity necessary to overcome the adverse influence of positive pitching moments under low-g conditions.

(U) The results of the parametric studies can be summarized as safe-launch boundaries which establish safe flight conditions for releasing a given store from a given aircraft/rack configuration. The criteria used in defining satisfactory separation are: no motion of the store nose or tail above the launch position, and sufficient average velocity to escape the aircraft flow field. On the graphs in Figure 10, a boundary is indicated for a range of pitching moments, where the area to the right of each curve denotes the safe region. If experimental load data were available as a function of Mach number and aircraft incidence, then a single curve would define the safe boundary for any particular aircraft/store/rack combination. The graphs indicate in a condensed form the sharp contrast between the separation characteristics of stores which pitch nose-up and those which pitch nose-down at release. For nose-down moments, small increases in ejection velocity can significantly increase the safe-launch region. This is because ejection velocity immediately displaces the store away from the aircraft, thus providing a "stall time" during which sufficient negative lift is generated to force the store out of the aircraft flow field. Also, separation characteristics improve with increasing airspeed, up to a certain point. On the other hand, proportionally much larger amounts of ejection velocity are required

to overcome the lifting influence of nose-up moments and achieve safe separation in the high-speed, low-g region of the flight regime.

(U) The question arises as to whether the unfavorable effects of pitching motion can be alleviated through the use of off-c.g. ejection. That is, application of an ejection moment to counter-balance the aerodynamic pitching moment. First consider the case of low-g conditions and low ejection velocity, in which the initial c.g. translation of the store takes place slowly in comparison with the period of the pitching motion. The external aerodynamic pitching moment is then essentially constant over the first pitch cycle. As shown in the upper graph of Figure 11, the store oscillates about a "trim angle" of M_0/M_α. Under these conditions, the introduction of an ejection angular impulse at release can reduce the amplitude of the first half-cycle of motion only at the expense of increasing the pitch amplitude over the second half-cycle. (This effect of off-c.g. ejection was observed in the tests of reference 3.) Furthermore, the ejection angular impulse does not alter the net lifting effect of the pitching motion, since the average pitch angle over the first cycle is still equal to M_0/M_α. Thus, in this situation, use of off-c.g. ejection is as likely to degrade separation behavior as to improve it. On the other hand, if the store translates more rapidly away from the aircraft (i.e. higher ejection velocity and/or higher g conditions), the external pitching moment can decay significantly from its captive value of M_0. As shown in the lower graph of Figure 11, the amplitude of the pitching motion is reduced as the store initial (and average) downward velocity increases, and the pitching moment appears to act as if it were impulsively applied. It is only in this limiting case that an ejection angular impulse can effectively cancel the pitching motion due to the flow field. To summarize, the favorable effects of off-c.g. ejection are associated mainly with situations in which the store passes rapidly out of the aircraft flow field. But in these situations, the problem of store-aircraft collisions is already non-existent, and pitch amplitude is already reduced significantly because of decay of the pitching moment. Additionally, off-c.g. ejection was seen to have an adverse effect in cases where the store passes slowly out of the aircraft flow field. In general, then, the most favorable point of application of the ejection impulse is over the store c.g.

ANALYTICAL SOLUTIONS

SOLUTION FOR LINEAR LOAD DECAY

(U) An approximate closed-form solution to the pitch plane equations of motion (Figure 1) can be easily obtained by neglecting pitch damping, and taking $\alpha \simeq \theta$. Then the equations for linear decay of the aircraft interference loads become

$$m\ddot{z} = Z_\alpha\,\theta + Z_o\,(1 - z/z_1) + mg_n \tag{1}$$

$$z(o) = o \qquad \dot{z}(o) = v_e$$

$$I\,\ddot{\theta} = M_\alpha\,\theta + M_o\,(1 - z/z_1) \tag{2}$$

$$\theta(o) = \theta_o \qquad \dot{\theta}(o) = w_e$$

Equations (1) and (2) can be decoupled to yield

$$\dddot{z} + (a + \omega_o^2)\,\ddot{z} + \omega_o^2\,c\,z = \omega_o^2\,(c\,z_1 + g_n) \tag{3}$$

$$\ddddot{\theta} + (a + \omega_o^2)\,\ddot{\theta} + \omega_o^2\,c\,\theta = \omega_o^2\,\frac{M_o}{M_\alpha}\,\frac{g_n}{z_1} \tag{4}$$

where

$$\omega_o = \left(-\frac{M_\alpha}{I}\right)^{1/2} \qquad a = \frac{Z_o}{mz_1} \qquad c = \frac{1}{mz_1}\left(Z_o - \frac{Z_\alpha}{M_\alpha}\,M_o\right) \tag{5}$$

Oscillatory and damping type roots are identified as

$$\omega = \pm\left[\left(\frac{a+\omega_o^2}{2}\right) + \left(\left[\frac{a+\omega_o^2}{2}\right]^2 - \omega_o^2\,c\right)^{1/2}\right]^{1/2} \simeq \pm\left[\omega_o^2 - c\right]^{1/2} \tag{6}$$

$$\lambda = \pm\left[-\left(\frac{a+\omega_o^2}{2}\right) + \left(\left[\frac{a+\omega_o^2}{2}\right]^2 - \omega_o^2\,c\right)^{1/2}\right]^{1/2} \simeq \pm\left[-c\right]^{1/2} \tag{7}$$

$$\Omega = \pm\,(\omega^2 + \lambda^2)^{1/2} \tag{8}$$

The oscillatory root ω represents a perturbation of the store's natural pitching frequency, due to decay of the interference loads. Later it will be seen that the factor c can be interpreted as the vertical gradient of the average aerodynamic acceleration per pitch cycle.

(U) The solutions to equations (1) and (2) can be written as

$$z(t) = -\frac{Z_\alpha}{m\Omega^2}\left[\left(\frac{M_o}{M_\alpha} + \theta_o\right)\left(\cos\omega t - \cosh\lambda t\right) + \left(w_e - \frac{M_o}{M_\alpha}\,\frac{v_e}{z_1}\right)\left(\frac{\sin\omega t}{\omega} - \frac{\sinh\lambda t}{\lambda}\right)\right] + \left[g_n + \frac{1}{m}\left(Z_o - \frac{Z_\alpha}{M_\alpha}\,M_o\right)\right]\left(\frac{\cosh\lambda t - 1}{\lambda^2}\right) + \frac{v_e}{\lambda}\,\sinh\lambda t \tag{9}$$

$$\theta(t) = \frac{\omega_o^2}{\Omega^2}\left[\left(1 + \frac{g_n}{z_1\,\omega_o^2}\right)\frac{M_o}{M_\alpha}\,(\cos\omega t - \cosh\lambda t)\right.$$

$$\left. - \frac{M_o}{M_\alpha}\frac{v_e}{Z_1}\left(\frac{\sin\omega t}{\omega} - \frac{\sinh\lambda t}{\lambda}\right)\right] \qquad (10)$$

$$+ \frac{M_o}{M_\alpha}\frac{g_n}{z_1\,\omega_o^2}\left(\frac{\cosh\lambda t - 1}{\lambda^2}\right) + \frac{w_e}{\omega}\sin\omega t + \theta_o\cos\omega t$$

where terms involving $(1 - \omega^2/\omega_o^2)$ have been neglected. Also, λ is taken to be real for negative c. If c is positive λ becomes imaginary, and in equations (9) and (10), cosh λt and sinh λt are to be replaced by cos λt and sin λt, respectively.

(U) Comparison of the analytical solution (no pitch damping) given by equations (9) and (10) with the more exact computer solution of the equations in Figure 1, is shown in Figure 12. The rather close agreement indicates that damping has little effect on initial store motion.

SOLUTION FOR CONSTANT LOADS

(U) Since equations (9) and (10), are not easily interpreted, it is instructive to consider the limiting case of constant interference loads ($z_1 \to \infty$ in equations (9) and (10)), which can be written as

$$z(t) = -\frac{Z_\alpha}{m\,\omega_o^2}\left[\theta(t) - \theta_o\right] + \left[g_n + \frac{1}{m}\left(Z_o - \frac{Z_\alpha}{M_\alpha}M_o\right)\right]\frac{t^2}{2}$$

$$+ V_e\left(1 - \frac{Z_\alpha}{M_\alpha}\ell_e\right)t \qquad (11)$$

$$\theta(t) = \frac{M_o}{M_\alpha}(\cos\omega_o t - 1) + \frac{w_e}{\omega_o}\sin\omega_o t + \theta_o\cos\omega_o t \qquad (12)$$

The constant load solution is approximately valid if no appreciable c.g. motion occurs during the first pitch cycle. The pitching motion consists of the particular solution for constant external moment M_o, plus the complementary solution for initial conditions. The heaving motion contains an oscillatory lift term which is relatively unimportant in comparison with the more dominant secular terms. The term $(Z_o - \frac{Z_\alpha}{M_\alpha}M_o)$ represents the average lift per cycle, since for constant M_o, the average pitch angle is M_o/M_α. Also note that Z_α/M_α, the reciprocal of the static margin, is positive for statically stable stores. Thus positive M_o results in negative acceleration, up toward

the aircraft, while negative M_o provides positive acceleration away from the aircraft. Additionally, the influence of M_o is reduced as the static margin is increased. (Strictly speaking, this statement applies only if the static margin increase is obtained by a forward shift of the store c.g. If the static margin is increased by increasing the size of the store tail fins, then the value of M_o will change in a manner dependent upon the particular flow pattern about the store. However, a simple analysis suggests that unless M_o is due entirely to the load on the tail fins, M_o/M_α is reduced if M_α is increased.)

PARAMETRIC DEFINITION OF SAFE-LAUNCH BOUNDARIES

(U) Safe-launch boundaries as presented previously in Figure 10 may also be defined analytically by parametric constraint relations obtained from solutions of the motion equations. As the first condition for safe separation it is required that there be no motion of the store nose or tail above the launch position. Denoting by Z_n and Z_t, respectively, the positions of the store nose and tail relative to the aircraft,

$$z_n = z - R_n \cdot \theta$$
$$z_t = z + R_t \cdot \theta \tag{13}$$

where R_n and R_t denote distances from the store c.g. to nose and tail tip, respectively. The condition above is approximately satisfied by requiring that

$$z_n\,(T/2) \geq 0 \text{ and } z_t\,(T/2) \geq 0 \tag{14}$$

where T is the store natural period of oscillation. Using the constant load solutions (equations (11) and (12)) for z and θ, the first constraint relation becomes, say for the tail,

$$g_n + \frac{2}{\pi}\left(-\frac{\rho A D}{2I}\,C_{M_\alpha}\right)^{1/2} v_e\,V + \frac{\rho A}{2m}\left[\left(C_{Z_o} - \frac{C_{Z_\alpha}}{C_{M_\alpha}}\,C_{M_o}\right) + \frac{4}{\pi^2}\left(\frac{C_{Z_\alpha}}{C_{M_\alpha}} + \frac{mD}{I}\,R_t\right)C_{M_o}\right] V^2 \geq 0 \tag{15}$$

with a similar expression for the nose.

(U) The second condition for safe separation, that the store have sufficient average velocity to escape the aircraft flow field, is satisfied by requiring that

$$\dot{z}\big|_{z=z_1} \geq 0 \tag{16}$$

This condition can be expressed in parametric terms through an approximate first integral of equations (1) and (2), in which a more general load decay law of the form

$$\left.\begin{matrix} Z(z) = Z_o \\ M(z) = M_o \end{matrix}\right\} \left[1 - (z/z_1)^p\right] \tag{17}$$

is considered. (Linear load decay is the special case of p = 1 in equation (17).) The result is

$$g_n + \frac{v_e^2}{2z_1} + \frac{\rho A}{2m}\left(\frac{p}{p+1}\right)\left(C_{Z_o} - \frac{C_{Z_\alpha}}{C_{M_\alpha}} C_{M_o}\right) V^2 \geq 0 \tag{18}$$

(U) The safe-launch boundary is then obtained from the constraints imposed by equations (15) and (18). For nose-down pitching moments, equation (15) will usually represent the more stringent condition. In this case the safe boundary is defined with g_n proportional to V^2 and V. For nose-up moments, equation (18) will usually be more stringent, in which case g_n is proportional to V^2. These functional relationships are in agreement with the curves presented previously in Figure 10.

CONCLUSIONS

(U) Some important assumptions have been made in order to obtain the results presented in this paper. Nevertheless, the results appear in good qualitative agreement with observations from full-scale tests, at least for streamlined, statically stable stores.

(U) Under current operational procedures, it is typical for stores to be released with low ejection velocities, under high-speed, low-g flight conditions. Store motion is then dominated by the influence of even relatively small pitching moments, and stores may exhibit marginal separation behavior, in the sense that slight changes in release conditions can lead to radical changes in initial motion. Adequate prediction of such behavior requires extensive knowledge of interference loads along the initial trajectory.

(U) Marginal separation behavior can be avoided, or at least alleviated by ensuring that stores have adequate static stability, and by providing substantial ejection velocities (over the store c.g.) at release.

(U) By imposing appropriate lower limits on store static stability and ejection velocity, the number of combinations of aircraft, store, rack, and flight conditions that fall into the marginal category can be significantly reduced. Under such conditions, the prediction problem would become more tractable, since it would then be possible to distinguish between good and bad separation behavior on the basis of a limited amount of test data.

GLOSSARY OF SYMBOLS

A	Store maximum cross-sectional area
C_{M_α}	Pitching moment coefficient derivative, $\frac{\partial C_M}{\partial \alpha}$
$C_{M_{\dot{\alpha}}}$	Pitch damping moment coefficient derivative, $\frac{\partial C_M}{\partial (\dot{\alpha} D/2V)}$
C_{M_o}	Store captive pitching moment coefficient
C_{Z_α}	Normal force coefficient derivative, $\frac{\partial C_Z}{\partial \alpha}$
C_{Z_o}	Store captive normal force coefficient
D	Store maximum diameter
F_e	Ejection force (in the z-direction)
g	Gravitational acceleration
g_n	Aircraft normal acceleration, normal g factor times g
I	Store transverse moment of inertia
ℓ_e	Ejection moment arm (positive when ejection force is applied aft of store c.g.)
M	Mach number
m	Store mass
Q	Dynamic pressure, $1/2\ \rho V^2$
R_n	Distance from store c.g. to nose tip
R_t	Distance from store c.g. to tail tip
T	Store natural period of pitch oscillation, $2\pi \left[\frac{I}{-M_\alpha}\right]^{1/2}$
t	Time
t_e	Duration of ejection force
V	Airspeed at time of store release
v_e	Ejection translational velocity (in the z-direction)
w_e	Ejection angular velocity (in the θ-direction)
z	Distance traveled by store relative to aircraft (measured in direction normal to aircraft flight vector at store release)
z_1	Distance below the aircraft (i.e. in the z-direction) at which free-stream conditions are assumed to exist
α	Store incidence angle
α_F	Aircraft incidence angle
θ	Store pitch angle
ρ	Air density
ϕ	Aircraft dive angle at time of store release

Note: Aerodynamic coefficients are referred to the store maximum cross-sectional area and the store maximum diameter.

REFERENCES

1. Cornell Aeronautical Laboratory. Prediction of the Initial Motion of a Bomb Carried and Released Under the Wing of an Airplane at High Subsonic Speed (U), by S. J. Deitchman. Buffalo, N. Y., CAL, December, 1956. (CAL Report GC-910-C-10, publication UNCLASSIFIED.)

2. Northwestern University, Aerial Measurements Laboratory. External Stores Separation under Subsonic Conditions, Phase V, Instrumented Mk. 83 Fly-Around Tests (U), by R. Sadler and M. Wiley. Evanston, Ill., AML, June 1965. (AML Memo 432, publication UNCLASSIFIED.)

3. Cornell Aeronautical Laboratory. Subsonic Wind Tunnel Tests of the Separation Characteristics of Several Externally Mounted Store Shapes for the United States Naval Weapons Laboratory (U), by E. B. Fisher. Buffalo, N. Y., CAL, July 1961. (CAL Report AA-1481-W-1, publication UNCLASSIFIED.)

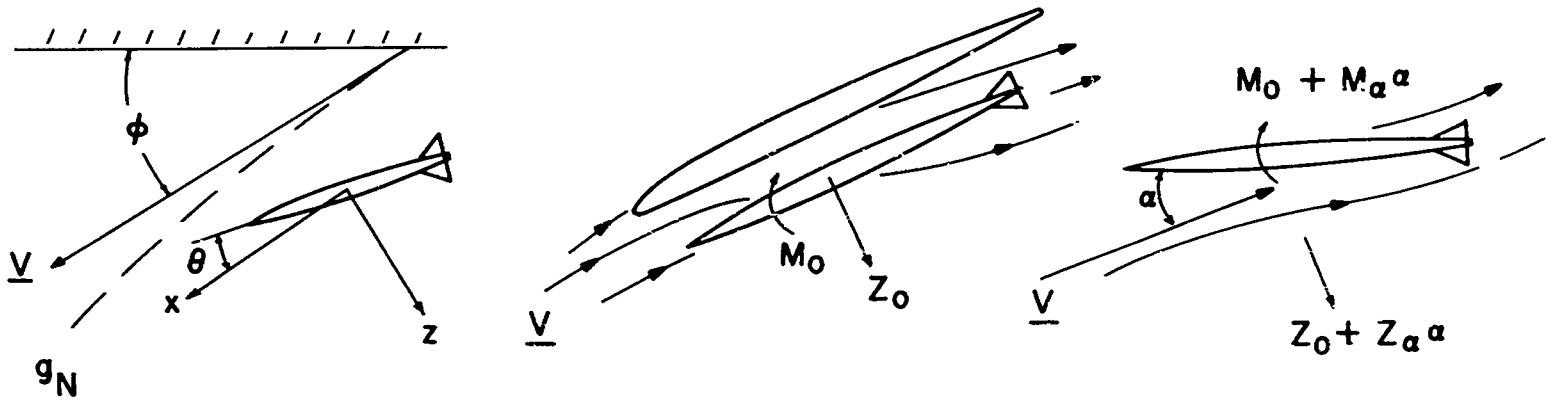

$$m\ddot{z} = Z_\alpha \alpha + Z_0 U(z) + m g_N$$

$$I\ddot{\theta} = M_\alpha \alpha + M_0 U(z) + M_{\dot{\alpha}} \dot{\alpha}$$

$$\alpha \approx \theta + \dot{z}/V$$

$$z(0) = 0 \qquad \dot{z}(0) = V_e = 1/m \int_0^{t_e} F_e \cdot dt$$

$$\theta(0) = \theta_0 \qquad \dot{\theta}(0) = W_e = Ie/I \int_0^{t_e} F_e \cdot dt$$

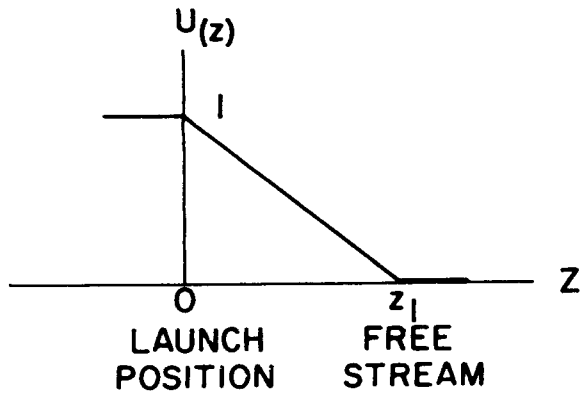

(U) FIG. 1. Dynamic Model.

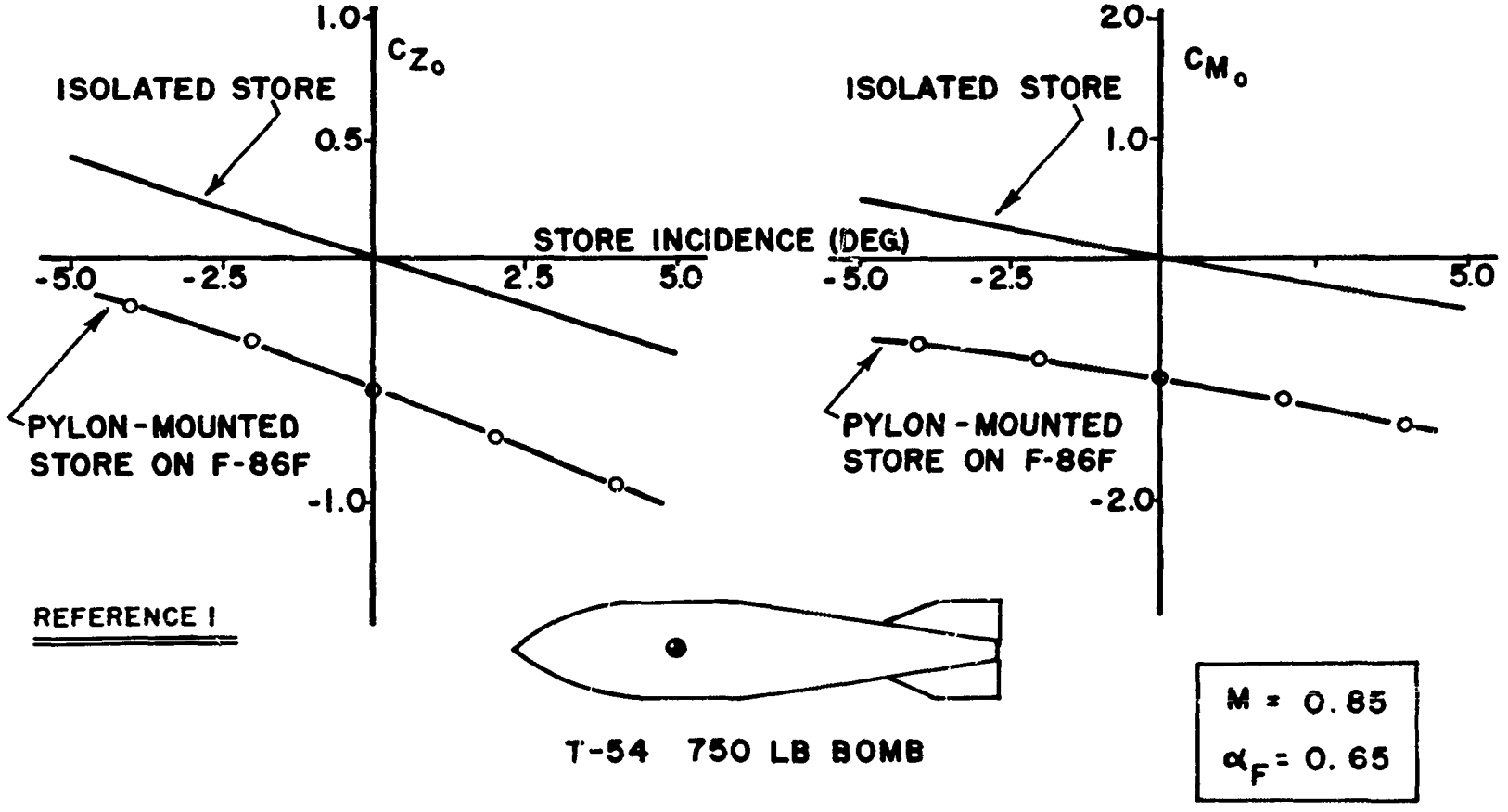

(U) FIG. 2. Variation of Store Loads with Incidence. T-54 Bomb. F-86F Aircraft. .3 Semi-Span Station.

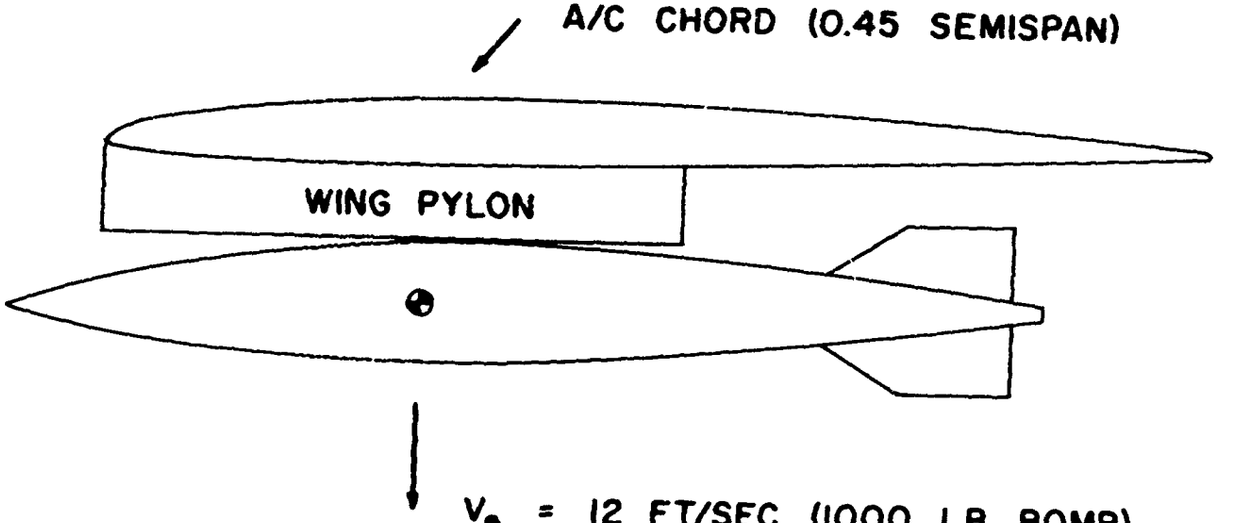

MK 83 1000 LB LOW DRAG BOMB ON AERO 20A RACK (WING PYLON).

A4 AIRCRAFT WING STATION.

(U) FIG. 3. Typical Single Store Carriage Arrangement.

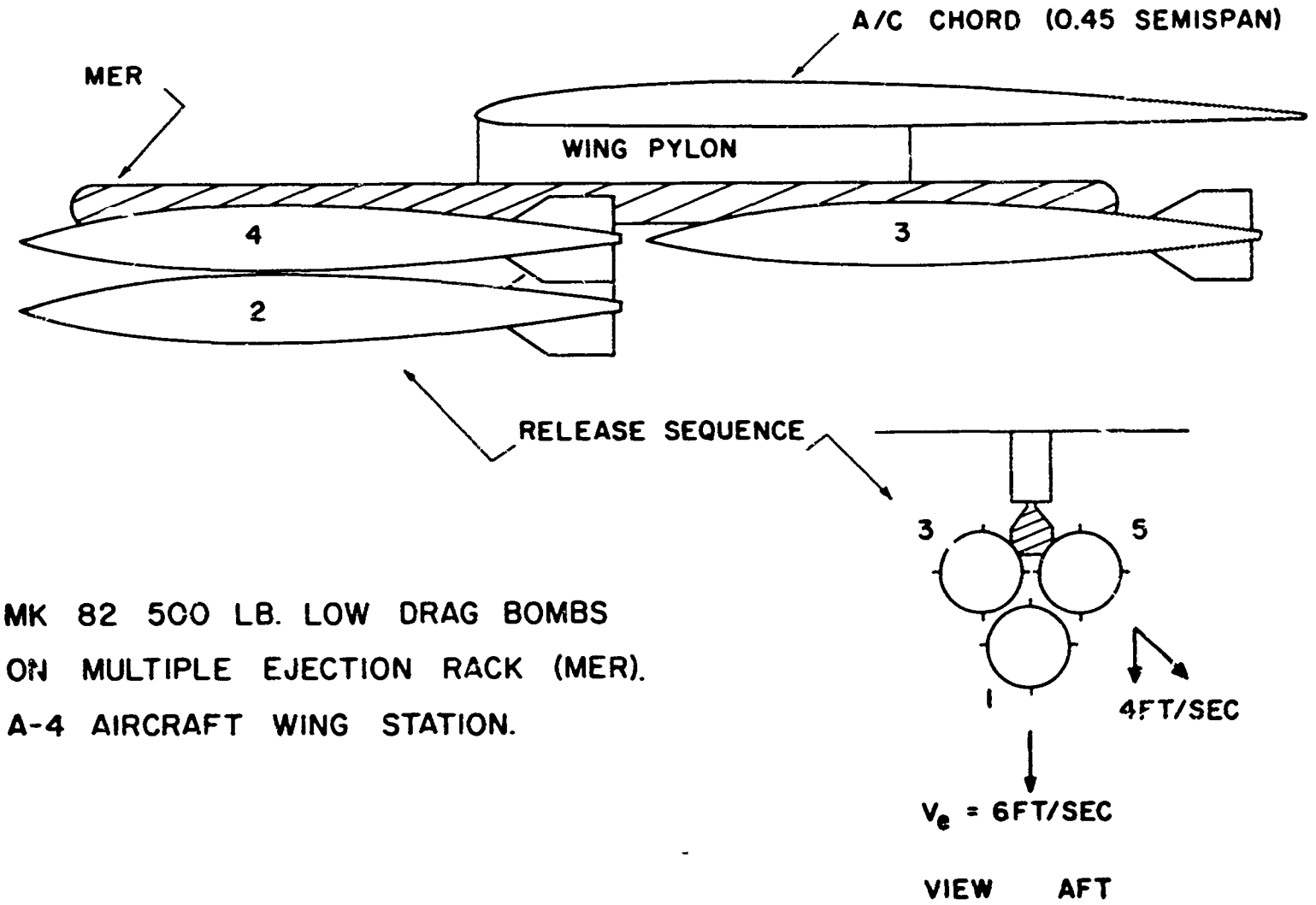

(U) FIG. 4. Typical Multiple Store Carriage Arrangement.

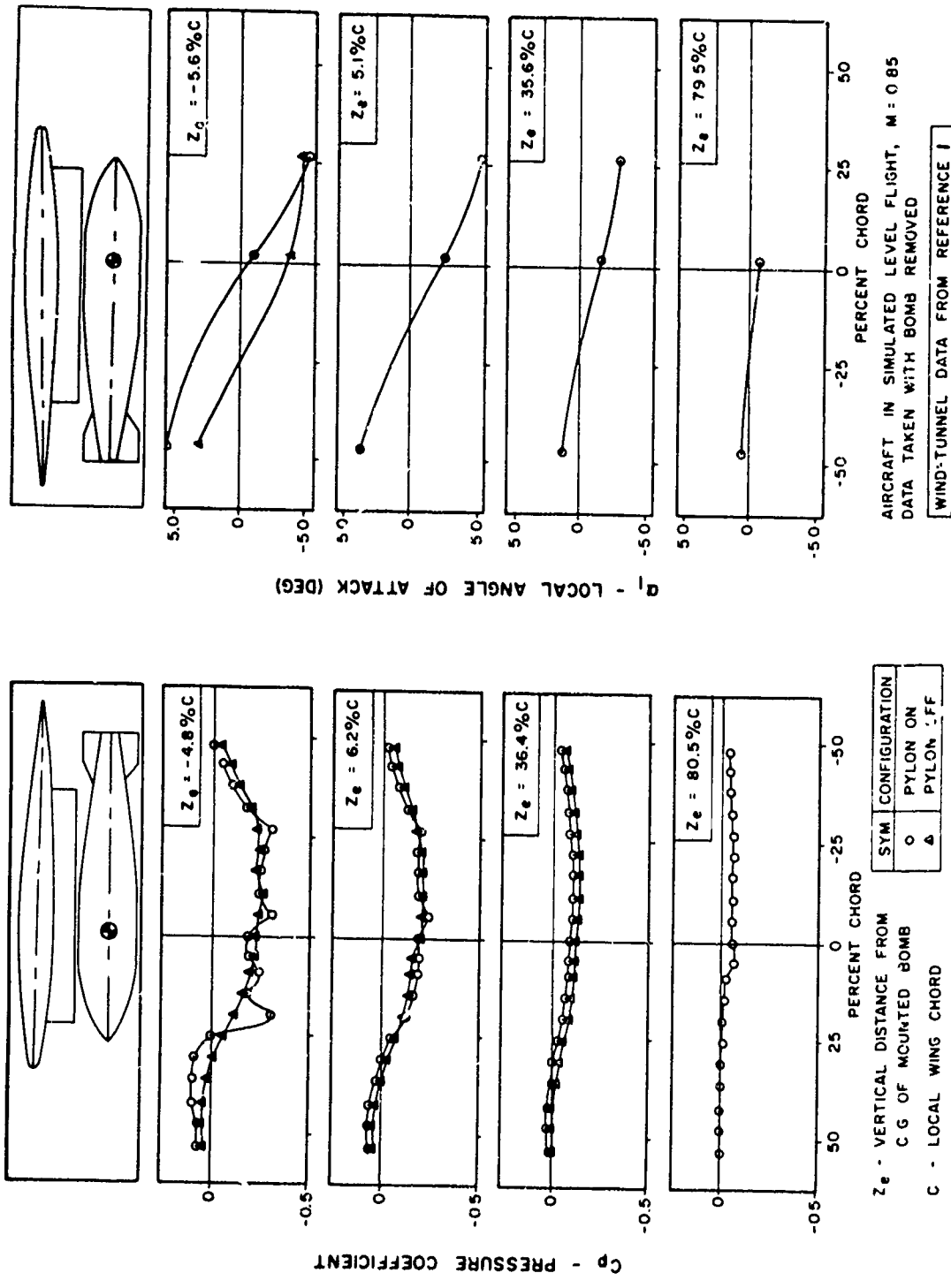

(U) FIG. 5. Flow Field Below the Wing of the F-86F Aircraft at .3 Semi-Span.

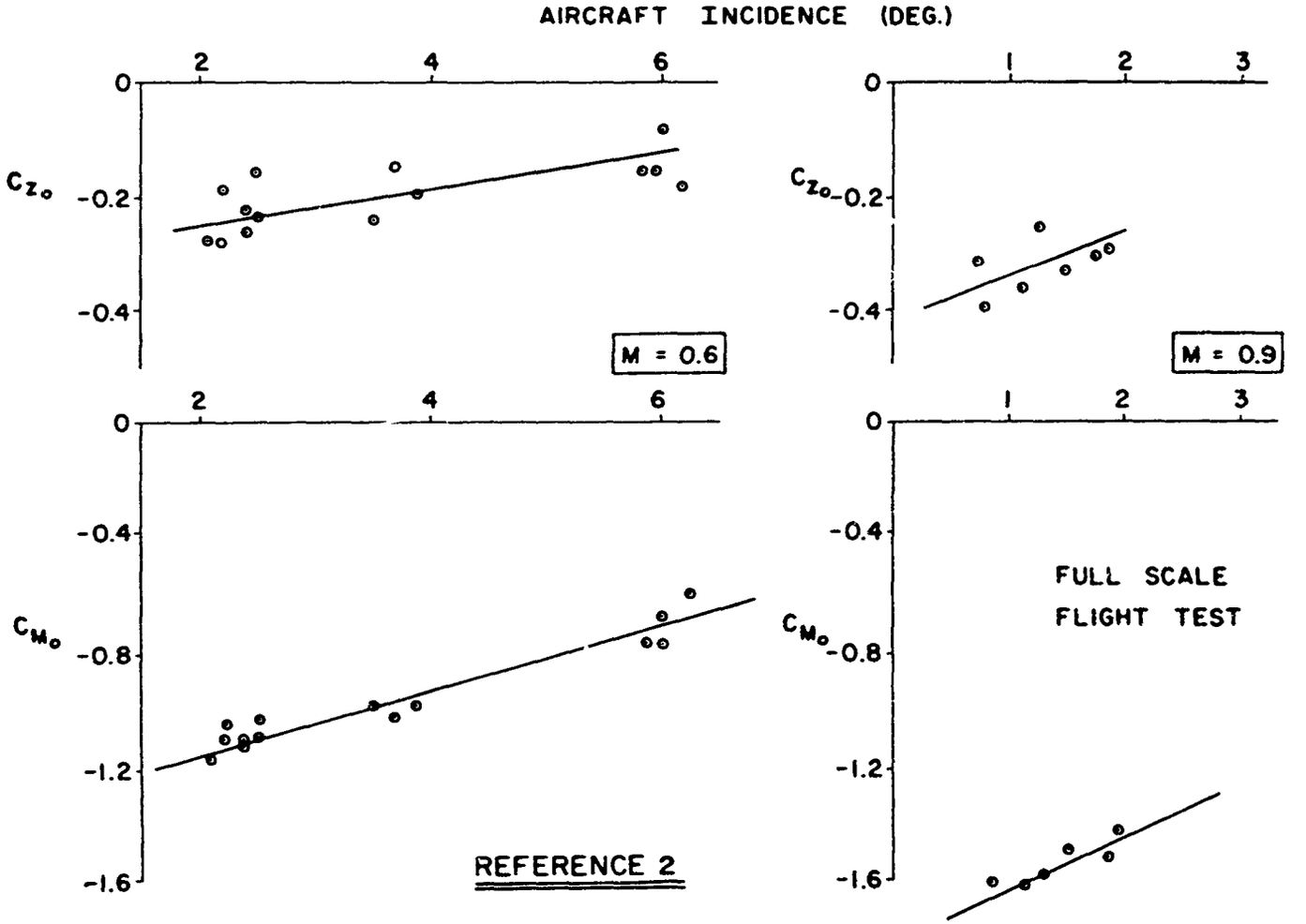

(U) FIG. 6. Captive Store Loads. 1000 lb. Low Drag Bomb. A4 Aircraft at 0.45 Semispan.

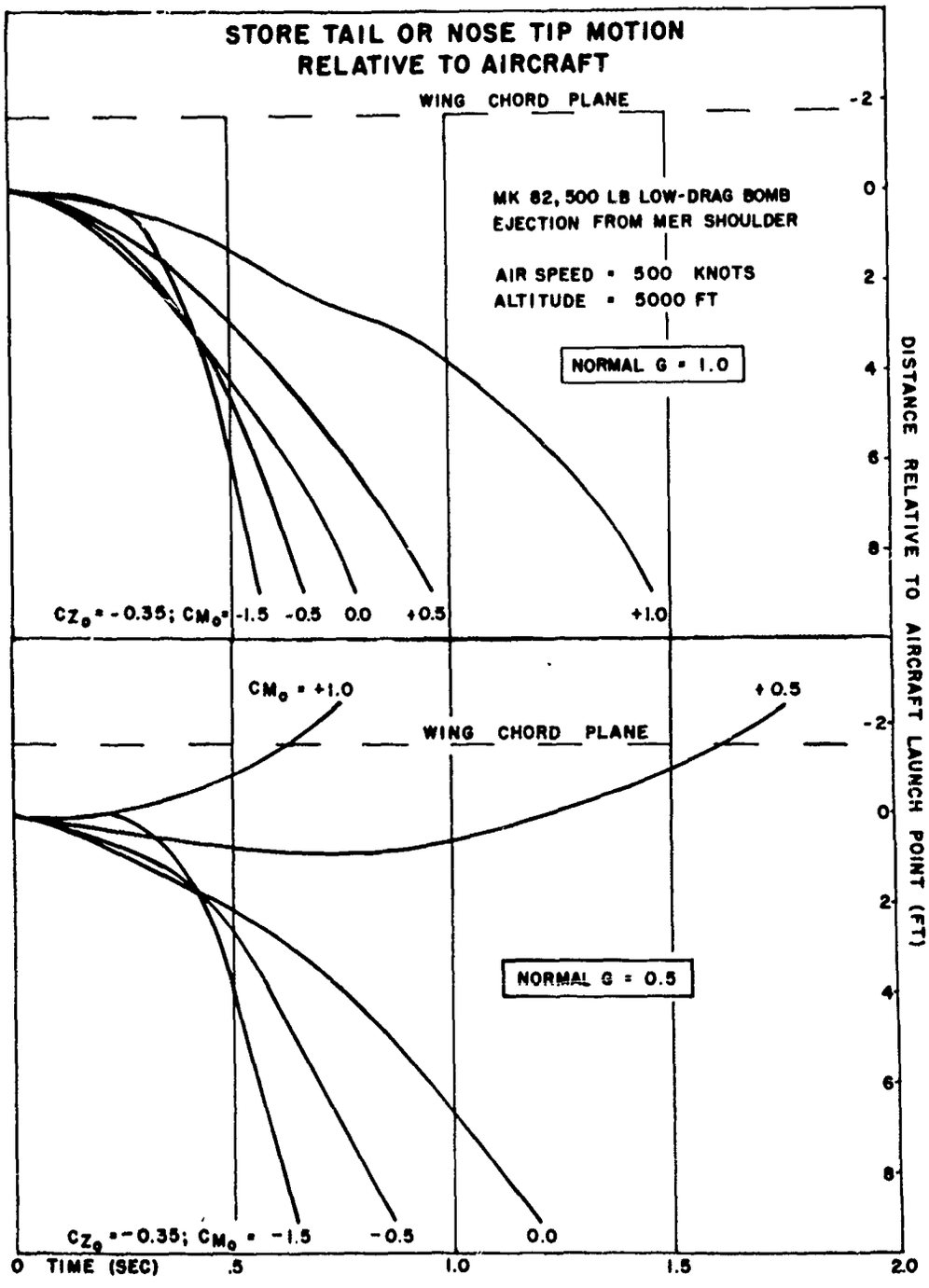

(U) FIG. 7. Effect of Normal G on Initial Store Motion.

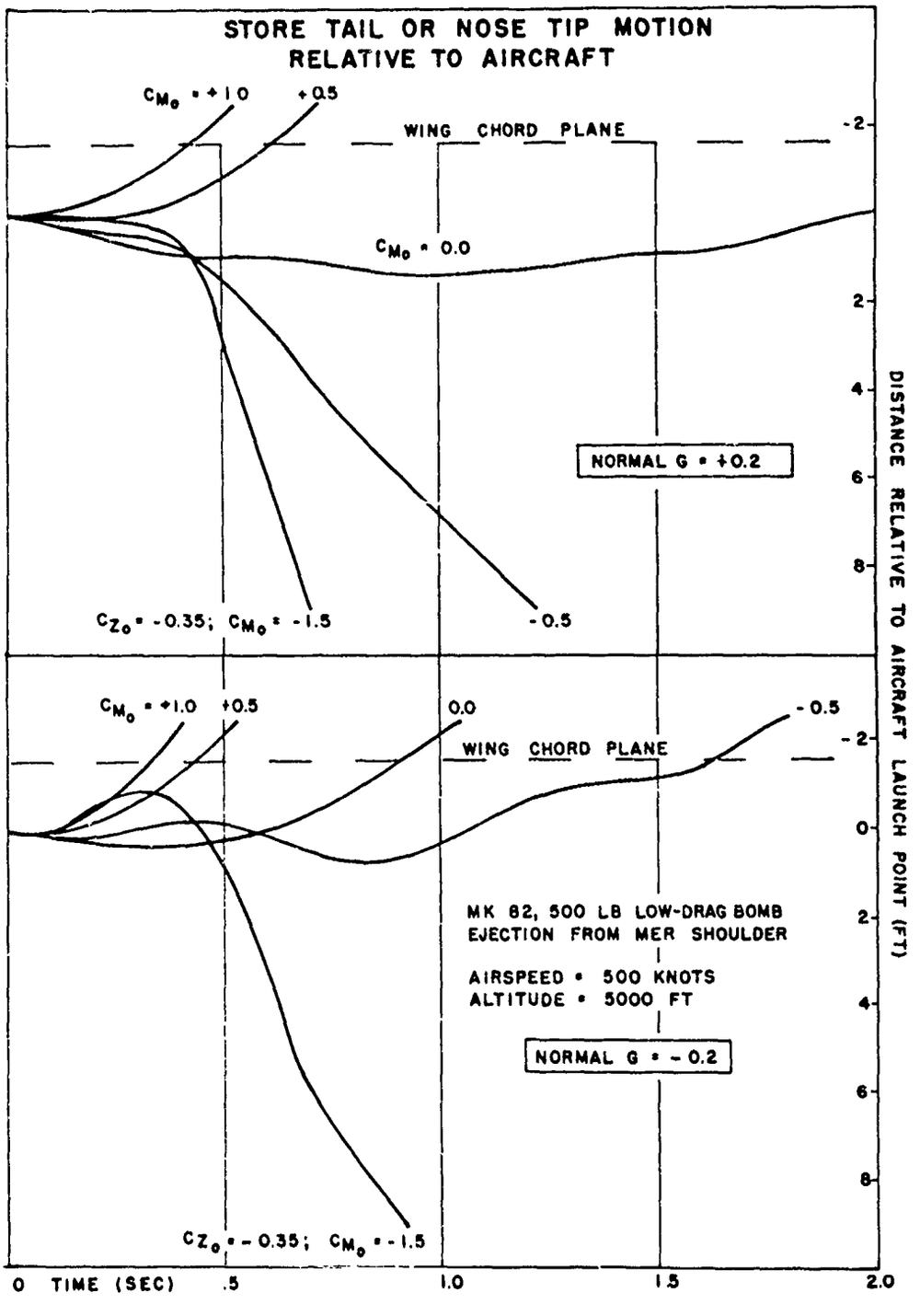

(U) FIG. 7. (Continued).

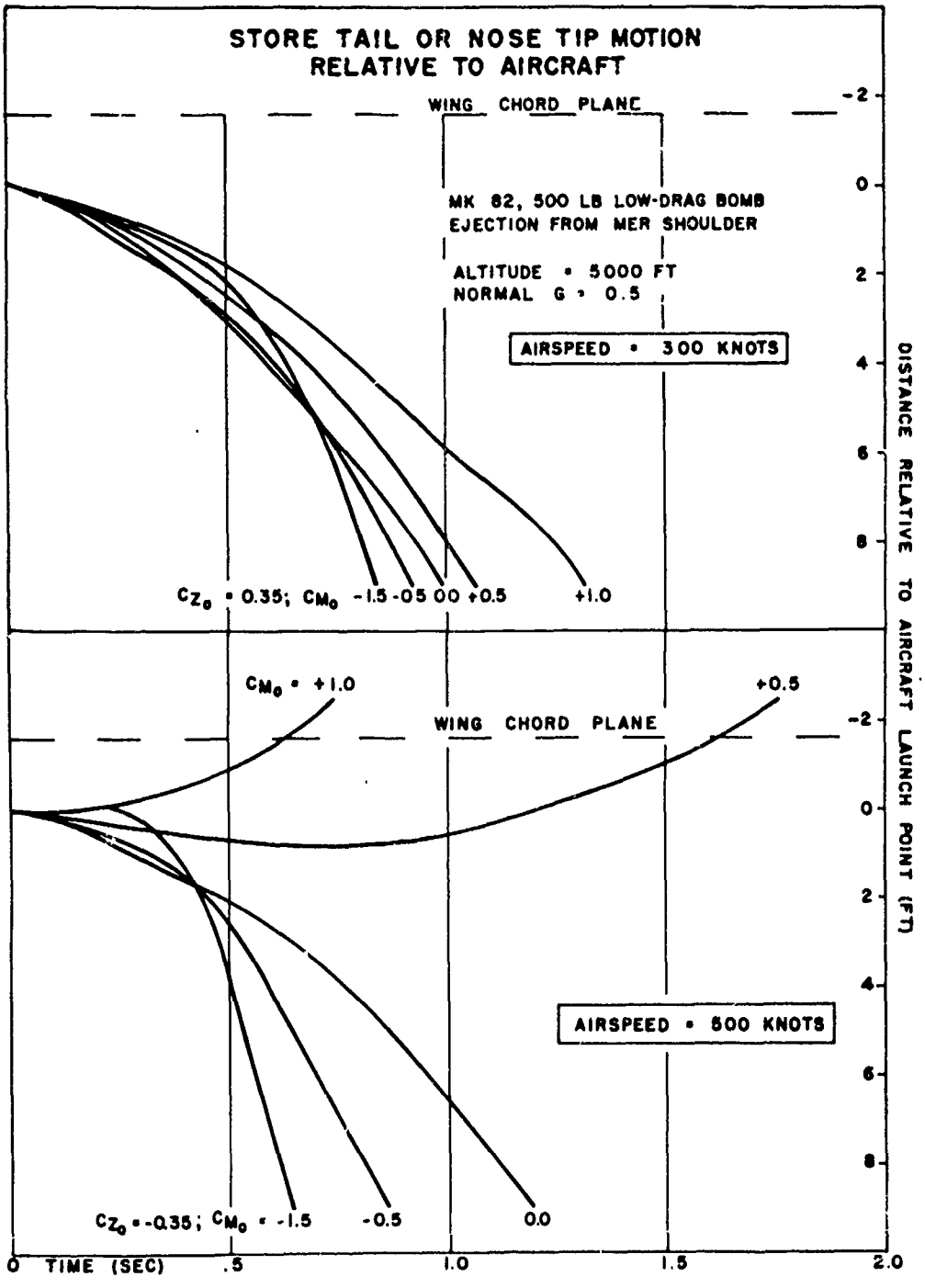

(U) FIG. 8. Effect of Airspeed on Initial Store Motion.

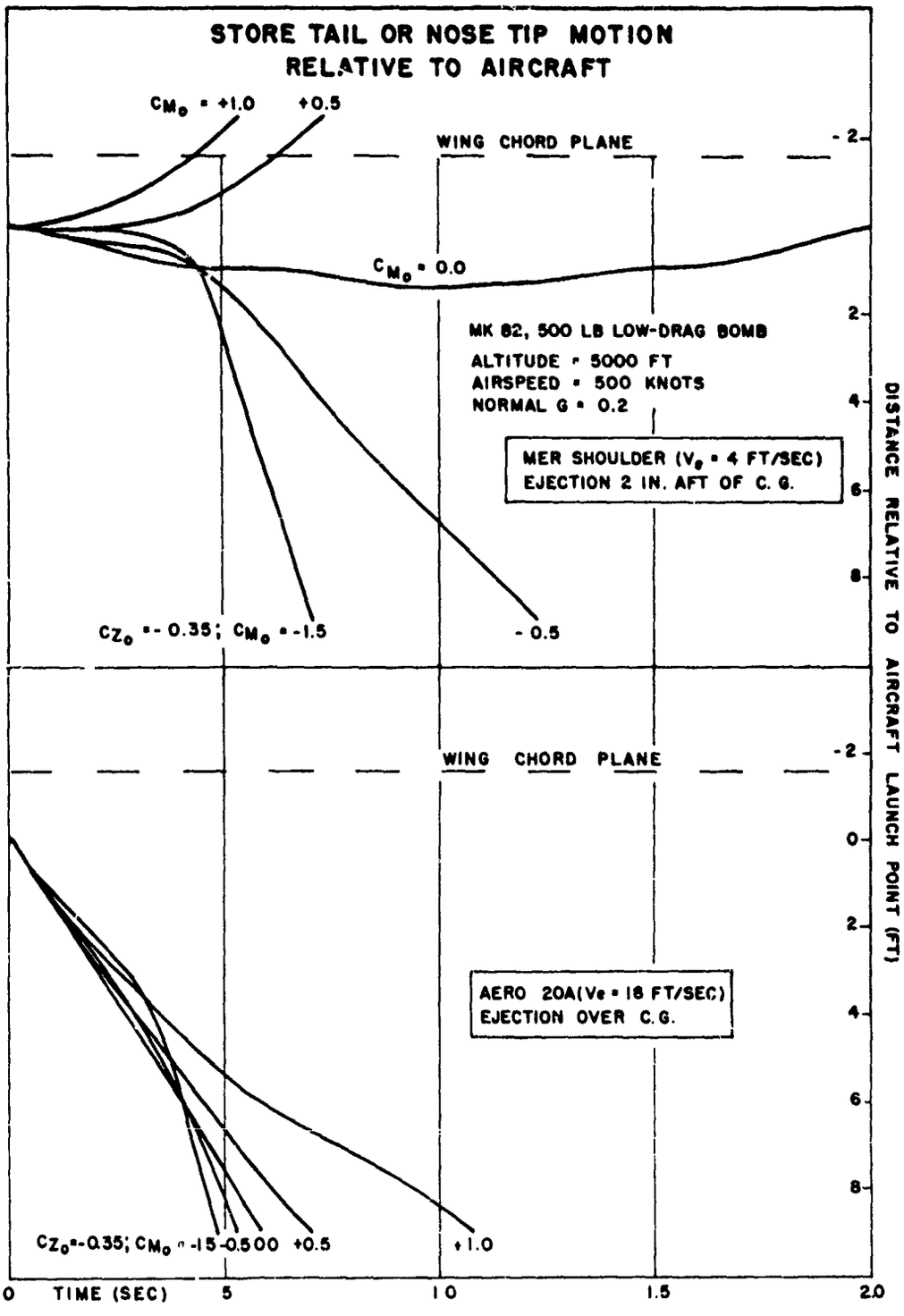

(U) FIG. 9. Effect of Ejection Velocity on Initial Store Motion.

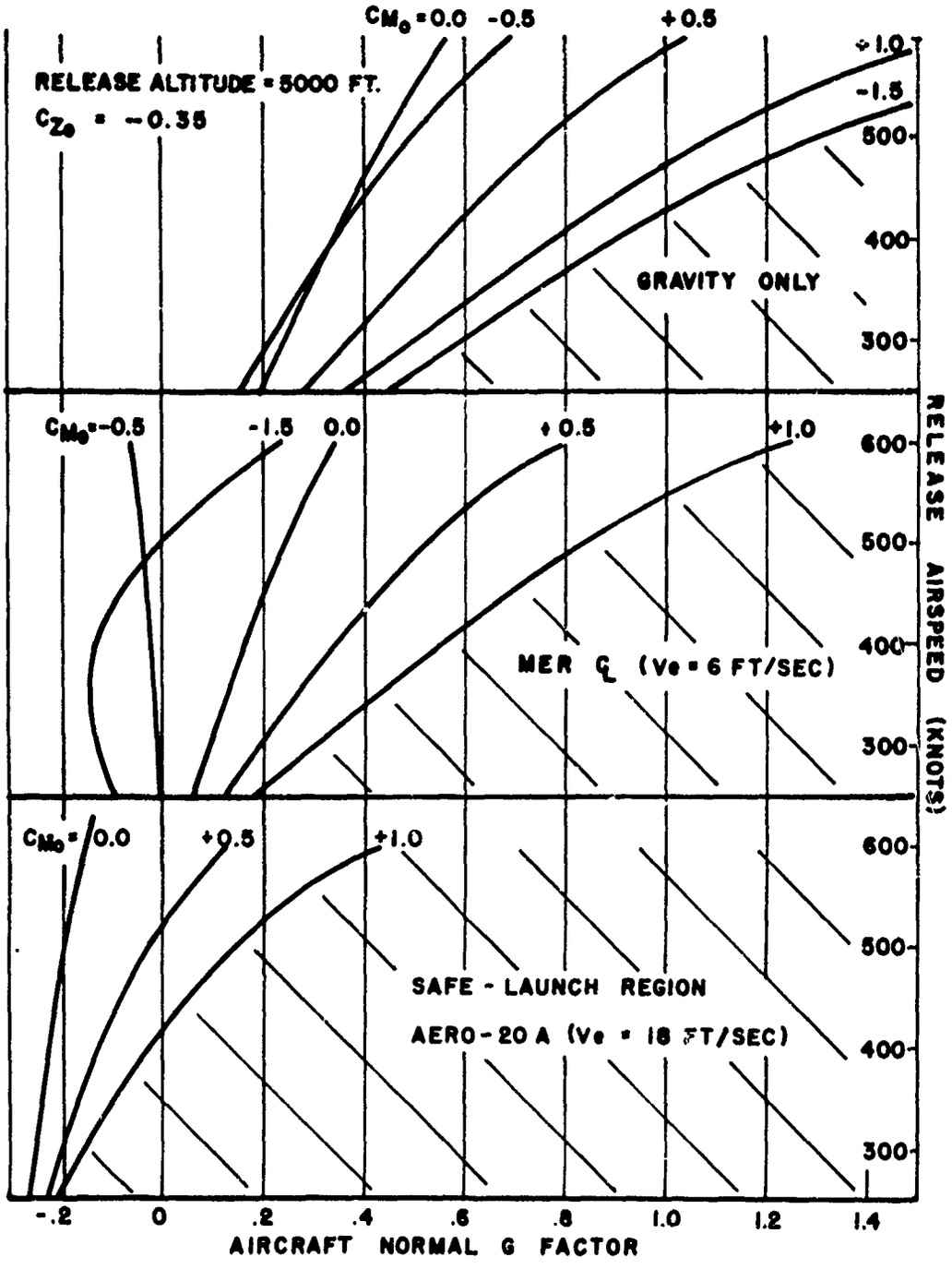

(U) FIG. 10. Safe-Launch Boundaries, MK 82 500 lb. Low-Drag Bomb.

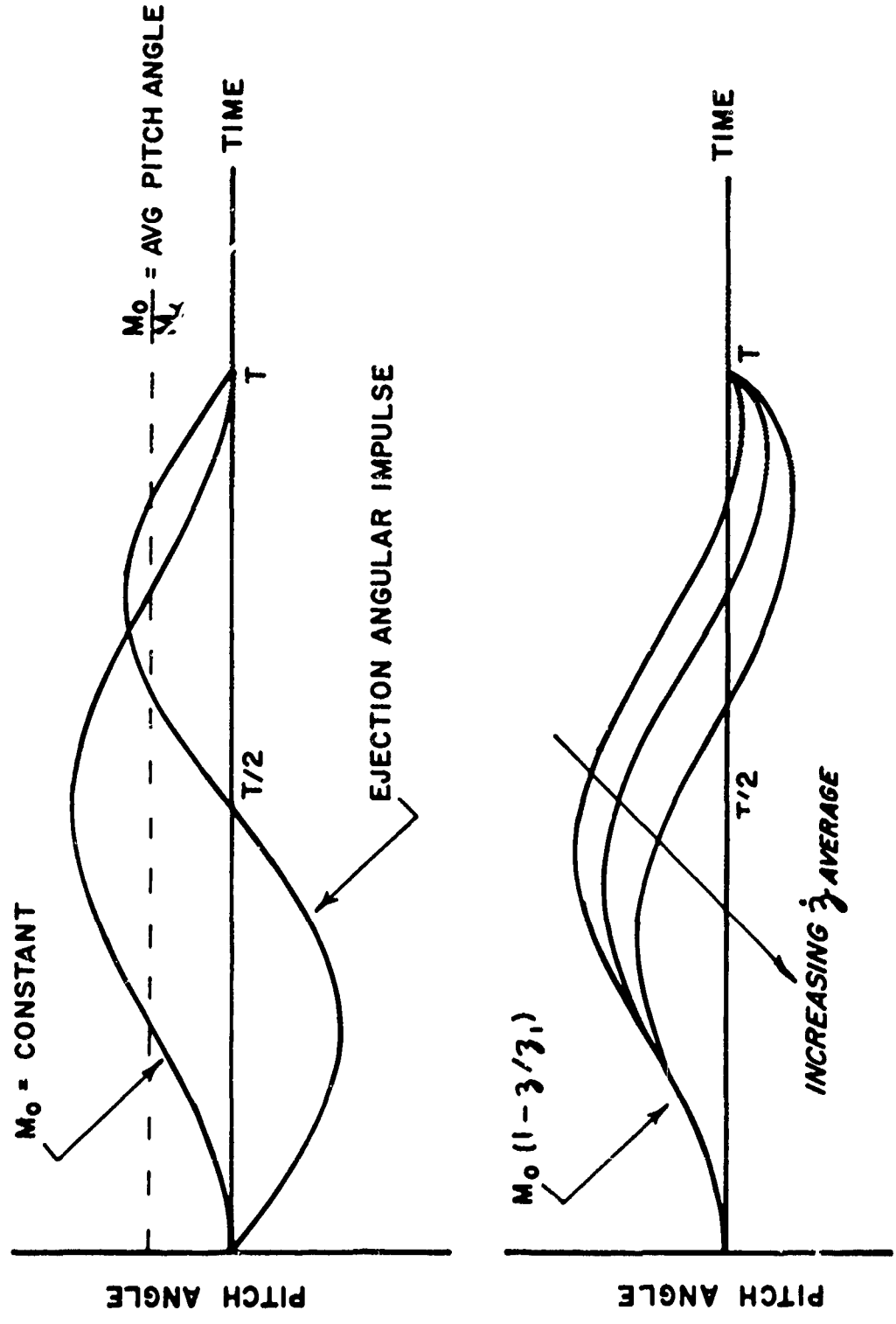

(U) FIG. 11. Some Characteristics of Store Transient Pitching Motion.

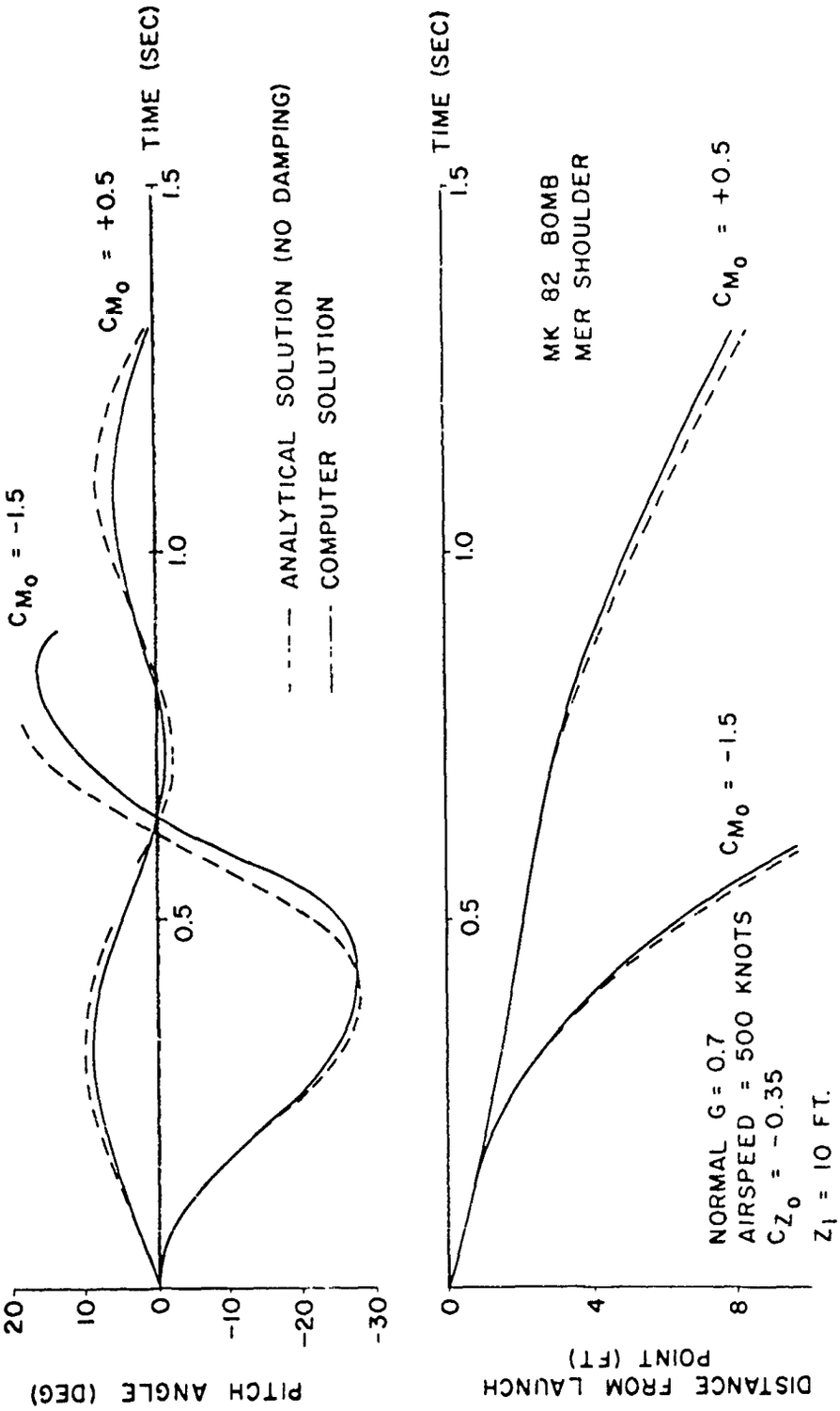

(U) FIG. 12. Comparison of Analytical and Computer Solutions for Dynamic Response to Linear Decay of Loads.

Paper No. 47

PREDICTION OF STORE SEPARATION TRAJECTORIES AT THE NAVAL WEAPONS CENTER (U)

(Paper UNCLASSIFIED)

by

J. V. Netzer
Naval Weapons Center
China Lake, Calif. 93555

ABSTRACT. (U) Because existing theoretical prediction techniques did not satisfactorily predict separation characteristics of conventional ordnance released from multiple-carriage bomb racks on high-speed aircraft, the Naval Weapons Center investigated a semi-empirical prediction technique based on previous flight data. It was hypothesized that if the captive flight air loads were known, along with the free-stream aerodynamic characteristics, then the manner in which these loads varied from one to the other would depend primarily on distance from the release aircraft.

(U) In order to use this information to predict the separation motions, the presently used digital six-degree-of-freedom program was modified to simulate store separation. The data obtained are now being used to predict separation trajectories to match existing flight test data. This trajectory matching consists of using the grid data and empirically varying the way the initial captive loads change to free-stream conditions below the aircraft. The results of these studies and simulations are given.

INTRODUCTION

(U) The Naval Weapons Center is very much aware of the problems that are associated with separating stores from multiple carriage racks on high speed aircraft. Compounding the problem also are the present tactics which are dictating high dive conditions during release. Our experience, during a time of having extreme difficulties with the separation of the Rockeye II dispenser, indicated that very little capability existed to predict and understand the motion that occurred during separation of these complex configurations under practical release conditions. Also, the wind tunnel techniques for exploring the separation phenomenon were just beginning and very little data were available. It appeared, therefore, that the most fruitful method for the Naval Weapons Center to undertake would be an empirical prediction technique based on available flight test data.

(U) It was hypothesized that if the aerodynamic loads were known during captive flight along with the normal free stream aerodynamic data, the manner in which the captive flight loads varied to free stream conditions would be dependent primarily on the distance from the release aircraft. This assumes that the changes in the aerodynamics of the store due to its attitude are independent of the aircraft flow field.

(U) This paper presents the program that was undertaken to develop the capability of simulating the motion of a store as it separates from the aircraft.

EXPERIMENTAL DATA REQUIRED

(U) The MK 7 Dispenser (Rockeye II) as shown in Fig. 1 was selected as the basis for the development of the simulation model. This configuration has had very extensive flight testing on the NWC ranges from which a great deal of trajectory and attitude data are available. Also since this dispenser is initially unstable at release, the flow field has a very predominate role in the initial motion that occurs. The following experimental data have been obtained for the MK 7 Mod 2 dispenser:

1. Wind tunnel data of both static and dynamic coefficients.

2. Captive flight loads using a six-component internal balance in a full scale weapon.
3. Wind tunnel grid tests in the proximity of an A-4 aircraft model.
4. Full scale flight tests on the NWC ranges.

WIND TUNNEL PROGRAM

(U) A complete series of wind tunnel tests have been performed to obtain all the aerodynamic data that are normally used in a stability and trajectory analysis. This information is also used in the simulation of the separation from the aircraft since we assumed that the effect of the aircraft flow field only adds incremental changes to the aerodynamics of the stores. The test program that was prepared is as shown:

1.	Static coefficients	$f(M, \alpha, \phi)$
2.	Pitch damping coefficients	$f(M, \alpha, \phi)$
3.	Roll damping coefficients	$f(M, \alpha, p)$
4.	Magnus coefficients	$f(M, \alpha, p)$

(U) Static data have been obtained from both the Naval Ships Research and Development Center (NSRDC) and the Naval Ordnance Laboratory (NOL). The tests conducted at NSRDC were on a four-tenths scale model and included both the Mod 1 and Mod 2 configurations with fins open and closed. The Mach range was up to .85. The NOL tests were more complete, although only the Mod 2 fins open was tested. These tests included the transonic region up to Mach 1.5. The remainder of the test program was done at the NOL facilities although the Magnus tests have not yet been completed.

CAPTIVE FLIGHT AIRLOADS

(U) A large portion of the effort in this program has been directed toward the development of the capability to measure the loads on the store during captive flight. In the past, NWC has built several airborne balances in an attempt to obtain this type of information. Success was very limited, however, due to problems in instrumentation, aircraft vibration, interaction in the balance, and an accurate determination of the flight characteristics during recording of the data. With the seriousness of the store separation problems that have developed, the need for these captive flight loads was again apparent. These measured loads would provide a better understanding of the complex flow field around the aircraft and also provide full scale checks for the wind tunnel data.

(U) When the Pastushin balance became available, it presented an opportunity to determine if our previous balance problems could be

overcome and also provide some very useful and timely captive load data.

(U) This balance as shown in Fig. 2 was installed in the shell of a Rockeye II dispenser. After calibration and development of the data reduction program, the flight tests were started. To date ten flights have been made on the Mod 1 configuration and eight flights on the Mod 2. The flight schedules are shown in Tables 1 and 2.

(U) The data that have been obtained for the MK 7 Mod 2 configuration are shown in Fig. 3 through Fig. 8. As seen, the pitching moments and yawing moments become very large with increasing Mach number. On the plus side, however, the normal force is small and even becomes negative, for some locations, with increasing Mach numbers.

(U) Table 1. Captive Flight Air Loads on A-4 Aircraft
Flight Schedule

	Rack	Rack Sta	Other Rack Sta Loaded	A/C Sta	Rockeye Mod
2	TER	1	2	Port 75	1
3	MER	4	5,6	Fuselage	1
4	MER	5	6	Fuselage	1
5	MER	3	4,5	Port 75	1
6	MER	4	5	Port 75	1
7	MER	2	3,4,5,6	Fuselage	1
8	MER	3	4,5,6	Fuselage	1
9	MER	5	-	Port 75	1
10	TER	2	-	Port 75	1

All flights V = 225, 300, 350, 400, 450, V_{MAX}

(U) Table 2. Captive Flight Air Loads on A-4 Aircraft
Flight Schedule

	Rack	Rack Sta	Other Rack Sta Loaded	A/C Sta	Rockeye Mod
11	AERO 20A	-	-	Port 113.5	2
12	AERO 20A	-	-	Port 75	2
13	TER	1	2	Port 75	2
14	TER	2	-	Port 75	2
15	AERO 7A	-	-	Fuselage	2
16	TER	2	3	Fuselage	2
17	TER	2	3	Fuselage	2
18	TER	3	-	Fuselage	2

All flights V = 225, 300, 350, 400, 450, V_{MAX}

GRID TESTS

(U) Even though we assumed that the captive flight loads could be used to calculate the separation trajectories, a series of wind tunnel tests were proposed at NSRDC to obtain grid data in the proximity of an A-4 aircraft model. The grid method was selected over the captive trajectory method since this dispenser is being used for other weapons and a large variation of mass and inertia characteristics will occur with each application. These data will be used to predict the separation characteristics of the dispenser for comparisons with both the flight test data and the prediction based on the captive flight loads. The grid data will also give us the form in which the captive flight loads should be varied to free stream conditions below the aircraft. The program for the grid test is shown in Fig. 9. As can be seen, three basic grids have been outlined covering the A-4 aircraft. This could be considered as a minimal grid program. These tests are presently in progress and should be available by the end of May.

STORE SEPARATION PROGRAM

(U) In order to use these data to predict the motion of a store as it is released from an aircraft, the six-degree-of-freedom program available at NWC has been modified. This program is the McDonnell Six-Degree-of-Freedom Program that was adapted to our computer several years ago. The construction of this program is on a building block principle such that modifications, changes and additions can easily be incorporated.

(U) With the basic 6-D program available, the store release problem requires three additional functions:

1. Method of adding additional forces and moments to account for the aerodynamics of the store in the aircraft flow field.
2. Ejection simulation.
3. Simulation of the release aircraft flight path.

FLOW FIELD AERODYNAMICS

(U) The adding of the additional aerodynamic forces and moments to the free stream aerodynamics to account for the flow field effects has been accomplished through the use of influence coefficients. These influence coefficients are in the aircraft axis system and are allowed to vary in some defined manner as a function of the distance XYZ from the release aircraft. The summation of the aerodynamics is as shown:

$$C_N = C_N' + \Delta C_N$$

$$C_Y = C_Y' + \Delta C_Y$$

$$C_m = C_m' + \Delta C_m$$

$$C_n = C_n' + \Delta C$$

(U) The prime values are the free stream aerodynamics and the Delta coefficients are the influence coefficients. At the present time we are using a linear interpolation table look-up for the influence coefficients. This could possibly change with the development of the techniques being proposed by NSRDC.

EJECTION

(U) The ejection of the store is simulated through the use of the thrust routine that was in the program. This was expanded, however, to include the dual ejection capability of the newer racks. Also, since the rack ejection forces and time of ejector strokes vary considerably with store mass, the thrust forces and time can be input as functions of the store mass. A typical force time curve for the MER/TER rack is shown in Fig. 10.

AIRPLANE

(U) The controlling routine in the program is the airplane. This routine simulates the flight path of the aircraft and keeps track of the position of the store relative to it. This position data is then used to enter the tables of influence coefficients to obtain their values.

(U) The actual aircraft simulation grew out of the target routine that was developed for Sidewinder simulation. It provides for the simulation of the aircraft for the following options:

1. The airplane is constrained to a stationary point.
2. The airplane is moving in a straight line.
3. The airplane is moving with circular motion in the X-Y plane.
4. The airplane is moving with circular motion in the X-Z plane.

COMPARISON WITH FLIGHT TESTS

(U) The program has been exercised only during the past few months with the captive load data. The results to date are very promising although only a superficial comparison has been made thus far.

(U) The data from the captive flight tests of the Mod 0 and Mod 1 have been used to compute the separation characteristics of a number of early flight tests. The captive flight data were used to simulate a grid for these computations. Table 3 shows these comparisons on the basis of the first initial pitch angle off of the rack.

(U) Table 3. Rockeye II Mod 0, Mod 1 - Comparison of Predicted vs Actual Initial Pitch Angles

Configuration	Velocity (KTS)	Predicted ∝ Max	Flight Data ∝ Max
A4 ℄ MER 4	400	-21°	-21°
	450	-24°	-27°/-24°
	470	-24°	-27°
A4 WS MER-4	225	20°	+13°
	325	10°	10°/9°
	470	6°	6°
A4 ℄ MER-3	350	10°	14°
	400	13.5°	8°/9°
	465	15°	6°

(U) Using the data that was previously shown for the Mod 2, one flight test has been simulated in greater detail. This drop was made in a 46-degree dive from Station 2 of the TER rack on the wing of the A-4. Figure 11 shows the pitch and yaw data obtained from this flight with the simulation superimposed. The agreement is quite good considering the fact that all the captive flight data have been taken only in level flight. The variation in pitch with distance below the aircraft is shown in Fig. 12.

SUMMARY AND RECOMMENDATIONS

(U) This program that has been developed at the Naval Weapons Center has shown that with a reasonable knowledge of the loads on the store during captive flight, the motion during separation can be computed with reasonable results. What happens as the motion becomes more violent and unsafe to the launch aircraft has not yet been considered.

(U) There are a number of recommendations that should be made to give those people who are doing store separation studies a better chance at success. These are:

1. The aircraft flight characteristics at release should be known with better accuracy.

2. The motion of the store during that short interval of time while in flow field should be measured accurately.

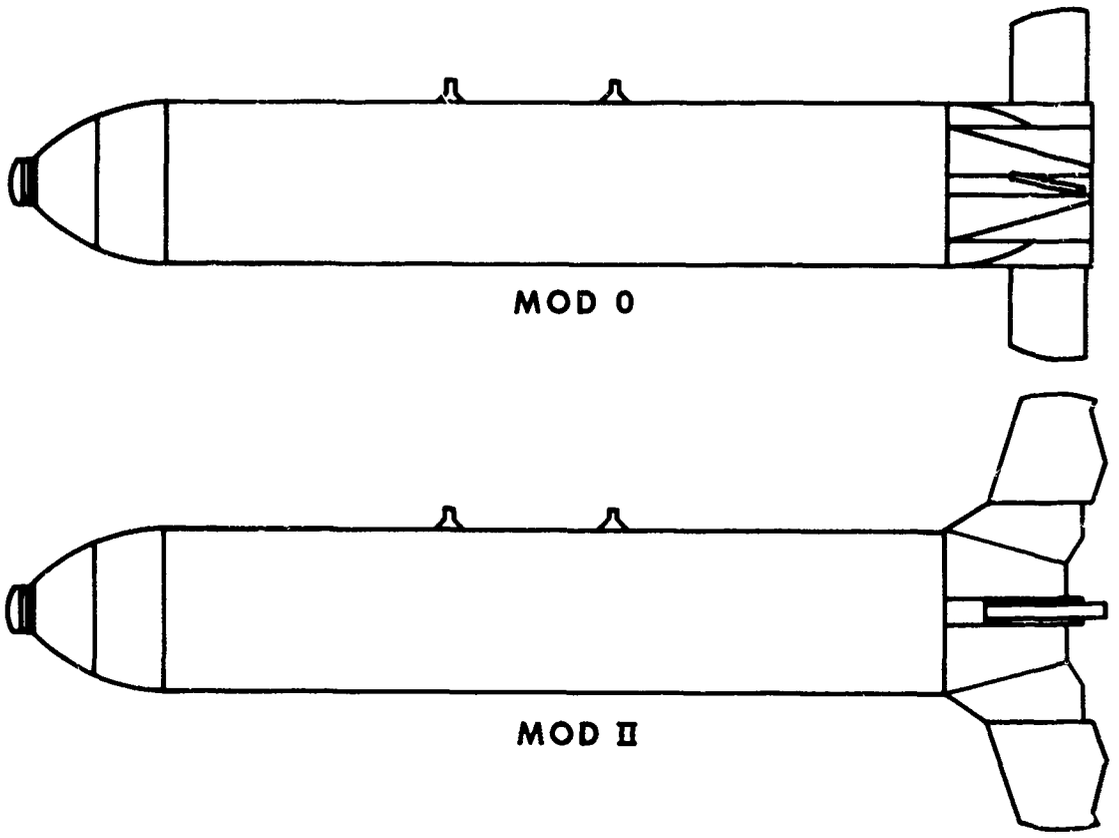

(U) FIG. 1. MK 7 Dispenser (Rockeye II).

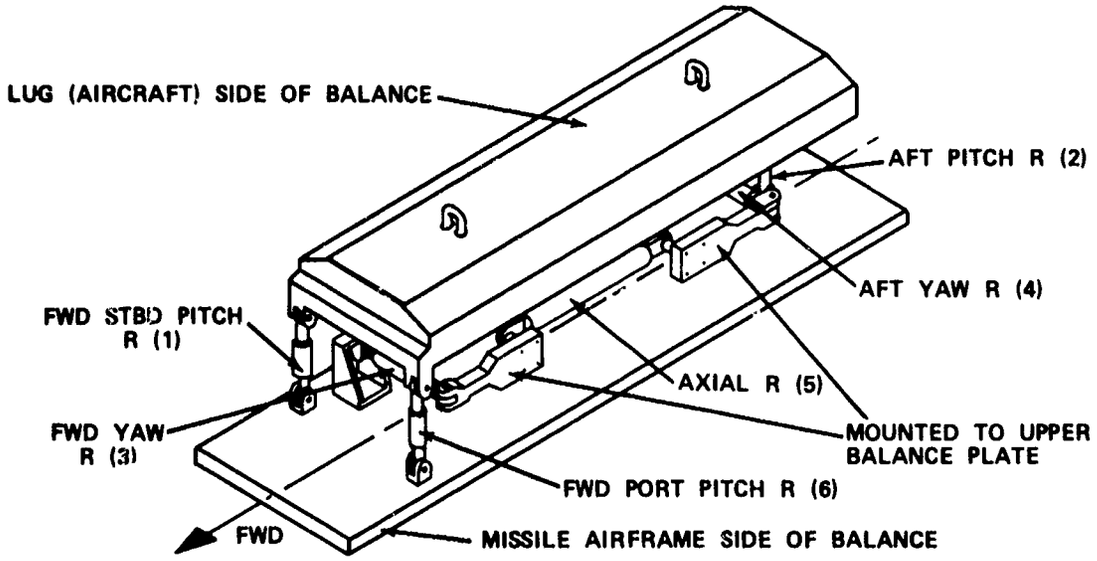

(U) FIG. 2. Pastushin Balance.

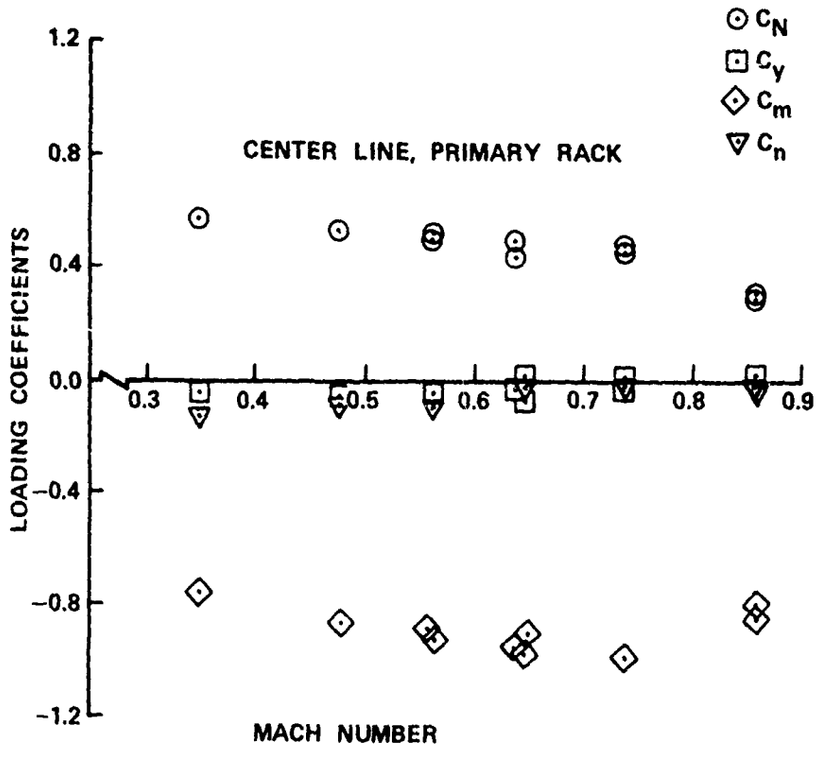

(U) FIG. 3. MK 7 Mod 2 Captive Flight Loads A-4 Aircraft.

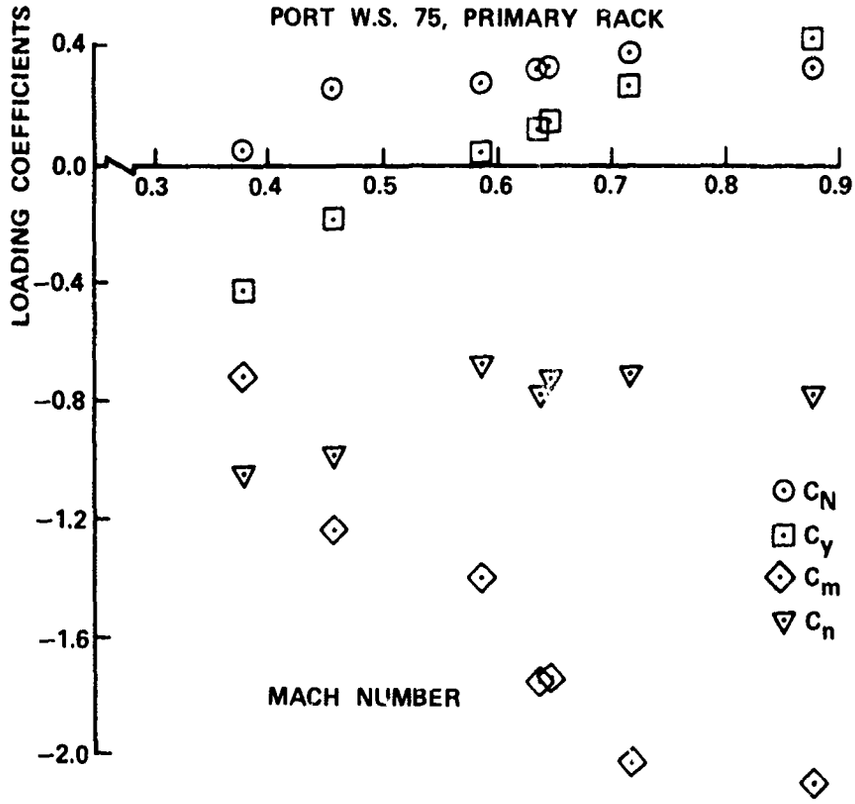

(U) FIG. 4. MK 7 Mod 2 Captive Flight Loads A-4 Aircraft.

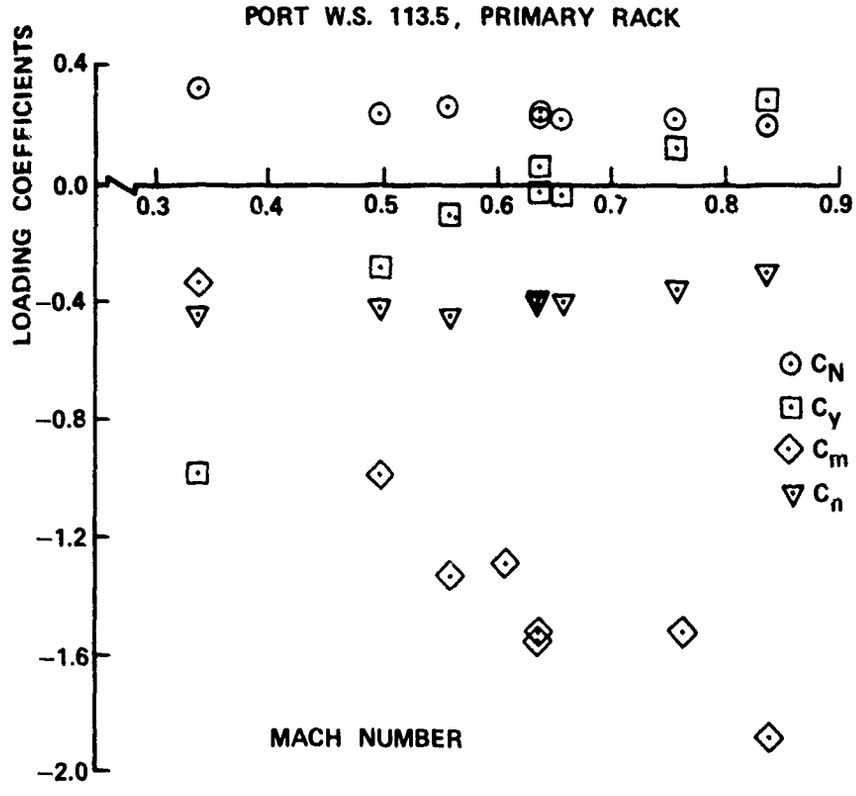

(U) FIG. 5. MK 7 Mod 2 Captive Flight Loads A-4 Aircraft.

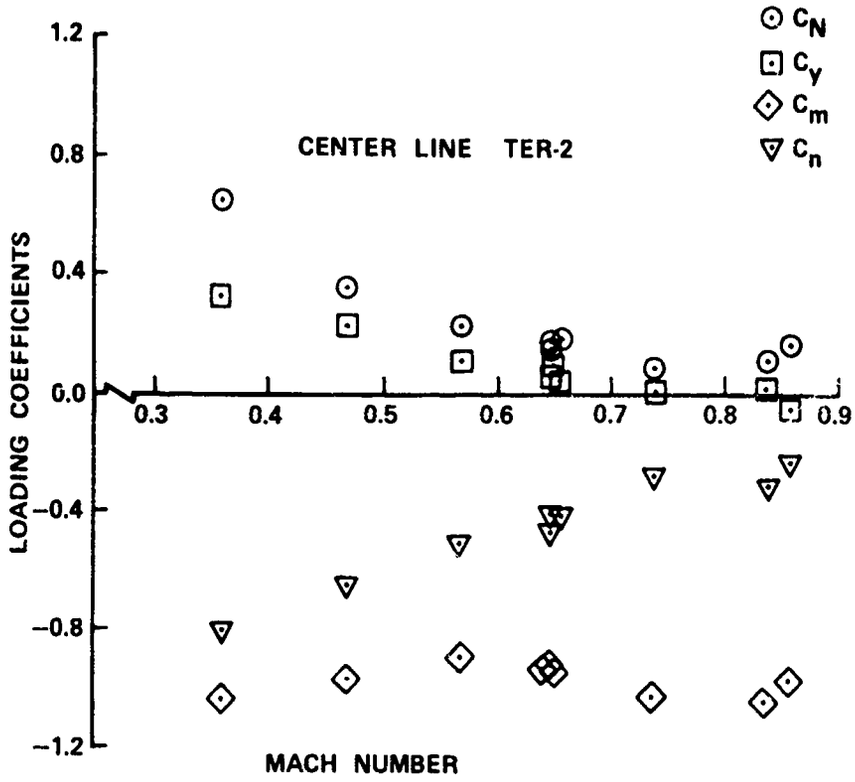

(U) FIG. 6. MK 7 Mod 2 Captive Flight Loads A-4 Aircraft.

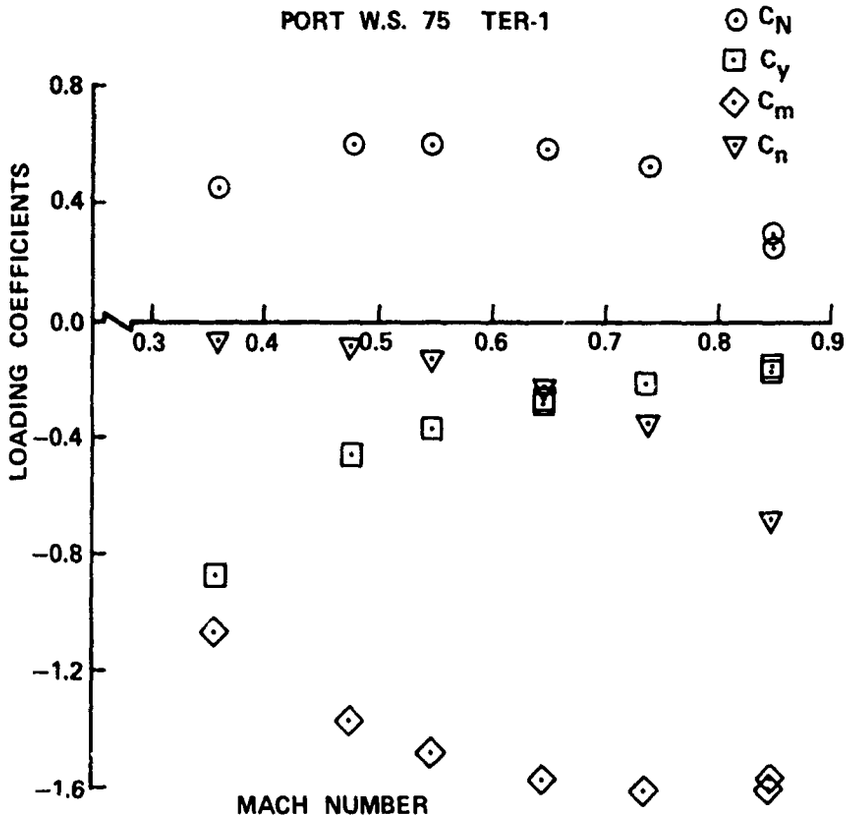

(U) FIG. 7. MK 7 Mod 2 Captive Flight Loads A-4 Aircraft.

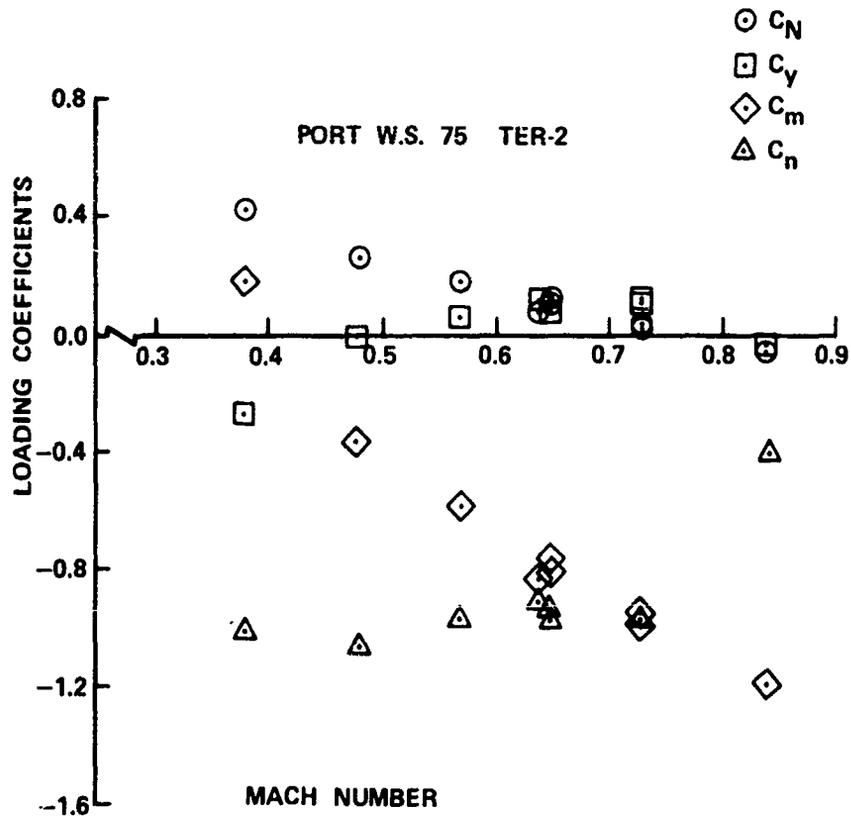

(U) FIG. 8. MK 7 Mod 2 Captive Flight Loads A-4 Aircraft.

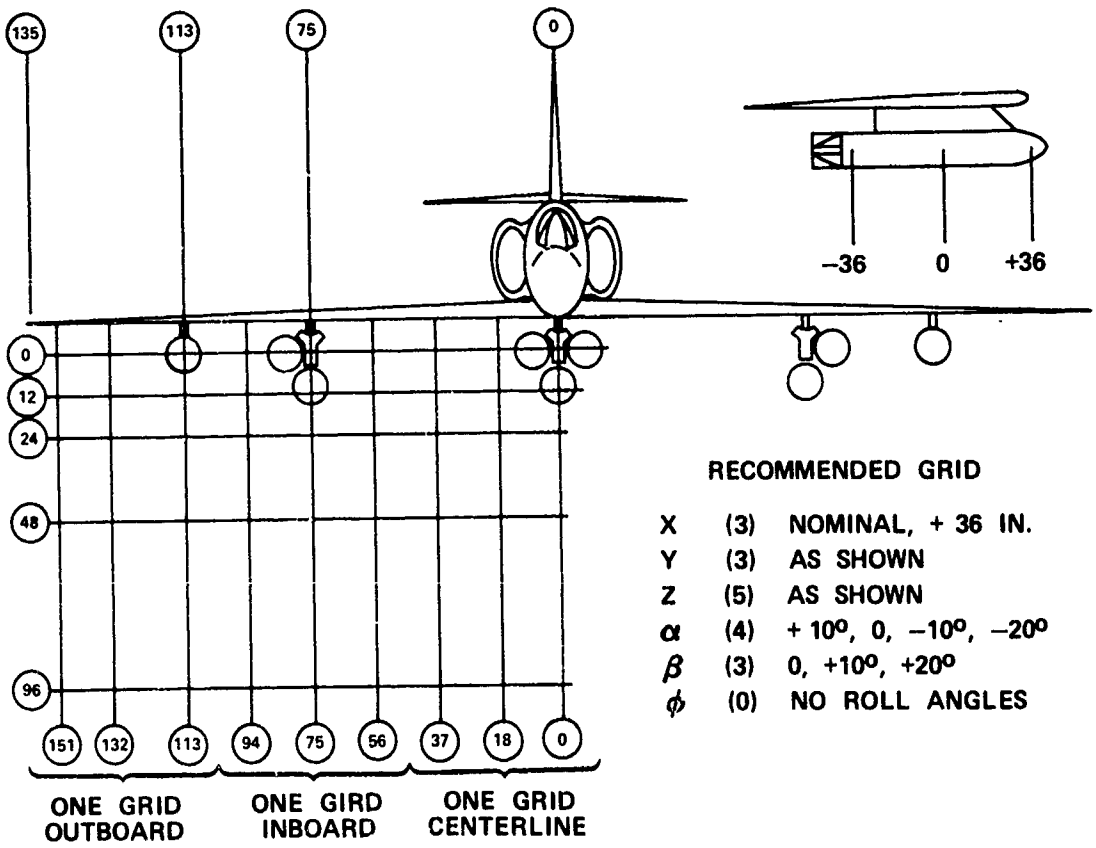

(U) FIG. 9. Typical Grid Test.

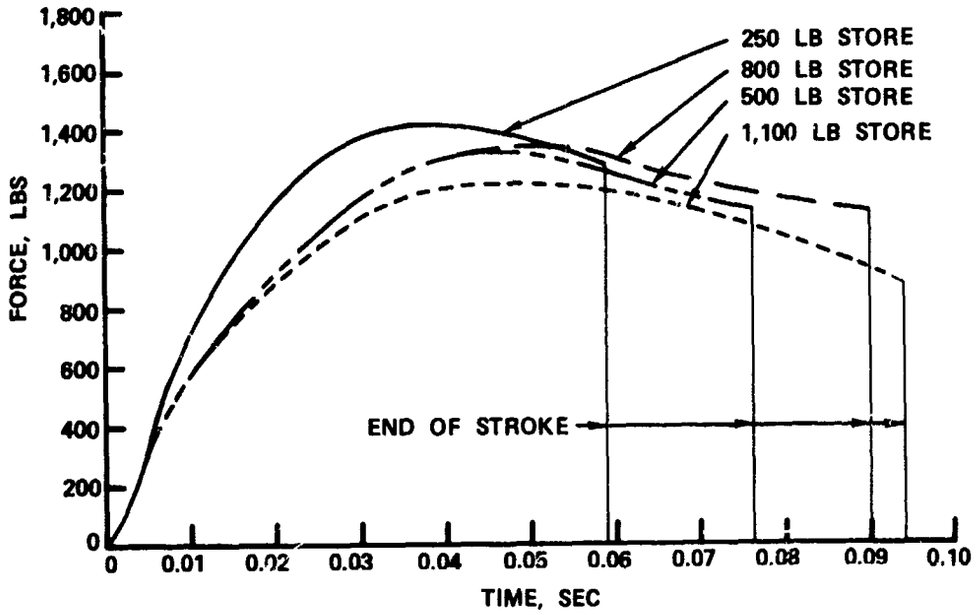

(U) FIG. 10. MER/TER Ejection Characteristics.

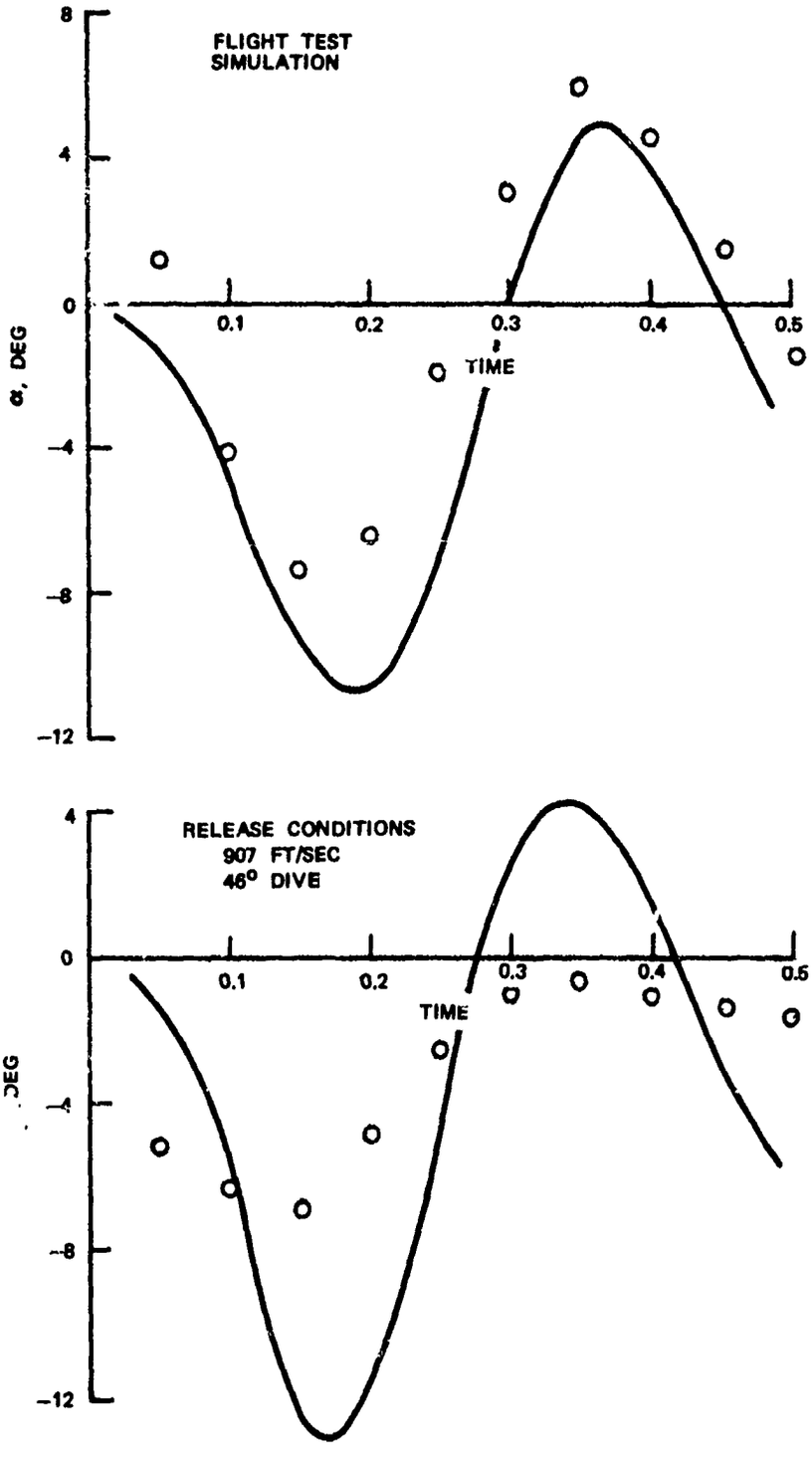

(U) FIG. 11. Simulated Pitch and Yaw Time Histories.

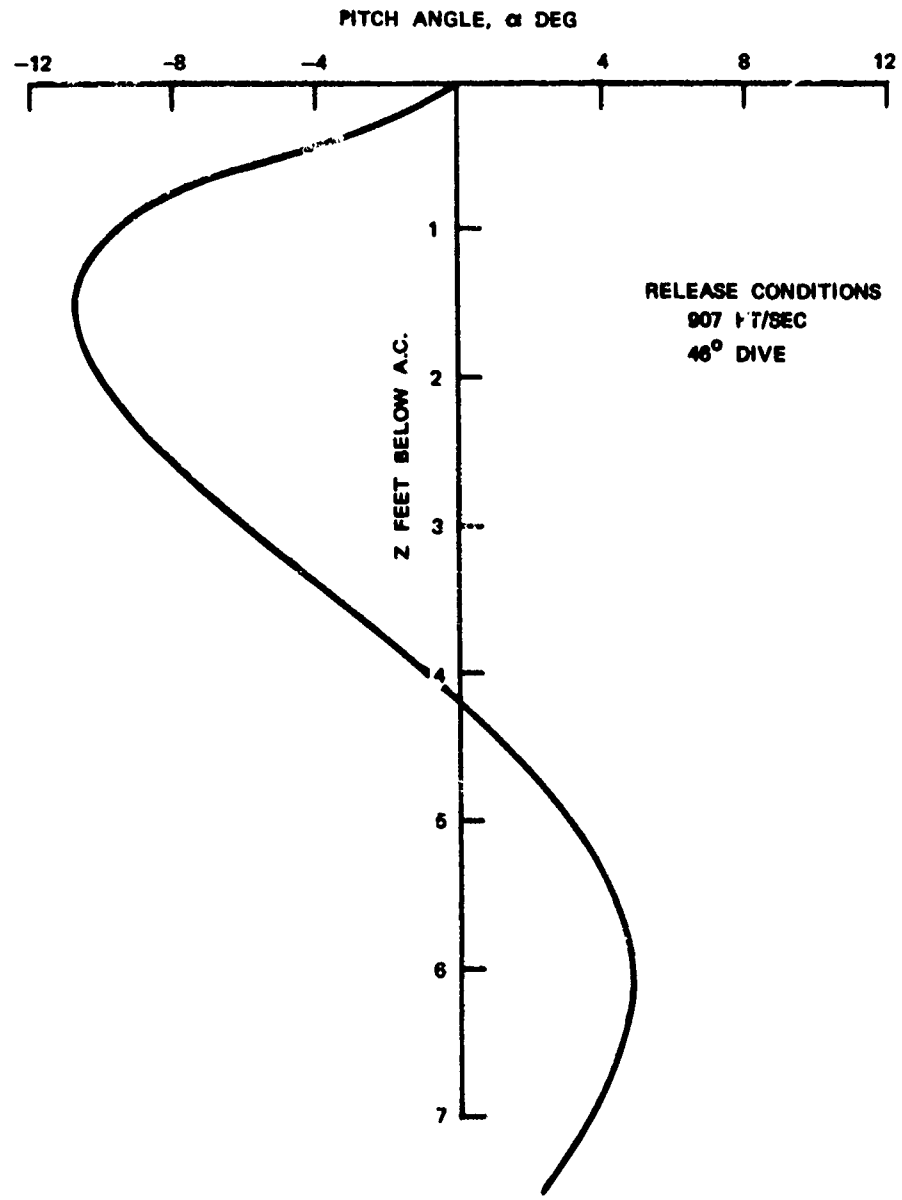

(U) FIG. 12. Variation in Pitch with Distance Below Aircraft.

Paper No. 49

AN ANALYTICAL, NUMERICAL PROGRAM FOR CALCULATING THE AERODYNAMIC FORCES EXTERNAL TO AIRCRAFT (U)

(Paper UNCLASSIFIED)

by

Hyman Serbin
15219 Sunset Boulevard, Room 201
Pacific Palisades, Calif. 90272

ABSTRACT. (U) An analytical method for calculating the aerodynamic forces on a store within the flow field of an aircraft has been developed based on the assumptions: (a) the aircraft is a slender body, (b) the store has no appreciable effect on the aircraft flow field, and (c) the store is a slender body oriented at a small angle relative to the ambient flow. The method of analysis is based on the Munk-Jones slender body theory according to which the flow at each cross section of the aircraft is treated independently. The velocity field so obtained is applied to the store, again by slender body theory. The impulse required to generate the cross flow generates a reaction on the store, the aerodynamic force.

(U) The analysis has been converted into a computer program with options of calculating either the local angles of the flow field or the aerodynamic forces on a store at general positions relative to the aircraft. Numerical comparison with NACA tests shows qualitative agreement. Areas of refinement in the theory are indicated.

INTRODUCTION

(U) The design of external stores for aircraft requires a knowledge of the aerodynamic forces acting on the store. This information is usually obtained in wind tunnel tests. However, when a number of combinations of stores are considered, it is unfeasible to obtain this type of design data by testing. The availability of high speed computers has opened the possibility of applying aerodynamic theory to the calculation of forces on stores under interference conditions. One of the most versatile theories is Munk's theory of slender bodies. In its original form, as applied to airships, the theory led to the prediction of zero normal force. It was R. T. Jones who revitalized the theory by extending it to lifting surfaces of a simple shape (delta wings). The theory can be extended to more general aerodynamic shapes, and to the computation of forces on stores near aircraft. If it can be shown that the predictions of the theory are fairly accurate, then a computer program will be a useful tool for preliminary design and for the evaluation of design changes. In this paper, a first stage computer program is described, and a comparison with wind tunnel data is made.

PLAN OF THE INVESTIGATION

(U) The study proceeds in two phases:

a. Calculation of the flow field around the aircraft
b. Calculation of the aerodynamic forces on the store immersed in the flow field.

Part a is carried out on the basis of a decomposition of the flow field. This is done in two stages. The free stream velocity vector is decomposed into two components, one along the aircraft axis and the other perpendicular. To each of these components, there is a flow field (Fig. 1) with velocity components (u, v) in the plane of the cross section. The first flow field is specified by the distribution of normal velocity at the contour; the second by the cross flow velocity.

(U) The calculation of the velocity is carried out not in the physical plane but in a conformally equivalent plane (Fig. 1), in which the transformed contour appears as a slit. The axial flow field is again specified by a distribution of normal velocities and the cross flow by the remote velocity. The axial flow field is then decomposed into two parts, I and II. Flow field I is defined by a constant normal velocity and flow field II by a normal velocity distribution of zero efflux across the contour. Flow field III is then the cross flow field described above.

(U) The practical execution of the steps outlined above depends on the transformation of the physical cross section into a slit. There are again two cases. On the forward part of the airplane, the cross section is approximated by a circle. The mapping into a slit is given analytically. On the part of the airplane where the cross section cuts the wings, the mapping into the slit is accomplished by a sequence of numerical transformations which progressively flatten the aircraft cross section. In the limit the transformed contour becomes a slit. Practically, only five such transformations are used. Therefore, the physical cross section that one starts with should be "slender."

(U) The resultant flow field is the superposition of the three flow fields I, II, and III. The forces on the store are then calculated by applying slender body theory to the store immersed in a curving stream. The result of the analysis is a distribution of transverse forces along the axis of the store. All the aerodynamic coefficients, except drag and rolling moment, are then found by suitable integrations along the axis of the store.

(U) The complete analysis is embodied in a numerical program. This program starts with the geometrical description of the aircraft and the store, the flight conditions of the aircraft, and the geometrical relation between the store and the aircraft. The output includes the aerodynamic force coefficients C_Y, C_N and moment coefficients $C_{m'}$, C_n. Pressure distributions can be calculated from the data generated within the program.

SAMPLE CALCULATION

(U) The program has been applied to a canard missile operating near an aircraft with swept mid-wing (Fig. 2). Various locations of the missile were considered, all in the same cross section location under the left wing. The fore-aft was varied in terms of the parameter

$$\frac{x}{c} = \frac{\text{long. coordinate of missile ref. pt. relative to l. e. wing chord}}{\text{chord at wing semi-span}} \quad (1)$$

The components of the cross force on the missile are shown in Fig. 3. A meaningful comparison of the moments is more difficult to make. Combine the pitching and yawing moments into a single vector in the cross section plane. By a suitable choice of the reference point, the component of moment perpendicular to the vector force can be reduced to zero. This point can be called the "aerodynamic center." Figure 4 shows the comparison between the calculated and experimental values.

(U) There is substantial qualitative agreement between the calculated and experimental results. The principal disagreement in the force data is the direction of the force vector. The difference in the aerodynamic center varies from 1/2 to 1 fuselage diameter except for one position near the wing leading edge.

PROPOSED EXTENSIONS

(U) Further progress depends significantly on an improved solution of the aerodynamic forces on an isolated srore. Here the problem is to calculate the motion of shed vortices and their interaction on the lifting surfaces.

(U) In summary, the areas of investigation should be pursued:

1. Application of the program to a variety of configurations to assess the accuracy of the theory in the present form.
2. Calculation of the shed vortex sheets behind the store lifting surfaces and the induced aerodynamic forces.
3. Flow fields in multiply connected cross sections of the aircraft.
4. Next order refinement of slender body theory to account for three dimensional and compressibility effects.

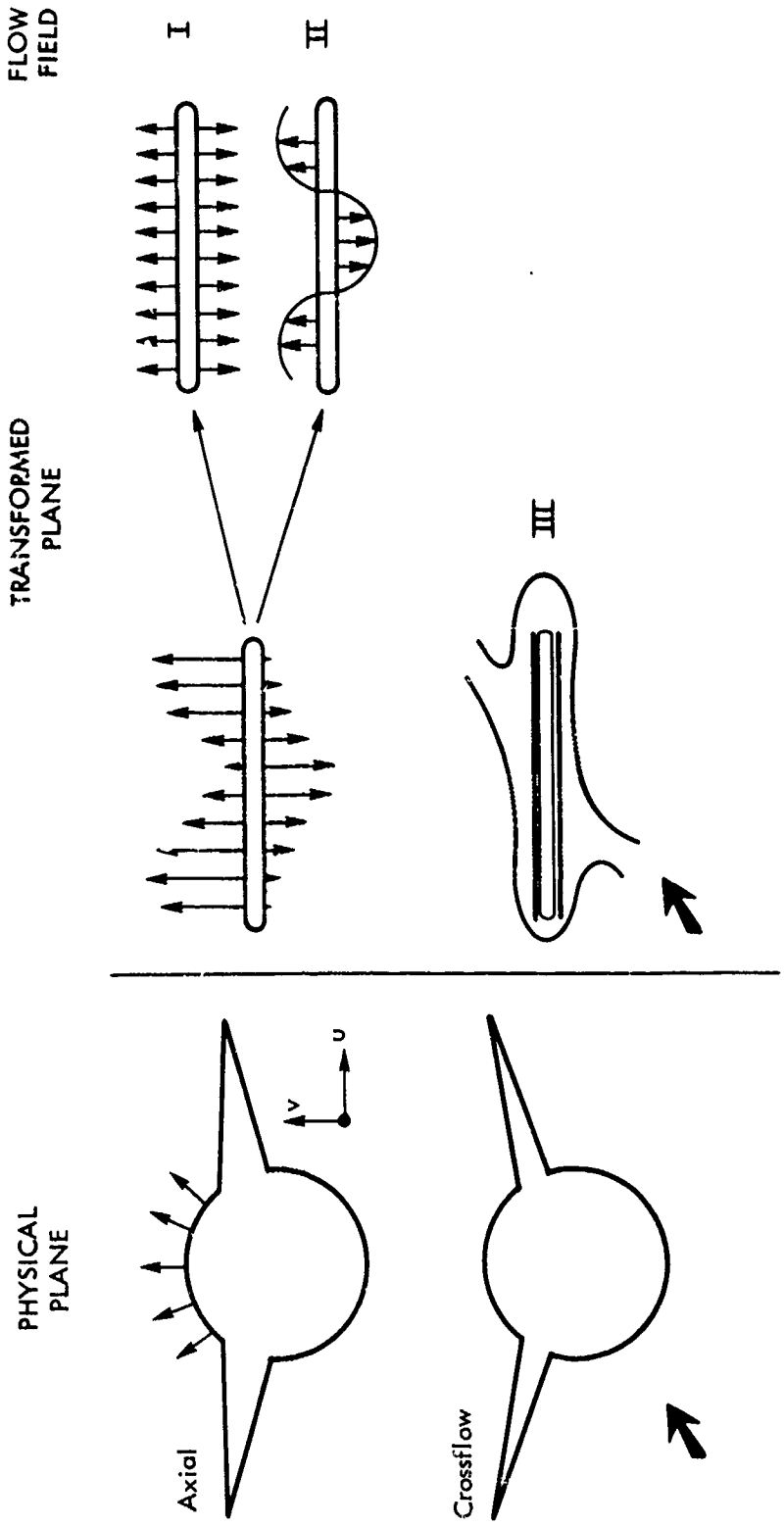

Fig. 1—Decomposition of the flow field

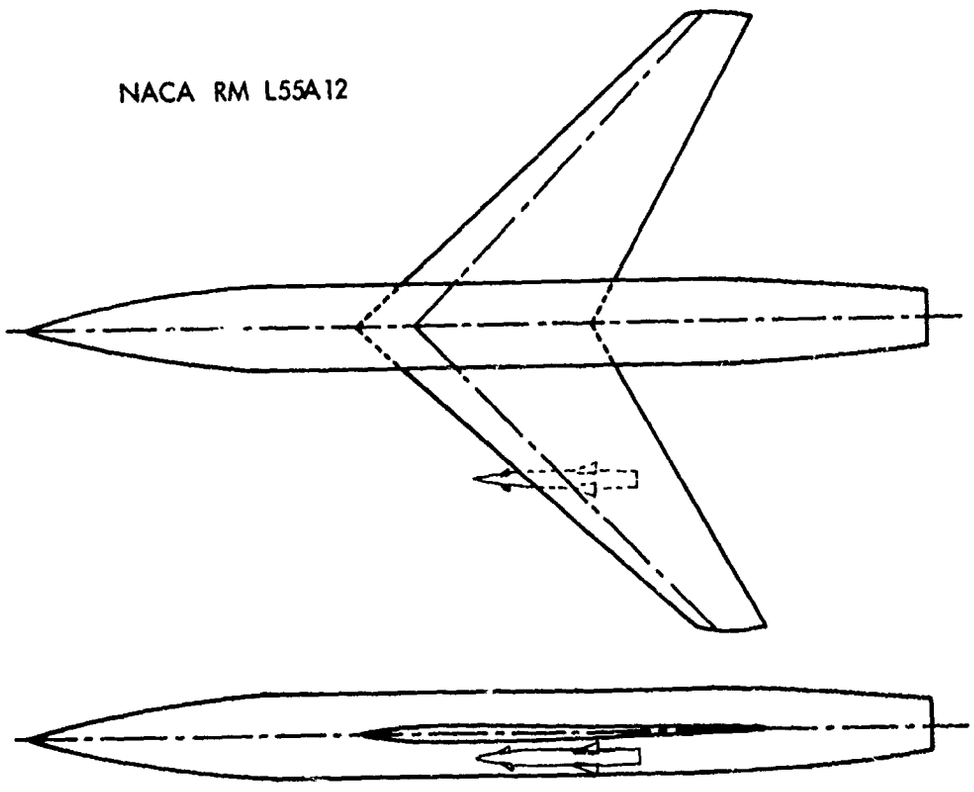

Fig. 2—Test setup showing missile in test locations

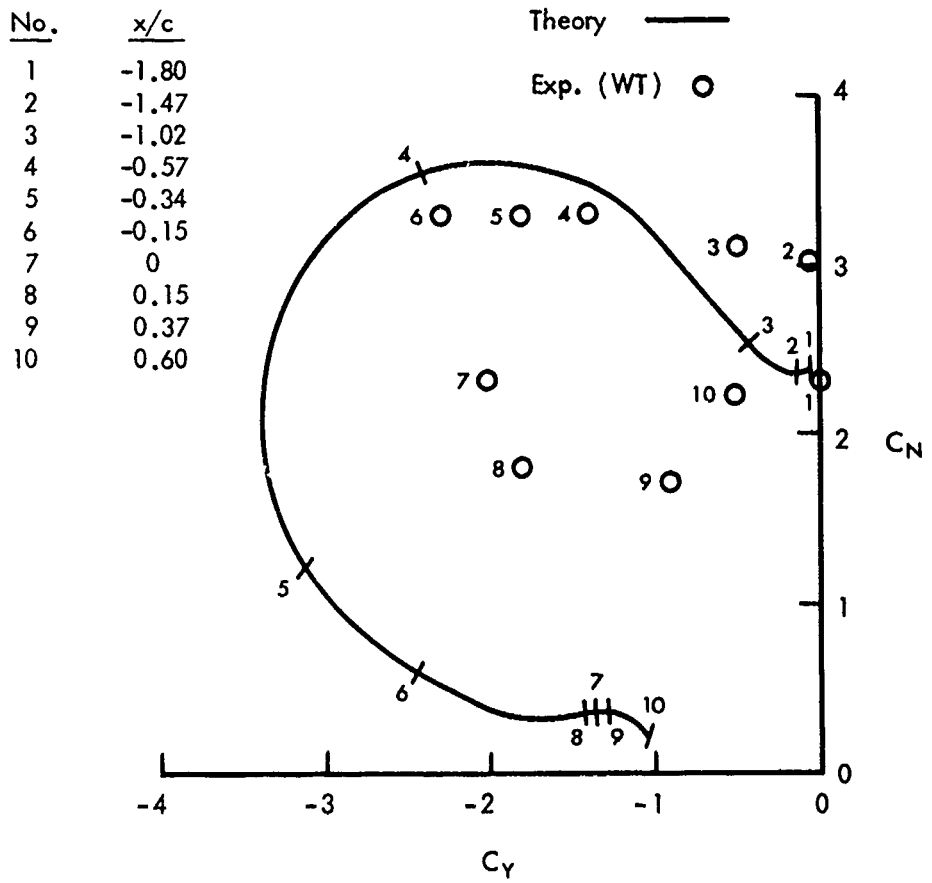

Fig. 3—Comparison of experimental and theoretical cross force

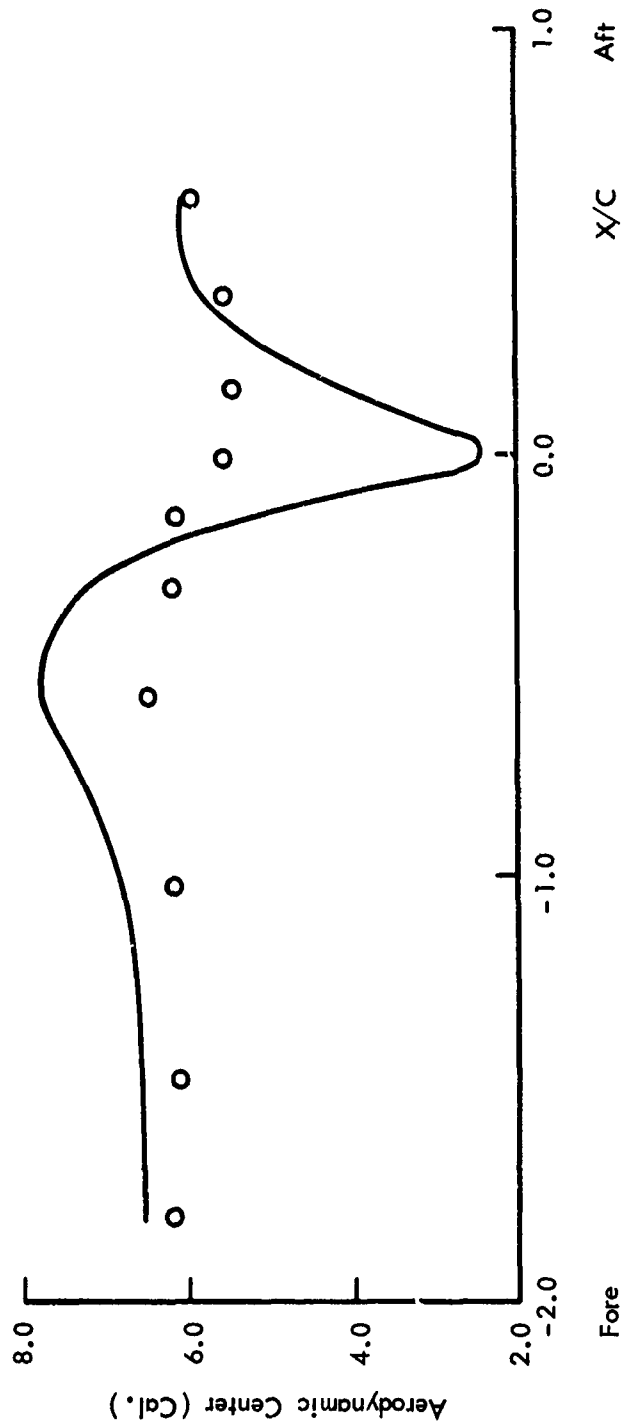

Fig. 4—Variation of aerodynamic center

UNCLASSIFIED

Security Classification

DOCUMENT CONTROL DATA - R & D

(Security classification of title, body of abstract and indexing annotation must be entered when the overall report is classified)

1 ORIGINATING ACTIVITY *(Corporate author)* Naval Weapons Center China Lake, California 93555	2a. REPORT SECURITY CLASSIFICATION UNCLASSIFIED 2b GROUP

3 REPORT TITLE

PROCEEDINGS OF THE 8TH NAVY SYMPOSIUM ON AEROBALLISTICS. VOLUME 4

4 DESCRIPTIVE NOTES *(Type of report and inclusive dates)*

5 AUTHOR(S) *(First name, middle initial, last name)*

6 REPORT DATE June 1969	7a TOTAL NO OF PAGES 272	7b. NO OF REFS 40
8a CONTRACT OR GRANT NO b. PROJECT NO c. d.	9a ORIGINATOR'S REPORT NUMBER(S) TS 69-199 9b OTHER REPORT NO(S) *(Any other numbers that may be assigned this report)*	

10 DISTRIBUTION STATEMENT

THIS DOCUMENT IS SUBJECT TO SPECIAL EXPORT CONTROLS AND EACH TRANSMITTAL TO FOREIGN GOVERNMENTS OR FOREIGN NATIONALS MAY BE MADE ONLY WITH PRIOR APPROVAL OF THE NAVAL WEAPONS CENTER.

11 SUPPLEMENTARY NOTES	12 SPONSORING MILITARY ACTIVITY Naval Air Systems Command Naval Ordnance Systems Command Naval Material Command Washington, D.C. 20360

13 ABSTRACT

DD FORM 1 NOV 65 1473 (PAGE 1)

S/N 0101-807-6801

UNCLASSIFIED

Security Classification

14 KEY WORDS	LINK A		LINK B		LINK C	
	ROLE	WT	ROLE	WT	ROLE	WT
Aeroballistics Navy Aeroballistics Symposium Missile Structures Aeroelasticity External Stores, Aircraft Store Separation Structures Loads						